UNIVERSITY OF CALIFORNIA,
IRVINE

Interactions among the Steroid and Xenobiotic Receptor (SXR/PXR), environmental toxicants and the gut microbiome and their effects on inflammation, oxidative stress, and cancer

DISSERTATION

submitted in partial satisfaction of the requirements
for the degree of

DOCTOR OF PHILOSOPHY

in Pharmacological Sciences
with a concentration in Pharmaceutical Sciences

by

Riann Jenay Egusquiza

Dissertation Committee:
Professor Bruce Blumberg, Chair
Professor Andrej Lupták
Assistant Professor Claudia Benavente

2019

DEDICATION

To

my Dadders

my biggest fan and supporter

Science means constantly walking a tightrope between blind faith and curiosity; between expertise and creativity; between bias and openness; between experience and epiphany; between ambition and passion; and between arrogance and conviction - in short, between an old today and a new tomorrow

- Heinrich Rohrer

TABLE OF CONTENTS

LIST OF FIGURES

CHAPTER 4 FIGURES Page

CHAPTER 4 SUPPLEMENTAL FIGURES Page

CHAPTER 5 FIGURES Page

LIST OF TABLES

ACKNOWLEDGMENTS

I would first like to thank my adviser Dr. Bruce Blumberg for his support and encouragement throughout my PhD journey. I am specifically grateful for him allowing me to pursue projects that were outside the normal scope of the lab research. I feel as though I am better qualified as an independent researcher because I was allowed to come up with my own ideas, learn how to plan and execute each new experiment myself, and, most importantly, follow where the data took me. Not all of my ideas worked out, but each one made me grow even more as a scientist. I cannot thank Bruce enough for this opportunity and the growth I have made in my time in his lab as a graduate student.

I would like to thank my committee members, Dr. Andrej Lupták and Dr. Claudia Benavente, for help in the editing of this dissertation and all the advice and support regarding my future. I would like to thank the Medicinal Chemistry and Pharmacology (MCP) gateway program and the Department of Pharmaceutical Sciences for challenging me and providing me with this wonderful opportunity to earn my doctorate.

I would not have made it through this journey without the support of the friends I have made here at UCI. I would specifically like to thank my dearest friend Stephanie Wu who has been there for me every step of the way and my shoulder to cry on in the toughest of times. I would also like to thank Dr. Bao Ho, Dr. Beverly Chou, Tom Ford-Hutchinson, Dr. Camila Zanette, and Guilherme Puglia for their constant support and friendship throughout my graduate career, and for demonstrating that there is life after grad school! I am very lucky to have met Omar Moquit during my last year here and am so very thankful for his support, encouragement, love, and necessary distractions, this year was much more special having him by my side.

The support I have received from my fellow lab members has also been instrumental in my success and happiness on this journey. I have been very lucky to have mentored many extremely amazing students over the years and I appreciate every single one of them for their work and friendship. I specifically want to acknowledge Kaelen Kay, Maria Ambrosio, and Shuyi (Gin) Wang who helped me so much with the work that went into this dissertation and my publication. I would also like to thank previous lab member Dr. Bassem Shoucri for being an excellent role model and setting the bar way too high for the expectations of a graduate student because it encouraged me to set the bar higher for myself. Finally, I would like to thank Dr. Raquel Chamorro-Garcia who has been the most amazing role model and friend in the lab, her support and constant encouragement has definitely made my experience here easier and more enjoyable.

Finally, I would like to thank my family. Without them, I would not be where I am today. I am beyond lucky to have a family that supports me with everything they have. I need to give a special shout out to my sister Ranie, who followed me down to Southern California for her own graduate studies and who has been my constant source of support, reassurance, and friendship. And to my biggest supporter of all, who I know is crying as he reads this, my dad. His love and support are endless. I am glad I can make him proud, and I am very proud to be his daughter.

CURRICULUM VITAE

Riann Jenay Egusquiza
PhD candidate, Pharmacological Sciences, University of California, Irvine
Email: regusqui@uci.edu

EDUCATION

University of California, Irvine
Medicinal Chemistry and Pharmacology PhD Gateway Program 9/2013-6/2014
Pharmacological Sciences, PhD 6/2014-6/2019

California State University, Fresno 8/2008-5/2013
Bachelor of Arts in Chemistry, GPA 3.84
Graduation date –May 18, 2013
Magna Cum Laude
With Departmental Honors

RESEARCH EXPERIENCE

Graduate Student Research 6/2014-6/2019
University of California, Irvine
Department of Pharmaceutical Sciences
Dr. Bruce Blumberg
Interactions of the Steroid and Xenobiotic Receptor with environmental toxicants and the gut microbiome and its effects on inflammation, oxidative stress, and cancer

- Use of mouse models to study cancer, inflammation, and oxidative stress
- Flow cytometry
- Mouse breeding and maintenance
- Perinatal and chronic exposure experiments
- Various mouse injection and collection techniques (oral gavage, intraperitoneal, subcutaneous, saphenous vein, tail vein)
- Isolation of mouse tissues and cells for gene expression, flow cytometry, and other techniques
- Microdissections of primordial germ cells (PGCs) from e13.5 mouse embryos
- Ex vivo assays using primary hepatocytes, splenocytes, and blood
- Cell culture of established cell lines and primary mouse cells
- Microbiome transplant experiments in mice using fecal material and bacteria isolates
- 16S rRNA sequencing analysis using QIIME
- RNA-seq analysis
- Experience in sequencing bioinformatics (R/Rstudio, HPC-cluster) and analysis

Independent Undergraduate Research 1/2012-9/2013
California State University, Fresno
Department of Chemistry
Dr. Joy Goto Laboratory
The effects of BOAA on the viability and locomotory behaviors of Drosophila melanogaster
- Use of *Drosophila* model for toxicity studies
- Perform locomotor ability assays after exposure to various neurotoxins
- Perform behavioral studies on decapitated flies given BOAA and control compounds

Stanford Summer Research Program (SSRP) 6/2012-8/2012
Stanford University School of Medicine
Department of Neurology
Dr. Marion Buckwalter Laboratory
Impaired astrocytic TGF-β signaling leads to neuronal damage in mice infected with Toxoplasma gondii
- Prepared mouse brain tissue samples
- Performed immunohistochemistry on free floating brain sections
- Light microscopy
- Quantified areas of neuronal death (ImageJ)

NASA Reduced Gravity Student Flight Opportunities Program 10/2010-1/2012
California State University, Fresno (preliminary experiments & post-flight data processing)
NASA Johnson Space Center & Ellington Field, Houston, TX (in-flight experiment)
The formation of kidney stone-like calcium oxalate crystals in microgravity
- Designed the syringe apparatus to contain the reaction during the microgravity flight
- Determined and formulated the solutions used for the reaction
- Trained other groups members on how to operate the syringe apparatus
- Conducted the experiment while in microgravity (NASA, Houston, TX)
- Collected and processed experimental crystal samples
- Used Scanning Electron Microscope and compound microscope to analyze crystals
- Performed several outreach presentations to several schools in the Central Valley, CA

PUBLICATIONS

Egusquiza, Riann J., et al. Altered metabolism of PCB-153 leads to increased oxidative stress and hemolytic anemia in mice lacking the Steroid and Xenobiotic Receptor, SXR/PXR. Manuscript submitted for publication. (2019).

Cekanaviciute, E., Dietrich, H.K, Axtell, R.C., Williams, A.M., **Egusquiza, R.**, Wai, K.M., Koshy, A.A. and Buckwalter, M.S. Astrocytic TGFβ signaling limits inflammation and reduces neuronal damage during toxoplasma infection of the CNS, *Journal of Immunology* (2014), 193(1):139-49

Egusquiza, Riann J., et al. Calcium Oxalate Crystal Formation in Various Gravity Environments. *Gravitational and Space Research* (2014), 2(2)

SCHOLARSHIPS, GRANTS & FELLOWSHIPS

PhRMA Foundation
- 2018 PhRMA Pre-doctoral Fellowship, Pharmacology & Toxicology

Gordon Research Conference
- 2018 Carl Storm Underrepresented Minority Fellowship

National Institute of Environmental Health Sciences (NIEHS)
- Diversity Supplement (2015-2017)

University of California, Irvine
- Graduate Opportunity Fellowship (2013-2017)

California State University, Fresno
- Paul Sergi Memorial Scholarship (2013)
- Undergraduate Research Grant, *Division of Undergraduate Studies,* (2011-2012, 2012-2013). Provided to fund my independent research project.
- rGrant, *Associated Students Inc.*, (2012) Provided to fund my independent study project.
- William and Susan Furze Scholarship (2012)
- J Eckle Starnes Scholarship, (2008-2009, 2011, 2012). Given to one Sanger High School graduate every year
- Professor Kenneth Chan Memorial Scholarship, *Department of Chemistry.* (2010-2011). Given to a freshman or sophomore chemistry major that shows strong promise in the field of chemistry research (1 of 2 recipients).
- Harry L Bahr Engineering Scholarship, (2008-2009). Given to undergraduates in the School of Engineering.

AWARDS

Amgen Scholar Foundation
- Spring 2018 Amgen Scholar Alumni Travel Award

University of California, Irvine
- Spring 2018 Associated Graduate Student Travel Award
- 2018 Pharmaceutical Sciences Department Travel Award
- 2015 NSF GSRP Honorable Mention
- 2013-2014 Amgen Scholar Award, 1 of 2 awardees

California State University, Fresno
- 2013 Chemistry Student of the Year
- Dean's List (5 semesters)
- President's List (4 semesters)
- Chemistry Honor's Program- One of three undergraduates accepted for the Fall of 2011

PRESENTATIONS

Environmental Endocrine Disruptors Gordon Research Conference (GRC)
Les Diableretes, Switzerland
June 3-8, 2018
Poster Presentation: Exposure to PCB-153 induces oxidative stress during in SXR knockout mice resulting in anemia and tumor development
Selected for poster preview talk

Environmental Endocrine Disruptors Gordon Research Seminar (GRS)
Les Diableretes, Switzerland
June 2-3, 2018
Oral Presentation: Exposure to PCB-153 induces oxidative stress during in SXR knockout mice resulting in anemia and tumor development

PPTOX IV
Torshavn, Faroe Islands
May 27-30, 2018
Poster Presentation: *In utero* and chronic exposure to PCB-153 induces oxidative stress in SXR knockout mice resulting in anemia and tumor development

Cancer Research in Progress
University of California, Irvine
November 15, 2015
Oral Presentation: The Role of the Steroid and Xenobiotic Receptor (SXR) in Inflammation and Lymphoma

Cancer Biology/Immunology Poster Session
University of California, Irvine
April 1, 2015
Poster Presentation: Investigating the role of diet and intestinal barrier function in the development of B-1a cell lymphoma induced by loss of the Steroid and Xenobiotic Receptor

Central California Research Symposium (CCRS)
California State University, Fresno
April 25, 2013
Oral Presentation: The effects of β-N-oxalylamino-L-alanine (BOAA) on the locomotory behavior of *Drosophila melanogaster*

245th American Chemical Society National Meeting
New Orleans, LA
April 7-11, 2013
Poster Presentation: Effects of β-N-oxalylamino-L-alanine (BOAA) on the viability and locomotory behavior of *Drosophila melanogaster*

California State University Program for Education and Research in Biotechnology (CSUPERB)

Anaheim, CA
January 3-5, 2013
Poster Presentation: The effects of β-N-oxalylamino-L-alanine (BOAA) on the locomotory behavior of *Drosophila melanogaster*

Annual Biomedical Research Conference for Minority Students (ABRCMS)
San Jose, CA
November 7-11, 2012
Travel Award Scholar
Poster Presentation: Impaired astrocytic TGF-β signaling leads to neuronal damage in mice infected with *Toxoplasma gondii*

Stanford Summer Research Program Symposium
Stanford University
August 22-23, 2012
Poster and Oral Presentation: Impaired astrocytic TGF-β signaling leads to neuronal damage in mice infected with *Toxoplasma gondii*

Central California Research Symposium (CCRS)
California State University, Fresno
April 13, 2012
Poster Presentation: The effects of β-N-oxalylamino-L-alanine on the viability and locomotory behavior of *Drosophila melanogaster*

California State University Program for Education and Research in Biotechnology (CSUPERB)
Santa Clara, CA
January 5-7, 2012
Poster Presentation: The formation of kidney stone-like calcium oxalate crystals in microgravity

TEACHING EXPERIENCE

University of California, Irvine- Department of Developmental and Cell Biology
Teaching Assistant, Genomics, Development, and Medicine (Bio Sci D145)
Winter Quarter 2017-2019

University of California, Irvine- Department of Chemistry
Teaching Assistant, General Chemistry Lab (Chemistry 1LC)
Spring Quarter 2014

MENTORING EXPERIENCE

- Hailey Brit Wheeler, undergraduate, January 2019- current
- Anastasya Melnikova, undergraduate, January 2019- current
- Nicole Balian, high school student, June 2018-May 2019, UCI Cancer Center Summer Youth Program 2018

- Kaelen Kay, undergraduate, March 2018- June 2019. Selected for UCI Summer Undergraduate Research Program (SURP). Earned Excellence in Research 2019.
- Maria Ambrosio, undergraduate, October 2017- June 2019. Earned Excellence in Research 2019.
- Sigal Wilner, Junior Specialist, December 2016- July 2018
- Gin Wang, high school student, September 2016-July 2018, UCI Cancer Center Youth Program 2017
- Xiao Li, undergraduate, June 2016-June 2017. Earned Excellence in Research.
- Grace Park, high school student, June 2016-August 2016, UCI Cancer Center Youth Program 2016
- Sohee Chung, undergraduate, September 2015- June 2017. Earned Excellence in Research 2017.
- Tejal Gala, high school student, June 2015- August 2015, UCI Cancer Center Youth Program 2015
- Samantha Reshel, PhD rotation student, January 2015-March 2015
- Mary Sargious, undergraduate, October 2014- October 2015

RELEVANT WORK EXPERIENCE

Creative Marketing and Research Fresno, CA 8/2010-7/2013
Laboratory Technician

Bureau of Reclamation Fresno, CA 2/2010-7/2013
Hydrologic Technician/Data input

ABSTRACT OF THE DISSERTATION

Interactions among the Steroid and Xenobiotic Receptor (SXR/PXR), environmental toxicants and the gut microbiome and their effects on inflammation, oxidative stress, and cancer

By

Riann Jenay Egusquiza

Doctor of Philosophy in Pharmacological Sciences
with a concentration in Pharmaceutical Sciences

University of California, Irvine, 2019

Professor Bruce Blumberg, Chair

The Steroid and Xenobiotic Receptor (SXR/PXR) is a nuclear receptor that regulates inducible xenobiotic metabolism. SXR is also implicated in other processes and perturbing its function can lead to adverse health consequences. The work described here investigates connections between SXR and adverse health consequences induced by the gut microbiome and xenobiotic chemicals.

The B-1a B cell lymphoma phenotype previously reported in SXRKO mice was lost following a change in the diet; it was not recovered after returning to the previous diet (**Chapter 1**), suggesting the microbiome may be involved. The studies in **Chapter 2** characterized the results of a fecal microbiome transplant from a mouse with a phenotype resembling the B-1a B cell lymphoma into wild-type and SXRKO mice. This transplant did not lead to B-1a B cell lymphoma in SXRKO mice. However, gene expression analysis revealed that SXRKO mice resisted some changes in gene expression induced by the gut microbiome, likely attributable to elevated intestinal inflammation. **Chapter 3** investigated differences between the microbiomes

in current and archival samples with and without tumors and revealed *Akkermansia sp*. and *Prevotella sp.* as candidate microbes linked to lymphoma in SXRKO mice. Expansion of these microbes in the gut increased the number of B-1a B cells in the peritoneal cavity of SXRKO mice and revealed differences in microbiome-induced gene expression changes between wild-type and SXRKO mice. These studies established SXR as a potential bridge between the gut microbiome and adverse impacts on the host.

Chapter 4 explored the role of SXR during exposure to the environmental toxicant PCB-153, revealing that SXRKO mice developed hemolytic anemia, increased oxidative stress and accumulation of hydroxylated metabolites. **Chapter 5** revealed that wild-type and SXRKO mice did not respond differently to oxidative stress or anemia induced by phenylhydrazine. These findings demonstrated that SXR is protective against xenobiotic-induced oxidative stress and the associated health consequences, due to its role in the metabolism and/or clearance of toxic metabolites.

The gut microbiome and oxidative stress both have large impacts on health. Taken together, these results demonstrate a protective role of SXR in these processes and the corresponding adverse health consequences.

INTRODUCTION

Nuclear receptors

Nuclear receptors are ligand-modulated transcription factors that regulate expression of specific genes in response to a broad spectrum of ligands, including hormones, biological metabolites, and xenobiotic chemicals[1, 2]. These receptors have shown to interact with each other and with other proteins to regulate genes involved in development, homeostasis, and metabolism[3, 4]. Biological and chemical interactions with these receptors can have significant effects on these processes.

Steroid and Xenobiotic Receptor, SXR/PXR

The steroid and xenobiotic receptor (SXR), also known as the pregnane X receptor (PXR) and formally known as NR1I2, is a nuclear receptor that is expressed at high levels in the liver and intestine and at lower, but detectable, levels in most other tissues[5, 6]. Ligands for this receptor are diverse and include hormones, bile acids, natural products, pharmaceutical drugs, and xenobiotic chemical toxicants[7, 8]. Upon ligand binding, SXR can induce the transcription of all three phases of xenobiotic metabolizing enzymes: phase I enzymes such as cytochrome P450 (CYP3A) genes, phase II conjugating enzymes such as glutathione S-transferase (GST), and phase III ABC drug transporters[6, 9, 10]. Therefore, SXR functions as a molecular sensor for a broad spectrum of ligands to regulate the metabolism and clearance of endogenous and xenobiotic chemicals. As predicted, SXR loss-of-function studies have demonstrated perturbed xenobiotic metabolism and confirmed the important role of SXR in the appropriate metabolism of these compounds[11, 12]. The

many functions of SXR in xenobiotic metabolism and clearance, and its ability to regulate expression of Cyp3A genes, which are activated by over 50% of pharmaceuticals[13], has guided the majority of research on SXR towards drug-drug interactions. However, many studies have demonstrated additional functions of SXR beyond xenobiotic metabolism, including roles in inflammation, lipid and glucose metabolism, atherosclerosis, and immune dysfunctions[5, 14-18]. These studies not only prove that SXR has other important physiological functions, but it also implicates SXR as a link between xenobiotic chemicals and physiological alterations to these other pathways.

SXR and inflammation

SXR engages in a mutually inhibitory interaction with nuclear factor kappa B (NF-κB), a master regulator of inflammation and a transcription factor that is involved in multiple cellular pathways[15, 19, 20]. Activation of one pathway led to inhibition of the other, and genetic knockdown of SXR resulted in elevated activity of NF-κB[15]. SXR null (SXRKO) mice displayed elevated expression of inflammatory cytokines in the liver and intestine, and histological and physiological evidence of intestinal inflammation[15, 21]. SXR has also been implicated in various inflammatory conditions, including inflammatory bowel disease (IBD)[22], non-alcoholic fatty liver disease (NAFLD)[23], and even cancer[14, 24].

B-1a B cell lymphoma in SXR-knockout mice

The pro-inflammatory environment of SXRKO mice was demonstrated to progress into tumors in multiple tissues accompanied by large increases in B-1a B cells in the blood, peritoneal cavity, and spleen, characteristic of B-1a B cell lymphoma[5]. This expansion of B-1a B lymphocytes in

SXRKO mice was not fully characterized, but was shown to occur in part due to increased NF-κB signaling[5]. These results established SXR as a tumor suppressor in B-1a B cells, and provided a possible link between xenobiotic chemicals and B-1a B cell lymphomagenesis. **Chapter 1** of this dissertation describes the discovery that this lymphoma phenotype disappeared in our colony of SXRKO mice after a change in the diet and the investigations that lead to the hypothesis that the gut microbiome impacts the development of B-1a B cell lymphoma in SXRKO mice.

SXR and the gut microbiome

The gut microbiome is the community of microorganism present in the gut that aids in metabolism and providing protection against intestinal pathogens. The microbiome can impact various metabolic processes and host immunity and, therefore, has the capability to directly or indirectly impact almost every physiological function in the host[25]. Perturbations to the gut microbiome can have extensive impacts on health and were shown to be associated with disease states, such as obesity and inflammatory bowel disease (IBD)[26-28]. Many xenobiotics and dietary factors produce significant impacts on the gut microbiome. Statins induce microbiota dysbiosis through a SXR-dependent mechanism[29]. It was also demonstrated that a bacterial metabolite, indole 3-propionic acid (IPA), interacted with SXR to regulate intestinal permeability[21]. These studies demonstrated that SXR interacts with the gut microbiome and are consistent with the possibility that these interactions could lead to the consequences associated with dysbiosis of the gut microbiome. **Chapters 2-3** of this dissertation describe the investigations into the impact of the gut microbiome on the development of the B-1a B cell lymphoma phenotype in SXRKO mice and reveal new functions for SXR in gut microbiome-induced changes to the host.

Interactions among SXR, polychlorinated biphenyls, and other environmental toxicants

Polychlorinated biphenyls (PCBs) are a class of environmental contaminants formerly widely used in various industrial products, including plastics, adhesives, and electrical equipment[30]. Continued production of these chemicals was banned in the late 1970's due to evidence of various harmful effects to human health associated with exposure[31]. Many PCBs interact with SXR, demonstrating both activation and inhibition[7, 32-34]. Other environmental toxicants, such as polybrominated diphenyl ethers (PBDEs), that demonstrate similar toxic effects also interact with SXR[35, 36]. Therefore, SXR serves a possible mechanistic bridge between exposure to these harmful toxicants and the resulting adverse consequences. **Chapter 4** of this dissertation discusses the discovery that SXRKO mice developed oxidative stress and hemolytic anemia with exposure to PCB-153, as a result of altered xenobiotic metabolism leading to increased accumulation of toxic metabolites.

Xenobiotic-induced oxidative stress and hemolytic anemia

Many xenobiotic compounds and their metabolites were shown to induce oxidative stress, and thus, promote adverse consequences[37-39]. Oxidative stress induced by some xenobiotics can lead to the premature lysis of red blood cells, or hemolytic anemia[40, 41]. Other xenobiotics, such as primaquine, require biological activation into a toxic metabolite to induce the oxidative stress and hemolytic properties[40]. SXR regulates inducible xenobiotic metabolism and thus can regulate both the production and clearance of xenobiotic metabolites. The roles of SXR in xenobiotic-induced oxidative stress, and in the associated physiological consequences, such as hemolytic anemia, have not yet been deeply studied. **Chapter 4** demonstrates that SXR plays a protective role against the oxidative stress induced by PCB-153 metabolites. **Chapter 5** demonstrates that

SXR does not have a protective role against phenylhydrazine-induced oxidative stress and hemolytic anemia. These results together reveal that SXR has a protective role against xenobiotic-induced oxidative stress, but it likely applies only to xenobiotics that require biological activation to induce toxicity.

Human relevance of SXR loss-of-function

There are currently 9,451 reported single nucleotide polymorphisms (SNPs) of human SXR in the NCBI dbSNP, many of which can impact the expression of SXR itself and/or that of its target genes[42, 43]. In addition, polymorphisms in human SXR were linked to multiple functional consequences, including altered metabolism, increased inflammation, and susceptibility to disease[44-46]. Pharmaceutical research aims to target inhibition of SXR to reduce drug-drug interactions that can lead to decreased drug efficacy and increased drug toxicity[47-49]. More investigation into the consequences of SXR inhibition or loss-of-function should be conducted before it is targeted in human health.

This study

The work described in this dissertation investigates the connections between SXR and adverse health consequences induced by the gut microbiome (Part I, Chapters 1-3) and xenobiotic chemicals (Part II, Chapters 4-5). **Chapter 1** describes the discovery that the B-1a B cell lymphoma phenotype present in our SXRKO mouse colony for more than 10 years was lost following a change in the diet and was not recovered after a switch back to the previous diet. This led me to hypothesize that the gut microbiome impacted the development of the lymphoma phenotype of SXRKO mice. **Chapter 2** describes attempts to recover the lymphoma phenotype

in SXRKO mice via fecal microbiome transplant from a mouse with a phenotype resembling the previous B-1a B cell lymphoma. **Chapter 3** describes investigations into the differences in the gut microbiome between SXRKO mice that displayed the B-1a B cell lymphoma phenotype and those that did not and the results of expanding the abundance of candidate microbes in the gut on the phenotype of SXRKO mice. **Chapter 4** describes the discovery of oxidative stress and hemolytic anemia in SXRKO mice following exposure to the environmental toxicant, PCB-153, and the accumulation of hydroxylated PCB-153 metabolites due to an altered metabolism profile. **Chapter 5** describes the investigation into the impact of a known inducer of oxidative stress and hemolytic anemia, phenylhydrazine, between wild-type and SXRKO mice. The chapters in Part I demonstrate that the gut microbiome and SXR interact and can impact the host, but did not demonstrate that the gut microbiome induces the B-1a B cell lymphoma phenotype of SXRKO mice. The chapters of Part II demonstrate that SXR has an important role in the metabolism and clearance of toxic xenobiotic metabolites that are capable of inducing oxidative stress and hemolytic anemia. Overall, these studies revealed that SXR loss-of-function has adverse health consequences that can be induced or impacted by the gut microbiome and xenobiotics, suggesting that pharmacological inhibition of SXR may have more risk than benefit and that human containing some SXR SNPs may be more susceptible to adverse effects associated with gut microbiome dysbiosis and certain xenobiotics.

CHAPTER 1

Diet has an indirect role on the B-1a B cell lymphoma phenotype of mice lacking the Steroid and Xenobiotic Receptor (SXR/PXR)

Summary

The Steroid and Xenobiotic Receptor (SXR/PXR) is a nuclear hormone receptor expressed highly in the liver and intestine where, upon activation by xenobiotics, it induces transcription of genes involved in all three phases of xenobiotic metabolism. SXR also engages in a mutually inhibitory relationship with NF-κB, a major regulator of inflammation, providing additional roles of SXR outside of xenobiotic metabolism. Casey et al. discovered that the pro-inflammatory environment of SXR knockout (SXRKO) mice led to the development of a B-1a B cell lymphoma phenotype, characterized by splenomegaly, elevated percentages of B-1a B cells in the blood, spleen, and peritoneal cavity, and lymphatic tumors in multiple tissues. In this study, we discovered that this B-1a B cell lymphoma phenotype was lost following a switch in diet, from a non-irradiated to irradiated rodent chow, in the SXRKO mouse colony. We conducted experiments to test whether the phenotype of SXRKO mice was dependent on the diet. Wild-type (WT) and SXRKO mice were either continued on the current irradiated diet or switched to the previous non-irradiated diet. These mice were also bred to generate an F1 generation exposed to each diet throughout development. Both the F0 and F1 generations were investigated for signs of B-1a B cell lymphoma at either 6 or 8 months of age. Switching the diet back to the previous non-irradiated chow did not restore the lymphoma phenotype, as determined by the percentage of B-1a B cells present in the spleen and peritoneal cavity and absence of tumors. However, there

was one F1 SXRKO mouse on the non-irradiated diet that displayed a pre-lymphoma phenotype, characterized by a large increase in the percentage of B-1a B cells in both the spleen and peritoneal cavity. 16S rRNA microbiome sequencing analysis revealed that the two diets did not result in many alterations to the gut microbiome. However, we found that the microbiome of the pre-lymphoma SXRKO mice appeared to be different, suggesting that the microbiome may be playing a role in the development of B-1a B cell lymphoma in SXRKO mice. Therefore, we hypothesize that the initial change in diet altered the gut microbiome of our SXRKO mouse colony leading to the loss of the phenotype. We infer that the previous non-irradiated diet is preferential to the bacteria that are important for the phenotype, since the switch to an irradiated diet eliminated the phenotype and because the one pre-lymphoma SXRKO mouse was maintained on the non-irradiated diet. Our results indicate that the diet may not play a direct role on the development of B-1a B cell lymphoma in SXRKO mice, but rather that the microbiome could potentially be having an impact. The microbiome obtained from the pre-lymphoma mouse provided us with the material needed to test this hypothesis, which is discussed in **Chapter 2** of this dissertation.

Introduction

The steroid and xenobiotic receptor (SXR/PXR), formally known as NR1I2, is a nuclear hormone receptor activated by a diverse array of chemicals, including xenobiotic compounds, pharmaceutical drugs, vitamins, hormones, and natural products[6, 50]. SXR is expressed highly in the liver and intestine where it heterodimerizes with the retinoid X receptor (RXR), and induces transcription of enzymes responsible for xenobiotic and hormone metabolism[50, 51]. These target genes include enzymes involved in all three phases of xenobiotic and drug metabolism, such as phase I cytochrome P450 (CYP3A) genes, phase II conjugating enzymes such as glutathione S-transferase (GST), and phase III ABC drug transporters[10, 52]. SXR null (SXRKO) mice display defects in inducible xenobiotic metabolism, making them hypersensitive to the effects of certain xenobiotics[12, 52]. In addition, constitutive activation of SXR leads to increased protection against these same xenobiotics[12].

SXR/PXR has been shown to engage in a mutually inhibitory interaction with nuclear factor kappa B (NF-κB), a master regulator of inflammation and a transcription factor that is involved in multiple cellular pathways[20, 53]. Activation of SXR results in NF-κB repression, and conversely, pharmaceutical activation of NF-κB leads to inhibited SXR activity[20, 53]. In addition, SXRKO mice display elevated mRNA levels of various inflammatory cytokines in the liver and intestine and histological evidence of acute inflammation, particularly in the intestine[53]. This interaction with NF-κB is responsible for additional physiologic functions of SXR/PXR that are independent of metabolism and provides a connection between xenobiotics and the immune system.

This pro-inflammatory environment of SXRKO mice was shown to progress to a B-1a B cell lymphoma with age, characterized by high increases in B-1a B cell content in the spleen,

peritoneal cavity, and blood, and the development of lymphatic tumors in multiple tissues[5]. How the acute inflammation progresses into B-1a B cell lymphoma in SXRKO mice is not known, but would provide extremely valuable information on how immune cancers and autoimmune diseases develop.

Diet and nutrition are factors that are long known to impact health[54]. Many natural products and vitamins interact with SXR/PXR. For example, both Vitamin E and K are activators of SXR[55, 56]. Natural products, such as St. John's Wart, also activate SXR[8]. In addition, dietary phytochemicals, or chemicals produced by plants, have been demonstrated to activate SXR and induce up-regulation of its target genes[57]. The results of these studies suggest that diet may modulate SXR activity. Therefore, it is possible that some dietary components can have differential effects on the host depending on whether they modulate SXR activity.

Diet is also a major factor that affects the gut microbiome - the community of microorganisms present in our gut[58]. The gut microbiome has recently been shown to induce large differences on host health and even to impact the development of certain phenotypes in mouse models[25, 59-63]. SXR has been demonstrated to interact with gut microbial metabolites to regulate intestinal permeability[21]. In addition, statin treatment was shown to cause gut dysbiosis, or an overall disruption to the gut microbiome, in mice via a SXR-dependent mechanism[29]. These data suggest that SXR can induce changes to the host physiology and health through direct and indirect interactions with the gut microbiome.

The mutually inhibitory relationship between SXR and NF-κB also provides mechanisms that may impact the interaction between the diet and host, especially since SXR is highly expressed in the intestines. In addition, SXR has been implicated in inflammatory gut conditions in both humans and in rodent models, which have also been associated with alternations to the

gut microbiome[45, 64]. Therefore, this connection to intestinal inflammation could implicate SXR in changes to the gut microbiome and the disease outcomes related to alterations to the gut microbiome.

The studies in this chapter discuss the various experiments to test the impact of the diet on the development of the lymphoma phenotype s of the B-1a B cell lymphoma phenotype of SXRKO mice following a change in the diet, and the characterization of a single SXRKO mouse displaying a B-1a B cell lymphoma-like phenotype and a distinct gut microbiota. Our results demonstrated that diet does not have a direct impact on the development of lymphoma in SXRKO mice, but are consistent with the possibility that alterations in the gut microbiome that are induced by dietary changes may be having an impact on the development of lymphoma.

Materials and Methods

Mouse maintenance: Wild-type and SXRKO animals were identically raised and housed at the University of California, Irvine on a standard diet. SXRKO mice were descendants of a gift from the Salk Institute; all other animals were descendants of 129S6/SvEv mice purchased from Taconic Biosciences (Germantown, NY). Mice were maintained on either the irradiated PicoLab Rodent Diet 20/5053 (LabDiet) or non-irradiated ProLab RMH 2500/5P14 (LabDiet) for all diet experiments as noted. Mice were housed in micro-isolator cages in a temperature-controlled room (25–28°C) with a 12-h light/dark cycle. Water and food were provided ad libitum. Animals experiments were carried out in accordance with the Institutional Animal Care and Use Committee at the University of California, Irvine, and were consistent with Federal guidelines.

Diet Experiments: 6-8 week old wild-type and SXRKO mice were either continued on the 5053 irradiated rodent chow or were switched to the 5P14 non-irradiated rodent chow. The blood of these mice was monitored monthly for blood B-1a B cell content. The B-1a B cell content of the spleen and peritoneal cavity were analyzed after euthanasia at 6 months of age. A subset of these mice was used to generate a F1 generation exposed to the diet during development. The F1 mice were euthanized at either 6 or 8 months of age to investigate the B-1a B cell content of the spleen and peritoneal cavity.

Blood collection: Approximately 50 µL of whole blood was collected from the saphenous vein of the mice using heparinized capillary tubes. Red blood cells (RBCs) were lysed by incubating cell suspension in ACK lysis buffer (150 mM NH4Cl, 10 mM KHCO3, 0.1 mM Na2EDTA) for 5 min. RBC-depleted blood cells were washed and resuspended in FACS buffer (PBS, 1% FBS, 0.02% sodium azide) at 400K cells/mL for antibody staining and flow cytometric analysis.

Peritoneal cavity lavage: Mice were euthanized by isoflurane overdose. Whole blood was collected by cardiac puncture. The skin was carefully cut to reveal the peritoneum without puncturing or nicking it. 9 mL of ice cold FACS buffer was injected into the peritoneum, avoiding injecting organs. The filled peritoneum was then physically agitated to dislodge any cells, then a syringe and 25-gauge needle were used to extract most of the peritoneal fluid. A pipet was then used to extract the small amount of remaining liquid from the peritoneum. RBCs were lysed by incubating cell suspension in ACK lysis buffer (150 mM NH4Cl, 10 mM KHCO3, 0.1 mM Na2EDTA) for 5 min. RBC-depleted cells were washed and resuspended in FACS buffer (PBS, 1% FBS, 0.02% sodium azide) for antibody staining and flow cytometric analysis.

Tissue collection: Liver, small intestine, colon, caecum, and spleen tissue were dissected, flash frozen in liquid N_2 and stored at -80˚C. A section of the spleen was set aside before flash freezing to undergo splenocyte isolation.

Spleen cell isolation: Spleen sections were physically dissociated using a petri dish and syringe plunger in 1 mL of ice-cold PBS containing 1% FBS. RBCs were lysed by incubating cell suspension in ACK lysis buffer (150 mM NH4Cl, 10 mM KHCO3, 0.1 mM Na2EDTA) for 5 min. RBC-depleted splenocytes were washed, resuspended in FACS buffer (PBS, 1% FBS, 0.02% sodium azide), and filtered through a 100 µm cell strainer to yield single cells for antibody staining and flow cytometric analysis.

Flow cytometry (FACS) analysis: RBC-depleted spleen, peritoneal cavity, and blood cells were diluted into aliquots of 200K cells, stained with an antibody cocktail of anti-mouse CD5-APC (eBioscience), CD19-PE (eBioscience), and IgD-FITC (eBioscience) for 30 min, washed with cold FACS buffer (PBS, 1% FBS, 0.02% sodium azide), and fixed with 1% paraformaldehyde.

Cells were measured on a BD LSR II cytometer. Data was analyzed using FlowJo software (Treestar).

Fecal sample collection and analysis: Fecal samples were collected from all mice, flash frozen, and stored at -80˚C. Fecal DNA was extracted using the PowerFecal DNA kit (MO BIO/Qiagen) according to manufacturer's protocol.

16s rRNA sequencing: microbial DNA was amplified for the V3-V4 variable regions of the 16S rRNA gene. DNA libraries were prepared by the UCI Genomics High Throughput Facility following the Illumina protocol for 16S rRNA metagenomic sequencing library preparation. 16S rRNA sequencing was performed on Illumina MiSeq with 2x300bp paired-end reads at the Institute for Integrative Genome Biology at the University of California, Riverside. Fastq files were processed using QIIME[65].

QIIME microbiome sequencing analysis

Paired-end reads were joined using the fastq-join function. Joined files were then quality filtered and merged into one data file with each sample labeled by the file name using the multiple_split_libraries_fastq.py function. The seqs.fna file from the previous command was then filtered to remove any chimeric sequences using Usearch6.1[66], installed within QIIME. Chimeric sequencing were identified using the identify_chimeric_seqs.py and the recent Greengenes reference sequence file (gg_13_8_otus.fasta)[67]. The discovered chimeric sequences were then removed from the seqs.fna file using the filter_fasta.py command. The chimeras.txt file obtained from the previous command and the added parameter of "-n". OTU picking was then conducted on the newly filtered sequencing file using the pick_de_novo_otus.py command using Usearch6.1 as the OTU picking method and Uclust for assigning taxonomy to the OTUs[68]. This step was conducted on the UCI high performance computer (HPC) cluster. Taxonomy

assignments were summarized into a readable format using the summarize_taxa_through_plots.py and the otu_table.biom file generated in the previous command. Visualizations and statistical analyses were conducted using Calypso[69]. QIIME script is available in Figure 1.8.

RNA isolation: Frozen tissue sections were homogenized rapidly in 1 mL of Trizol reagent (ThermoFisher Scientific). RNA was isolated from the tissue-Trizol homogenate by phenol/chloroform extraction. RNA was precipitated with an equal volume of 100% isopropanol, centrifuged and salt removed by washing with 70% ethanol. Final RNA product was resuspended in DNase/RNase-free sterile, ultrapure water (ultrafiltered, UV sterilized water from Barnstead Nanopure water system, hereafter called nanopure water), quantified by spectrophotometry, and integrity verified by denaturing agarose gel electrophoresis.

cDNA synthesis: cDNA was made using 2 µg of intact total RNA and Superscript III reverse transcriptase (Applied Bioscience) according to manufacturer's protocol. Synthesized cDNA was diluted 5-fold with nanopure water for downstream qPCR analysis.

Designing qPCR primers: Gene sequences were obtained from Ensembl genome browser. PerlPrimer was used to design and identify candidate forward and reverse primers. Primer oligos were ordered from Sigma-Aldrich and resuspended in 10 mM Tris pH 8.0, 0.1 mM EDTA buffer. Primer sequences are listed in Table 1.1.

Quantitative real time reverse transcriptase PCR (qPCR): Diluted cDNA was combined with SYBR green qPCR Master Mix (Applied Biosystems) and the primer mix for gene of interest then run on the Roche LightCycler 480. Technical replicate Ct values were averaged for each biological replicate. Mean Ct values were normalized to 36B4/Rplp0 (ΔCt), and relative fold

change mRNA levels were then calculated by using ΔΔCt method[70] with relative gene expression presented as mean fold change over vehicle control ± SEM.

Statistical analysis: Data visualization and statistical analyses were conducted in Prism 8 (GraphPad Software). Thirteen to twenty biological replicates were used all diet experiments and down-stream flow cytometry and qPCR mRNA expression analyses. Unpaired t-test was used to determine statistical significance. * = p-value <0.05, ** = p-value <0.01, ***= p-value <0.001, #= p-value <0.0001

Results

Loss of B-1a B cell lymphoma phenotype in SXR knockout mice following a change in diet

Analysis of the spleen and peritoneal cavity of SXRKO and WT mice with ages ranging from 4-9 months of age done in the Summer of 2014 revealed that the B-1a B cell lymphoma phenotype previously reported in 2011, by Casey et al., was no longer being presented in aged SXRKO mice. This loss of phenotype was evident by the lack of increased percentage of B-1a B cells in the spleen and peritoneal cavity, splenomegaly, and splenic tumors (Figure 1.1). We confirmed that these SXRKO mice still retained the mutation in the SXR/PXR gene (Figure 1.2) and that this resulted in the loss of SXR/PXR mRNA in tissues with known expression (Figure 1.1D). The SXRKO mice still presented the elevated expression of certain inflammatory genes, such as IL-6 and IL-1β (Figure 1.1E-F), which results from increased NF-κB activity and was previously reported to be a phenotype of SXRKO mice[53]. These results demonstrated that the SXRKO mice in our colony still retained the elevated inflammatory phenotype, but that something was interfering with the development of the B-1a B cell lymphoma phenotype in aged SXRKO mice.

Analysis of our records showed that one year prior to this analysis, the rodent chow given to our SXRKO colony was changed. The colony was originally maintained on the ProLab RMH 2500/5P14 (LabDiet), and in the summer of 2013 they were switched to an irradiated equivalent diet, PicoLab Rodent Diet 20/5053 (LabDiet) by ULAR staff. These two diets have comparable profiles in terms of the composition of protein, fat, and carbohydrates, but there are differences in the some of the ingredients used between the two diets. For example, the 5P14 diet contains porcine animal fat, porcine meat meal and fish meal to contribute to the dietary proteins and fat, while the 5053 diet does not contain the porcine animal fat or meat meal. There are also differing

levels of vitamins and minerals in the two diets (Table 1.3). The most significant difference between the two diets is the fact that the 5053 is irradiated, whereas the 5P14 diet was not. Irradiation is used on laboratory rodent diets to provide reliable microbial control. However, the process of irradiation can also damage organic molecules in the diet leading to ineffective antioxidants, vitamins, and other important food components. In addition, irradiation essentially kills any present microbes in the diet, and therefore, can impact the gut microbiome of the mice consuming it. We hypothesized that this change in diet eradicated the B-1a B cell lymphoma phenotype of our SXRKO mouse colony, either through a direct interaction with a component in one of the diets, or indirectly by altering the gut microbiome.

Diet does not directly affect the development of the B-1a B cell lymphoma phenotype of SXRKO mice

To test the hypothesis that the diet directly impacted the development of the B-1a B cell lymphoma phenotype in SXRKO mice, we conducted diet exposure experiments using the current and previous diet used in our mouse colony. Wild-type and SXRKO mice were either continued on the 5053 (irradiated) or switched to the 5P14 (non-irradiated) rodent chow starting at 6 weeks of age. The mice were maintained on the experimental diets until 6 months of age, when they were dissected and investigated for signs of B-1a B cell lymphoma. The endpoint of 6 months of age was chosen based on the original report that the lymphoma phenotype was present in 6 month old SXRKO mice[5]. Three independent diet studies conclusively showed that the switch back to the non-irradiated 5P14 diet was not sufficient to restore the B-1a B cell lymphoma phenotype in SXRKO mice, evident by the lack of increase of B-1a B cells in the spleen and peritoneal cavity determine by flow cytometry analysis (Figure 1.3). A subset of these diet experiment mice was used for breeding purposes to generate an F1 population that had been

exposed to the experimental diet throughout development to test whether exposure to the diet during early development was important. The F1 generation mice were continued on the experimental diet throughout lifespan and were sacrificed at two different time points: 6 months and 8 months of age. We extended the dissection age for a subset of animals in case the development of lymphoma was occurring later than what was previously reported. At 6 months of age, exposure starting *in utero* to the non-irradiated 5P14 diet did not return the B-1a B cell lymphoma of F1 SXRKO mice, determined by the lack of a large increase of splenic and peritoneal B-1a B cells compared to wild-type controls. The SXRKO males on the 5P14 diet had a small increase in splenic B-1a B cell percentage, but it was still not above the normal range (Figure 1.4A). SXRKO females appeared to actually have a decrease in B-1a B cell content for both tissues and both diets (Figure 1.4C-D). Monthly blood measurements did not reveal any increase in blood B-1a B cell content throughout the lifespan of these mice (Figure 1.4F-G). The F1 mice diet experiment mice also did not display B-1a B cell lymphoma at 8 months of age (Figure 1.5). However, there was one 8-month-old SXRKO female from this study on the 5P14 diet that had a large increase in the percentage of B-1a B cells in both the spleen and peritoneal cavity, characteristic of the previously reported lymphoma phenotype (Figure 1.5C-D). This mouse will be referred to as "Mouse #96" for the remainder of this dissertation.

Mouse #96, a source of microbiome study material for the lymphoma phenotype

A single F1 diet experiment female SXRKO mouse, Mouse #96, displayed a phenotype resembling the previously reported B-1a B cell lymphoma phenotype at 8 months of age. Although the switch back to the non-irradiated/5P14 diet demonstrated to not induce the lymphoma phenotype, we asked if the microbiome of Mouse #96 was different than the other diet experiment mice, which could have impacted its susceptibility to the development of the B-

1a B cell lymphoma. 16S rRNA sequencing of microbial DNA isolated from fecal samples revealed that there were little differences in the microbiome between the two diets, though there were a few significantly different changes (Figure 1.6, Table 1.2). However, the microbiome of Mouse #96 was indeed significantly different than other mice from the F1 diet experiment (Figure 1.7). Determining statistical significance of individual microbes was not possible since we only had one individual, however, we observed that certain microbes, such as *Coprobacillus* and *Prevotella*, were much more abundant in the microbiome of Mouse #96 compared to the other F1 diet experiment mice (Figure 1.7A-B). Since Mouse #96 has a phenotype resembling the B-1a B cell lymphoma phenotype and appeared to have a distinctly different microbiome than the other mice that did not display a phenotype, the microbiome from this mouse served as the study material to determine in the microbiome could impact the development of the B-1a B cell lymphoma phenotype of SXRKO mice.

Discussion

We observed complete loss of the previously observed B-1a B cell lymphoma phenotype of SXRKO following a change in the diet. Diet composition experiments were conducted to test if returning the SXRKO mice to the previous diet returned the phenotype. SXRKO mice placed on the previous 5P14 diet at 6-8 weeks of age then maintained until 6 months of age did not show an increase in B-1a B cell content in the peritoneal cavity, spleen, or blood, demonstrating that the diet did not return the lost phenotype.

The F1 SXRKO mice that had been exposed to the diet throughout development also did not have increased percentages of B-1a B cells in any tissue investigated at 6 months of age. Interestingly, a single F1 SXRKO female maintained on the previous 5P14 diet (Mouse #96) displayed a large percentage of B-1a B cells in both the spleen and peritoneal cavity at 8 months of age. These findings partly recapitulated characteristics of the previously reported B-1a B cell lymphoma phenotype. It is possible that we needed to extend the study or increase the number of generations maintained on the non-irradiated 5P14 diet in order to obtain more SXRKO mice with this phenotype.

Investigations of the microbiome of the F1 diet experiment mice using 16S rRNA sequencing revealed that the diet had little overt impact on the microbiome composition. However, it appeared that the microbiome of Mouse #96 was distinctly different as it contained increased abundance of certain microbes compared to the microbiome of other mice from the study. We hypothesize that the distinct microbiome of Mouse #96 was favorable to the development of the B-1a B cell lymphoma phenotype. Although the diet alone did not return the lymphoma phenotype, we believe that the previous diet allowed, or promoted the establishment of certain microbes that interacted with the SXRKO tissues to predispose the animals to

lymphoma. Then, changing to the irradiated 5053 diet resulted in alterations to the gut microbiome and, thus, altered the phenotype of SXRKO mice. Since Mouse #96 displayed a phenotype that resembled the B-1a B cell lymphoma phenotype and a distinctly different microbiome, it provided us with the material needed to investigate the connection between the microbiome and lymphoma phenotype in SXRKO mice.

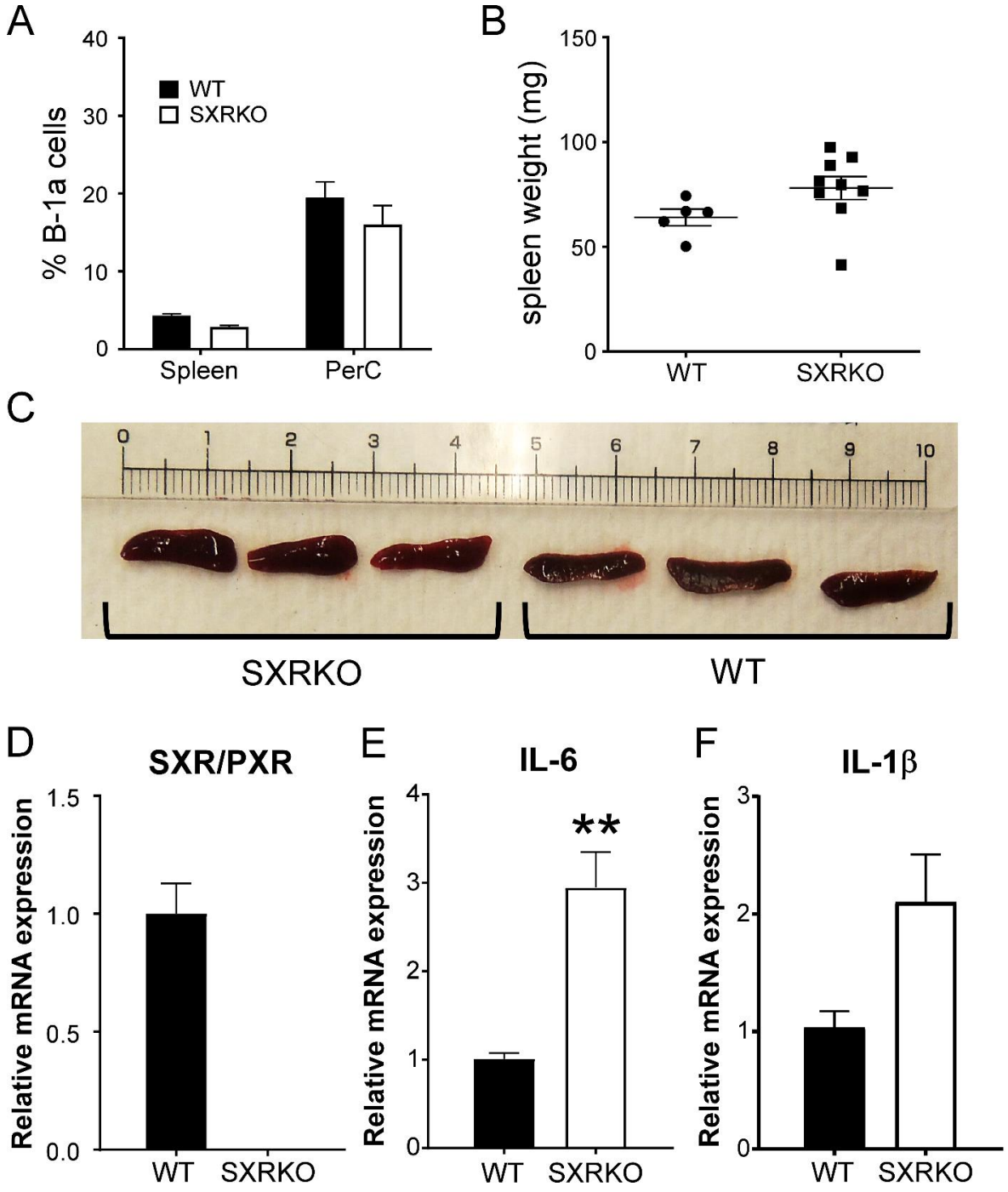

Figure 1.1 Absence of B-1a cell lymphoma phenotype in SXRKO mice one year after diet change

No change in B-1a cell content of either the spleen or peritoneal cavity (PerC) between WT and SXRKO mice, as measured by percentage of CD19+CD5+ lymphocytes determined by flow cytometry (A). SXRKO mice display slightly larger spleens by weight (B) but the spleens are not visually larger and do contain tumors (C). These SXRKO mice were confirmed to not express SXR/PXR mRNA (D). SXRKO mice retained the increased expression of certain inflammatory genes in liver, such as IL-6 (E) and IL-1β (F).

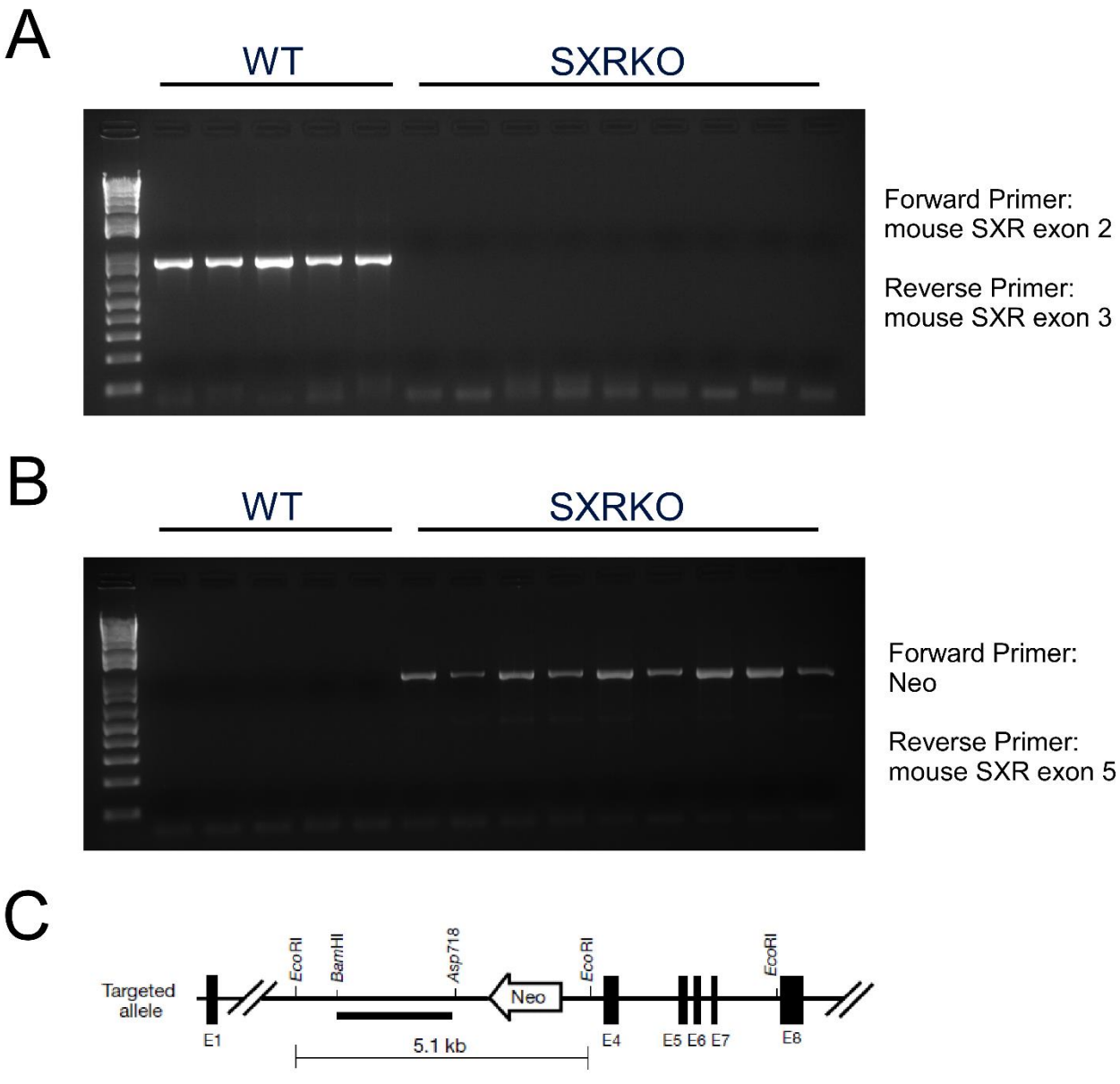

Figure 1.2: Genotypic analysis of WT and SXRKO mice not displaying B-1a cell lymphoma phenotype. PCR results of DNA from WT and SXRKO mice amplifying exon 2 and 3 of mouse SXR gene (A) and PCR results of DNA from WT and SXRKO mice targeting the Neomycin resistance gene present in the SXR gene sequence in SXRKO mice (B). Diagram of SXR gene sequence of SXRKO mice, obtained from Xie, et al. 2000, displaying location of intact exons and inserted Neomycin resistance gene (C).

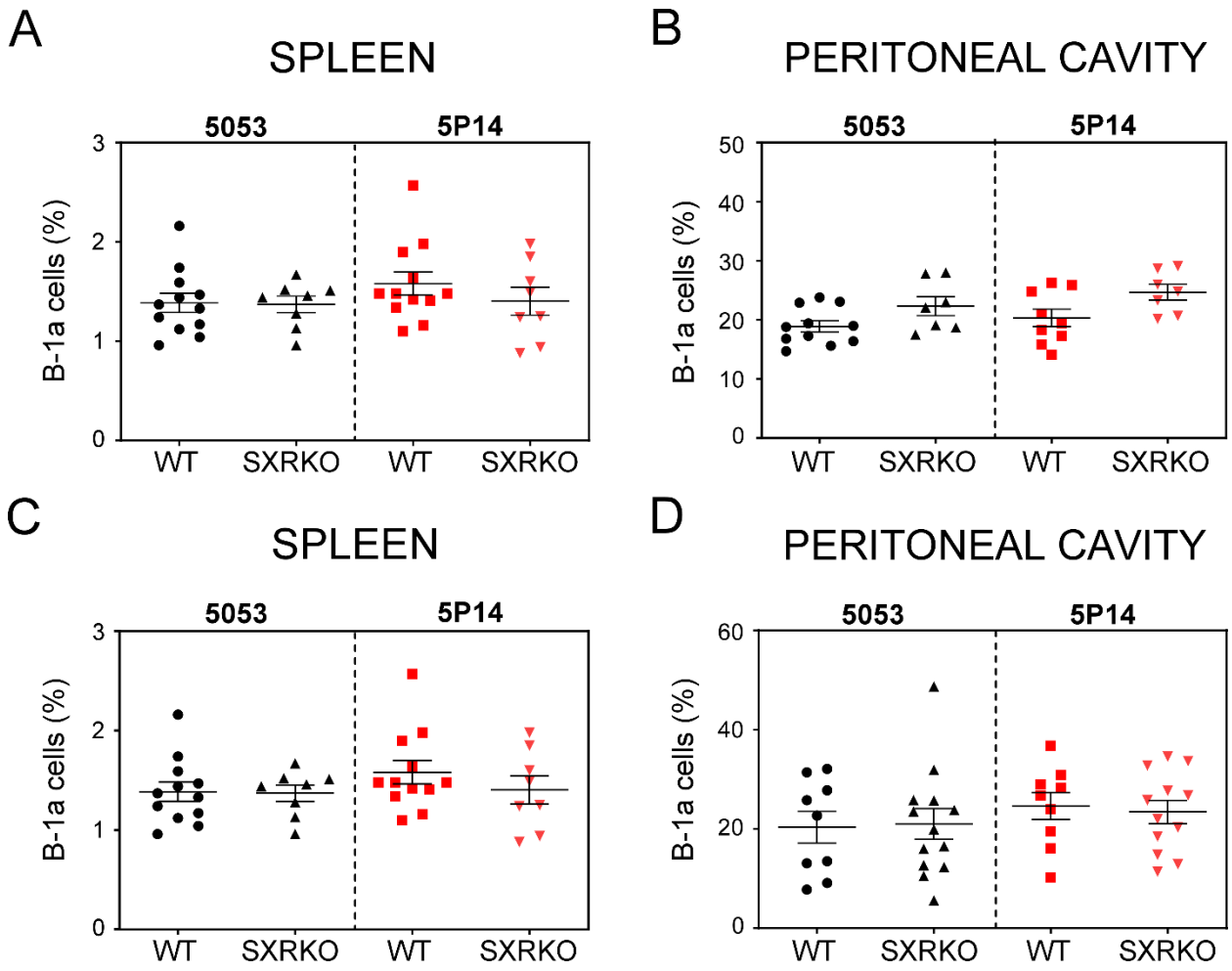

Figure 1.3 5P14 diet does not induce B-1a cell lymphoma in SXRKO mice
F0 male SXRKO mice do not display increased percentage of B-1a cells in the spleen (A) or peritoneal cavity (PerC) (B) compared to WT controls after being on diet for 4 months. F0 female SXRKO mice also display no increase in B-1a cell percentage in the spleen (C) or PerC (D) after 4 months of exposure to the diets compared to WT controls.

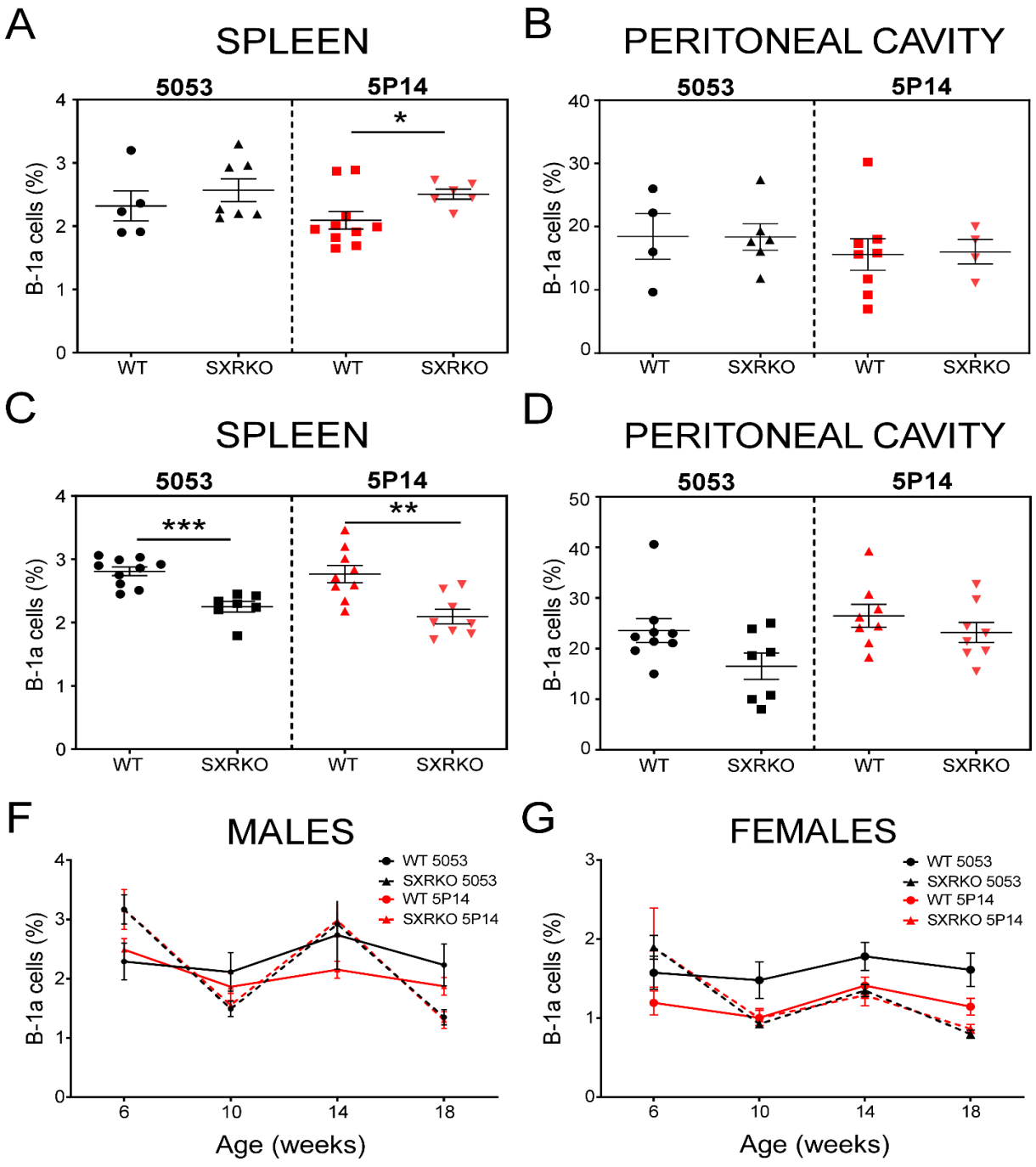

<u>Figure 1.4</u>: Percentage of B-1a cells in the spleen, peritoneal cavity, and blood of F1 diet experiment mice on either irradiated or non-irradiated diet at 6 months of age. Percentage of B-1a cells in the spleen (A) and peritoneal cavity (PerC) (B) of WT and SXRKO F1 male mice on either the irradiated (5053) or non-irradiated (5P14) diet at 6 months of age, determined by flow cytometry. Percentage of B-1a cells in the spleen (C) and PerC (D) of WT and SXRKO F1 female mice on either the irradiated (5053) or non-irradiated (5P14) diet at 6 months of age, determined by flow cytometry. Percentage of B-1a cells over time in the blood of male (E) and female (F) WT and SXRKO F1 mice maintained of either

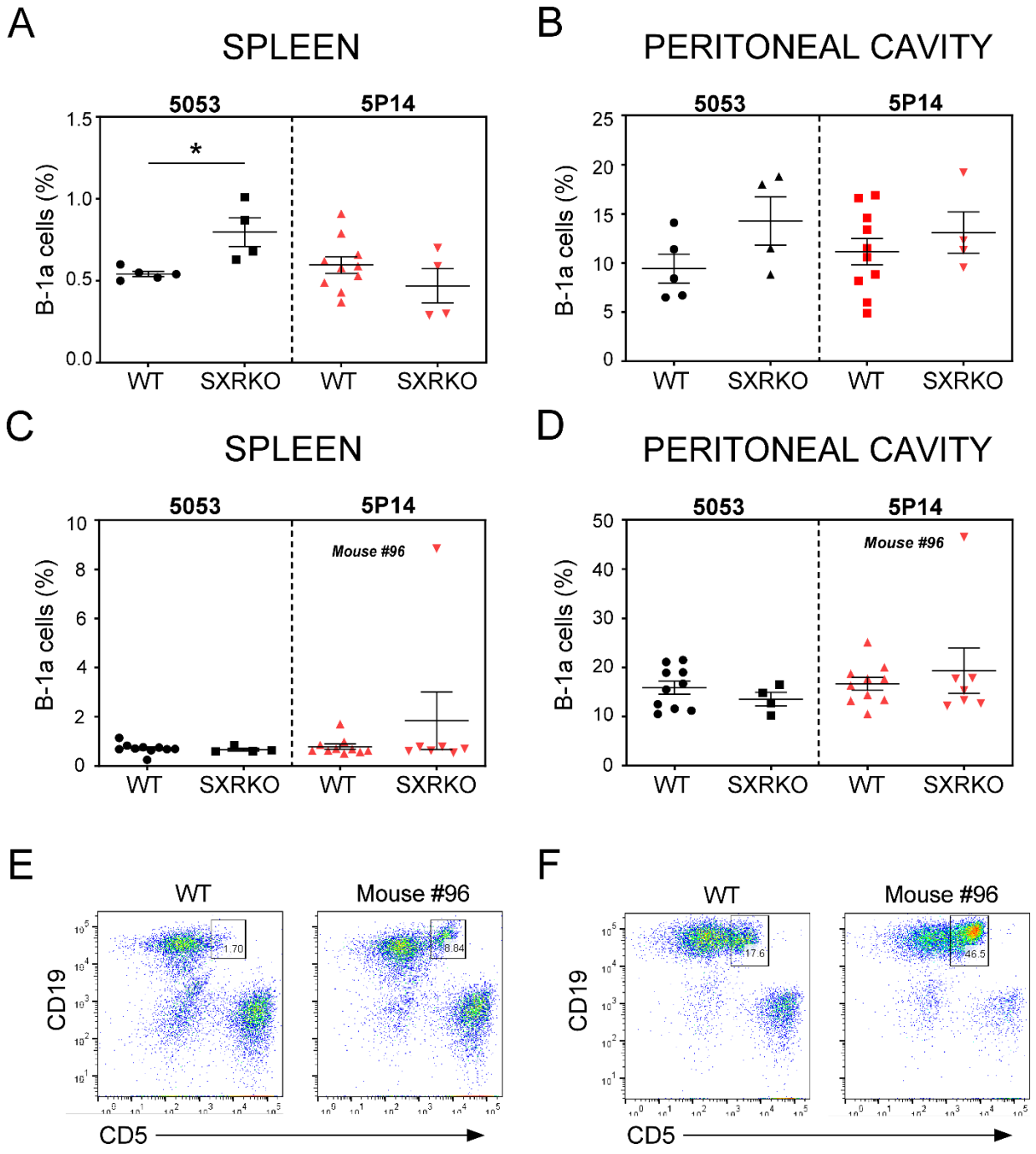

<u>Figure 1.5</u>: A single F1 diet experiment mouse displays B-1a cell lymphoma-like phenotype. Percentage of B-1a cells in the spleen (A) and peritoneal cavity (B) of F1 male WT and SXRKO mice and in the spleen (C) and peritoneal cavity (D) of F1 female WT and SXRKO mice after *in utero* and chronic exposure to the diets until 8 months of age. Mouse #96, displayed a lymphoma-like phenotype with a elevated percentages of B-1a cells in both the spleen and PerC (labeled in panel C and D). Representative flow plots of the spleen (E) and peritoneal cavity (F) of Mouse #96 (right) and a WT mouse on 5P14 diet (left), gating on CD19+/CD5+ B-1a cells.

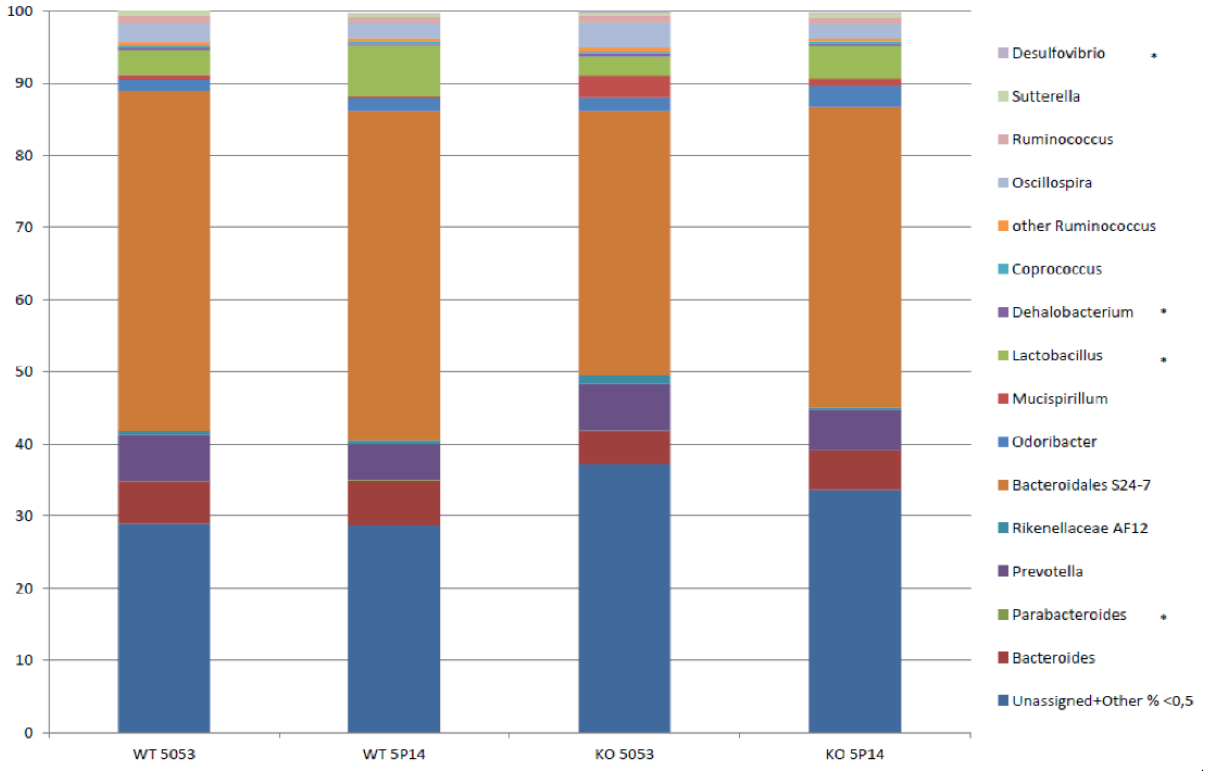

Figure 1.6: Genus level composition of the gut microbiome of diet experiment mice. Gut microbiome composition at genus level of F1 diet experiment mice at 8 months of age, determine by 16S rRNA sequencing, n=4 per group.

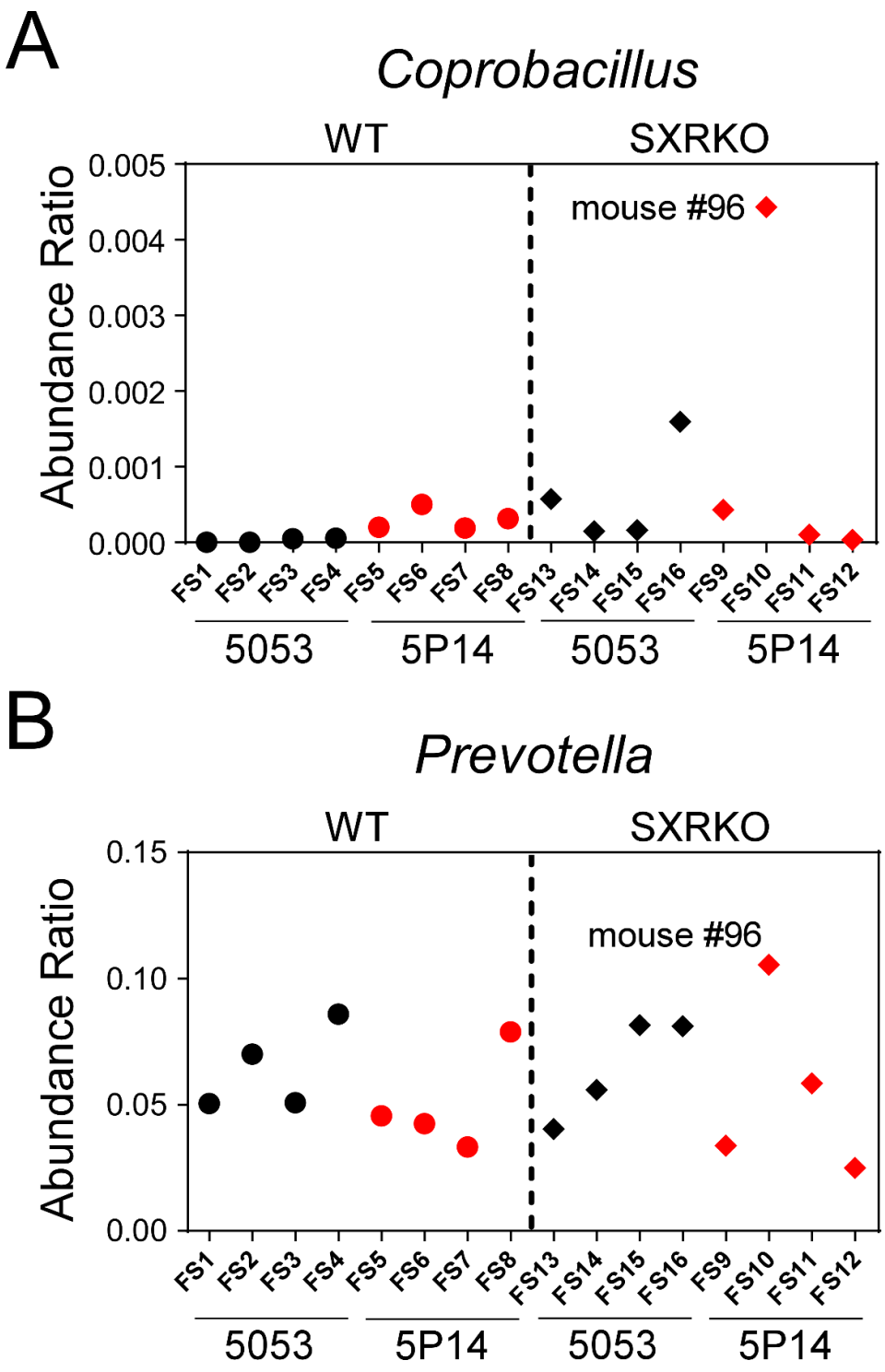

Figure 1.7: Mouse #96 has a distinct microbiome. Abundance ratios of Coprobacillus (A) and Prevotella (B) in the microbiome of F1 diet experiment mice, determined by 16S rRNA sequencing on DNA isolated from fecal samples. Samples are labeled by sample code (FS= fecal sample). Mouse #96/FS10 is labeled in both panels.

```
fastq-join sampleID_file_R1 sampleID_file_R2 -o sampleID_

multiple_join_paired_ends.py -i directory_containing_files -o
joined_output_folder

multiple_split_libraries_fastq.py - i directory_containing_joined_files -o
multiple_split_libraries_output_folder --demultiplexing_method
sampleid_by_file

identify_chimeric_seqs.py -i seqs.fna -m usearch61 -o
usearch_checked_chimeras/ -r gg_13_8_otus.fasta

filter_fasta.py -f seqs.fna -o seqs_chimeras_filtered.fna -s
usearch_checked_chimeras/chimeras.txt -n

pick_de_novo_otus.py -i seqs.fna -o otus_output_folder -p
de_novo_otus_parameters.txt

summarize_taxa_through_plots.py -i otu_table.biom -o taxa_summary_output
```

de_novo_otus_parameters.txt:

```
pick_otus:enable_rev_strand_match True

pick_otus:otu_picking_method usearch61
```

Figure 1.8: Example QIIME script for 16S rRNA sequencing analysis. QIIME script used for 16S rRNA microbiome sequencing analysis and contents of de_novo_otus_parameters.txt file

Table 1.1: qPCR and PCR primer sequences

Gene (mouse)	**Forward primer**	**Reverse primer**
36B4/Rplp0	AAGCGCGTCCTGGCATTGTCT	CCGCAGGGGCAGCAGTGGT
SXR/PXR	GATCATCCCTCTTCTGCCACAC	CAGGTTCCCGTTTCCGTGTC
IL-6	TAGTCCTTCCTACCCCAATTTCC	TTGGTCCTTAGCCACTCCTTC-
IL-1β	GCAACTGTTCCTGAACTCAACT	ATCTTTTGGGGTCCGTCAACT
SXR intron 2 (PCR)	CTTGGGACCTTGGCTTCTTATC	CTTCCTCGGAGCCTTGTTATTC
Neo-SXR exon 5 (PCR)	AGGTGAGATGACAGGAGATC	TCACAFCCACTGTGGAACAC

Table 1.2: Significant differences in microbiota (genus level) between diets

Genus	*P*- value[a] WT 5053 vs KO 5053	*P*- value[b] WT 5P14 vs KO 5P14	*P*- value[c] WT 5P14 vs WT 5053	*P*- value[d] KO 5P14 vs KO 5053
Parabacteroides	0.664	0.063	0.904	<0.001
Lactobacillus	0.214	0.201	0.022	0.193
Anaerostipes	1.00	0.069	0.252	0.039
Dehalobacterium	0.350	0.694	0.127	0.039
Desulfovibrio	0.426	0.491	0.306	0.006

aSignificant differences in log gene copy numbers of specific bacterial groups between WT 5053 and KO 5053 mouse groups.
bSignificant differences in log gene copy numbers of specific bacterial groups between WT 5P14 and KO 5P14 mouse groups.
cSignificant differences in log gene copy numbers of specific bacterial groups between WT 5P14 and WT 5053 mouse groups.
dSignificant differences in log gene copy numbers of specific bacterial groups between KO 5P14 and KO 5053 mouse groups.

Table 1.3: Comparison of diet composition of 5053 and 5P14 (LabDiet)

Nutrients (%, unless otherwise noted)	5053	5P14	Minerals (%, unless otherwise noted)	5053	5P14
Protein	**20**	**24**	**Ash**	**6.1**	**6.9**
Arginine	1.22	1.55	Calcium	0.81	0.95
Cystine	0.28	0.34	Phosphorus	0.63	0.69
Glycine	0.96	1.17	Phosphorus (non-phytate)	0.33	0.33
Histidine	0.5	0.59	Potassium	1.07	1.2
Isoleucine	0.97	1.16	Magnesium	0.22	0.25
Leucine	1.56	1.87	Sulfur	0.34	0.29
Lysine	1.16	1.4	Sodium	0.3	0.4
Methionine	0.7	0.43	Chloride	0.51	0.7
Phenylalanine	0.9	1.11	Fluorine	10	12
Tyrosine	0.59	0.73	Iron (ppm)	220	290
Threonine	0.77	0.92	Zinc (ppm)	87	110
Tryptophan	0.26	0.31	Manganese (ppm)	85	110
Valine	1	1.25	Copper (ppm)	13	17
Serine	1.03	1.27	Cobalt (ppm)	0.71	0.51
Asparic acid	2.19	2.61	Iodine (ppm)	0.97	1.4
Glutamic acid	4.34	5.23	Chromium (ppm)	0.81	1.2
Alanine	1.15	1.21	Selenium (ppm)	0.3	0.48
Proline	1.47	1.7	**Vitamins**	**5053**	**5P14**
Taurine	0.02	0.005	carotene (ppm)	1.5	2
Fat (ether extract)	**5**	**4.5**	Vitamin K (ppm)	3.3	3.2
Fat (acid hydrolysis)	**5.6**	**6**	thiamin hydrochlorine (ppm)	17	20
Cholesterol (ppm)	141	101	riboflavin (ppm)	8	12
Linoleic acid	2.19	1.53	niacin (ppm)	90	130
Linolenic acid	0.26	0.11	pantothenic acid (ppm)	17	24
Arachidionic acid	<0.01	0.004	choline chloride (ppm)	2000	2300
Omega-3 fatty acids	0.33	0.17	folic acid (ppm)	3	7.9
Total saturated acids	0.93	1.55	pyridoxine (ppm)	9.6	8
Total monosaturated fatty acids	0.99	1.24	biotin (ppm)	0.3	0.28
Fiber (crude)	**4.7**	**5.3**	B12 (mcg/kg)	51	49
Neutral detergent fiber	16.4	15.4	vitamin A (IU/gm)	15	22
Acid detergent fiber	6	6.3	Vitamin D_3 (IU/gm)	2.2	5
Nitrogen-free extract	**52.9**	**49.3**	Vitamin E (IU/kg)	99	52
Starch	33.9	21.5	Ascorbic acid (mg/gm)	-	-
Glucose	0.19	0.2	**Calories provided by (%)**	**5053**	**5P14**
Fructose	0.23	0.2	Protein	24.651	28.768
Sucrose	3.18	3.4	Fat (ether extract)	13.205	12.137
Lactose	1.34	0.6	Carbohydrates	62.144	59.095
Total digestible nutrients	**76.2**	**75.7**	**Other**	**5053**	**5P14**
Gross energy, kcal/gm	**4.07**	**4.05**	Irradiated	YES	NO
Physiological fuel value, kcal/gm	**3.41**	**3.34**			
Metabolizable energy, kcal/gm	**3.07**	**3.04**			

CHAPTER 2

The microbiome from a mouse with a lymphoma-like phenotype is distinct and transmissible but does not lead to transmission of the lymphoma phenotype in mice lacking the Steroid and Xenobiotic Receptor (SXR/PXR)

Summary

The microorganisms present in the gut, known as the gut microbiome, are important for digestive health, protection against intestinal pathogens, production of micronutrients and absorption of many macronutrients. It has now been demonstrated that the gut microbiome plays important roles in many other physiological functions including inflammation, immune cell development, and even neurological processes. In mouse models, perturbations to the gut microbiome can cause large changes to phenotypes and even lead to a complete loss of a phenotype. The B-1a B cell lymphoma phenotype characterized in aged SXR knockout (SXRKO) mice, which was first reported in 2011 (Casey et al 2011), was no longer observed in our mouse colony following a change in the diet. Placing the SXRKO mice back on the 5P14 diet did not return the B-1a B cell lymphoma phenotype in most mice, but did result in one female SXRKO mouse (Mouse #96) that displayed a large increase of B-1a B cells in both the spleen and peritoneal cavity at 8 months of age, characteristic of the previously reported B-1a B cell lymphoma phenotype. The microbiome of Mouse #96 appeared to be distinctly different than that of mice displaying no aberrant B-1a B cell phenotype leading us to hypothesize that the phenotype was associated with the gut microbiome. We performed a microbiome transplant of fecal material from Mouse #96 on both wild-type (WT) and SXRKO mice to investigate if the microbiome promoted the

elevated B-1a B cell phenotype. The transplanted mice were then bred to determine if the changes in the microbiome were transmissible to the F1 generation and to study if exposure to the microbiome during development had a differential impact on the phenotype of SXRKO mice. 16S rRNA analysis revealed that the microbiome transplant from Mouse #96 was successful and transmitted to the F1 generation. The sequencing results also revealed that the experimental microbiome, originating from Mouse #96, led to a distinctly different microbiome than that of mice transplanted with a WT control microbiome. The experimental microbiome transplant did not result in a B-1a B cell phenotype in either WT or SXRKO mice, demonstrating that the phenotype was not dependent on the microbiome or that the transplant lacked a component of the microbiome that was important for the cancer phenotype. Gene expression analysis on the colon of these mice demonstrated that SXRKO mice tended to be resistant to gene expression changes induced by the microbiome. Further analysis is needed to determine the mechanism behind this observation and to investigate if it has any impact on the phenotype of SXRKO mice.

Introduction

The community of microorganism present in our gut, known as the gut microbiome, exists in a symbiotic relationship with the host, aiding in metabolism and providing protection against intestinal pathogens. The microbiome can impact various metabolic processes and host immunity and, therefore, has the capability to directly or indirectly impact almost every physiological function in the host[25]. Perturbations to the gut microbiome can have extensive impacts on health and were shown to be associated with disease states, such as obesity and inflammatory bowel disease (IBD)[26-28]. Experiments in mouse models demonstrated a direct link between the microbiome and the development of disease, showing that alterations to the microbiome can lead to disease[61, 71, 72]. The composition of the microbiome was also shown to be a necessary component for the development of certain phenotypes in mouse models and ablation or perturbations of the gut microbiota led to a reduction or loss of the observed phenotype[62].

The gut microbiome is very dynamic and has been shown to be impacted by many factors, such as alcohol consumption, cigarette smoking, and exercise. Stress, disrupted circadian rhythm, and presence of existing conditions or diseases have also shown to induce changes to the gut microbiome composition. Diet is a major inducer of rapid and direct alterations to the gut microbiome[58, 62]. Diet induced changes to the gut microbiome can be both reversible and irreversible, leading to a variety of physiological impacts to the host.

Mice lacking the SXR/PXR (SXRKO mice) display increased widespread inflammation due to the mutually inhibitory relationship between SXR/PXR and NF-κB, a major transcription factor involved in the inflammatory response[53]. This increased inflammatory state of SXRKO mice was shown to lead to the development of a B-1a B cell lymphoma phenotype, characterized

by elevated levels of B-1a lymphocytes present in the blood, spleen, and peritoneal cavity, accompanied by tumors in various tissues[5].

Chapter 1 described the discovery that this B-1a B cell lymphoma phenotype disappeared following a change in the diet of our SXRKO colony and that simply returning the SXRKO mice to the previous diet did not rescue the phenotype. However, the diet experiment produced one SXRKO mouse that displayed a high increased percentage of B-1a B cell in both the spleen and peritoneal cavity, characteristic of the previously reported B-1a B cell lymphoma phenotype[5]. We refer to this single SXRKO mouse with B-1a B cell lymphoma as Mouse #96. 16S rRNA sequencing analysis revealed that the microbiome of Mouse #96 was different than that of other mice in our colony. Therefore, we hypothesized that the microbiome composition of SXRKO mice impacts the development of the B-1a B cell lymphoma phenotype. Mouse #96 provided the material to test whether the aberrant B-1a B cell lymphoma phenotype is linked to the microbiome.

We used fecal samples obtained from Mouse #96 to perform fecal microbiome transplants into both wild-type and SXRKO mice and investigated F0 and F1 mice for signs of B-1a B cell lymphoma to determine if the microbiome was a contributing factor.

Materials and Methods

Mouse maintenance: Wild-type (C57Bl6/J) and SXRKO mice were identically raised and housed at the University of California, Irvine on a standard diet. SXRKO mice were descendants of a gift from the Salk Institute. SXRKO mice were backcrossed to a C57Bl6/J background for six generations. All mice were maintained on standard non-irradiated ProLab RMH 2500/5P14 (LabDiet). Mouse cages were enriched with wood chip bedding and cotton nestlets. All experiments were carried out in accordance with the UCI Institutional Animal Care and Use Committee.

Microbiome/Fecal Transplant: In order to expand the amount of available fecal samples from Mouse #96, a few SXRKO males and females (n=2, n=4 respectively) were treated with an antibiotic cocktail (1 g/L Ampicillin, 1 g/L Metronidazole, 0.5 g/L Vancomycin, 1 g/L Neomycin) via drinking water for 4 weeks to clear the existing commensal microbiome. Mice received a fecal transplant from Mouse #96, via oral gavage, two days following the end of the antibiotic treatment. To obtain material for fecal transplant, fecal samples from Mouse #96 were placed in PBS and then dissociated with repetitive pipetting. The feces from these transplanted mice were then collected and used as our "test" microbiome samples. Fecal samples from non-transplanted wild-type mice were collected in parallel to use as the "control" microbiome. Next, both wild-type and SXRKO mice (n=4 to 5 per group) were pretreated with antibiotics for 4 weeks to clear their commensal microbiomes and then administered either test or control fecal transplants via oral gavage. These mice were then bred at 20 weeks old and their pups were studied (n=4 to 10 per group). Both F0 and F1 generations were euthanized and analyzed at 10 months of age.

Blood collection: Approximately 50 µL of whole blood was collected from the saphenous vein of the mice. Blood was collected using heparinized capillary tubes. Red blood cells (RBCs) were lysed by incubating cell suspension in ACK lysis buffer (150 mM NH4Cl, 10 mM KHCO3, 0.1 mM Na_2EDTA) for 5 min. Cells were washed and resuspended in FACS buffer (PBS, 1% FBS, 0.02% sodium azide) at 400K cells/mL for flow cytometry antibody staining.

Peritoneal cavity lavage: Mice were euthanized by isoflurane overdose and cervical dislocation. The skin was carefully cut to reveal the peritoneum without puncturing or nicking it. Approximately 9 mL of ice cold FACS buffer was injected into the peritoneum, avoiding injecting into internal organs. The filled peritoneum was then agitated to dislodge any cells attached to tissues. A syringe and 25-gauge needle were used to extract the large amount of liquid from the peritoneum. A pipet was then used to extract the small amount of remaining liquid from the peritoneum. RBCs were lysed by incubating cell suspension in ACK lysis buffer (150 mM NH4Cl, 10 mM KHCO3, 0.1 mM Na_2EDTA) for 5 min. RBC-depleted cells were washed and resuspended in FACS buffer (PBS, 1% FBS, 0.02% sodium azide) for flow cytometry antibody staining.

Tissue collection: Liver, small intestine, colon, caecum, and spleen tissue were dissected, flash frozen in liquid N_2 and stored at -80˚C. A section of the spleen was set aside before flash freezing to undergo splenocyte isolation.

Spleen cell isolation: Spleen sections were physically dissociated using a petri dish and syringe plunger in 1 mL of ice-cold PBS containing 1% FBS. RBCs were lysed by incubating cell suspension in ACK lysis buffer (150 mM NH_4Cl, 10 mM $KHCO_3$, 0.1 mM Na_2EDTA) for 5 min. RBC-depleted splenocytes were washed, resuspended in FACS buffer (PBS, 1% FBS, 0.02%

sodium azide), and sent through a 100 µm cell strainer to prepare for flow cytometry antibody staining.

Flow cytometry (FACS) analysis: RBC-depleted spleen, peritoneal cavity, and blood cells were diluted in cold FACS buffer (PBS, 1% FBS, 0.02% sodium azide), aliquoted at 200K cells, and stained with and antibody cocktail of anti- mouse CD5-APC (eBioscience), CD19-PE (eBioscience), and IgD-FITC (eBioscience) for 30 min. Cells were measured on a BD LSR II cytometer. Data was analyzed using FlowJo software (Treestar).

Fecal sample collection and analysis: Fecal samples were collected from all mice, flash frozen, and stored at -80˚C. Fecal DNA was extracted using the PowerFecal DNA kit (MO BIO/Qiagen) according to manufacturer's protocol.

16s rRNA sequencing: microbial DNA was amplified for the V3-V4 variable regions of the 16S rRNA gene. DNA libraries were prepared by the UCI Genomics High Throughput Facility following the Illumina protocol for 16S rRNA metagenomic sequencing library preparation. 16S rRNA sequencing was performed on Illumina MiSeq with 2x300bp paired-end reads at the Institute for Integrative Genome Biology at the University of California, Riverside. Fastq files were processed using QIIME[65].

QIIME microbiome sequencing analysis: Paired-end reads were joined using the fastq-join function. Joined files were then quality filtered and merged into one data file with each sample labeled by the file name using the multiple_split_libraries_fastq.py function. The seqs.fna file from the previous command was then filtered to remove any chimeric sequences using Usearch6.1[66], installed within QIIME. Chimeric sequencing were identified using the identify_chimeric_seqs.py and the recent Greengenes reference sequence file (gg_13_8_otus.fasta)[67]. The discovered chimeric sequences were then removed from the seqs.fna

file using the filter_fasta.py command, the chimeras.txt file obtained from the previous command and the added parameter of "-n". OTU picking was then conducted on the newly filtered sequencing file using the pick_de_novo_otus.py command using Usearch6.1 as the OTU picking method and Uclust for assigning taxonomy to the OTUs[68]. This step was conducted on the UCI high performance computer (HPC) cluster. Taxonomy assignments were summarized into a readable format using the summarize_taxa_through_plots.py and the otu_table.biom file generated in the previous command. Visualizations and statistical analyses were conducted using Calypso[69].

RNA isolation: Frozen tissue sections were homogenized rapidly in 1 mL of Trizol reagent (ThermoFisher Scientific). RNA was isolated from the tissue-Trizol homogenate by phenol/chloroform extraction. RNA was precipitated with an equal volume of 100% isopropanol, centrifuged and salt removed by washing with 70% ethanol. Final RNA product was resuspended in DNase/RNase-free sterile, ultrapure water (ultrafiltered, UV sterilized water from Barnstead Nanopure water system, hereafter called nanopure water), quantified by spectrophotometry, and checked for integrity by denaturing agarose gel electrophoresis.

cDNA synthesis: cDNA was made using 2 µg of intact RNA and Superscript III reverse transcriptase (Applied Bioscience) according to manufacturer's protocol. Synthesized cDNA was diluted 5-fold with nanopure water for downstream qPCR analysis.

Designing qPCR primers: Gene sequences were obtained from Ensembl genome browser. PerlPrimer was used to design and identify candidate forward and reverse primers. Primer oligos were ordered from Sigma-Aldrich and resuspended in Tris-EDTA buffer. Primer sequences are listed in Table 2.1.

Quantitative real time reverse transcriptase PCR (qPCR): Diluted cDNA was combined with SYBR green qPCR Master Mix (Applied Biosystems) and the primer mix for gene of interest and run on the Roche LightCycler 480. Expression values were compared to the housekeeping gene 36B4/Rplp0 to determine relative mRNA expression. For qPCRs to quantify bacteria abundance, Ct values for 16S rRNA gene was divided by the weight of the fecal sample to get approximate bacterial abundance in fecal sample (arbitrary unit (AU)/weight of fecal sample).
Statistical analysis: Data visualization and statistical analyses were conducted in Prism 8 (GraphPad Software). Unpaired t-test was used to determine statistical significance. * = p-value <0.05, ** = p-value <0.01, ***= p-value <0.001, #= p-value <0.0001

Results

Microbiome transplant from Mouse #96 results in a distinct microbiome

To investigate whether the microbiome of Mouse #96 was responsible for the B-1a B cell lymphoma phenotype observed, we used fecal material to conduct a microbiome transplant into both wild-type (WT) and SXRKO mice and measured the splenic and peritoneal B-1a B cell content. The fecal material used to conduct the microbiome transplant originated from either Mouse #96, which will be referred to as the "test" microbiome, or from WT mice in our colony that did not display an elevation of B-1a B cell percentage, which will be referred to as the "control" microbiome. 12 week old WT and SXRKO mice received the microbiome transplant via oral gavage following four weeks of antibiotic treatment to clear the existing microbiome and one-week break (Figure 2.1). The microbiomes of the mice were monitored by qPCR to determine total microbial content before and after the antibiotic treatment and after the microbiome transplant, confirming a reduction of commensal bacteria after antibiotic treatment and subsequent reconstitution of a microbiome following the fecal microbiome transplant (Figure 2.2). These mice were bred to generate the F1 generation exposed throughout development (Figure 2.1). 16S rRNA sequencing analysis of fecal DNA revealed that the microbiome transplant was successful and that the microbiomes from the control and test groups were distinctly different and were transferred to the F1 generation (Figure 2.3, Figure 2.4). In addition, the sequencing revealed that the microbiome of the test transplant group clustered with the microbiome of Mouse #96 and test fecal gavage material clustered, and had similar microbial diversity as determined by the Shannon Index (Figure 2.3A-B). There was some spread in the variance within each microbiome group, but this was shown not to be because of gender or mouse genotype (Figure 2.4B). We hypothesize that these differences were due to natural

variance in the reconstitution of the microbiome, although overall the microbiomes within each group were more similar to each other than to those of the other microbiome group.

There were few changes detected between Mouse #96 and the test microbiome samples. For example, there was an increase in unclassified *Mogibacteriacaeae* in the test microbiome group that was not increased in Mouse #96 (Figure 2.5E). However, for the most part, the changes in the microbiome of Mouse #96 was reflected in the test microbiome group. For example, a large increase in *AF-12* and *Odoribacter*, and large decrease in *Anaeroplasma* were observed in both Mouse #96 and the test microbiome transplant mice when comparing to the control transplant mice (Figure 2.5A-B, D).

Phenotype of Mouse #96 was not transmitted with a fecal microbiome transplant

Both the F0 and F1 mice from the microbiome transplant study were euthanized at 10 months of age and investigated for signs of B-1a B cell lymphoma. No changes in B-1a B cell content were observed in the F0 mice between WT and SXRKO from either microbiome group (Figure 2.6). For the F1 mice exposed to the microbiome throughout development, no changes in B-1a B cell content in either the spleen or peritoneal cavity were observed between male WT and SXRKO of either microbiome group (Figure 2.7A-B). F1 female SXRKO mice from the test microbiome group displayed an increased percentage of B-1a B cells in the peritoneal cavity compared to WT mice of the same transplant group (Figure 2.7D). However, there was no increase in the spleen percentage of B-1a B cells in F1 SXRKO females with the test microbiome (Figure 2.7 C), indicating the absence of B-1a B cell lymphoma.

Female SXRKO mice display elevated expression of NF-κB subunit p65 and sirtuins in the colon

Although the microbiomes tested in this study did not induce the development of the B-1a B cell lymphoma, we asked if the different microbiomes caused any gene expression

alterations to the gut of the host and whether those changes were different between WT and SXRKO mice. We investigated gene expression in the colon, which is the major site of microbiota-host interactions. We focused on inflammatory genes, due to the interaction between SXR and NF-κB, and genes related to the microbiome, such as the sirtuin family of genes. Consistent with previous findings, female SXRKO mice displayed increased NF-κB activity with elevated expression the key subunit, p65, compared to WT mice (Figure 2.8A). This was observed in both microbiome groups, although the difference was significant only in the control microbiome. Interestingly, increased p65 expression was not observed in male SXRKO mice (Figure 2.9A)

Sirtuins are NAD, dependent protein deacetylases that regulate various pathways such as gene silencing and DNA repair. Sirtuin 1 (Sirt1) can reduce inflammation by deacetylating the p65 subunit of NF-κB[73, 74]. Sirtuins have also been shown to be important mediators of microbiota-host interactions[75, 76]. We discovered that F1 female SXRKO mice displayed increased expression of Sirt1 compared to WT controls in both microbiome groups (Figure 2.8B). Sirt6 was also increased in SXRKO females compared to WT controls, though this difference was only observed in the control microbiome group (Figure 2.8C). Interestingly, Sirt6 mRNA expression was also different between the microbiome groups of WT mice with an increase observed in the test microbiome group (Figure 2.8C). There were no changes in gene expression levels for both sirtuins in the colons of F1 male mice (Figure 2.9B-C). The increased expression of Sirt1 and Sirt6 in female SXRKO mice is likely attributable to the increased expression of NF-κB in these mice.

SXRKO mice are resistant to microbiome-induced gene expression changes in the colon

Nuclear factor erythroid 2–related factor 2 (Nrf2) is an inducible transcription factor involved in cellular response to oxidants and electrophiles. Nrf2 can inhibit NF-κB activity[77], functioning similarly to Sirt1 and SXR. In addition, Sirt1 is an upstream regulator of the Nrf2 pathway[78]. Nrf2 also shares similar target genes involved in xenobiotic detoxification with SXR[79]. We observed trends for increased expression of Nrf2 induced by the test microbiome in the colon of F1 WT females (Figure 2.8 D). Interestingly, SXRKO females did not display these trends in gene expression (Figure 2.8D). Nrf2 was shown to heterodimerize with the proto-oncogene, c-Jun, to induce transcription of detoxifying enzyme and antioxidant response genes[80]. We observed a similar trend of increased c-Jun mRNA expression in the test microbiome group in female WT mice and a lack of increased expression in SXRKO females in the test microbiome group (Figure 2.8E). These results demonstrated that loss of SXR can result in resistance to microbiome induced changes in expression of Nrf2 and c-Jun mRNA in the host colon. Whether loss of SXR leads to resistance to other microbiome induced gene expression changes to the host still needs to be investigated. Similar to the p65 and sirtuin expression profiles, we did not observe these changes in male mice (Figure 2.9 D-E).

Discussion

Fecal microbiome transplants utilizing samples from Mouse #96 resulted in a distinct microbiome that matched that of the originating Mouse #96 microbiome. Despite having a microbiome matching that of Mouse #96, we did not observe any large increase in the percentage of B-1a B cells in the spleen or peritoneal cavity of SXRKO mice from the test microbiome group. These results demonstrated that the microbiome of Mouse #96 we were able to transfer was not sufficient to produce an increased number of B-1a B cells.

Although our 16S rRNA sequencing results suggested that the microbiome of Mouse #96 was successfully transplanted into the experimental mice and that the experimental microbiome matched that of Mouse #96, it is possible that some microorganisms did not successfully colonize and that this is responsible for the failed transmission of the B-1a B cell phenotype. Many factors, such as temperature, housing conditions and water source, can impact the gut microbiome and could have prevented successful colonization of a microbe(s) key to the phenotype[81]. The only way to accurately test the hypothesis that the microbiome is important for the development of the B-1a B cell lymphoma phenotype in SXRKO mice is to have a current colony of mice that display the phenotype and then investigate the effect of ablating or perturbing the microbiome. Unfortunately, determining the impact of these factors on the microbiome and phenotype of our mice and determining what individual microbes may be important cannot be easily achieved since we do not have a colony of mice currently presenting the B-1a B cell lymphoma phenotype.

We were able to observe gene expression differences between SXRKO and WT mice induced by the microbiome. There was a trend toward increased Nrf-2 and Jun mRNA expression in the colon of WT mice with the test microbiome compared to the control

microbiome. However, this trend was not observed in SXRKO mice. There was an increase in sirtuins (Sirt1 and Sirt6) and p65 mRNA expression in female SXRKO mice compared to WT controls. We infer that the increased p65 and sirtuin gene expression of SXRKO mice made them resistant to gene expression changes induced by the microbiome since we observed trends for gene expression changes between the two microbiomes in the wild-type mice, but no trends in the SXRKO mice and because inflammation and sirtuins have demonstrated to impact the gut microbiome[75]. More studies will be required to confirm this and to investigate what other microbiome-induced gene expression changes may be absent in SXRKO mice.

The gene expression changes observed between WT and SXRKO mice may play a part in differential responses to the gut microbiome. Only F1 female mice showed these alterations in gene expression and this was the only group to display an aberrant B-1a B cell percentage. Whether these two observations are linked is yet to be determined. Many phenotypes were shown to be sexually dimorphic and connected to differences in the microbiome[82, 83]. Therefore, this phenomenon is not uncommon, but the molecular mechanism for the phenotype we observed has not been determined yet.

Overall, the results of this study demonstrated that a fecal microbiome transplant from a SXRKO mouse displaying a pre-lymphoma phenotype did not result in the transmission of the phenotype in either WT or SXRKO mice, despite an apparently successful transplantation. However, it does not completely rule out the possibility that the microbiome is an important component in the B-1a B cell lymphoma phenotype of SXRKO mice since we do not have the appropriate mice to accurately test it. We did observe gene expression changes in the colon between WT and SXRKO mice that were accompanied by differential changes in expression of some genes that appeared to be induced by the microbiome. This suggests that SXR does play a

role in the interactions between the microbiome and host at the gene expression level. Additional studies are needed to fully characterize this interaction.

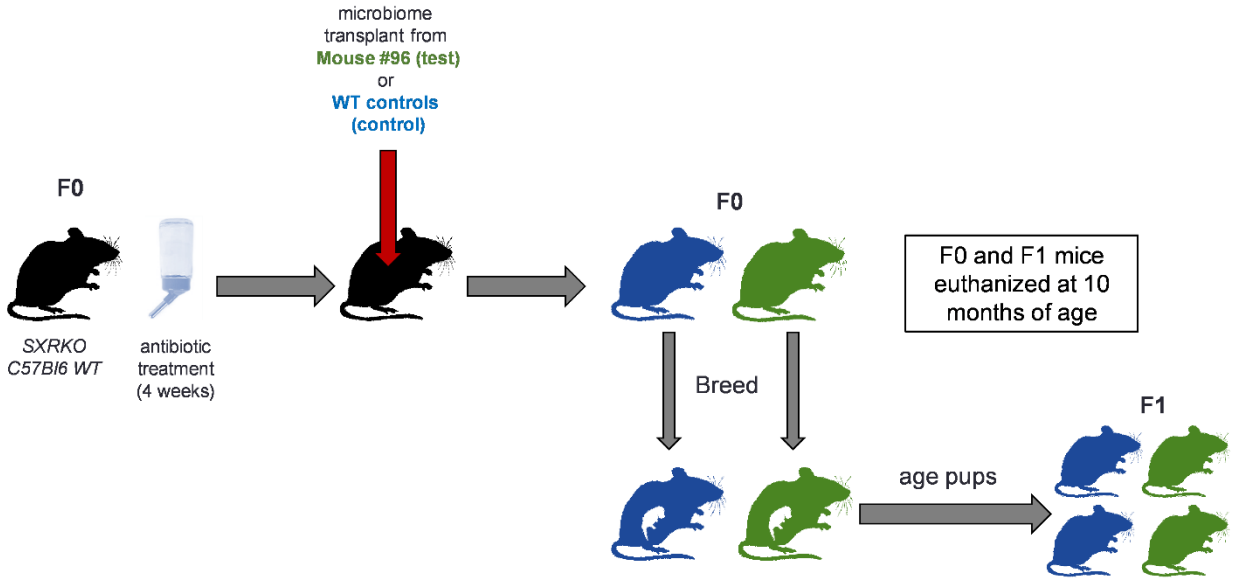

Figure 2.1: Experimental design for fecal microbiome transplant experiment

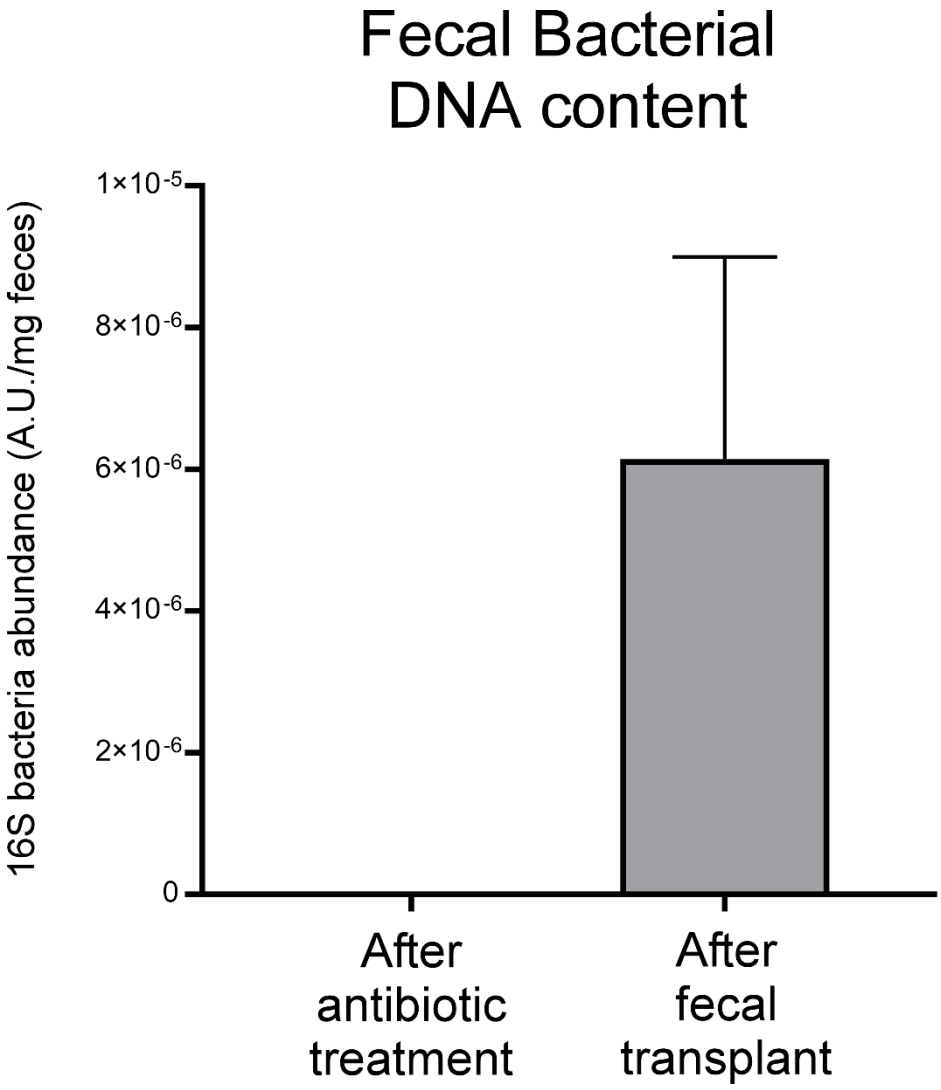

Figure 2.2: qPCR validation of 16S rRNA gene abundance in feces of F0 mice following antibiotic treatment and fecal transplant.

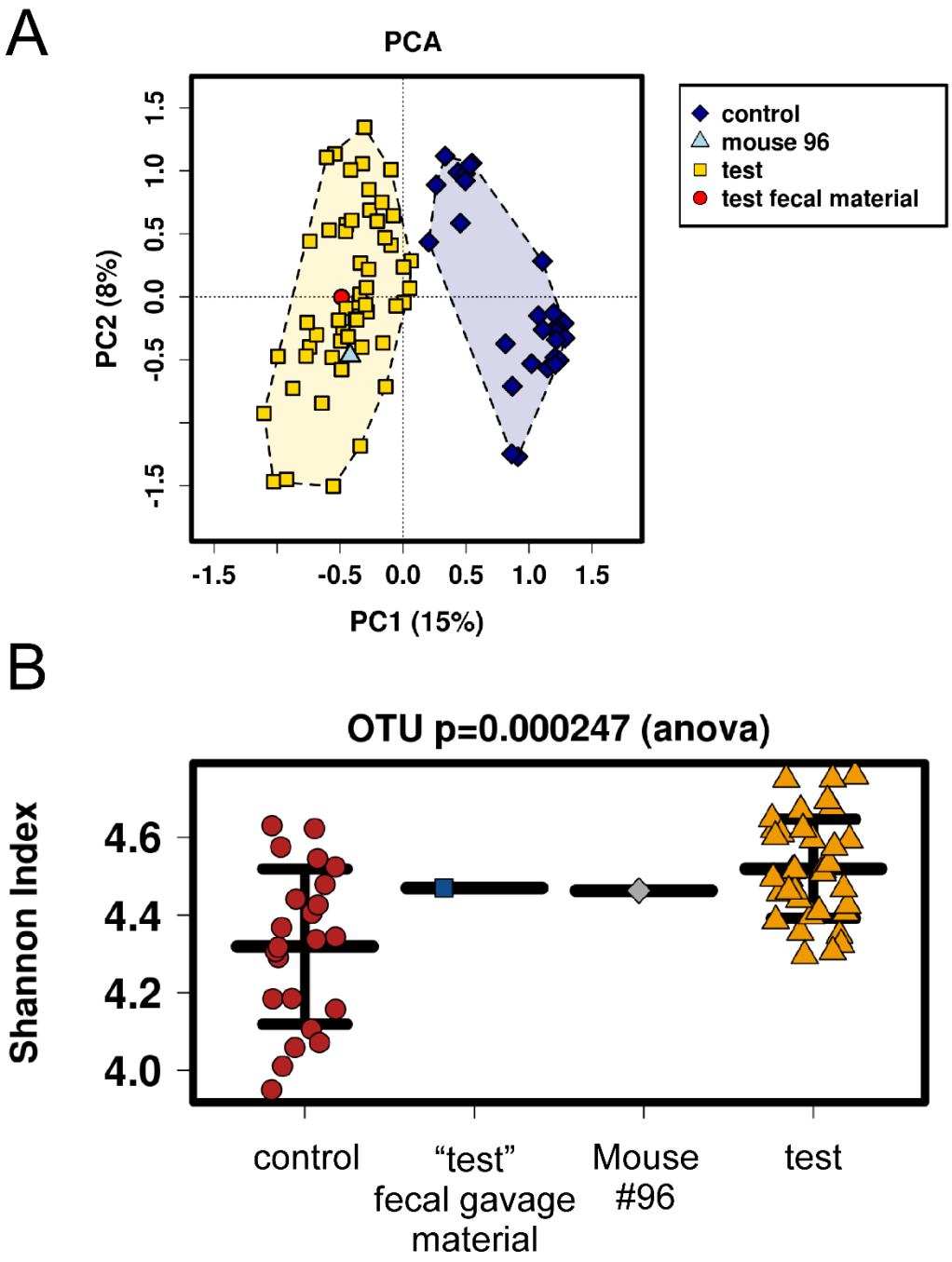

Figure 2.3 Fecal microbiome transplant results in a distinct microbiome matching that of Mouse #96. Principle Component Analysis (PCA) plot of 16S rRNA sequencing of fecal samples from microbiome transplant mice, demonstrating that fecal transplant was successful (A). The microbiome originating from Mouse #96 has increased diversity, as determined by Shannon index, compared to control microbiome (B)

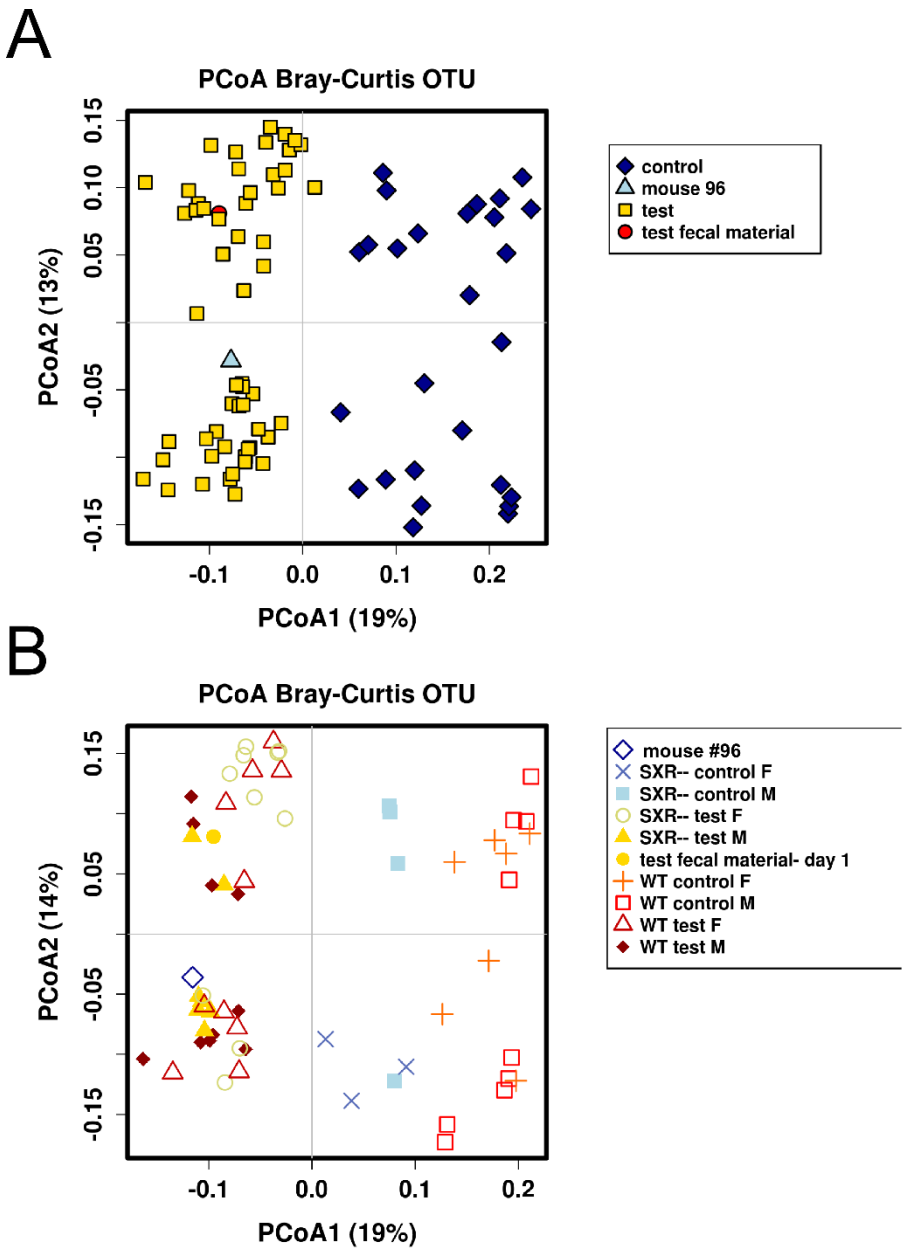

Figure 2.4: Fecal microbiome transplant results in a distinct microbiome matching that of Mouse #96. Principle Coordinate Analysis (PCoA) plots indicate that the microbiome of transplant mice cluster mostly based on the transplant group "test" or "control" (A). There appears to be no clustering based on gender or mouse genotype (B).

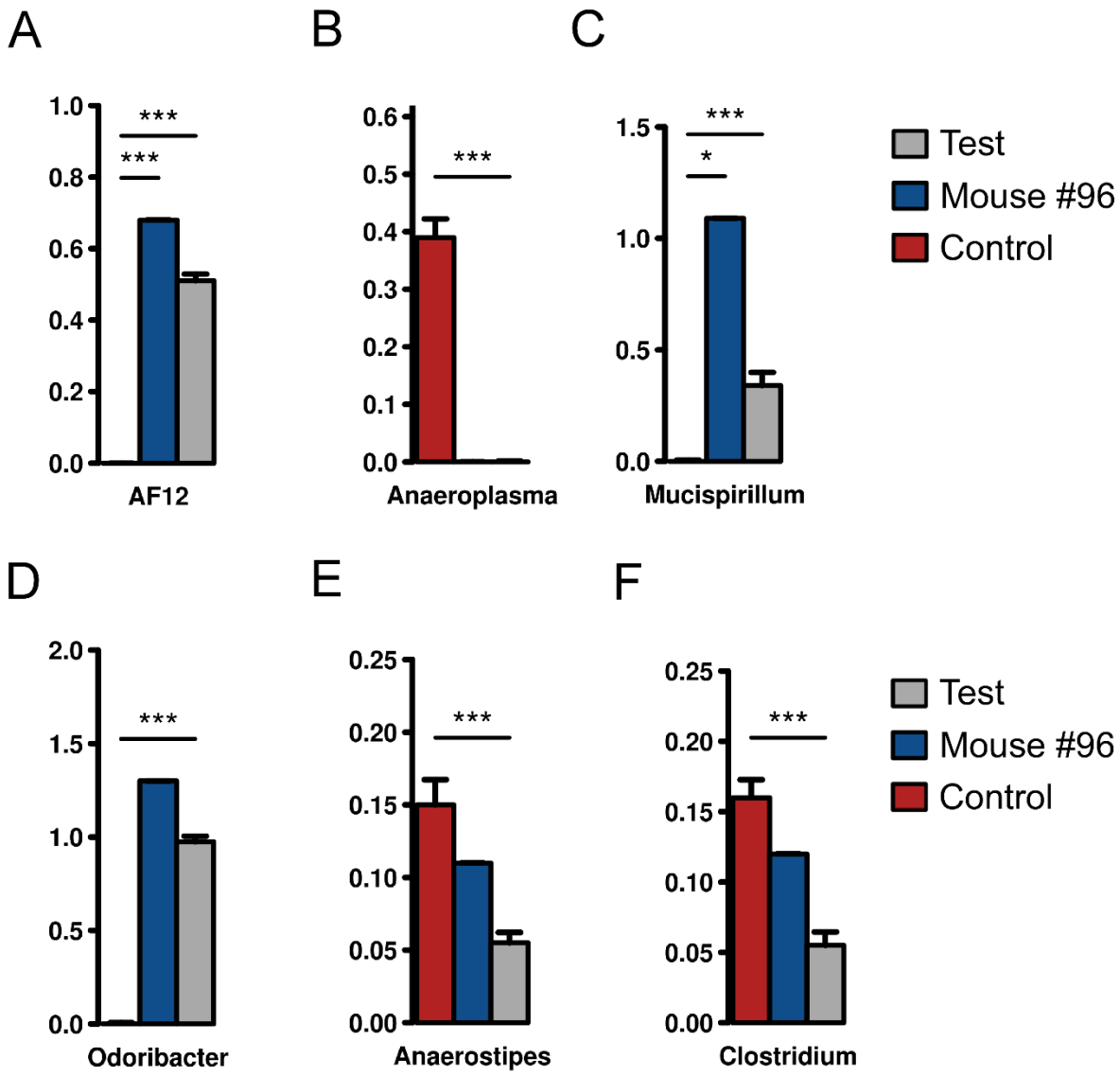

Figure 2.5 Abundance of various microbes in the feces of mice from both transplant groups and Mouse #96. Percentage of microbiota abundance of genus AF-12 (A), Anaeroplasma (B), Mucispirillum (C), Odoribacter (D), Anaerostipes (E), and Clostridium (F) in feces from 10 month old F1 transplant mice, comparing to that of Mouse #96.

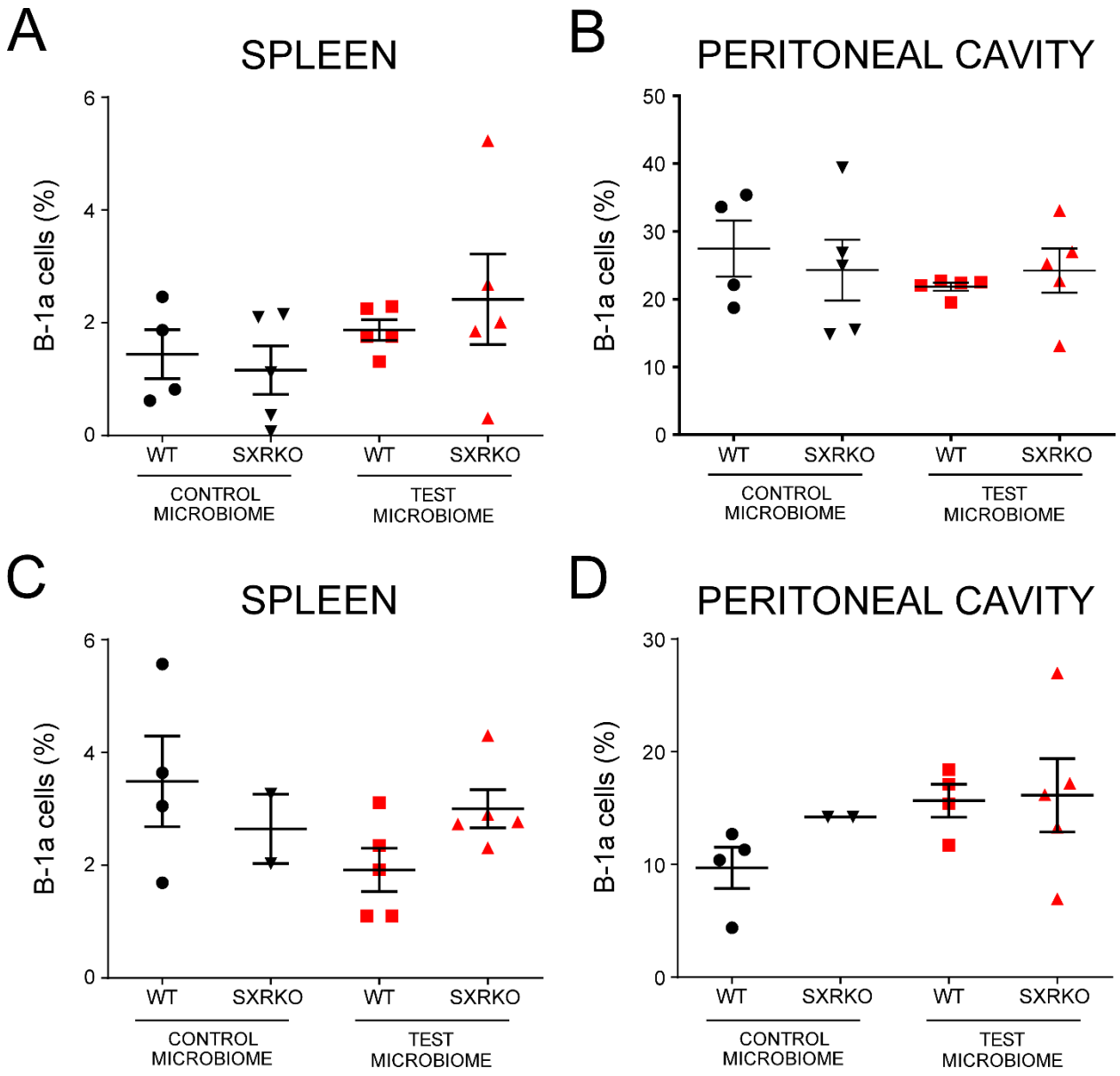

<u>Figure 2.6</u>: F0 WT and SXRKO mice of either transplant microbiome group do not display B-1a cell lymphoma. Percentage of B-1a cells in spleen (A) and peritoneal cavity (B) of F0 male mice, determined by flow cytometry analysis. Percentage of B-1a cells in the spleen (C) and peritoneal cavity (D) of F0 female mice, determined by flow cytometry analysis.

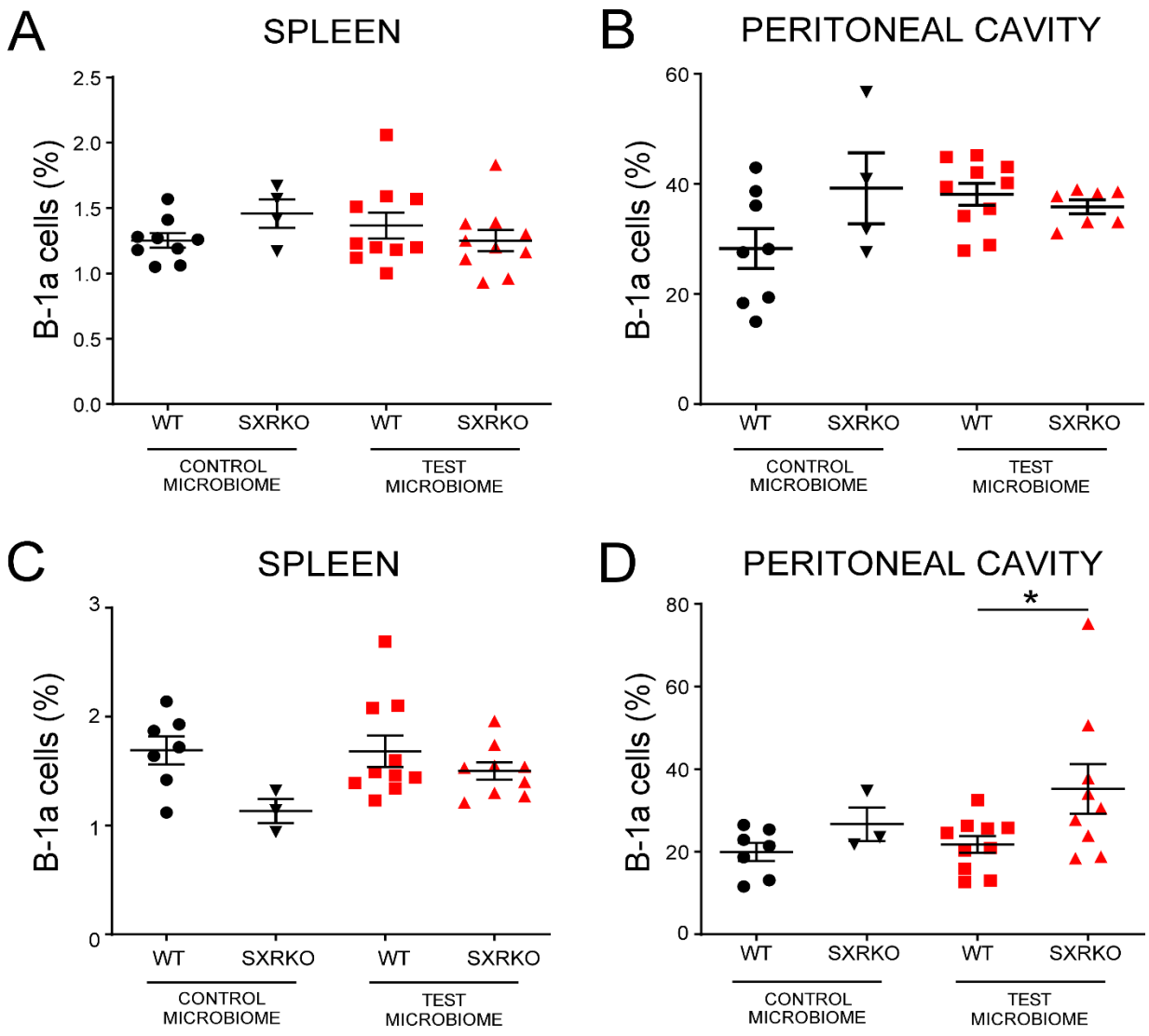

<u>Figure 2.7</u>: F1 WT and SXRKO mice of either transplant microbiome group do not display B-1a cell lymphoma. Percentage of B-1a cells in spleen (A) and peritoneal cavity (B) of F1 male mice, determined by flow cytometry analysis. Percentage of B-1a cells in the spleen (C) and peritoneal cavity (D) of F1 female mice, determined by flow cytometry analysis.

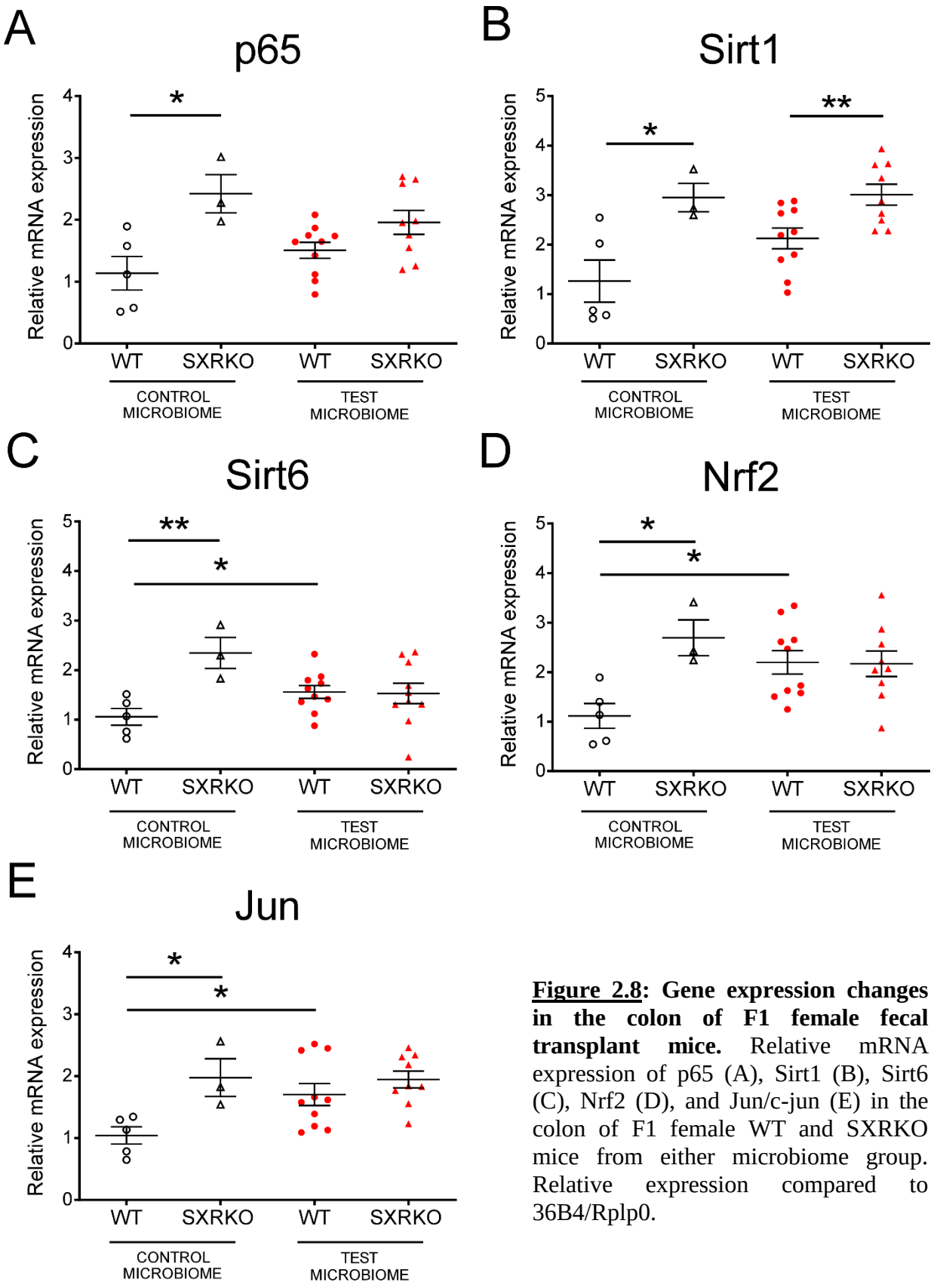

<u>Figure 2.8</u>: Gene expression changes in the colon of F1 female fecal transplant mice. Relative mRNA expression of p65 (A), Sirt1 (B), Sirt6 (C), Nrf2 (D), and Jun/c-jun (E) in the colon of F1 female WT and SXRKO mice from either microbiome group. Relative expression compared to 36B4/Rplp0.

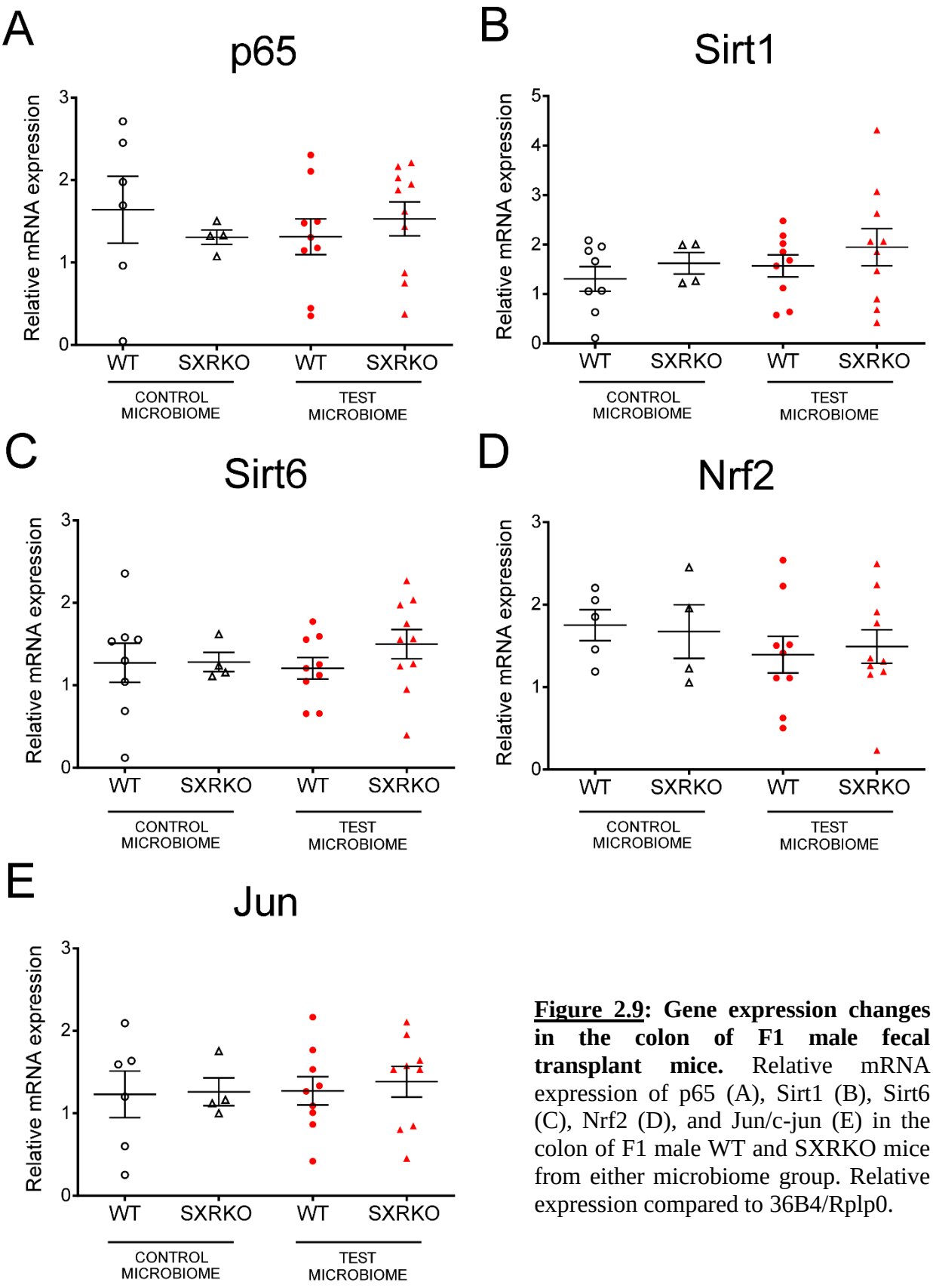

Figure 2.9: Gene expression changes in the colon of F1 male fecal transplant mice. Relative mRNA expression of p65 (A), Sirt1 (B), Sirt6 (C), Nrf2 (D), and Jun/c-jun (E) in the colon of F1 male WT and SXRKO mice from either microbiome group. Relative expression compared to 36B4/Rplp0.

Table 2.1: qPCR primer sequences

Gene	Forward primer	Reverse primer
Mouse 36B4/Rplp0	AAGCGCGTCCTGGCATTGTCT	CCGCAGGGGCAGCAGTGGT
Universal 16S rRNA	ACTCCTACGGGAGGCAGCAGT	ATTACCGCGGCTGCTGGC
Mouse p65	AGAGAAGCACAGATACCACC	TCAGCCTCATAGTAGCCATCC
Mouse Sirt1	TATCCTTTCAGAACCACCAAAGCG	TCAGGAATCCCACAGGAGACAG
Mouse Sirt6	TCCCAAGTGTAAGACGCAGTACG	CAACGAGTCCTCCCAGTCCA
Mouse Nrf2	GAAAGACAAGAGCAACTCCA	TACAGTCTTCAAAGTACAAGGC
Mouse Jun	GCCAGCAACTTTCCTGACCC	TGAGTATAGGTTCCTCTTCTCCCT

CHAPTER 3

Increasing abundance of *Akkermansia muciniphila* and *Prevotella copri* in the gut microbiome leads to increased B-1a B cell content in the peritoneal cavity of mice lacking the Steroid and Xenobiotic Receptor (SXR/PXR), but does not induce development of B-1a B cell lymphoma

Summary

The gut microbiome affects numerous physiological functions including inflammation, immune cell development, and even neurological processes. In addition, single microbial species have shown to induce specific effects on the host that go as far as promoting, or treating disease. Mice lacking the Steroid and Xenobiotic Receptor (SXR/PXR) were reported to develop a B-1a B cell lymphoma phenotype. This phenotype disappeared following a change in the diet of our SXR knockout (SXRKO) mouse colony and was not recovered following a switch back to the original diet. We hypothesized that the initial change in diet led to the loss of certain microbial species that were important for the development of the B-1a B cell lymphoma phenotype in SXRKO mice. We aimed to determine what microbes were different between mice that displayed a B-1a B cell lymphoma phenotype and those that did not by conducting 16S rRNA sequencing on archival samples and samples from our current colony of mice that no longer displayed a lymphoma phenotype. From this analysis, we selected two candidate microbes: *Prevotella* and *Akkermansia*. We administered these microbes to wild-type and SXRKO mice and evaluated animals for signs of B-1a B cell lymphoma at 10 months of age. Increasing the abundance of both microbes in the gut resulted in increased percentages of B-1a B cells in the peritoneal cavity of SXRKO mice compared to wild-type controls. There were no increases in the percentage of

B-1a B cells in the spleen, indicating that there was no B-1a B cell lymphoma in the treated animals. We speculate that the increase of peritoneal cavity percentage of B-1a B cells in SXRKO mice is due to increased intestinal permeability leading to elevated levels of bacteria reaching the peritoneal cavity and, therefore, inducing an elevated immune response.

Introduction

The complex community of microorganisms present in the gut, known as the gut microbiome, has been shown to impact both health and disease[59]. Perturbations to the gut microbiome composition, or dysbiosis, have been associated with gut-related diseases in humans, such as inflammatory bowel disease[27, 28], as well as extra-intestinal conditions, such as obesity, cardiovascular disease, and autism[25, 59, 84]. Rodent studies have also demonstrated these associations and provided more direct links between the microbiome and disease states of the host[62, 85-88]. Microbiomes have shown to differ between common mouse strains originating from different vendors, and even among different rooms at an individual vendor, and these differences have demonstrated to impact phenotypes[89-91].

In addition to overall microbiome dysbiosis, differences in the abundance of individual microbes has also been shown to impact the development of human and rodent disease phenotypes. For example, segmented filamentous bacteria (SFB) were shown to impact immune development in mice and the development of mouse disease models through their ability to induce IL-17 producing T-helper (Th-17) cells[89, 90, 92]. While the presence of this microbe has been demonstrated to impact mostly gut related inflammatory conditions, the presence of SFB also impacts the development of an autoimmune arthritis in mice; germ-free mice had a strong attenuation of the arthritis phenotype and the addition of SFB alone recovered the phenotype[93]. Other commensal gut microbes have also demonstrated to impact mouse models. For example, *Prevotella copri* was also shown to increase susceptibility to arthritis in a murine disease model[88], and *Helicobacter pylori* and *Helicobacter felis* have been shown to be required for the development and progression of cancers of the gut in several murine models, mimicking H. pylori induced stomach cancer in humans[94, 95].

SXR/PXR is a ligand activated nuclear receptor involved in xenobiotic metabolism expressed highly in the liver and intestine[6]. SXR also has a mutually inhibitory relationship with NF-κB, a major transcription factor involved in the inflammatory response[53]. SXR null (SXRKO) mice display elevated levels of inflammatory cytokines in the intestine and colon[53]. In addition, SNPs of the SXR locus have been associated with increased susceptibility to IBD[45]. Despite the connections between IBD and SXR, the interaction between SXR and the gut microbiome, and to the disease outcomes associated with alterations to the gut microbiome, have not been highly investigated.

Some studies have demonstrated interactions between SXR and the gut microbiome. For example, induce microbiota dysbiosis through a SXR-dependent mechanism[29]. It was also demonstrated that a bacterial metabolite, indole 3-propionic acid (IPA), interacts with SXR/PXR to regulate intestinal permeability[21]. This study also showed that SXRKO mice have increased intestinal permeability and inflammation. Increased intestinal permeability, or "leaky gut", has been demonstrated to lead to increased translocation of bacteria or bacterial components through the gut mucosa to the peritoneal cavity, bloodstream, and extraintestinal organs to induce immunological impacts[96-99].

Chapter 1 discussed how a B-1a B cell lymphoma phenotype, first reported in 2011 and characterized by increased percentages of B-1a B lymphocytes in various tissues and tumors in multiple tissues[5], was lost in our colony of SXRKO mice following a change in the diet and it was not recovered following a switch back in the diet. Due to the overwhelming evidence that diet greatly impacts the gut microbiome[58, 62, 100] and that gut microbes can have huge impacts on mouse phenotypes, we hypothesized that the change in diet altered the gut microbiome of our SXRKO mouse colony leading to the loss of the B-1a B cell lymphoma phenotype.

In an attempt to discover what microbes were different in mice that displayed the lymphoma phenotype and those that did not, as well as which ones had changed due to the diet, we conducted 16S rRNA sequencing on current day and archival samples from mice with intestinal B-1a B cell lymphoma. From this analysis, we obtained candidate microbes to investigate further. *Prevotella copri* and *Akkermansia muciniphila* populations were greatly increased in abundance in the gut microbiome of wild-type (WT) and SXRKO mice. F0 and F1 mice from this study were investigated at 10 months of age for signs of the B-1a B cell lymphoma phenotype. Expansion of both microbes in the gut led to increased percentages of B-1a B cells in the peritoneal cavity of SXRKO mice compared to WT controls. Additional gene expression analysis revealed that SXRKO mice had increased expression of genes encoding tight junction proteins in the intestine compared to WT mice. Therefore, our results suggested that expansion of *Prevotella copri* and *Akkermansia muciniphila* in the gut of SXRKO mice led to an increased percentage of B-1a B cells in the peritoneal cavity as a result of increased intestinal permeability and/or inflammation. Whether this finding would eventually lead to increased percentages of B-1a B cells in other tissues and be involved in the development of the B-1a B cell lymphoma phenotype is not known and still needs to be investigated in the future.

Materials and Methods

Mouse maintenance: Wild-type and SXRKO (C57BL/6J) mice were equally maintained and housed by the Blumberg lab at the University of California, Irvine. SXRKO mice were descendants from a colony of 129S6/SvEv mice from the Salk institute and were backcrossed onto C57BL/6J background strain for 6 generations to obtain an essentially pure C57BL/6J background. Mice were maintained on standard rodent chow, ProLab RMH 2500/5P14 (LabDiet). Water and food were provided ad libitum. Mouse cages were enriched with wood chip bedding and additional cotton nestlets. All experiments were carried out in accordance with the Institutional Animal Care and Use Committee at the University of California, Irvine, and were consistent with Federal guidelines.

Fecal sample collection and analysis: Fecal samples were collected from all mice, flash frozen, and stored at -80˚C. Fecal DNA was extracted using the PowerFecal DNA kit (MO BIO/Qiagen).

Extraction of DNA from paraffin-embedded intestine samples: Excess paraffin was trimmed away from paraffin-embedded tissue sections then the remaining tissue was placed in a microcentrifuge tube. DNA was extracted using the QIAamp DNA FFPE Tissue Kit (QIAGEN) according to manufacturer's protocol. DNA was precipitated with 100% ethanol and sodium acetate, washed with ethanol, and resuspended in 10 mM Tris pH 8.0, 0.1 mM EDTA buffer.

16s rRNA sequencing: microbial DNA was amplified for the V3-V4 variable regions of the 16S rRNA gene. DNA libraries were prepared by the UCI Genomics High Throughput Facility following the Illumina protocol for 16S rRNA metagenomic sequencing library preparation. 16S rRNA sequencing was performed on Illumina MiSeq with 2x300bp paired-end reads at the Institute for Integrative Genome Biology at the University of California, Riverside. Fastq files were processed using QIIME[65].

QIIME microbiome sequencing analysis: Paired-end reads were joined using the fastq-join function. Joined files were then quality filtered and merged into one data file with each sample labeled by the file name using the multiple_split_libraries_fastq.py function. The seqs.fna file from the previous command was then filtered to remove any chimeric sequences using Usearch6.1[66], installed within QIIME. Chimeric sequencing were identified using the identify_chimeric_seqs.py and the recent Greengenes reference sequence file (gg_13_8_otus.fasta)[67]. The discovered chimeric sequences were then removed from the seqs.fna file using the filter_fasta.py command. The chimeras.txt file obtained from the previous command and the added parameter of "-n". OTU picking was then conducted on the newly filtered sequencing file using the pick_de_novo_otus.py command using Usearch6.1 as the OTU picking method and Uclust for assigning taxonomy to the OTUs[68]. This step was conducted on the UCI high performance computer (HPC) cluster. Taxonomy assignments were summarized into a readable format using the summarize_taxa_through_plots.py and the otu_table.biom file generated in the previous command. Visualizations and statistical analyses were conducted using Calypso[69].

Culturing of Prevotella copri and Akkermansia muciniphila: Freeze-dried human fecal isolates of *Prevotella copri* and *Akkermansia muciniphila* from were obtained from DSMZ (Germany). Pellets were resuspended in PYG Tween FA/GLC media (Anaerobe Systems) under anaerobic conditions (0% O_2, 5% CO_2, 2.5% H_2). Bacteria concentration was determined by measuring optical density at 600 nm (OD_{600}). Bacteria was expanded during the exponential growth period by dilution bacteria 1:10 fresh PYG Tween FA/GLC media. *Prevotella copri* took approximately 24 hours to reach stationary phase. *Akkermansia muciniphila* took approximately 48 hours to reach stationary phase.

Bacterial reconstitution experiments: 6-8 week old male and female WT and SXRKO mice were treated with an antibiotic cocktail (1 g/L Ampicillin, 1 g/L Metronidazole, 0.5 g/L Vancomycin, 1 g/L Neomycin) via drinking water for 4 weeks to clear the existing commensal microbiome. Antibiotic treatment water was replaced every 48 hours. Two days after the end of the antibiotic treatment, mice received 100 µL of solution containing approximately $2.6x10^7$ CFU of *Prevotella copri*, *Akkermansia muciniphila*, or a 1:1 mixture of the two microbes via oral gavage for three doses given every other day. Control mice received 100 µL of media alone. Upon successful bacteria reconstitution, these mice were then bred at 20 weeks old and their pups were studied. Both F0 and F1 generations were analyzed at 10 months of age for signs of B-1a B cell lymphoma. Diagram of experimental design found in Figure 3.4.

Peritoneal cavity lavage: Mice were euthanized by isoflurane overdose and cardiac puncture. The skin was carefully cut to reveal the peritoneum without puncturing or nicking it. 9 mL of ice cold FACS buffer was injected into the peritoneum, avoiding injecting organs. The filled peritoneum was then agitated to dislodge any cells then a syringe and 25-gauge needle were used to extract the large amount of liquid from the peritoneum. A pipet was then used to extract the small amount of remaining liquid from the peritoneum. RBCs were lysed by incubating cell suspension in ACK lysis buffer (150 mM NH4Cl, 10 mM KHCO3, 0.1 mM Na2EDTA) for 5 min. Cells were washed and resuspended in FACS buffer (PBS, 1% FBS, 0.02% sodium azide) at 400K cells/mL for antibody staining and flow cytometric analysis.

Tissue collection: Liver, small intestine, colon, caecum, and spleen tissues were dissected, flash frozen in liquid N_2 and stored at -80˚C. A section of the spleen was set aside before flash freezing to undergo splenocyte isolation.

Spleen cell isolation: Spleen sections were physically dissociated using a petri dish and syringe plunger in 1 mL of ice-cold PBS containing 1% FBS. RBCs were lysed by incubating cell suspension in ACK lysis buffer (150 mM NH4Cl, 10 mM KHCO3, 0.1 mM Na2EDTA) for 5 min. Cells were washed, resuspended in FACS buffer (PBS, 1% FBS, 0.02% sodium azide), and filtered through a 100 µm cell strainer to yield single cells for antibody staining and flow cytometric analysis.

Flow cytometry (FACS) analysis: RBC-depleted spleen and peritoneal cavity cells were diluted in cold FACS buffer (PBS, 1% FBS, 0.02% sodium azide), aliquoted at 200K cells, stained with and antibody cocktail of anti- mouse CD5-APC (eBioscience), CD19-PE (eBioscience), and IgD-FITC (eBioscience) for 30 min. Cells were measured on a BD LSR II cytometer. Data was analyzed using FlowJo software (Treestar).

RNA isolation: Frozen tissue sections were homogenized rapidly in 1 mL of Trizol reagent (ThermoFisher Scientific). RNA was isolated from the tissue-Trizol homogenate by phenol/chloroform extraction. RNA was precipitated with an equal volume of 100% isopropanol, centrifuged and salt removed by washing with 70% ethanol. Final RNA product was resuspended in DNase/RNase-free sterile, ultrapure water (ultrafiltered, UV sterilized water from Barnstead Nanopure water system, hereafter called nanopure water), quantified by spectrophotometry, and integrity verified by denaturing agarose gel electrophoresis.

cDNA synthesis: cDNA was synthesized using 2 µg of intact total RNA and Superscript III reverse transcriptase (Applied Bioscience) according to manufacturer's protocol. Synthesized cDNA was diluted 5-fold with nanopure water for downstream qPCR analysis.

Designing qPCR primers: Gene sequences were obtained from Ensembl genome browser. PerlPrimer was used to design and identify candidate forward and reverse primers. Primer oligos

were ordered from Sigma-Aldrich and resuspended in 10 mM Tris pH 8.0, 0.1 mM EDTA buffer. Primer sequences can be found in Table 3.1.

Quantitative real time reverse transcriptase PCR (qPCR): Diluted cDNA was combined with SYBR green qPCR Master Mix (Applied Biosystems) and the primer mix for gene of interest and run on the Roche LightCycler 480. Technical replicate Ct values were averaged for each biological replicate. Mean Ct values were normalized to 36B4/Rplp0 (ΔCt), and relative fold change mRNA levels were then calculated by using ΔΔCt method[70] with relative gene expression presented as mean fold change over vehicle control ± SEM. For qPCRs to quantify bacteria abundance, Ct values for bacteria of interest was normalized by total 16S rRNA gene Ct value to get percent of total bacteria and/or divided by the weight of the fecal sample to get approximate bacterial abundance in fecal sample (arbitrary unit (AU)/weight of fecal sample).

Statistical analysis: Data visualization and statistical analyses were conducted in Prism 8 (GraphPad Software), except for 16S rRNA sequencing analysis, which was conducted in Calypso[69]. Unpaired t-test was used to determine statistical significance. * = p-value <0.05, ** = p-value <0.01, ***= p-value <0.001, #= p-value <0.0001

Results

16S rRNA sequencing of current and archival samples to obtain candidate microbes that might be important for the B-1a B cell lymphoma phenotype of SXRKO mice

We conducted 16S rRNA sequencing of both current and archival samples aiming to reveal what microbes were different between mice displaying a lymphoma phenotype and those that did not. The archival samples included DNA extracted from paraffin-embedded intestinal tissue from SXRKO mice that displayed intestinal tumors, SXRKO mice that did not display tumors, and wild-type (WT) mice. This analysis revealed that the microbiome composition of the tumor-bearing mice was the most different compared to the other groups when investigating the operational taxonomic units (OTUs) that resulted from the 16S rRNA sequencing analysis (Figure 3.1). Several bacterial genera showed a statistically significant difference in abundance in the tumor-bearing SXRKO mice compared to either WT mice or SXRKO mice that did not present tumors (Table 3.2). For example, the genera *Prevotella* and *Sphingomonas* were significantly more abundant in SXRKO mice with tumors compared to WT controls (Figure 3.2A, D) and *Sutterella* and *Lactobacillus* were increased in SXRKO mice with tumors compared to both WT and non-tumor bearing SXRKO mice (Figure 3.2B-C).

We also compared the results of the archival samples, using the paraffin-embedded tissue sections, to the microbiome composition of mice in our current colony, utilizing fecal samples from the F1 diet experiment mice described in **Chapter 1**, including Mouse #96. This comparison revealed significant differences in the genera *Acinetobacter*, *Akkermansia*, *Methylobacterium*, and *Sphingomonas*, all of which were increased in the archival tumor-bearing SXRKO mice compared to the current SXRKO mice samples (Figure 3.3, Table 3.3). These differences should be viewed with some caution since we are comparing two different sources of

microbial DNA (paraffin-embedded intestinal tissue vs fecal sample). The fecal samples contain vastly more microbes than the proximal gut, and the composition of microbes present in these two areas is also different[101].

From the 16S rRNA sequencing results, we decided to further investigate the microbes *Prevotella* and *Akkermansia*. *Prevotella* abundance was significantly increased in tumor-bearing SXRKO mice compared to WT mice in the archival paraffin-embedded intestinal tissues (Figure 3.2A). Several *Prevotella* species have been demonstrated to be increased in patients with colorectal cancer and *Prevotella* abundance is impacted by the diet[102-104], making it a relevant candidate bacterium to investigate in our study. *Akkermansia* was chosen because it has been associated with colon tumorigenesis in murine models[105, 106], and was increased in the archival SXRKO samples compared to current samples from SXRKO mice that do not display tumors or the B-1a B cell lymphoma phenotype (Figure 3.3B).

Increased colonization of Prevotella and Akkermansia in the gut induced increases in B-1a B cell percentage in the peritoneal cavity of SXRKO mice

We asked if increasing the abundance of *Prevotella* and *Akkermansia* in the gut of SXRKO would push the development of the B-1a B cell lymphoma phenotype. To do this, human gut isolates of *Akkermansia muciniphila* and *Prevotella copri* were cultured and then administered to mice via oral gavage, following a 4 week antibiotic treatment course to reduce the commensal microbiome. WT and SXRKO mice received either *Prevotella copri*, *Akkermansia muciniphila*, or the 1:1 mixture of the two (Figure 3.4). The microbiomes of these mice were monitored before and after the antibiotic treatment and after the reconstitution of the selected microbes. These results demonstrated that *Akkermansia* was successful colonized in mice that received either *Akkermansia* alone or the combination (Figure 3.5A). *Prevotella*,

however, failed to colonize without the presence of *Akkermansia* (Figure 3.5B). Therefore, we removed the *Prevotella*-only group from analysis for this experiment (Figure 3.4). After successful colonization of the bacteria, the mice were bred to obtain a F1 generation that was developmentally exposed to the new microbiome. Both the F0 and F1 mice were aged until 10 months of age and investigated for signs of B-1a B cell lymphoma. F0 male SXRKO mice had increased percentage of B-1a B cells in the peritoneal cavity independent of the bacteria treatment group, although it was only statistically significant in the mice administered *Akkermansia* alone (Figure 3.6 B). This was interesting because we had not seen an increase in B-1a B cell content in this tissue of SXRKO mice in other experiments (**Chapter 1 and 2**). Even although there was an increase in B-1a B cell percentage in the peritoneal cavity of SXRKO males, this was not associated with any increase in the splenic B-1a B cell content, indicating these mice did not have a B-1a B cell lymphoma. (Figure 3.6A). No change was observed in either tissue for the F0 females in the bacteria groups (Figure 3.6C-D). There was a difference between WT and SXRKO in the peritoneal cavity of F0 female mice administered media only. However, it appears that the difference is due to a decrease in WT B-1a B cell content (Figure 3.6C).

The F1 SXRKO mice from the *Akkermansia* or *Akkermansia+Prevotella* bacterial groups demonstrated increased percentages of B-1a B cells in the peritoneal cavity compared to WT controls, and this was observed for both males and females (Figure 3.7 B, D). For these mice, we also did not observe any increase in B-1a B cell content in the spleen, indicating the absence of B-1a B cell lymphoma (Figure 3.7 A, C). Increased percentage of B-1a B cell content in the peritoneal cavity was observed in both F0 and F1 generations, although it was strongest in the F1 generation. This suggests that the expansion of *Prevotella copri* and *Akkermansia muciniphila* in

the gut led to some innate immune response in SXRKO mice and that earlier and/or developmental exposure to the altered microbiome yielded a stronger phenotype.

Increased expression of tight junction related genes and Sirtuin 1 in the colon of SXRKO mice

Since we observed an increase in the percentage of B-1a B cells present in the peritoneal cavity of SXRKO mice that possessed increased abundance of *Akkermansia muciniphila* and *Prevotella copri* in the gut, we asked whether this could be due to increased intestinal permeability of the bacteria or bacterial components. SXRKO mice have been previously reported to have increased intestinal permeability. Therefore, we investigated the mRNA expression of genes encoding tight junction proteins in the colon, including tight junction protein 1 (Tjp1), occluding (Ocln), and E-cadherin (Cdh1). We observed trends for inherent increases in Tjp1, Ocln, and Cdh1 in the colon of F1 male SXRKO mice compared to WT controls (Figure 3.8A-C). F1 female SXRKO mice displayed trends for increased expression for all tight junction genes, most notably with Tjp1, in the colon for all bacteria groups compared to WT mice of the respective group (Figure 3.9A-C). Ocln expression was also increased in jejunums of F1 male SXRKO mice in the media only group compared to WT controls (Figure 3.10B). These results demonstrated increased expression of genes related to tight junctions in the gut, which is likely a response to the altered gut microbiome and/or increased intestinal permeability.

Sirtuins have shown to have anti-inflammatory properties in the intestine. Recently, a knockout of Sirt2 resulted in increased intestinal permeability in mice. We previously observed increased sirtuin expression in SXRKO mice (**Chapter 2**). In this study, we observed an increase in Sirt1 expression in SXRKO mice in the media only group compared to WT controls, although it did not reach statistical significance (Figure 3.8D, 3.9D).

Discussion

We identified several bacterial groups that were different between SXRKO mice that possessed tumors and SXRKO and WT mice that did not. We also identified a number of microbes significantly different between the archival samples and present day samples. Both analyses provided us with candidate microbes that could have been important for the development of the B-1a B cell lymphoma phenotype.

We performed bacterial reconstitution experiments with *Akkermansia*, which was increased in archival samples compared to present day samples, and *Prevotella*, which was increased in tumor bearing SXRKO mice compared to non-tumor bearing mice from the same experiment and cohort. Increasing the abundance of both microbes in the gut led to increased percentages of B-1a B cells in the peritoneal cavity of SXRKO mice compared to wild-type controls. This increase was observed in both the F0 and F1 generation.

The increase in B-1a B cell content in the peritoneal cavity was not accompanied by an increase in B-1a B cell percentage in the spleens, indicating an absence of the B-1a B cell lymphoma phenotype. It is possible that the candidate microbes we chose to investigate were not the only ones important for the development of the B-1a B cell lymphoma phenotype. Unfortunately, we did not possess the necessary samples to accurately compare the microbiomes between the mice that had the lymphoma phenotype vs those that do not, since we do not have a current colony of SXRKO mice displaying the phenotype and fecal samples were not saved from the previous colonies that did. There were also other microbes that were present at statistically significant levels in the analyses that we conducted that we were not able to investigate *in vivo*. It is possible that one of these other microbes is important for the progression of the B-1a B cell lymphoma phenotype either alone, or in combination with *Prevotella* or *Akkermansia*.

It is also possible that we did not observe the B-1a B cell lymphoma in this experiment because we did not let the mice age long enough. It was reported that SXRKO mice display increased B-1a B cell percentages at 5 months of age and tumors between 6-7 months of age[5]. Although we went beyond this age, it is possible that these mice could have been developing the phenotype slower due to nonideal conditions.

Age related microbiome dysbiosis can lead to increased intestinal permeability. With increased intestinal permeability, higher amounts of bacteria and bacterial components can cross the mucosal barrier and enter the peritoneal cavity and blood stream. There is no evidence that bacterial infection can induce a B-1a B cell lymphoma, however, it has been demonstrated to encourage autoimmune disorders, which are associated with an increased risk for developing lymphomas[107]. The peritoneal cavity contains large number of lymphocytes, many of which are innate immune cells that are the first responders against pathogens[108]. B-1a B lymphocytes are a subset of innate immune cells that are found at a high percentage in the peritoneal cavity, are autoreactive and, therefore, implicated in autoimmunity[108, 109]. We infer that the increases in peritoneal B-1a B cell content observed in this study is likely due to increased amount of bacteria and/or bacterial components reaching the peritoneal cavity as a result of the increased intestinal permeability. Whether this increased intestinal permeability of SXRKO mice could lead to or promote the development of B-1a B cell lymphoma has yet to be determined.

Since SXRKO mice have previously been reported to have increased intestinal permeability, we speculate that the increased expression of multiple tight junction genes and sirtuins observed in this study is due to the elevated intestinal permeability and inflammation that has previously been reported in SXRKO mice. Overall, this study suggests that perturbations to the gut microbiome leads to an increased innate immune response in the peritoneal cavity of

SXRKO mice, observed as an increase in B-1a B cell content, which is likely due to the elevated intestinal inflammation and permeability reported in these mice.

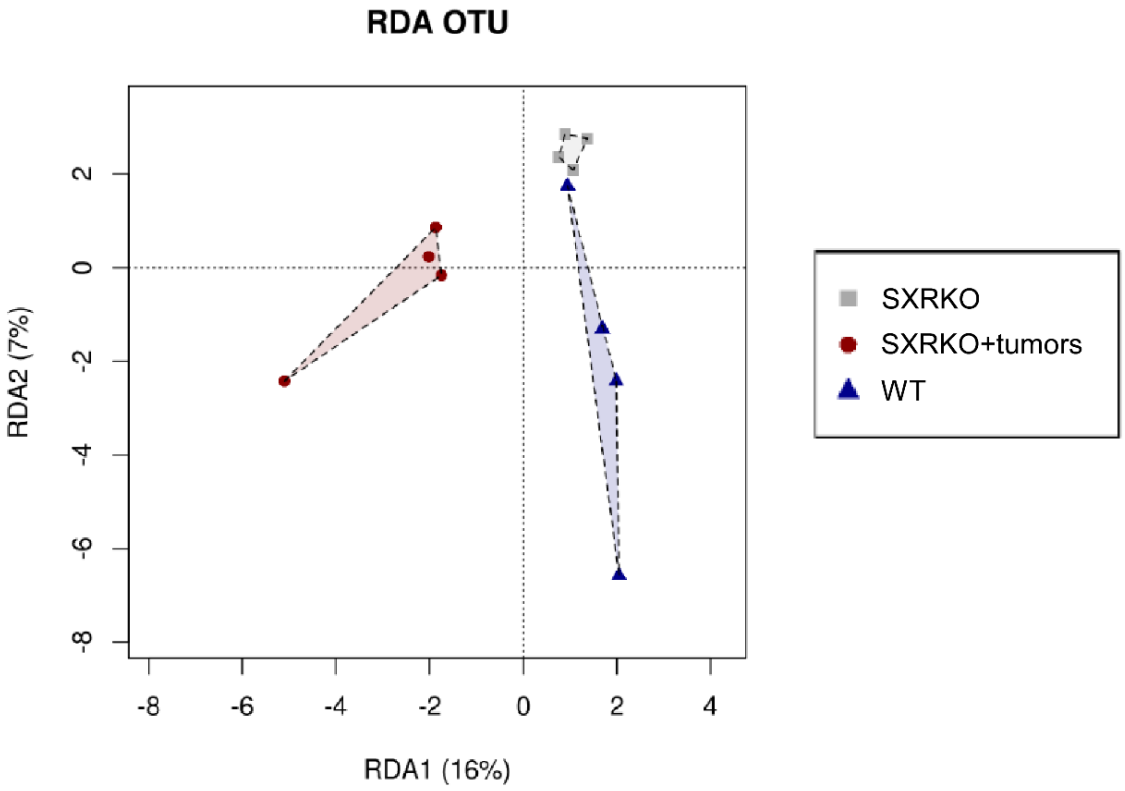

<u>Figure 3.1</u>: Redundancy Analysis (RDA) of OTUs obtained from 16S rRNA sequencing of paraffin-embedded intestinal tissue from WT, SXRKO, and tumor-bearing SXRKO mice.

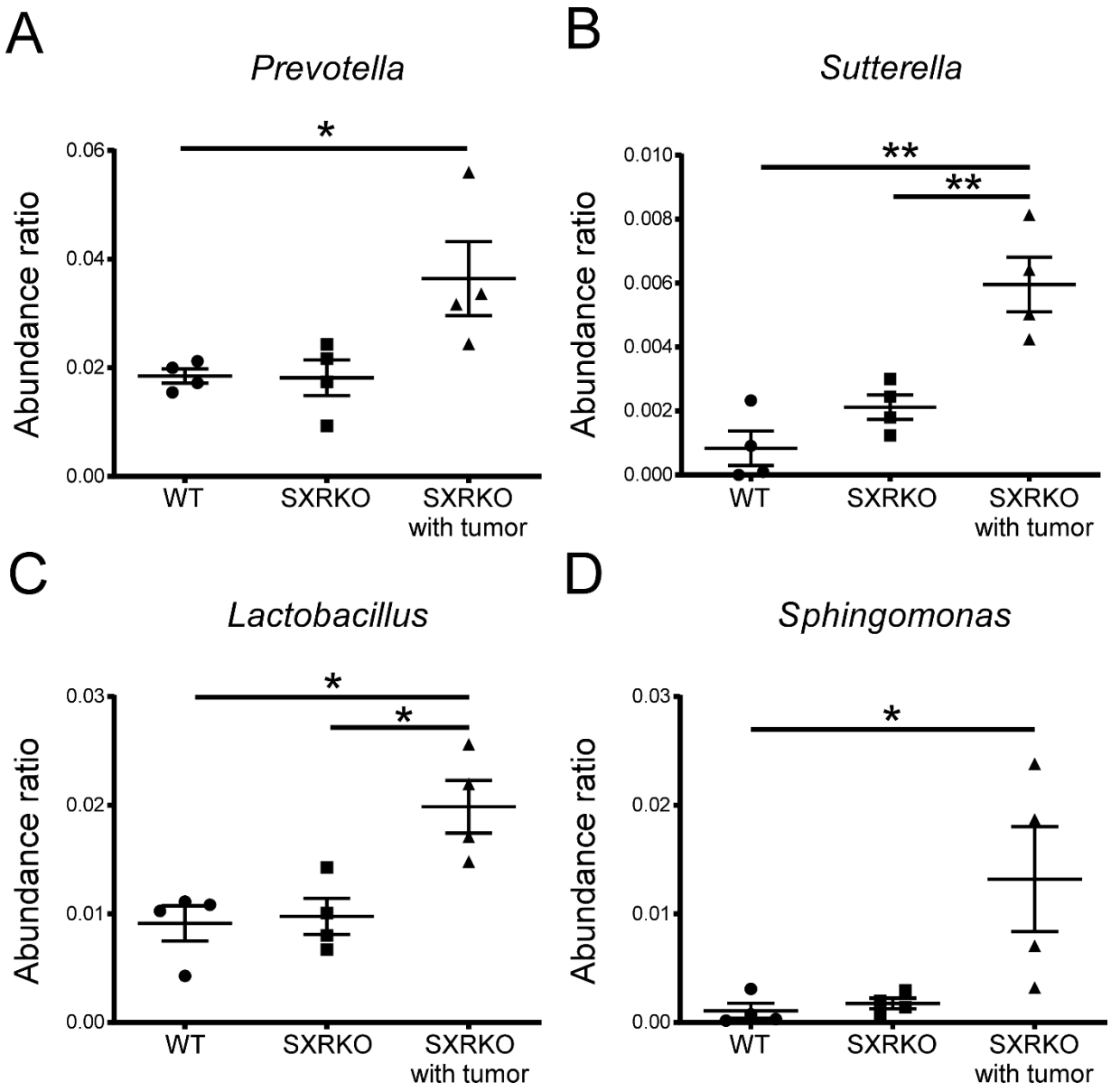

<u>Figure 3.2</u>: Abundance ratios of significantly different genera in paraffin-embedded intestinal tissue of tumor bearing SXRKO mice compared to non-tumor bearing SXRKO mice and WT mice. Abundance ratios of genera *Prevotella* (A), *Sutterella* (B), *Lactobacillus* (C), and *Sphingomonas* (D) determined by 16S rRNA sequencing analysis of paraffin-embedded intestinal tissue from WT, SXRKO, and tumor bearing SXRKO mice.

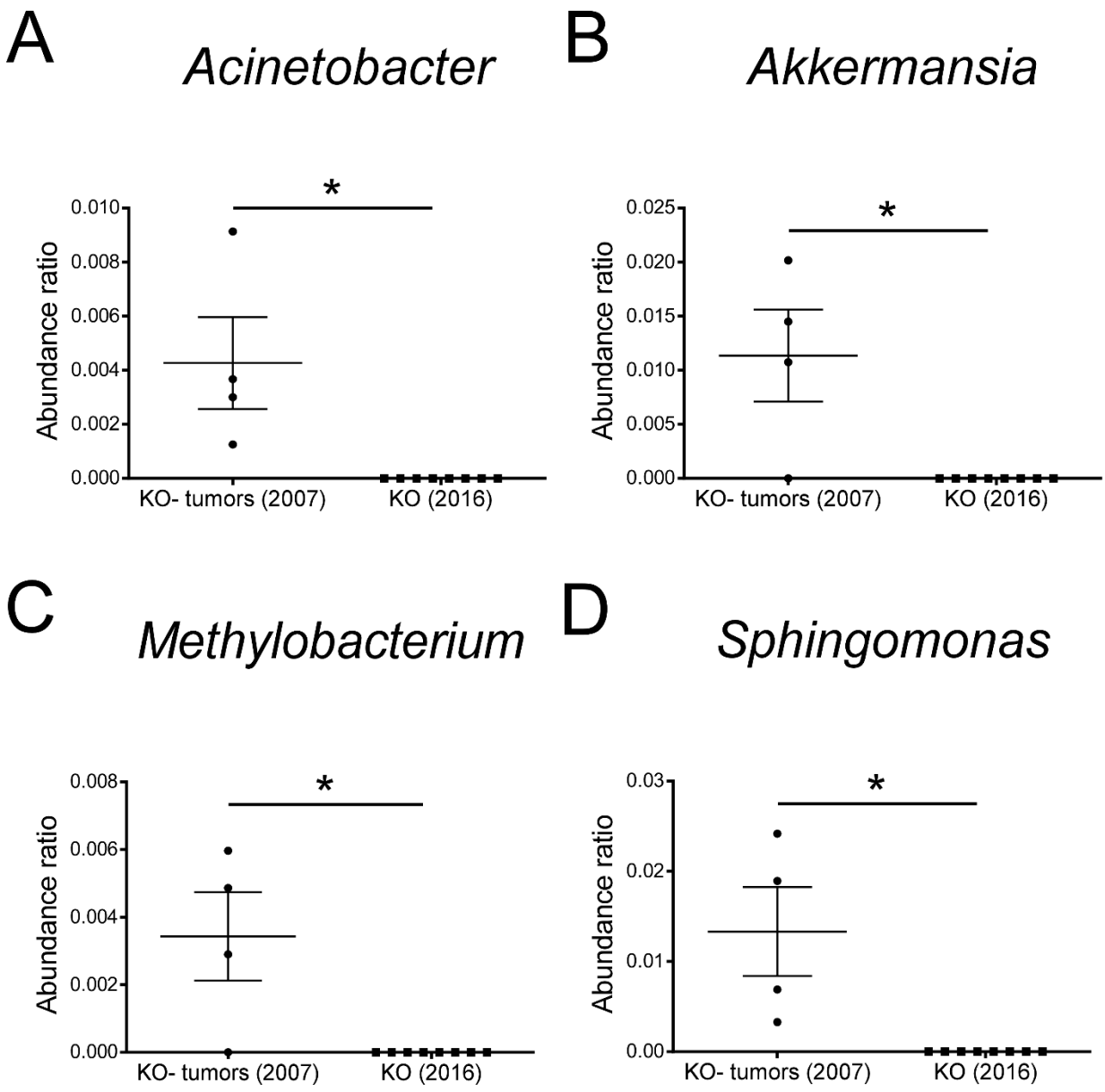

<u>Figure 3.3</u>: Abundance ratios of significantly different genera between historic paraffin-embedded intestinal tissue of SXRKO mice and current fecal samples from non-tumor bearing SXRKO mice. Abundance ratios of genera *Acinetobacter* (A), *Akkermansia* (B), *Methylobacterium* (C), and *Sphingomonas* (D) determined by 16S rRNA sequencing analysis of paraffin-embedded intestinal tissue from SXRKO from 2007 and fecal samples from 2016 SXRKO colony.

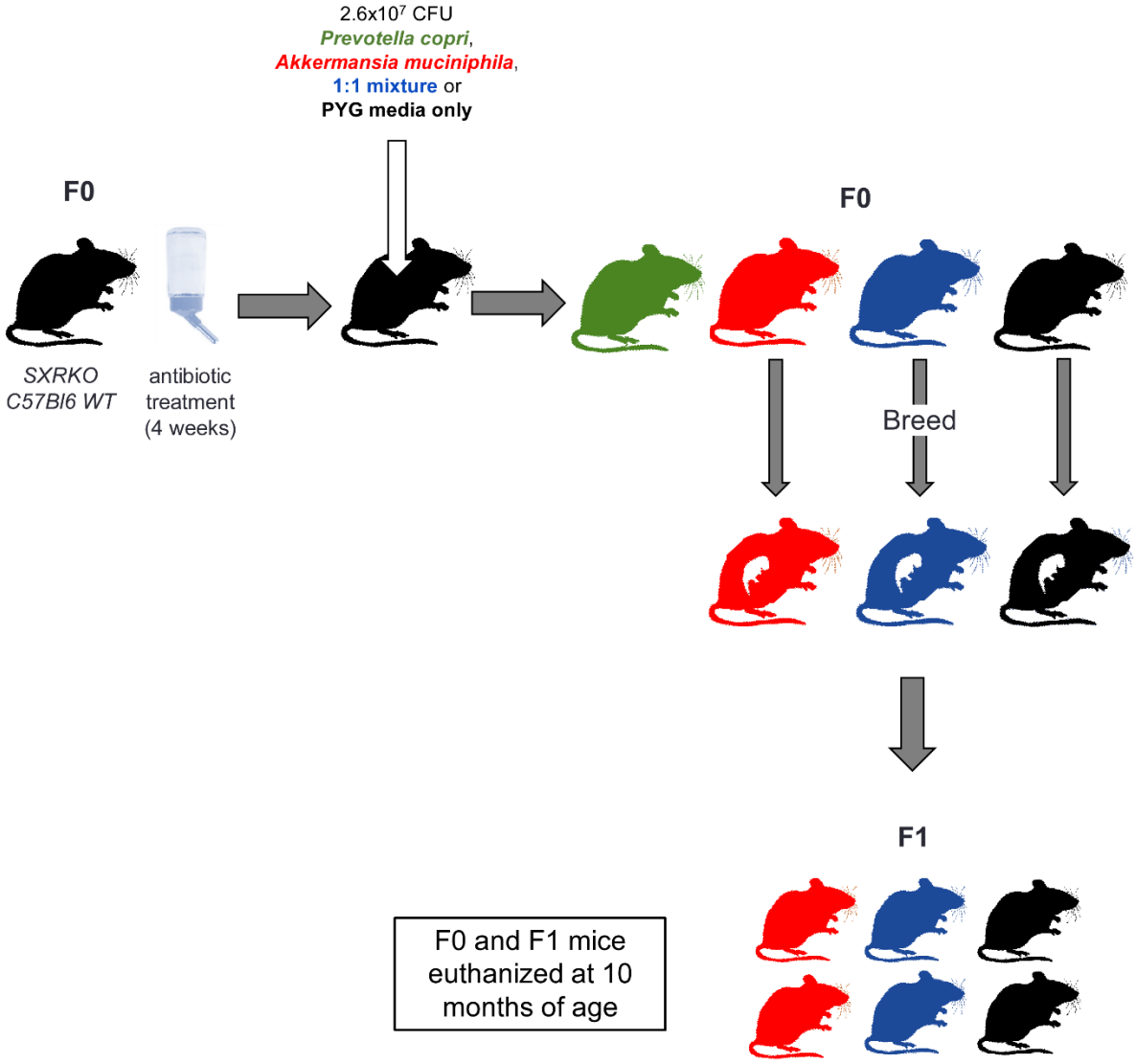

Figure 3.4: Experimental design for microbiome bacteria expansion experiment

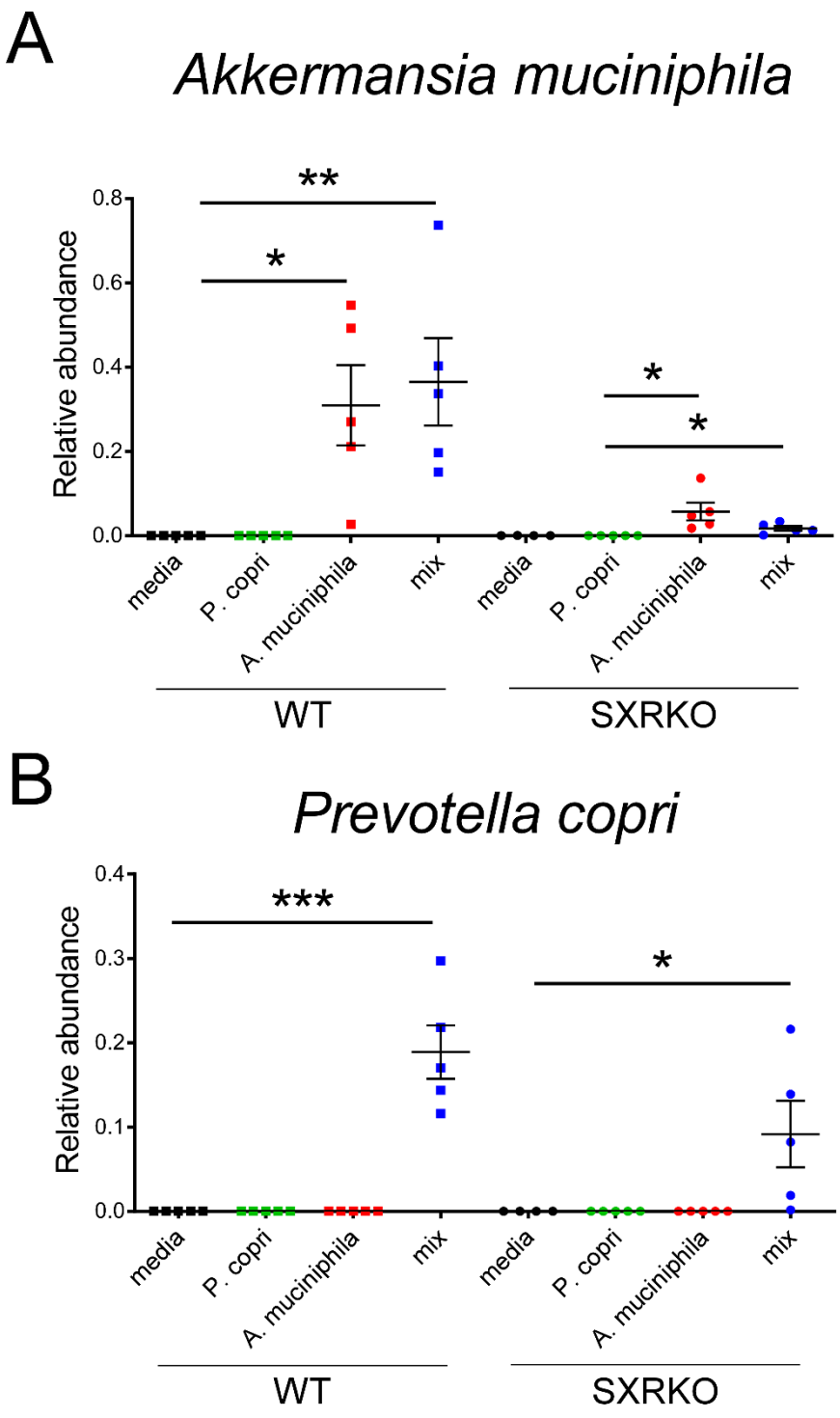

<u>Figure 3.5</u>: Relative abundance of *Akkermansia muciniphila* and *Prevotella copri* after bacteria reconstitution. Abundance of *Akkermansia muciniphila* (A) and *Prevotella copri* (B) in WT and SXRKO mice 10 days after oral gavage of media, *Prevotella copri*, *Akkermansia muciniphila*, or 1:1 mixture of both bacteria. Abundance was determined by qPCR quantification and normalized to 16S rRNA qPCR quantification.

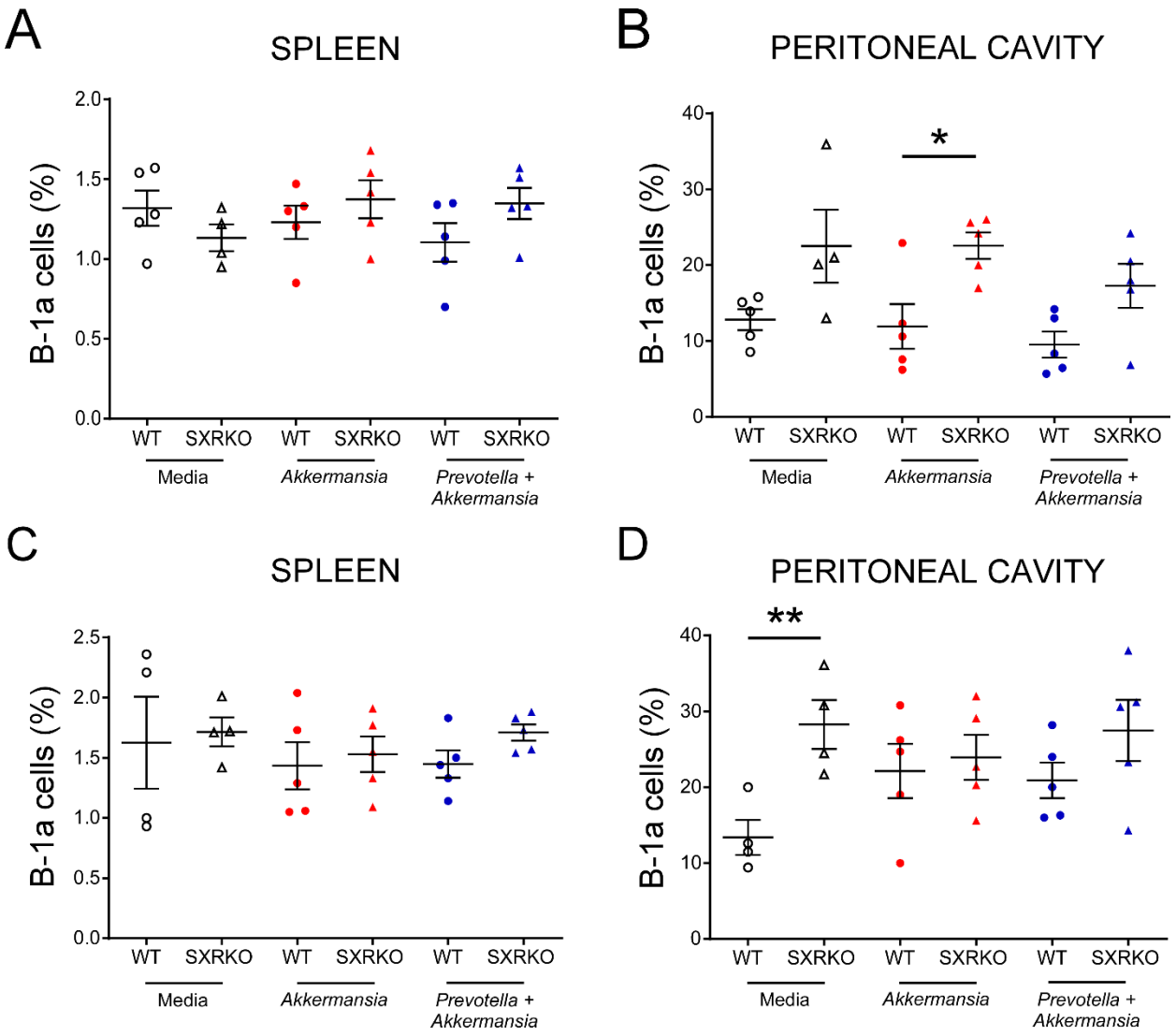

<u>Figure 3.6</u>: B-1a cell content in the spleen and peritoneal cavity of F0 WT and SXRKO mice with microbiota expanded with *Akkermansia* or a mixture of *Prevotella* and *Akkermansia*. Percentage of B-1a cells determined by flow cytometry in the spleen (A) and peritoneal cavity (B) of F0 males and spleen (C) and peritoneal cavity (D) of F0 females. Mice were administered *Akkermansia muciniphila*, 1:1 mixture of *Prevotella copri* and *Akkermansia muciniphila*, or media following antibiotic cocktail treatment to expand the abundance of indicated bacteria.

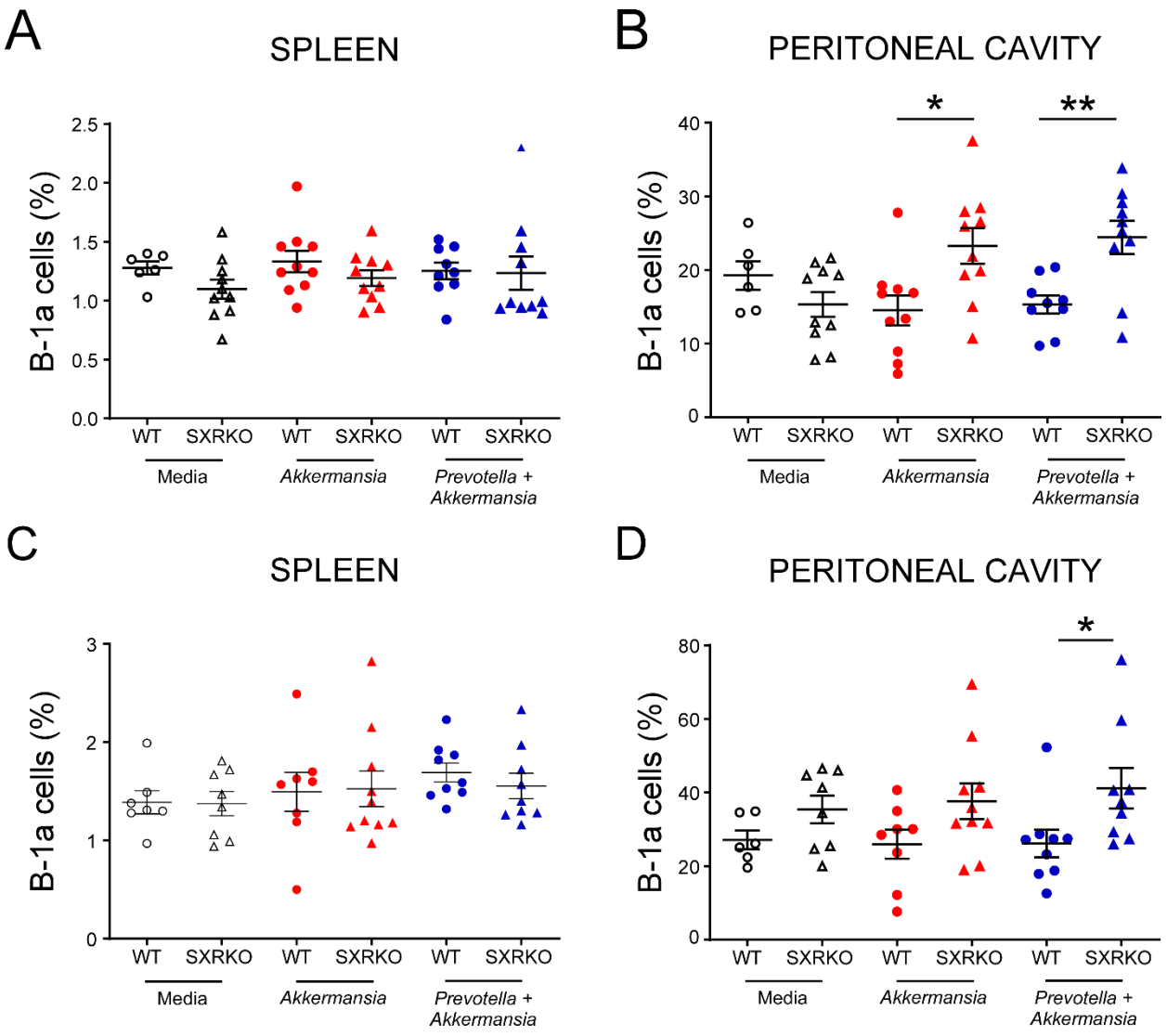

<u>Figure 3.7</u>: B-1a cell content in the spleen and peritoneal cavity of F1 WT and SXRKO mice with microbiota expanded with *Akkermansia* or a mixture of *Prevotella* and *Akkermansia*. Percentage of B-1a cells determined by flow cytometry in the spleen (A) and peritoneal cavity (B) of F1 males and spleen (C) and peritoneal cavity (D) of F1 females. F0 parents were administered *Akkermansia muciniphila*, 1:1 mixture of *Prevotella copri* and *Akkermansia muciniphila*, or media following antibiotic cocktail treatment to expand the abundance of indicated bacteria.

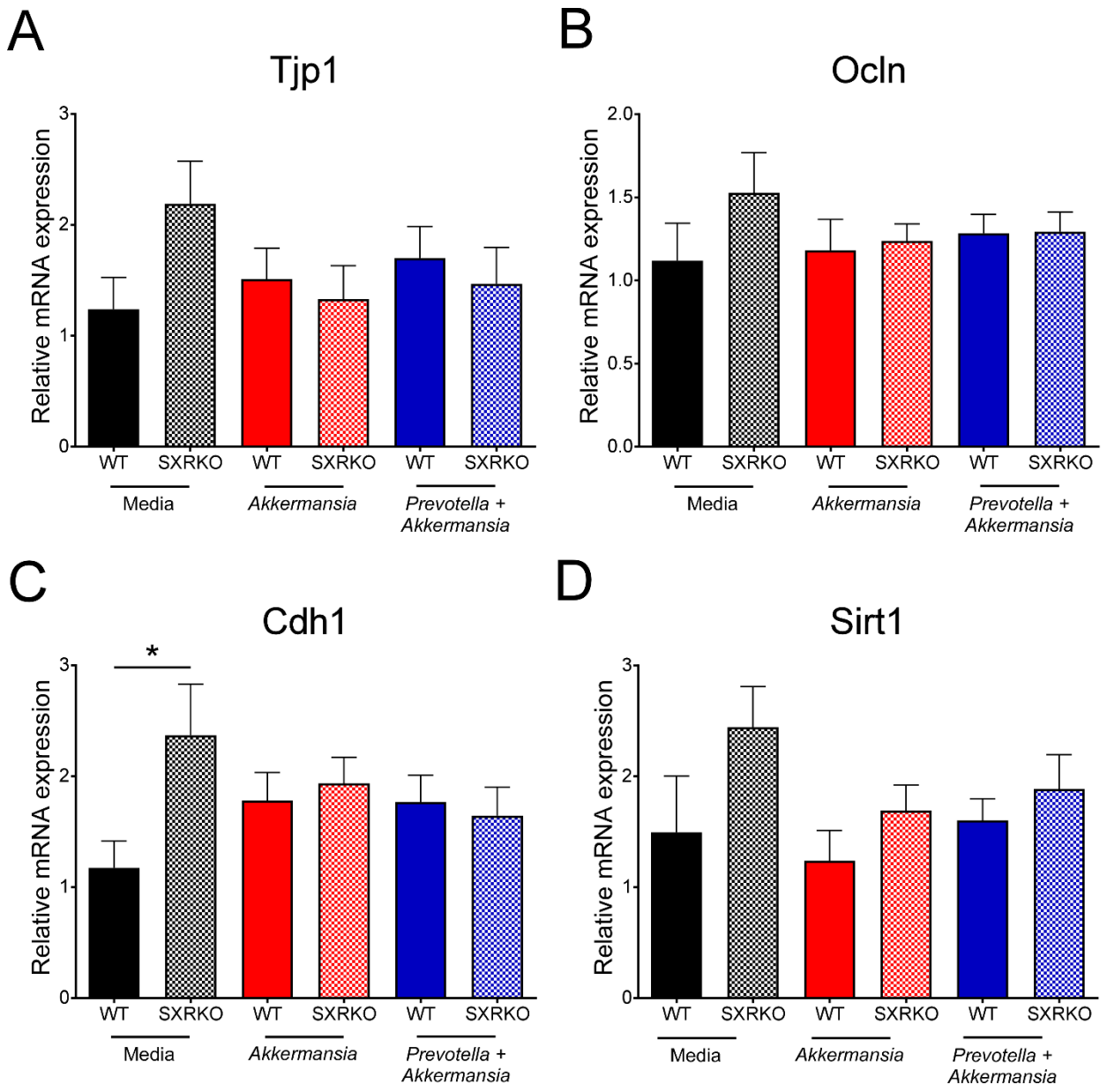

<u>Figure 3.8</u>: Colon mRNA expression of F1 male WT and SXRKO mice with microbiota expanded with *Akkermansia* or a mixture of *Prevotella* and *Akkermansia*. Relative mRNA expression of Tjp1 (A), Ocln (B), Cdh1 (C), and Sirt1 (D) in the colon of F1 males. F0 parents were administered *Akkermansia muciniphila*, 1:1 mixture of *Prevotella copri* and *Akkermansia muciniphila*, or media following antibiotic cocktail treatment to expand the abundance of indicated bacteria. Gene expression is normalized to 36B4/Rplp0.

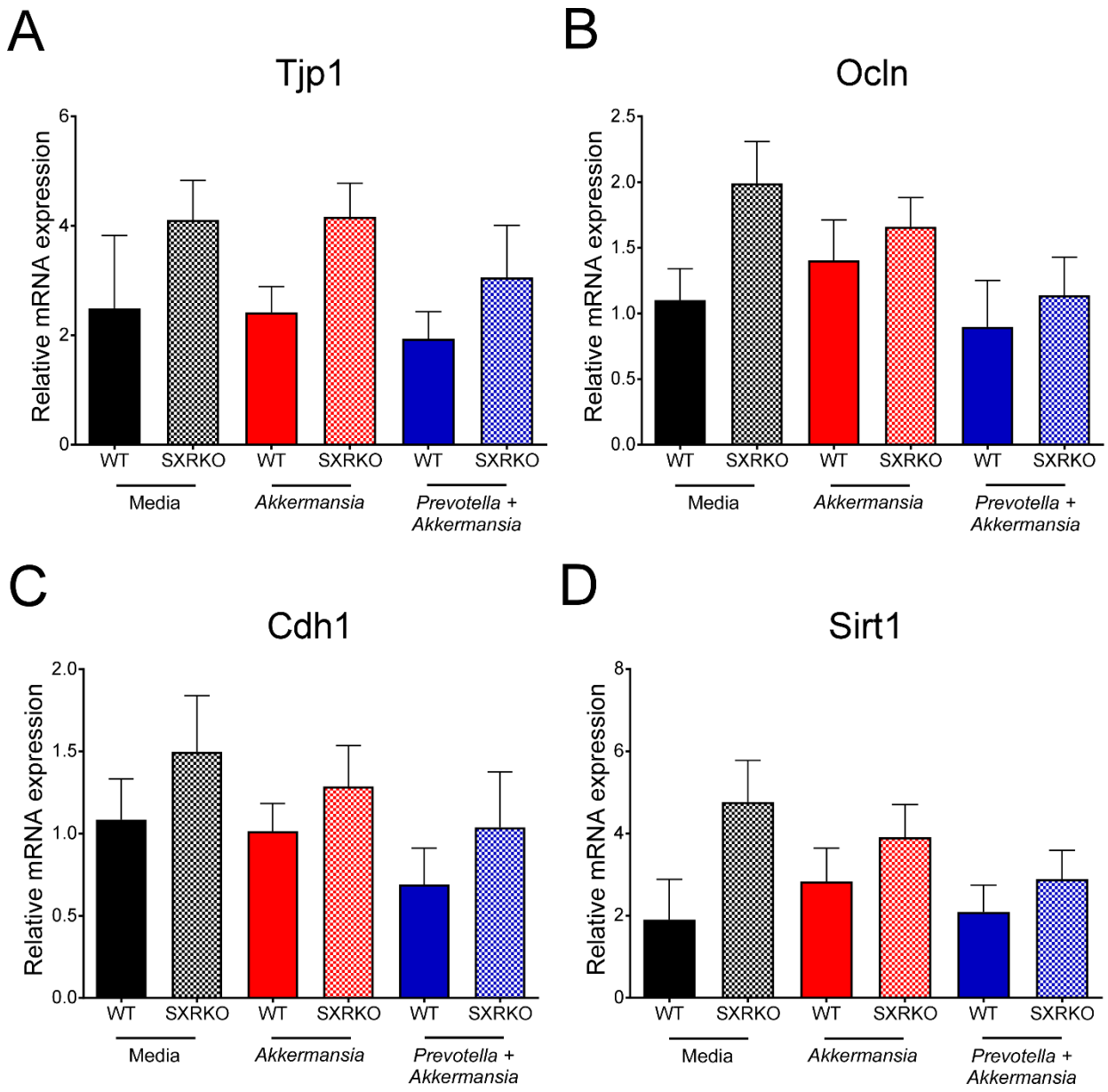

<u>Figure 3.9</u>: Colon mRNA expression of F1 female WT and SXRKO mice with microbiota expanded with *Akkermansia* or a mixture of *Prevotella* and *Akkermansia*. Relative mRNA expression of Tjp1 (A), Ocln (B), Cdh1 (C), and Sirt1 (D) in the colon of F1 females. F0 parents were administered *Akkermansia muciniphila*, 1:1 mixture of *Prevotella copri* and *Akkermansia muciniphila*, or media following antibiotic cocktail treatment to expand the abundance of indicated bacteria. Gene expression is normalized to 36B4/Rplp0.

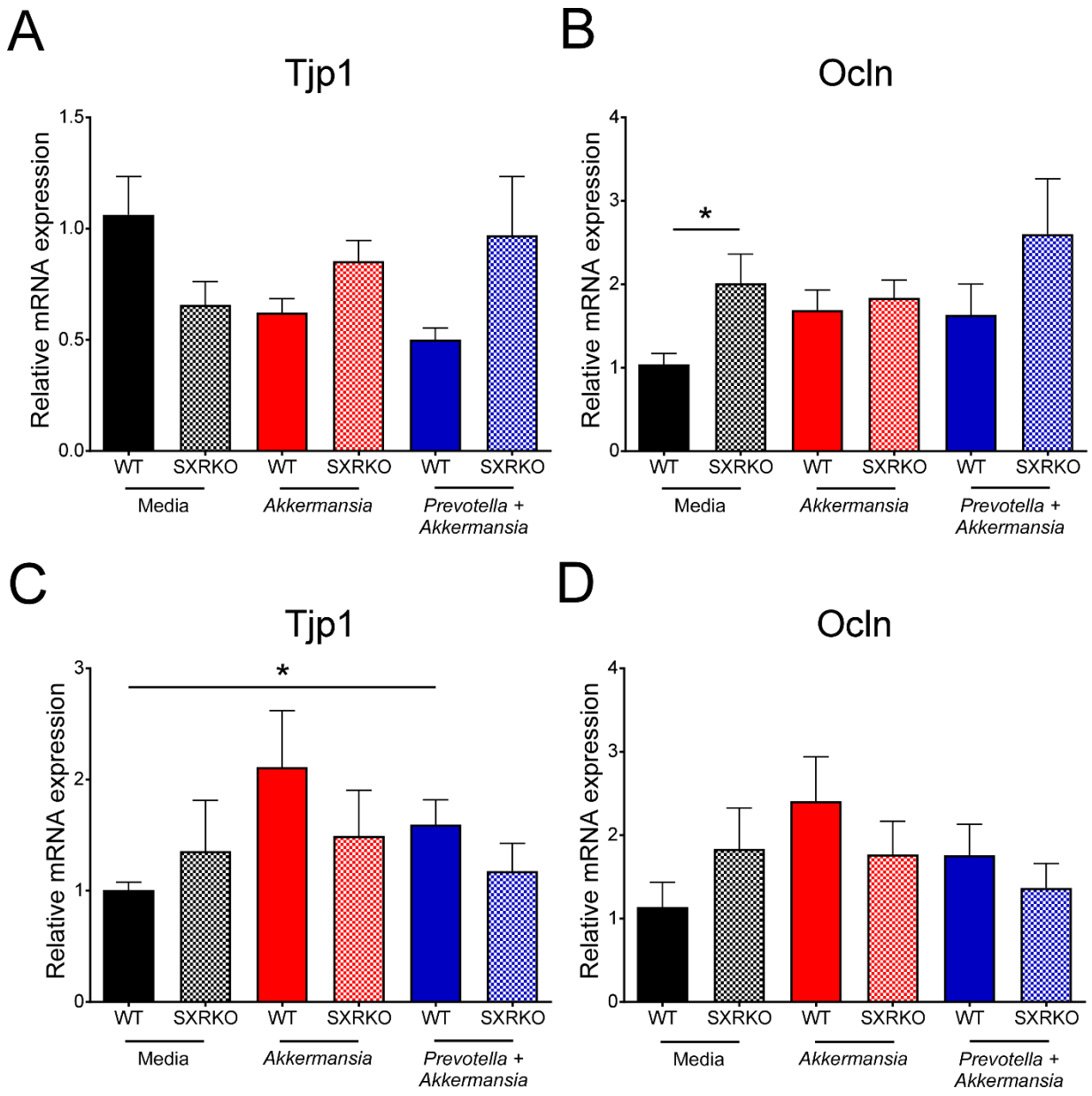

<u>Figure 3.10</u>: Jejunum mRNA expression of F1 WT and SXRKO mice with microbiota expanded with *Akkermansia* or a mixture of *Prevotella* and *Akkermansia*. Relative mRNA expression of Tjp1 (A), Ocln (B) in the jejunum of F1 males and Tjp1 (C), Ocln (D) in the jejunum of F1 females. F0 parents were administered *Akkermansia muciniphila*, 1:1 mixture of *Prevotella copri* and *Akkermansia muciniphila*, or media following antibiotic cocktail treatment to expand the abundance of indicated bacteria. Gene expression is normalized to 36B4/Rplp0.

Table 3.1: qPCR primer sequences

Gene or microbe	**Forward primer**	**Reverse primer**
Mouse 36B4/Rplp0	AAGCGCGTCCTGGCATTGTCT	CCGCAGGGGCAGCAGTGGT
Universal 16S rRNA	ACTCCTACGGGAGGCAGCAGT	ATTACCGCGGCTGCTGGC
Akkermansia muciniphila	CAGCACGTGAAGGTGGGGAC	CCTTGCGGTTGGCTTCAGAT
Prevotella copri	CCGGACTCCTGCCCCTGCAA	GTTGCGCCAGGCACTGCGAT
Mouse Tjp1	GCCTCAAGTTCCTGAAGCCC	TCCACGTTCACATTGCTTAGTCC
Mouse Ocln	GGCAAGCGATCATACCCAGAG	GAAGTCATCCACACTCAAGGTCAG
Mouse Cdh1	GCGGATAACCAGAACAAAGACCA	GCAGCAGGATCAGAATCAGCAG
Mouse Sirt1	TATCCTTTCAGAACCACCAAAGCG	TCAGGAATCCCACAGGAGACAG

Table 3.2 Statistically significant differences at genus level between paraffin-embedded tissue groups

Genus	p-value[a] WT vs SXRKO	p-value[b] SXRKO vs SXRKO with tumors	p-value[c] WT vs SXRKO with tumors
Sutterella	0.100	0.006	0.002
Sphingomonas	0.458	0.057	0.048
Lactobacillus	0.789	0.014	0.010
Prevotella	0.934	0.052	0.041
Methylobacterium	0.528	0.046	0.061
Anaerostipes	0.012	0.423	0.024

[a]Comparing log gene copy number for bacteria genera between WT paraffin-embedded intestinal tissue and SXRKO paraffin-embedded intestinal tissue

[b]Comparing log gene copy number for bacteria genera between non-tumor bearing SXRKO paraffin-embedded intestinal tissue and tumor-bearing SXRKO paraffin-embedded intestinal tissue

[c]Comparing log gene copy number for bacteria genera between WT paraffin-embedded intestinal tissue and tumor-bearing SXRKO paraffin-embedded intestinal tissue

Table 3.3 Statistically significant differences at genus level between historic and current SXRKO samples

Genus	p-value[a] tumor bearing SXRKO paraffin-embedded intestinal tissue (2007) vs SXRKO fecal sample (2016)
Acinetobacter	0.049
Akkermansia	0.037
Anaerofustis	0.356
Methylobacterium	0.040
Sphingomonas	0.034

[a]Comparing log gene copy number for bacteria genera between tumor bearing SXRKO paraffin-embedded intestinal tissue (2007) and SXRKO fecal samples (2016)

CHAPTER 4

Altered metabolism of PCB-153 leads to increased oxidative stress and hemolytic anemia in mice lacking the Steroid and Xenobiotic Receptor, SXR/PXR

Riann Egusquiza[1], Maria Ambrosio[2], Gin Wang[2], Kaelen Kay[2], Chunyun Zhang[3], Hans-Joachim Lehmler[3] and Bruce Blumberg[1,2,4]

[1]Department of Pharmaceutical Sciences, University of California, Irvine, CA, USA

[2]Department of Developmental and Cell Biology, University of California, Irvine, CA, USA

[3]Department of Occupational and Environmental Health, University of Iowa, Iowa City, IA, USA

[4]Corresponding author: blumberg@uci.edu

Summary:

Background: Polychlorinated biphenyls (PCBs) are environmental toxicants; PCB exposure has been associated with adverse effects on wildlife and humans. However, the mechanisms underlying these adverse effects are not fully understood. The Steroid and Xenobiotic Receptor (SXR/PXR, NR1I2) is a nuclear hormone receptor that regulates inducible metabolism of drugs and xenobiotics and is activated or inhibited by various PCB congeners.

Objectives: The aim of this study was to investigate the effects of exposure to PCB-153, the most prevalent PCB congener in human tissues, on mice lacking SXR (SXRKO) and to elucidate the role of SXR in PCB-153 metabolism and promotion of its harmful effects.

Methods: Wild-type and SXRKO mice were chronically or perinatally exposed to a low dose (54 µg/kg/day) of PCB-153. Blood, livers, and spleens were analyzed using RNA-seq and molecular techniques to investigate impacts of exposure on metabolism, oxidative stress, and hematological parameters.

Results: SXRKO mice perinatally exposed to PCB-153 experienced elevated oxidative stress leading to hemolytic anemia and premature death. Transcriptomal analysis revealed that expression of genes involved in metabolic processes were altered in SXRKO mice. Elevated levels of the PCB-153 metabolite, 3-OH-PCB-153, were found in exposed SXRKO mice compared to exposed wild-type mice. Blood hemoglobin levels were reduced in throughout the lifespan and occurrence of intestinal tumors was increased at 10 months of age in chronically exposed SXRKO mice.

Discussion: Our results demonstrated that altered metabolism induced by SXR loss-of-function resulted in the accumulation of harmful hydroxylated metabolites upon exposure to PCB-153, leading to oxidative stress, hemolytic anemia, and tumor development. These results suggest a more general role of SXR in maintaining balanced oxidation/reduction and proper metabolism to protect against xenobiotic-induced oxidative stress. This role of SXR could be generally applicable to other environmental toxicants, as well as pharmaceutical drugs.

Introduction

Polychlorinated biphenyls (PCBs) are a class of environmental contaminants formerly widely used in industrial products, including plastics, adhesives, and electrical equipment [30]. Continued production of these chemicals was banned in the late 1970's due to evidence of harmful effects of exposure on human health [31]. These effects ranged from acute to developmental and included inflammatory responses, neurological abnormalities and an increased risk for multiple types of cancer [110, 111]. Despite the ban on their production, PCBs are still found in the environment due to their high chemical stability. Many PCB congeners are also resistant to biological degradation, which leads to bioaccumulation in animals and humans [112, 113]. The highest levels of human exposure to PCBs resulted from dietary consumption of contaminated food, mainly fish and poultry, and inhalation of contaminated air and house dust [114-116].

PCBs were detected at high levels (between 0.5-4 mg/kg), in human breast milk, raising additional concerns about potential effects of exposure during development [110, 116, 117]. Associations were observed between prenatal and perinatal PCB exposure and reduced birth weight, immunological disruptions, and neurological abnormalities that can lead to physiological and cognitive consequences later in life in both animals and humans [118-120]. Their continued presence in humans, food sources, and indoor and outdoor air indicates that PCBs are a still a current and persistent risk to the environment and future generations [114, 121-123].

The mechanisms through which PCBs contribute to acute and lifelong effects following developmental exposure remain poorly understood. There are 209 PCB congeners that differ in the number and location of chlorine substituents. PCBs are often characterized into two groups based on similarity to tetrachlorodibenzodioxin (TCDD, colloquially called 'dioxin'), a known carcinogen. Like TCDD, dioxin-like PCBs (DL-PCBs) activate the aryl hydrocarbon receptor

(AhR), which underlies many of their adverse health effects [124-126]. Non-dioxin-like PCBs (NDL-PCBs) that do not activate the AhR also induce adverse effects *in vitro* and in animal exposure studies and have been associated with harmful effects, such as cancers, in exposed humans, yet the underlying mechanisms remain largely uncharacterized [127-132]. Determining the mode of action of NDL-PCBs is important for treatment of exposed individuals and to understand the action of alternative chemicals with similar structures (e.g. polybrominated biphenyls and polybrominated diphenyl eithers) that may act through the same pathways and induce similar adverse effects.

Some NDL-PCBs can interfere with estrogen, androgen, and thyroid signaling, resulting in adverse reproductive consequences [133, 134]. However, the ability of these chemicals to induce tumor progression, alter immune processes, or increase risk for various cancers in exposed individuals is not understood, nor are the adverse effects on children exposed during early development. NDL-PCBs interact with the Constitutive Androstane Receptor (CAR) and the Steroid and Xenobiotic Receptor (SXR/PXR), both of which are broad-specificity, xenobiotic sensing receptors [7, 32, 33, 42]. NDL-PCBs directly bind to and induce expression of target genes for these receptors. SXR was more strongly activated than was CAR in certain human cell lines, whereas CAR was more robustly activated in rat hepatocytes [32, 33]. Some of the same highly-chlorinated, NDL-PCB congeners that activated SXR in rodents showed antagonistic activity against human SXR [34].

PCB-153 (2,2',4,4',5,5'-hexachlorobiphenyl) is a highly chlorinated NDL-PCB that was reported to be the most prevalent congener found in human tissue and breast milk, and in contaminated fish [110, 116]. Unlike some other NDL-PCBs, PCB-153 does not interfere with thyroid signaling [134]. Despite its inactivity on common PCB induced pathways, PCB-153 increased tumor incidence in

rodents and was associated with increased risk for non-Hodgkin's lymphoma and other cancers in exposed humans [128, 135, 136]. In addition, PCB-153 was reported to be the most potent NDL-PCB congener on SXR induction of target genes in some human cell lines and rat hepatocytes [32, 33]; although, we showed that it was a human SXR antagonist in primary human hepatocytes and human LS-180 cells [34].

SXR, also known as the Pregnane X Receptor (PXR) and formally known as NR1I2, is a nuclear hormone receptor expressed at high levels in the liver and intestine and at lower, but detectable levels in most other tissues [6, 137]. When it is activated by ligands (drugs, endobiotic and xenobiotic chemicals), SXR/PXR up-regulates expression of genes encoding all three phases of xenobiotic metabolizing enzymes: phase I enzymes such as cytochrome P450 (CYP3A) genes, phase II conjugating enzymes such as glutathione S-transferase (GST), and phase III ABC drug transporters [6, 9, 10]. Predictably, SXR null (SXRKO) mice display defects in inducible xenobiotic metabolism, making them hypersensitive to the effects of certain xenobiotics [52].

Here we showed that SXR loss-of-function resulted in impaired metabolism of PCB-153 that led to increased levels of hydroxylated PCB-153 metabolites, oxidative stress and hemolytic anemia in perinatally exposed mice. Chronic exposure to a low dose of PCB-153 also resulted in tumor development in SXRKO mice. These results demonstrated that SXR is important for the proper metabolism of PCB-153 by preventing accumulation of harmful hydroxylated metabolites. We also identified hemolytic anemia as a previously uncharacterized effect of PCB-153 exposure. These results uncovered an unexpected role for SXR in maintaining balanced oxidation/reduction and proper metabolism to protect against xenobiotic-induced oxidative stress. These results could be generally applicable to other environmental toxicants, as well as pharmaceutical drugs.

Materials and Methods

Animal maintenance and exposure

Wild type (WT) and SXRKO (C57BL/6J) mice were maintained and housed at the University of California, Irvine. SXRKO mice were descendants from a colony of 129SVEV mice from the Salk institute (a gift of Prof. Ron Evans) and were backcrossed onto the C57BL/6J background for 6 generations to obtain SXRKO mice with an essentially pure C57BL/6J background. Mice were housed in micro-isolator cages in a temperature-controlled room (23–25°C) with a 12-h light/dark cycle. Water and food (5P14 ProLab RMH 2500, LabDiet) were provided ad libitum. Animals were treated humanely, and all procedures were approved by the Institutional Animal Care and Use Committee of the University of California, Irvine.

PCB-153 exposure

2,2',4,4',5,5'-Hexachlorobiphenyl (PCB-153) was purchased from ChemService Inc. Stock solutions were prepared at 20 mM in DMSO at 20 mM. Stocks were further diluted in DMSO to 1 mM concentration and stored at -80˚C until use. Chemical exposure was administered via the drinking water. Mice received 1 µM PCB-153 or vehicle (0.1% DMSO) in 0.5% carboxymethylcellulose prepared in autoclaved tap water. Water containing PCB-153 or vehicle was replaced twice weekly. WT and SXRKO females (8-10 weeks old) were randomly assigned to exposure groups (DMSO or PCB-153); exposure began 3 days prior to breeding. PCB or vehicle-containing water was removed for breeding and resumed following 3 days of mating, then continued throughout pregnancy and lactation. After weaning, male offspring continued on the exposure they received *in utero*. Exposure was continued until euthanasia at 4 weeks, or 10 months of age (Figure 4.1A). Female offspring were not investigated because we observed no effects in females in a pilot PCB-153 exposure study (data not shown).

The dose of PCB-153 used in this study is equivalent to 0.25 µmol/kg/day or 54 µg/kg/day, assuming that mice consumed 1.5 mL/10 g of body weight of water a day. The no observed adverse effect level (NOAEL) for PCB-153 for rodents is between 1 and 250 mg/kg/day depending on the biological endpoint investigated [138]. The worst case, environmentally-relevant dose of PCB-153 is 1.7 µmol/kg/day [129]. We chose the dose of 0.25 µmol/kg/day (54 µg/kg/day), because it is relevant to human exposure levels, we observed effects in a pilot study, and it is five times lower than the rodent NOAEL.

Complete blood count

Whole blood (50 µL) was collected bimonthly into heparinized capillary tubes from the saphenous vein beginning at 6 weeks until 9 months of age. Blood parameters were measured on a VetABC hematology analyzer (scil Animal Care Company) within 4 hours of blood collection. Blood parameters measured included: white blood cell count (WBC), red blood cell count (RBC), hematocrit (HCT), hemoglobin (HGB), mean corpuscular volume (MCV), mean cell hemoglobin (MCH), mean corpuscular hemoglobin concentration (MCHC), red blood cell distribution width (RDW), platelet count (PLT), lymphocyte count (LYM), monocyte count (MON), and granulocyte count (GRA).

Tissue and cell collection

Mice were euthanized by isoflurane overdose. Whole blood was collected by cardiac puncture. Aliquots of whole blood (20 µL) were flash frozen and stored at -80˚C until further analysis. Remaining blood was centrifuged to isolate plasma. Plasma was stored at -80˚C. Livers and spleens were dissected, flash frozen in liquid N_2 and stored at -80˚C. A section of each spleen was set aside before flash freezing for splenocyte isolation.

Spleen and bone marrow cell isolation

Spleens were physically dissociated using a Petri dish and syringe plunger in 1 mL of cold PBS containing 1% fetal bovine serum (FBS) (Omega Scientific). Hind legs were dissected, tibias and femurs were isolated, and bone marrow cells were extracted by flushing cold PBS + 1% FBS buffer into the marrow cavity using a 25-gauge needle. Erythrocytes were lysed by incubating cell suspensions in ACK lysis buffer (150 mM NH_4Cl + 10 mM $KHCO_3$ + 0.1 mM Na_2EDTA) for 5 min. Cells were washed and resuspended in FACS buffer (PBS+ 1% FBS + 0.02% sodium azide) for flow cytometry antibody staining.

Flow cytometry analysis

Splenic and bone marrow cells were diluted in cold FACS buffer (PBS+ 1% FBS + 0.02% sodium azide), divided into $4x10^4$ cell aliquots, stained with an antibody cocktail of anti-mouse TER119-APC (TONBO biosciences), CD71-PE (eBioscience), and CD45-Alexa Fluor700 (BioLegend) for 30 min. Cells were analyzed on a BD FortessaX20 cytometer and data processed using FlowJo software (Treestar).

Erythrocyte MDA/lipid peroxidation measurement

Flash frozen blood samples were mixed with 1 mL of sterile, ultrapure water (ultrafiltered, UV sterilized water from a Barnstead Nanopure water system, hereafter called nanopure water) to lyse the red blood cells (RBCs). RBC membranes were pelleted and supernatants discarded. RBC membranes were washed with nanopure water and pelleted again. Malondialdehyde (MDA) levels were obtained using the Lipid Peroxidation MDA Assay Kit (Sigma Aldrich) following the manufacturer's protocol. Supernatants were measured on a fluorescence plate reader with excitation at 532 nm and emission at 553 nm.

Hemoglobin measurement

Flash frozen blood samples were diluted 1:200 in nanopure water. Hemoglobin content was determined using the Hemoglobin Assay Kit (Sigma Aldrich) according to manufacturer's protocol. Colorimetric products were measured at 400 nm.

GSH/GSSG level determination

Flash frozen blood samples were diluted with 500 µL of nanopure water and deproteinized using 1/5 volume of 100% Trichloroacetic acid (Sigma Aldrich). Supernatants were neutralized by slowly adding sodium bicarbonate until pH= 4-6. GSH and total glutathione levels were determined using the GSH/GSSG Ratio Detection Assay Kit (Abcam) according to the manufacturer's protocol. Fluorometric product were excited at 490 nm and emission measured at 520 nm.

Ex vivo hemolysis assay

Blood was collected from untreated 4 week old wild-type and SXRKO mice (n = 3) by cardiac puncture using a needle and heparinized syringe. Blood was centrifuged and plasma was removed. Packed erythrocytes were washed twice with 1x PBS (pH 7.4) then diluted 1:50 in 1x PBS (pH 6.2). A more acidic pH was used in order to obtain higher sensitivity to agent induced hemolysis [139]. Red blood cells were treated with different concentrations of PCB-153 or with positive control (1% SDS) for 2 hours at 37˚C. Cells were pelleted and supernatants were transferred to a clear 96-well plate. Absorbance of free heme in the supernatant was measured at 405 nm.

RNA extraction

Frozen tissue sections were homogenized rapidly in 1 mL of Trizol reagent (Thermo Fisher

Scientific). RNA was isolated from the tissue-Trizol homogenate by chloroform extraction. RNA was precipitated with an equal volume of 100% isopropanol, centrifuged and salt removed by washing with 70% ethanol. Final RNA product was resuspended in DNase/RNase-free nanopure water, quantified by spectrophotometry, and integrity verified by denaturing agarose gel electrophoresis.

RNA-seq library prep and sequencing

Extracted RNA was further purified using a Zymo Quick-RNA Microprep Kit. RNA-seq libraries were prepared by the UCI Genomics High Throughput Facility using 1 µg of RNA and the Illumina TruSeq stranded mRNA library prep kit. Two separate libraries were made for the liver and spleen samples with 20 samples each using Illumina reagents. Each library was sequenced on a HiSeq4000 instrument using single-stranded 100 bp read length, with one library per flow cell lane. We obtained an average of 18.6±2.6 million reads per sample.

RNA-seq analysis and visualization

Sequence quality was checked in the Fastq files using FastQC (Babraham Bioinformatics)[140]. Fastq files were then aligned to the mouse MM10 genome assembly (ENSEMBL) using the STAR aligner [141] on the UC Irvine high performance computing cluster. The resulting BAM files were also checked with FastQC. The average number of uniquely mapped reads was 84.7±2.3%. Spleen sample "WD2" was removed from downstream analysis due to lower mapping quality (76.1%) compared to all other spleen samples. Reads were counted using Rsubread/featureCounts (R, Bioconductor)[142] and differential expression analysis was conducted using DESeq2 (R, Bioconductor) [143]. Differentially expressed genes (DEGs) were selected using a Benjamini-Hochberg adjusted p value (p-adj) < 0.05 and absolute value ($\log_2$FC) > 0.3. Normalized counts obtained from DESeq2 analysis were used to generate heatmaps. Heatmaps

were plotted using pheatmap package in R. Raw and processed RNA-seq data files are available at Gene Expression Omnibus (GSE135916). The annotated HPC and R scripts used for the RNA-seq analysis are in the Appendix.

Gene Ontology Analysis

Differentially expressed genes were input into MouseMine (Mouse Genome Informatics) again using a Benjamini-Hochberg corrected p-value <0.05 to determine significance. For GO term enrichment, terms were reduced to 25 terms using Revigo [144] and independent selection of desired terms. GO term enrichment plots were made using ggplot2. Enrichment is plotted as (# of DEGs within the term)/(total # of genes in the term) X 100.

qPCR validation of DEGs

cDNA was synthesized using 2 µg of extracted intact RNA and Superscript III Reverse Transcriptase (Thermo Fisher Scientific) according the manufacturer's protocol. Synthesized cDNA was diluted 5-fold for qPCR analysis. Diluted cDNA was combined with SYBR green qPCR Master Mix (Thermo Fisher Scientific) and the primer mix for gene of interest and analyzed using a Roche LightCycler 480. Technical replicate Ct values were averaged for each biological replicate. Mean Ct values were normalized to 36B4/Rplp0 or Actb, for liver or spleen respectively, (ΔCt), and relative fold change mRNA levels were then calculated by using ΔΔCt method [70] with relative gene expression presented as mean fold change over vehicle control ± SEM. Primers were designed using PerlPrimer software. qPCR primer sequences are given in Supplemental Table 4.1

Extraction of PCB-153 and 3-OH-PCB 153 from liver

Liver samples (247±62 mg) were spiked with PCB-117 and 4'-OH-PCB-159 (50 ng each) as surrogate recovery standards. After homogenization in 2-propanol (3 mL), samples were extracted with diethyl ether (1 mL) and hexane:diethyl ether (9:1 v/v, 2.5 mL) following a published procedure [145]. Combined extracts were washed with phosphoric acid (0.1 M solution in 0.9% aqueous sodium chloride, 5 mL) and derivatized with diazomethane (0.5 mL) overnight at 4°C. Sulfur removal and sulfuric acid treatment steps were employed before analysis as described [146, 147].

Extraction of PCB-153 and 3-OH-PCB-153 from plasma

Plasma samples (71±51 mg) were spiked with PCB-117 and 4'-OH-PCB-159 (50 ng each) as surrogate recovery standards and denatured with hydrochloric acid (6 M, 1 mL) and 2-propanol as reported previously [148, 149]. All samples were extracted with hexane:methyl *tert*-butyl ether (1:1 v/v, 5 mL), then re-extracted with hexane (3 mL). The combined organic extracts were washed with potassium chloride solution (1 %, 4 mL) and underwent the derivatization and clean-up procedures as above.

Quantitation of PCB-153 and 3-OH-PCB-153

Quantitative analyses of PCB-153 and 3-OH-PCB 153 in sample extracts were carried out on an Agilent 7890A gas chromatography equipped with a SPB-1 capillary column (60 m × 250 μm × 0.25 μm film thickness; Supelco, St Louis, MO, USA) and a ^{63}Ni-micro electron capture detector (μECD) as previously reported [148-150]. Helium was used as carrier gas with a constant flow rate of 2 mL/min. The injector and detector temperatures were 240°C and 300°C, respectively. The column temperature program was initially set as 50 °C, held for 1 min, then gradually increased to 200 °C by 30 °C/min, increased to 250 °C by 1 °C/min and increased to final temperature of 280 °C by 10°C/min and held there for 3 min. The PCB-153 and 3-OH-PCB-153 were identified

by the retention time of their authentic standards. The relative retention time (RRT) of all analytes was within 0.5 % of the RRT of the respective standard. The PCB 153 and 3-OH-PCB 153 were quantified with the internal standard method as described [146]. Levels were corrected for recoveries below 100%.

QA/QC of PCB-153 and 3-OH-PCB-153 measurements

The responses of PCB-153 (R^2=0.999), 3-OH-PCB-153 (R^2=0.999), PCB-117 (recovery standard, R^2=0.999), 4'-OH-PCB-159 (recovery standard, R^2=0.999) and PCB-204 (internal standard, R^2=0.999) on the GC-ECD were linear from 1 to 1000 ng/mL. The limits of detection (LOD) of PCB-153 and 3-OH-PCB-153 were calculated from method blanks as LOD = mean blanks + k × standard deviation blanks (k is the student's t value for a degree of freedom of n-1=5 for liver and n-1=5 for serum at the 99 % confidence level). The LODs for analyses of liver samples were 0.09 ng and 0.03 ng for PCB-153 and 3-OH-PCB-153, respectively. The LODs for analyses of serum samples were 0.11 ng and 0.07 ng for PCB-153 and 3-OH-PCB-153, respectively. The background level of PCB-153 and 3-OH-PCB-153 in control liver samples were 0.15±0.07 ng/g (n=19) and 0.11±0.03 ng/g (n=19), respectively. The background levels of PCB-153 and 3-OH-PCB-153 in control serum samples were 0.83±1.64 ng/g (n=18) and 0.85±2.38 ng/g (n=18), respectively. The recoveries of PCB-153 and 3-OH-PCB-153 spiked into control liver samples were 78±6 % (range: 73-87%; n = 5) and 86±9 % (range: 78-99%; n = 5), respectively. The recoveries of PCB-153 and 3-OH-PCB-153 spiked into control serum samples were 83±6 % (range: 74-90%; n = 6) and 70±17 % (range: 51-102%; n = 6), respectively. For liver analyses, the recoveries of the surrogate standards added to every samples were 95±12 % (range: 55-111 %; n=40) and 91±14 % (range: 56-120 %; n=40) for PCB-117 and 4'-OH-PCB-159, respectively. For serum analyses, the recoveries of the surrogate standards added to every

samples were 88±8 % (range: 74-102 %; n=47) and 99±14 % (range: 59-120 %; n=47) for PCB-117 and 4'-OH-PCB-159, respectively.

Statistical analysis

Data visualization and statistical analyses were conducted in Prism 8 (GraphPad Software), excluding RNA-seq analysis, which was completed in R and other software packages as indicated above. Thirteen to twenty biological replicates were used for exposure experiments and *in vivo* and FACS analyses. Down-stream biochemical analyses, RNA-seq analysis, and qPCR gene validations used 5 biological replicates per group. A p-value of <0.05 was considered statistically significant for all assays other than RNA-seq analysis, which used adjusted p-values based on Benjamini-Hochberg test.

Results

Low-dose PCB-153 exposure in SXRKO mice led to premature death and reduced blood hemoglobin

Wild-type (WT) and SXRKO females were exposed to approximately 54 µg/kg BW/day of PCB-153, or vehicle (0.1% DMSO), in the drinking water throughout pregnancy and lactation. The offspring were continued on the same exposure after being weaned from the mother until either 4 weeks or 10 months of age and were monitored to investigate the role of SXR on the action of developmental and chronic exposure to a NDL-PCB (Figure 4.1A).

We observed premature death at 5 weeks of age in approximately 20% of male SXRKO offspring from the PCB-153 group in two independent experimental cohorts; no deaths were observed in the vehicle exposed SXRKO mice or in any of the WT exposure groups (Figure 4.1B, Supplemental Table 4.2). Necropsy revealed no obvious causes of death (data not shown) and no additional deaths occurred after this age (Figure 4.1B). Blood parameters were monitored every 9-10 weeks in mice that survived after 5 weeks of age. A large decrease in hemoglobin levels was observed at 6 weeks of age in PCB-153-exposed, compared to vehicle (DMSO)-exposed SXRKO mice (Figure 4.1C). Decreased hemoglobin levels were observed consistently throughout the lifespan of the SXRKO mice exposed to PCB-153; the largest differences were observed at younger ages. There were no differences between the exposure groups among wild-type mice at any age (Supplemental Figure 4.1, Supplemental Table 4.3). No other blood parameters were consistently different between groups; although, a decreased hematocrit (HCT) and increased red blood cell distribution width (RDW) were transiently observed in PCB-153 exposed SXRKO mice at 6 weeks of age compared to vehicle exposed controls (Supplemental Table 4.4).

SXRKO mice exposed to PCB-153 displayed hemolytic anemia at 4 weeks of age

To further investigate the cause of death that occurred at 5 weeks of age in the PCB-153 exposed SXRKO mice and the possible connection to the decreased blood hemoglobin values, we investigated an independent cohort at 4 weeks of age and focused our investigation on the tissues involved in the production of red blood cells (RBCs) and iron homeostasis: blood, bone marrow, spleen, and liver.

An increased percentage of erythroid precursors (TER119+, CD71+), the progenitors of RBCs, was observed in the bone marrow and spleen via FACS analysis in SXRKO mice exposed to PCB-153 at 4 weeks of age (Figure 4.2A-D). No changes were observed in exposed WT mice (Figure 4.2B,D). This was accompanied by a decrease in blood hemoglobin (Figure 4.2E), consistent with our observations performed in older animals (Figure 4.1C). PCB-153 exposed SXRKO mice also displayed decreased body weights compared to vehicle exposed and wild-type controls (Figure 4.2F). There were no changes in relative spleen or liver weights for exposed pups or dams (Supplemental Figure 4.2).

Since the spleen is the site of stress erythropoiesis and because it is involved in the filtering and recycling of RBCs, we conducted RNA-seq analysis to evaluate alterations in splenic gene expression between PCB-153 and vehicle exposed SXRKO mice (Table 4.1). Numerous changes were observed, encompassing 380 gene ontology (GO) biological processes (BP) terms. Significant enrichments were found in terms that included heme metabolism, cell cycle, and immune system pathways (Supplemental Figure 4.3). SXRKO mice exposed to PCB-153 displayed increased expression of genes related to erythroid development, supporting the phenotypic finding of increased splenic erythropoiesis (Figure 4.3A). Krupple like factor 1 (Klf1), a transcription factor important for erythroid lineage commitment and erythrocyte

maturation [151], was significantly increased in SXRKO mice exposed to PCB-153 and this expression pattern was validated by qPCR (Figure 4.3B). Several other key differentially expressed genes (DEGs) for this pathway were validated with qPCR analysis (Supplemental Figure 4.4). PCB-153 exposed SXRKO mice also displayed elevated expression of genes related to heme metabolism (Figure 4.3C). This included important components in heme synthesis, such as ferrochelatase, Fech, one of the main components in the heme biosynthesis pathway and biliverdin reductase B (Blvrb), one of the most important enzymes involved in the catabolism of free heme (Figure 4.3C-D). Selected DEGs in this GO term were validated by qPCR (Supplemental Figure 4.4). The expression levels of genes in these GO terms parallels the observed level of splenic erythropoiesis which may explain the increased range of expression values in the PCB-153 exposed SXRKO mice (Supplemental Figure 4.5). The increase in both heme synthesis and catabolism, in conjunction with the increased erythropoiesis and decreased hemoglobin, led us to infer that SXRKO mice exposed to PCB-153 were undergoing hemolytic stress leading to anemia. Increased heme synthesis and erythropoiesis likely resulted from attempts to replenish the loss of RBCs and/or hemoglobin. We did not observe direct hemolysis of RBCs obtained from either wild-type or SXRKO mice by PCB-153 in an *ex vivo* hemolysis assay (Supplemental Figure 4.6), indicating that a physiological aspect of SXRKO mice likely promotes the hemolytic properties of PCB-153.

Exposure of SXRKO mice to PCB-153 led to elevated oxidative stress in spleen and RBCs

In addition to elevated heme synthesis and erythroid development, transcriptomal analysis in the spleens revealed enrichment for genes in GO terms related to oxidative stress (Supplemental Figure 4.3, Supplemental Figure 4.7A). SXRKO mice exposed to PCB-153 had a different expression profile for genes involved in responses to reactive oxygen species (ROS), with

increases in expression of key antioxidant genes including peroxiredoxin 2, Prdx2, and glutathione peroxidase 1, Gpx1 (Figure 4.4A, Supplemental Figure 4.7A-B), and the transcription factor Foxo3 (Supplemental Figure 4.7A), which is induced by ROS in erythrocytes to up-regulate antioxidant genes [152, 153]. This coincided with alterations in the expression of genes involved in glutathione metabolism and synthesis in the spleen (Figure 4.4C). PCB-153 exposed SXRKO animals showed increased expression of glutathione S-transferases (GSTs), such as microsomal glutathione S-transferase 3 (Mgst3) and glutathione S-transferase pi 3 (Gstp3), and increased expression of Gclc and Gclm, which encode for the two subunits of glutamate-cysteine ligase, the first, rate-limiting enzyme of glutathione synthesis (Figure 4.4C, Supplemental Figure 4.7C-D). RBCs of PCB-153 exposed SXRKO mice also displayed a lower ratio of reduced glutathione (GSH) to total glutathione content (Figure 4.4D), indicating elevated oxidative stress. RBC membranes of SXRKO mice exposed to PCB-153 showed signs of increased malondialdehyde (MDA) content, indicative of increased lipid peroxidation and oxidative damage, but this did not reach statistical significance (Figure 4.4B). These mice also exhibited altered gene expression of GO terms related to DNA damage in the spleen (Supplemental Figure 4.8). These findings support the RNA-seq results pointing toward increased oxidative stress experienced by SXRKO mice exposed to PCB-153.

Altered xenobiotic and glutathione metabolism profile in livers of SXRKO mice

SXR is expressed at high levels in the liver, a principal site of xenobiotic metabolism. The liver transcriptomes in WT and SXRKO mice were compared to determine whether the phenotypic differences were the result of distinct metabolic responses to PCB-153. We found a low number of differentially expressed genes associated with PCB-153 exposure in the livers of either WT or SXRKO mice compared to the vehicle exposed counterparts in the RNA-seq data set (Table 4.2).

However, the results revealed inherent differences between WT and SXRKO mice in terms such as xenobiotic metabolism, oxidation-reduction processes, and glutathione metabolic process (Figure 4.5, Supplemental Figure 4.9). These inherent differences included differential expression of many cytochrome P450 genes. Several isoforms of the CYP2B family of P450s catalyze phase I metabolism of NDL-PCBs [154]. Expression of Cyp2b9 and Cyp2b10 were elevated in SXRKO mice compared to WT (Figure 4.5A-B). We infer that this CYP2B gene expression profile of SXRKO mice could potentially cause increased metabolism and/or hydroxylation of PCB-153. However, many other CYP genes were down-regulated in SXRKO mice compared to WT, revealing an overall disrupted xenobiotic metabolism gene expression profile (Figure 4.5A). SXRKO mice also showed decreased expression of several glutathione S-transferases (GSTs), such as Gstp1 (Figure 4.5C-D) and increased expression of several sulfotransferases (SULTs), such as Sult2a1 (Supplemental Figure 4.10C-D), compared to WT controls.

Impaired PCB-153 metabolism in SXRKO mice

We hypothesized that the inherent differences observed in the liver transcriptome between WT and SXRKO mice could lead to differential metabolism of PCB-153 and/or increased susceptibility to oxidative stress. Expression of UDP-glucuronyl transferase (UGT) genes was elevated in PCB-153 exposed SXRKO mice compared to exposed WT. This up-regulation of UGT genes was only observed in PCB-153 exposed SXRKO mice (Supplemental Figure 4.10A). Various UGT enzymes are involved in the conjugation of PCB-153 metabolites, notably hydroxylated PCB metabolites [154, 155]. Levels of 3-OH-PCB-153 were elevated in the plasma and livers of PCB-153 exposed SXRKO mice compared to WT PCB-153 exposed mice (Figure 4.6). There was no increase in the levels of unmetabolized PCB-153 (Figure 4.6A,D), demonstrating

that SXRKO mice have impaired metabolism or clearance of the hydroxylated metabolites, leading to their increased accumulation. We infer that increased expression of UGT genes is a response to increased abundance of OH-PCB-153 in exposed SXRKO mice. One UGT gene, Ugt3a1, was down-regulated in unexposed SXRKO mice compared to unexposed WT mice (Supplemental Figure 4.10B). This inherent decrease in Ugt3a1 gene expression in SXRKO mice might play a role in the observed accumulation of 3-OH-PCB-153.

SXRKO mice chronically exposed to PCB-153 developed intestinal tumors

Chronic exposure to PCB-153 (54 µg/kg BW/day) led to the development of upper small intestinal tumors in SXRKO mice that were observed at 10 months of age. These tumors occurred in approximately 12% (4/34) of the PCB-153 exposed SXRKO mice and were located near the jejunum/duodenum junction (Figure 4.7A-B, Supplemental Figure 4.11A-B). These results derived from three independent exposure studies, one of which included a human SXR knock-in (hSXRki) transgenic mouse strain [156]. No wild-type or hSXRki mice in either exposure group developed intestinal tumors in any of the studies. Tumor bearing SXRKO mice also displayed enlarged spleens accompanied by robustly increased erythropoiesis (Figure 4.7C-D, Supplemental Figure 4.11C). Since only the tumor bearing mice showed splenic erythropoiesis, and splenic erythropoiesis is a common side effect of tumor development, we infer that the erythropoiesis observed at 4 weeks of age and at 10 months of age were probably the result of independent mechanisms. 10 month old SXRKO mice chronically exposed to PCB-153 displayed reduced body weights (Supplemental Figure 4.11D), matching the reduced body weights observed at 4 weeks of age (Figure 4.2F). We propose that the altered xenobiotic metabolism gene expression profile in the livers of SXRKO mice results in impaired metabolism and clearance of PCB-153, and associated toxic metabolites, leading to elevated oxidative stress

that acts on the RBCs to induce hemolytic anemia (Figure 4.8). It is plausible that this increased oxidative stress and consequential DNA damage experienced by SXRKO mice exposed to PCB-153 also contributed to the development of the intestinal tumors in chronically exposed animals.

Discussion

Polychlorinated biphenyls (PCBs) are highly persistent environmental contaminants known to cause many detrimental acute and developmental effects in humans and wildlife [110]. PCB exposure during early development often leads to more severe and longer lasting effects than does adult exposure [120, 157, 158]. Therefore, determining the underlying molecular mechanisms responsible for the effects elicited by acute, chronic, and developmental exposures and how to protect against them is vital to protect public health. While much is known about the mechanisms through which DL-PCBs act, a large knowledge gap remains concerning the mechanisms of action for NDL-PCBs. This study demonstrated that loss of SXR/PXR resulted in elevated toxicity of PCB-153, likely due to accumulation of harmful metabolites that induce oxidative stress. This highlights the importance of SXR/PXR in protection against exposure to NDL-PCBs and likely other xenobiotics with reactive metabolites.

Here we showed that perinatal exposure of SXRKO mice to PCB-153 led to hemolytic anemia, a previously unreported effect of exposure to this toxicant. The anemia was characterized by reduced hemoglobin levels that persisted throughout the lifespan with increased compensatory and stress erythropoiesis observed by 4 weeks of age. Splenic erythropoiesis is commonly associated with anemia, which results from ineffective medullary erythropoiesis or another form of RBC stress [159, 160]. Increased erythropoiesis in PCB-153 exposed SXRKO mice was observed in both the spleens and bone marrow, ruling out ineffective medullary erythropoiesis as the cause of the anemia. Increased expression of heme catabolic genes, such as Blvra and Blvrb, is consistent with the possibility that SXRKO mice exposed to PCB-153 also experienced elevated RBC destruction, characteristic of hemolytic anemia [161].

ROS and oxidative stress cause cell damage leading to RBC destruction and anemia [162-164].

Oxidative stress-induced hemolytic anemia has been associated with exposure to some xenobiotics, and is thought to be caused by altered glutathione synthesis or glutathione redox cycle regulation [40, 161]. Glutathione (GSH) is tripeptide that acts as both an antioxidant and detoxifying agent [165]. GSH reduces hydrogen peroxides and other reactive oxygen species (ROS), this process produces the oxidized form of glutathione, GSSG [166]. SXRKO mice perinatally exposed to PCB-153 have decreased levels of GSH (the reduced form of glutathione), in whole blood, indicating elevated oxidative stress. Here we also observed increased expression of mRNAs encoding key antioxidants, Gpx1 and Prdx2, which may indicate a physiological compensation to combat the increased oxidative stress.

Our chronic exposure study demonstrated that exposure to PCB-153 *in utero* until 10 months of age resulted in intestinal tumor formation in some SXRKO mice. PCBs and/or their metabolites were reported to be genotoxic, and this is widely believed to be a primary mechanism through which PCB exposure led to cancers [39, 167, 168]. Tumor bearing mice in our chronic exposure study also displayed anemia and elevated erythropoiesis. Splenic erythropoiesis was reportedly associated with tumor development in mouse models and it was shown recently that erythroblasts of tumor-bearing mice can further stimulate tumor progression [169]. Since only the tumor bearing, 10 month old mice displayed erythropoiesis in our study, we inferred that tumor formation in aged, chronically exposed mice was not induced by the erythropoiesis we observed in young perinatally exposed SXRKO mice. Instead we hypothesized that tumors arose from elevated oxidative stress and genotoxicity elicited by PCB-153 exposure and SXR loss-of-function; although, anemia/erythropoiesis may have helped promote tumor development.

In addition to oxidation and reduction, GSH also participates in the detoxification of xenobiotics, but requires catalysis by glutathione S-transferase (GST). SXRKO mice showed altered

expression of mRNAs encoding glutathione S-transferases in the liver, with decreased Gstp1 and Gstp2 and increased Gstp3 expression. GSTs also detoxify harmful metabolites of oxidative stress [170]. These differences suggested that SXRKO mice have altered detoxification by GSH, leading to increased levels of oxidative stress inducing metabolites and reduced levels of GSH. This would make SXRKO mice more susceptible to oxidative stress. GST deficiencies have been reported in human anemia cohorts [171, 172]. Another study linked GST polymorphisms with sickle cell anemia [173].

Transcriptomal analysis of livers revealed other inherent differences in gene expression between wild-type and SXRKO mice, mostly related to xenobiotic metabolism or oxidation-reduction processes, thus, we inferred that there may be resulting differences in PCB-153 metabolism. We observed increased levels of the hydroxylated metabolite of PCB-153, 3-OH-PCB-153, in both the plasma and livers of exposed SXRKO mice compared to exposed WT. Hydroxylated PCB metabolites are known to induce oxidative stress and DNA damage; this mechanism was hypothesized to be responsible for many of their adverse health effects [167, 174]. Therefore, we propose that the oxidative stress induced hemolytic anemia in SXRKO mice was probably caused by elevated levels of hydroxylated PCB-153 metabolites.

PCBs are hydroxylated by various cytochrome P450 enzymes, although it is thought that the Cyp2b family plays the largest role [154]. We observed increased expression of mRNAs encoding Cyp2b9 and Cyp2b10 in the livers of SXRKO mice, which could explain the increased level of hydroxylated metabolites. The altered expression of GSTs in the liver of SXRKO mice could also contribute to the elevated levels of OH-PCB153 due to their involvement in the detoxification of arene oxide metabolites of PCBs [154]. UDP-glucuronosyltransferases (UGTs) are phase II metabolizing enzymes that conjugate a glucuronic acid to the hydroxyl group of

hydrophobic compounds to aid in their clearance from the body [175]. These enzymes conjugate various OH-PCB metabolites [154, 155]. Decreased Ugt3a1 expression in SXRKO mice with both vehicle and PCB-153 exposure provides a possible explanation for the elevated levels of 3-OH-PCB-153 metabolite. Many other UGT genes were up-regulated in the livers of PCB-153 exposed SXRKO mice, but this up-regulation was not observed in WT exposed mice.

Sulfotransferases (SULTs) are phase II metabolizing enzymes that conjugate a sulfonyl onto a hydroxyl group of xenobiotics to aid in its solubility and clearance [176]. SXRKO mice had elevated expression of several SULTs compared to WT controls. This appears to contradict to our results of increased accumulation of 3-OH-PCB-153; however, it has been reported that some OH-PCB metabolites can inhibit SULT activity [177, 178]. In addition, Sult2e1 was only up-regulated in PCB-153 exposed SXRKO mice compared to exposed WT mice and this specific SULT isoform has been shown to bind to hydroxylated PCBs [179]. The increased expression of several UGT genes and Sult3e1 in PCB-153 exposed SXRKO mice is likely a compensatory response to the increased presence of 3-OH-PCB-153. The up-regulation of these enzymes can result in an increase in phase II metabolites of 3-OH-PCB-153, which may also induce oxidative stress.

Surprisingly, PCB-153 exposure had no significant effects on the liver transcriptomes of WT mice, and only a small effect on the liver transcriptomes of SXRKO mice. The lack of induction of typical xenobiotic metabolizing enzymes is probably the result of using a dose lower than the no observed adverse effect level (NOAEL) of PCB-153, which for mice is between 1 and 125 mg/kg BW/day depending on the biological endpoint [138]. Other studies showed that doses of 3.6 mg/kg BW/day may be required to observe gene expression changes in the mouse liver [180]. PCB-153 was shown to be highly resistant to metabolism [181], which is likely the cause of the lack of

induction of xenobiotic metabolizing genes in the exposed WT mice in our study. We observed gene expression changes, oxidative stress, hemolytic anemia, premature lethality, and tumor development with exposure of SXRKO mice to a much lower dose of PCB-153 than in other studies. We propose that the altered metabolism profile of SXRKO mice led to the accumulation of the highly toxic hydroxylated metabolites of PCB-153 which then elicited these toxic effects.

Our results suggest that exposure to PCB-153 during sensitive developmental time periods can lead to hemolytic anemia induced by elevated oxidative stress. Moreover, SXR loss-of-function increased susceptibility to this effect of PCB-153 via alterations in xenobiotic and glutathione metabolism leading to impaired metabolism and/or clearance of toxic PCB metabolites. We observed reduced body weights that coincided with reduced blood hemoglobin levels in SXRKO mice perinatally exposed to PCB-153 and this was consistently seen with chronic exposure up to 10 months of age. We speculate that the reduced body weight and premature death at 5 weeks of age observed in PCB-153 exposed SXRKO mice may be linked directly to the anemia phenotype. Mice experience rapid growth from birth up until 5-6 weeks of age, which requires increased production of red blood cells [182, 183]. We infer that anemia became fatal in some mice at 5 weeks of age due to an unmet need for RBCs and hemoglobin. Exposure to PCBs during *in utero* or early development was associated with reduced birth weight, growth rate, adolescent body weight, and these growth abnormalities have also been associated with anemia [119, 157, 184]. Therefore, our study revealed anemia as a possible component of the mechanism underlying these adverse effects of prenatal or perinatal PCB exposure. Anemia is a highly under-investigated outcome in PCB exposed human cohorts and in laboratory animal exposure studies. Only one study reported an anemia phenotype in rats, and this used a high dose (50 mg/L or 14 µmol/kg/day) of PCB-105 for 13 weeks of exposure [185], more than 50-fold higher than the dose

used in our study. A chronic exposure study in Rhesus monkeys to a mixture of PCBs led to anemia at a concentration of 200 μg/kg/day (or 0.55 μmol/kg/day) for a period of 27 months or longer [186]. To our knowledge, we are the first to report anemia as an effect of low-dose perinatal PCB exposure.

We recognize that the results from this study may not apply to all PCBs, or even all NDL-PCBs, because many studies have shown congener-specific effects. However, we believe it important to investigate PCB-153 since it is the most prevalent congener found in the environment, human tissue, and in breast milk [110, 116]. Many replacement chemicals, such as polybrominated biphenyls (PBBs) and polybrominated diethers (PBDEs), were synthesized following the PCB ban. These chemicals have similar structures and properties to PCBs and many were demonstrated to induce Cyp gene expression, inflammation, and to interact with SXR. In addition, hydroxylated metabolites of these chemicals have been demonstrated to induce oxidative stress [37, 187]. Whether SXR plays a key role in the protection and/or clearance of these chemicals, *in vivo,* remains to be investigated in the future.

There are currently 9,451 reported SNPs of human SXR on the NCBI dbSNP, many of which can impact the expression of SXR itself and/or that of its target genes [42, 43]. Polymorphisms in SXR have been linked to many functional consequences, including altered metabolism, increased inflammation, and susceptibility to disease [44-46]. Some xenobiotics and pharmaceutical drugs were shown to suppress SXR signaling [188, 189]. Antagonists of SXR are actively being developed to be used as pharmaceutical drugs [48]. Our studies suggest that both genetic and chemical inhibition of SXR might predispose humans to increased oxidative stress and lead to more toxic effects from exposure to PCBs. We expect that SXR is important for the metabolism and clearance of other metabolites of many PCB congeners. SXR is responsible for the metabolism

of many xenobiotics; thus, adverse effects of impaired SXR function may not be exclusive to PCB exposure. SXR is likely to be protective against other drugs and xenobiotics with the potential to produce reactive metabolites. There is evidence that hydroxylated metabolites of other xenobiotics, such as those of the antimalarial agent primaquine, can induce oxidative stress and hemolytic anemia [40]. Whether SXR also plays a role in the proper metabolism of these xenobiotics and protection against their reactive metabolites is yet to be investigated, but our results indicated that caution is warranted before inhibiting SXR/PXR function as a general method to promote increased efficacy of drugs that might otherwise be metabolized via an SXR/PXR-dependent process.

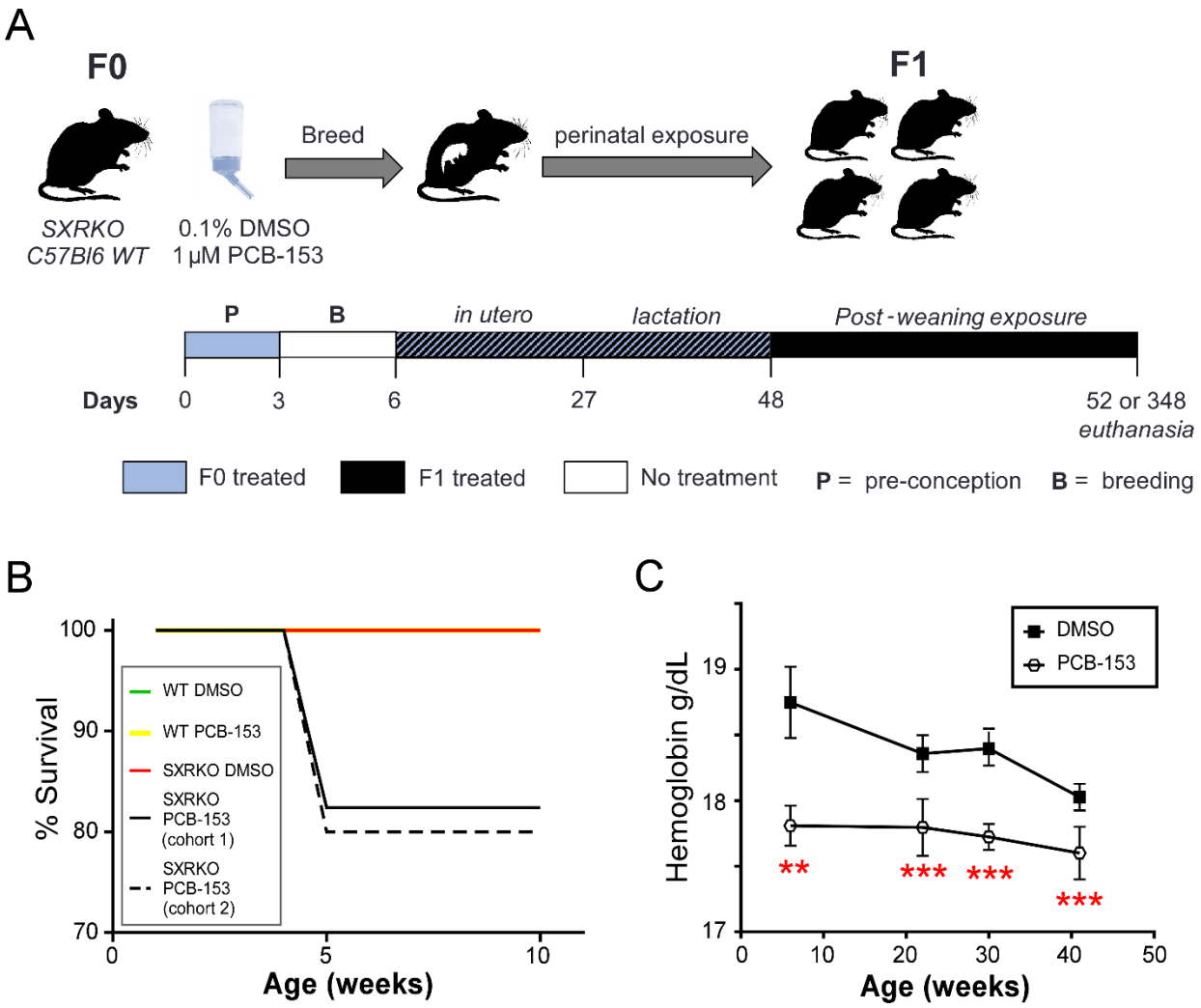

<u>Figure 4.1</u>: *Premature death and decreased blood hemoglobin in SXRKO mice exposed to PCB-153.* Exposure scheme for perinatal exposure to PCB-153 (A). Survival of wild-type (WT) or SXR/PXR knockout (SXRKO) mice perinatally exposed to PCB-153 or vehicle (DMSO) (B). Hemoglobin measurements of SXRKO mice exposed to DMSO or PCB-153 throughout lifespan (C). * = p-value <0.05, ** = p-value <0.01, ***= p-value <0.001

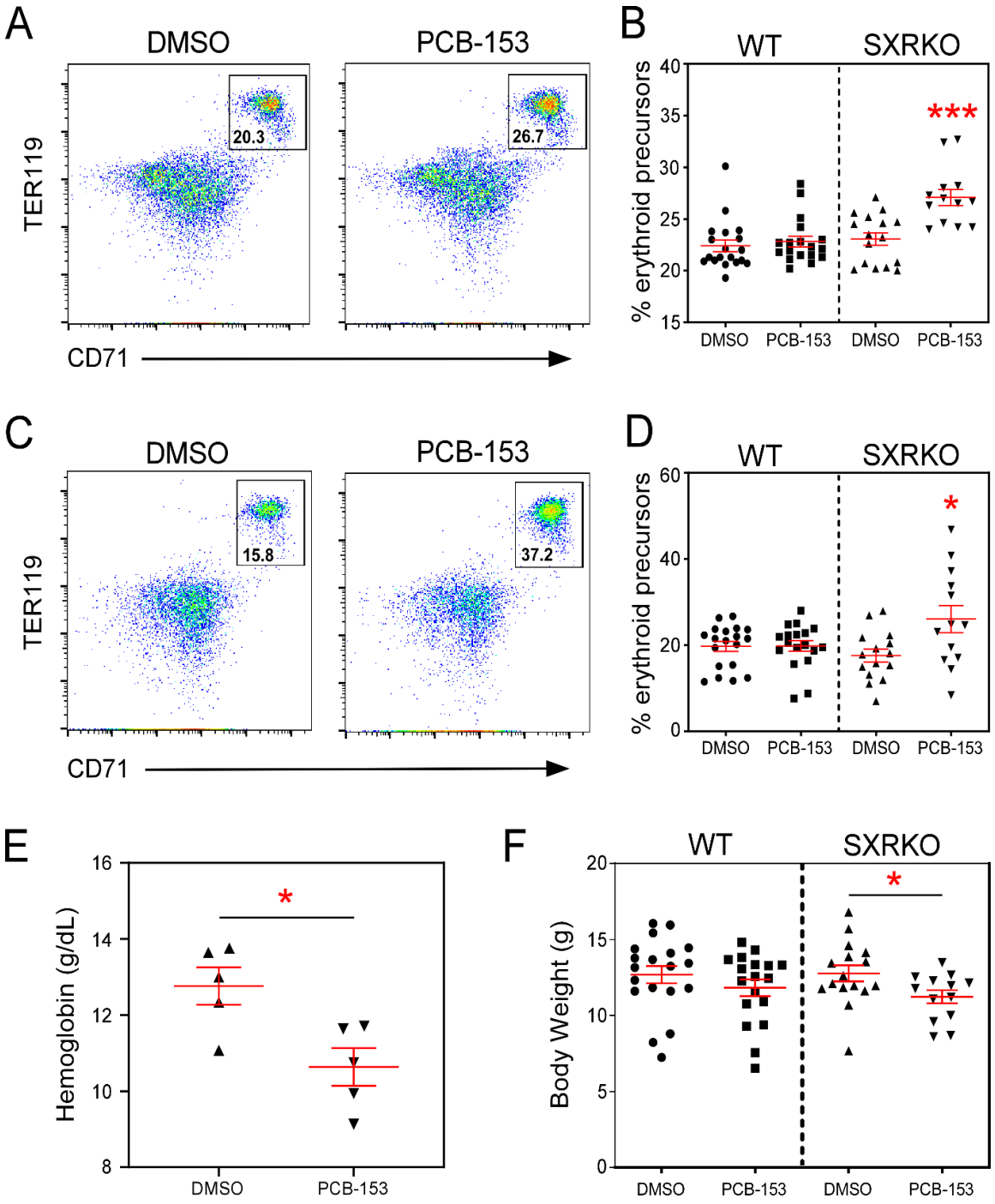

<u>Figure 4.2</u>: ***Increased erythropoiesis in 4 week old SXRKO mice perinatally exposed to PCB-153.*** Representative FACS plots of bone marrow (A) or spleen (C) of SXRKO mice exposed to DMSO and PCB-153, gating on erythroid precursors. Quantifications of erythroid precursors in bone marrow (B) and spleen (D) of 4 week old perinatally exposed mice. Blood hemoglobin levels of SXRKO mice at 4 weeks of age perinatally exposed to either DMSO or PCB-153 (G). Body weights of perinatally exposed mice at 4 weeks of age (H). * = p-value <0.05, ** = p-value <0.01, ***= p-value <0.001

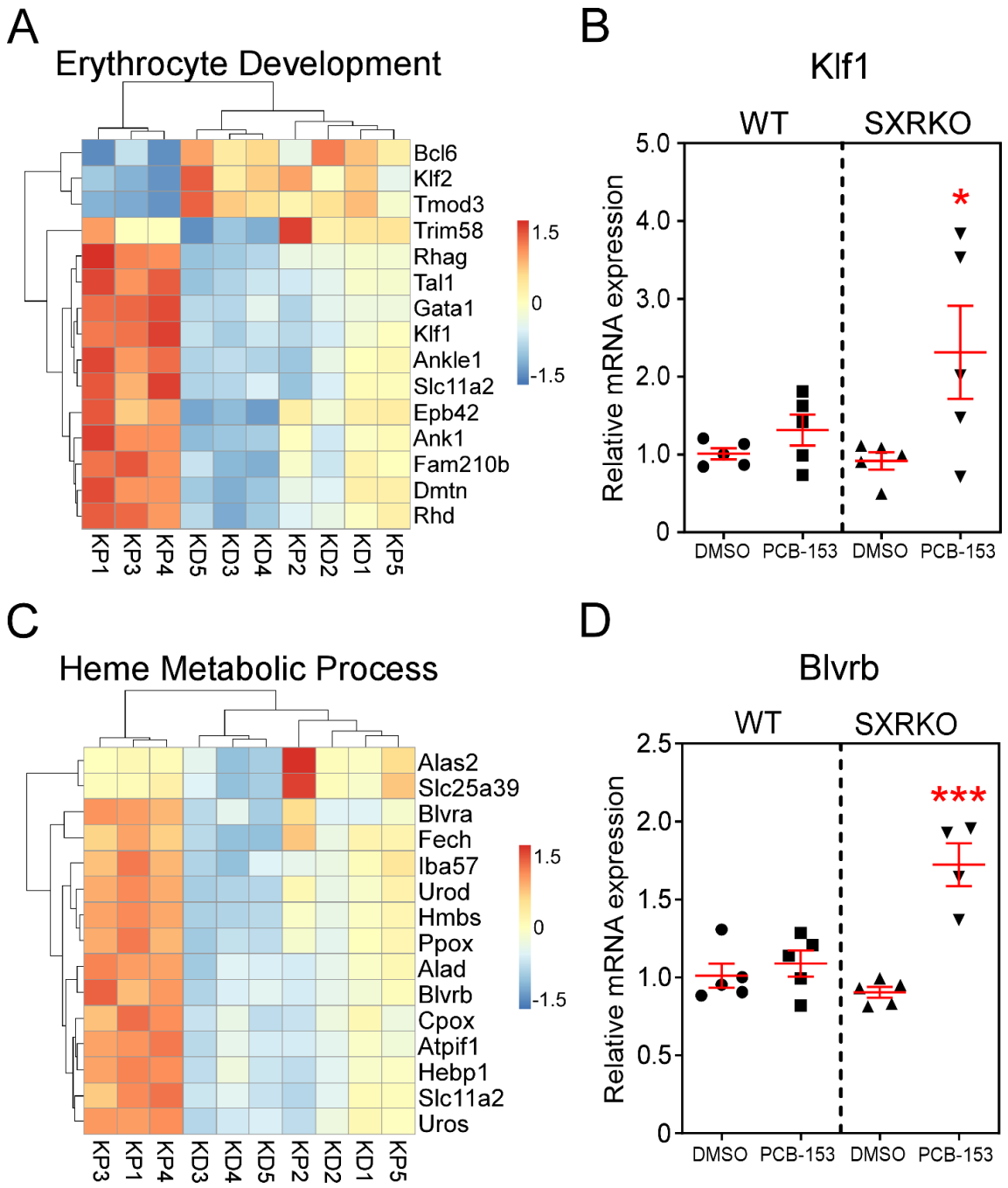

<u>Figure 4.3</u>: ***Increased expression of erythrocyte development and heme metabolism genes in SXRKO mice exposed to PCB-153.*** Differentially expressed genes (DEGs) involved in erythrocyte development in the spleen between SXRKO mice exposed to DMSO and PCB-153 (A). qPCR gene expression analysis confirmed expression pattern of Kupple-like factor 1 (Klf1) erythroid transcription factor (B). SXRKO mice exposed to PCB-153 have increased expression of heme metabolism genes (C), including genes involved in heme catabolism, such as Blvrb (D). D= DMSO exposure, P= PCB-153 exposure, W= wild-type mice, K= SXRKO mice. * = p-value <0.05, ** = p-value <0.01, ***= p-value <0.001

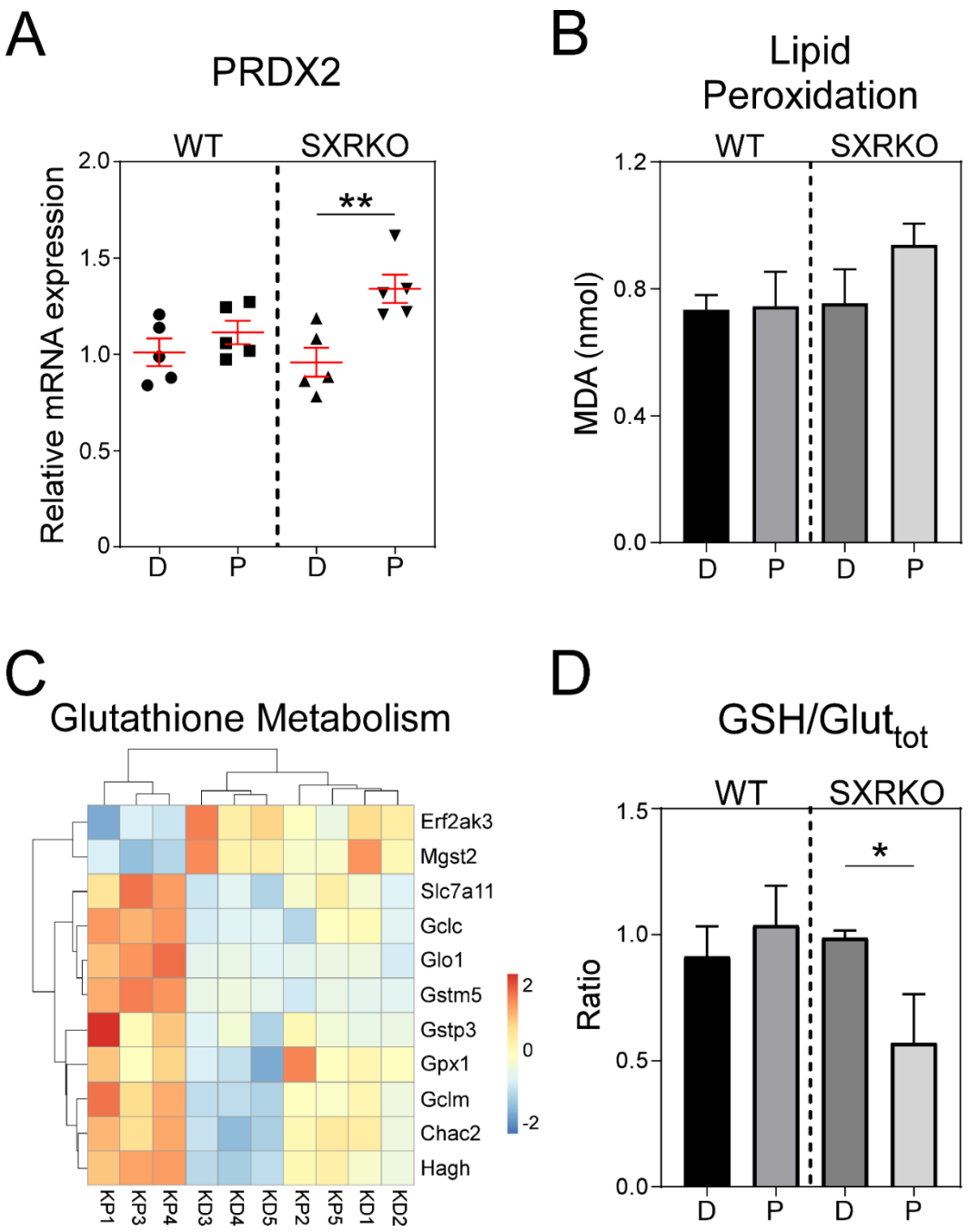

<u>Figure 4.4</u>: ***Elevated oxidative stress in spleen and RBCs of PCB-153 exposed SXRKO mice.*** Increased expression of reactive oxygen species (ROS) response genes, such peroxiredoxin 2 (Prdx2) (A) in spleen of SXRKO mice exposed to PCB-153 compared to vehicle. Malonaldehyde (MDA) levels show trend of increased lipid peroxidation of RBC membranes from PCB-153 exposed SXRKO mice (B). SXRKO mice exposed to PCB-153 display increased expression of glutathione metabolism genes (C). Ratio of reduced glutathione (GSH) to total glutathione is decreased in RBCs of SXRKO mice exposed to PCB-153 (D). D= DMSO exposure, P= PCB-153 exposure, W= wild-type mice, K= SXRKO mice. * = p-value <0.05, ** = p-value <0.01, ***= p-value <0.001

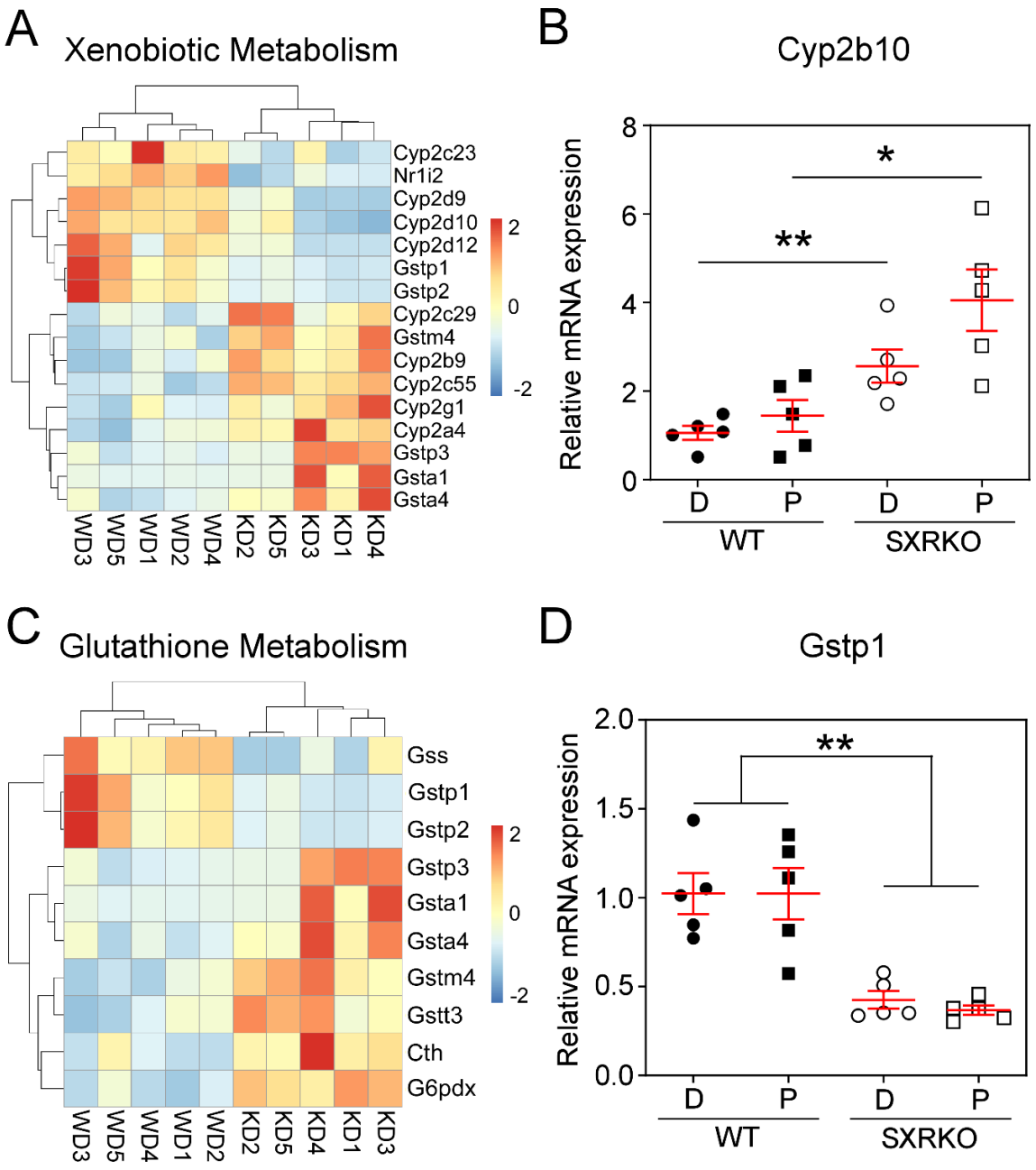

<u>Figure 4.5</u>: ***Altered xenobiotic and glutathione metabolism in the liver between SXRKO and WT mice.*** Liver RNA-seq analysis revealed inherent differences in xenobiotic metabolism genes (A), including various CYP genes, such as Cyp2b10, which was validated by qPCR (B). Several genes related to glutathione metabolism were also different in the liver between SXRKO and WT mice (C). Expression pattern of Gstp1 was confirmed by qPCR (D). D= DMSO exposure, P= PCB-153 exposure, W= wild-type mice, K= SXRKO mice. * = p-value <0.05, ** = p-value <0.01, ***= p-value <0.001

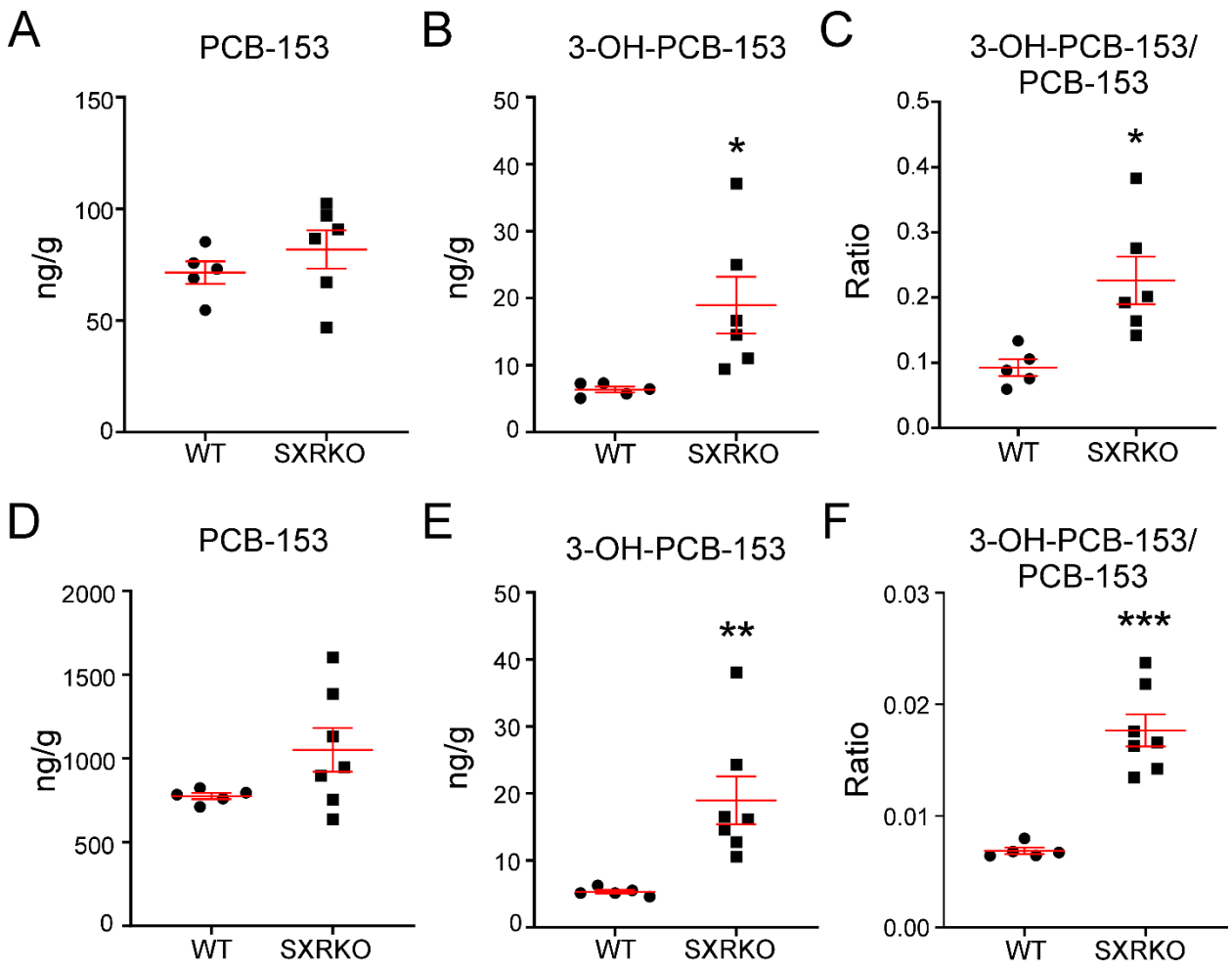

<u>Figure 4.6</u>: ***Elevated levels of hydroxylated PCB-153 metabolites in exposed SXRKO mice.*** Levels of PCB-153 (A) and 3-OH-PCB-153 (B), and the ratio of 3-OH-PCB-153 to PCB-153 (C) in the plasma. Levels of PCB-153 (D), 3-OH-PCB-153 (E), and the ratio of 3-OH-PCB-153 to PCB-153 (F) in liver of PCB-153 exposed WT and SXRKO mice. * = p-value <0.05, ** = p-value <0.01, ***= p-value <0.001

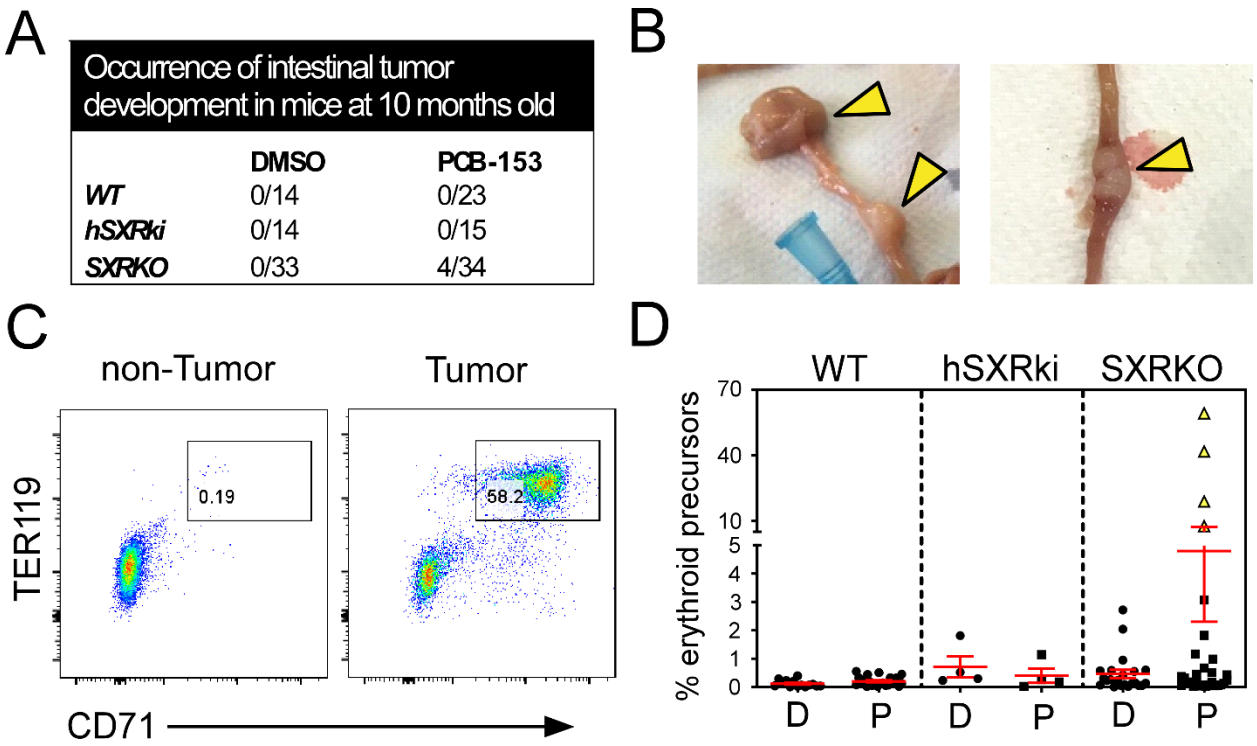

<u>Figure 4.7</u>: *SXRKO mice chronically exposed to PCB-153 until 10 months of age develop intestinal tumors*. Intestinal tumors were found in the upper intestine of ~12% of SXRKO mice chronically exposed to PCB-153 at 10 months of age, no tumors were found in PCB-153 exposed WT or human SXR/PXR knock-in (hSXRki) mice or any of the vehicle (DMSO) exposed mice (A). Representative images of the tumors located near the duodenum-jejunum junction of the upper intestine (B). Representative FACS plots of the spleen of a non-tumor vs tumor bearing mouse, gating on erythroid precursors (C). Quantification of erythroid precursor percentage in the spleen of chronically exposed mice, tumor bearing mice are indicated with yellow symbols (D). * = p-value <0.05, ** = p-value <0.01, ***= p-value <0.001

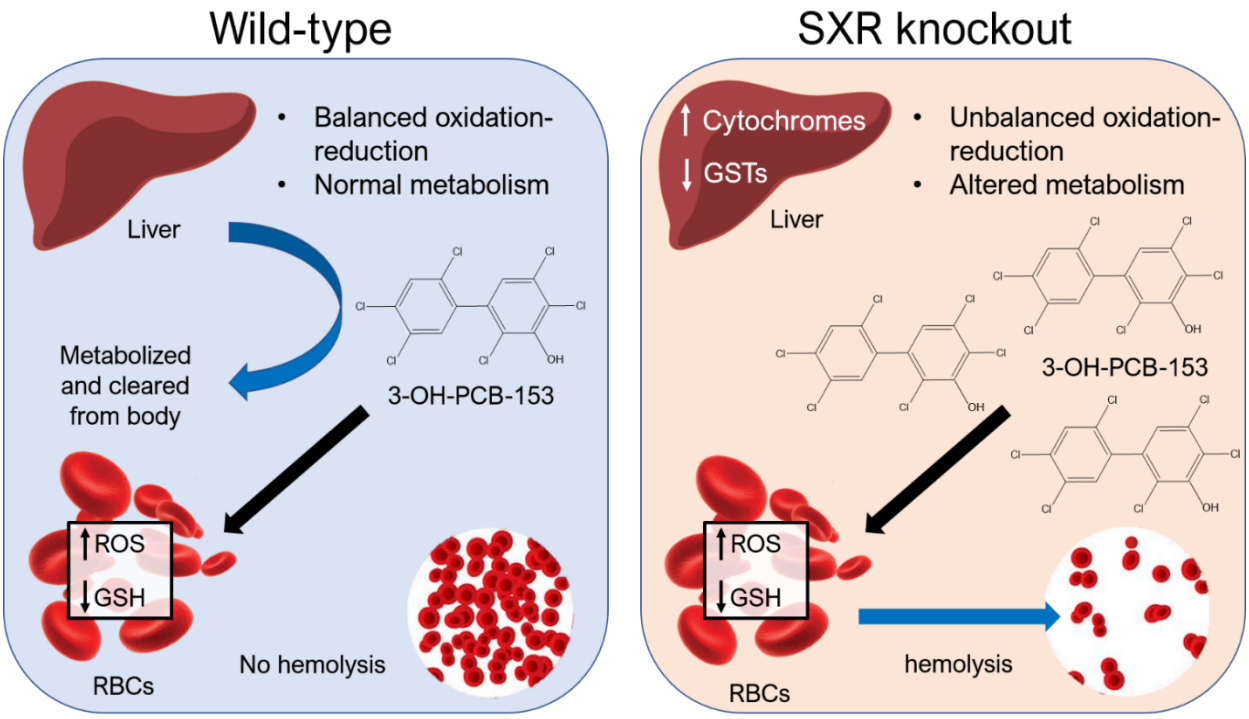

<u>Figure 4.8</u>: ***Proposed mechanism of oxidative stress and anemia phenotype induced by PCB-153 in SXRKO mice.***

Table 4.1: Spleen RNA-seq results

	SXRKO DMSO vs WT DMSO	SXRKO PCB vs WT PCB	SXRKO PCB vs SXRKO DMSO	WT PCB vs WT DMSO
Total DEGs	23	198	1598	4
Up-regulated	16	125	965	1
Down-regulated	7	73	633	3
GO terms (BP)	**0**	**24**	**380**	**0**

Number of total, up-regulated, and down-regulated differentially expressed genes (DEGs) for each comparison and the resulting number of significant gene ontology (GO) terms for biological processes (BP). DEGs were determined by DESeq2 with adj p-value<0.05 and absolute value of log2 (FC)>0.3. GO term significance determined by Benjamini-Hochberg correction test (adj p-value <0.05) in MouseMine.

Table 4.2: Liver RNA-seq results

	SXRKO DMSO vs WT DMSO	SXRKO PCB vs WT PCB	SXRKO PCB vs SXRKO DMSO	WT PCB vs WT DMSO
Total DEGs	260	394	60	0
Up-regulated	142	180	19	0
Down-regulated	118	214	41	0
GO terms (BP)	**47**	**103**	**9**	**0**

Number of total, up-regulated, and down-regulated differentially expressed genes (DEGs) for each comparison and the resulting number of significant gene ontology (GO) terms for biological processes (BP). DEGs were determined by DESeq2 with adj p-value<0.05 and absolute value of log2 (FC)>0.3. GO term significance determined by Benjamini-Hochberg correction test (adj p-value <0.05) in MouseMine.

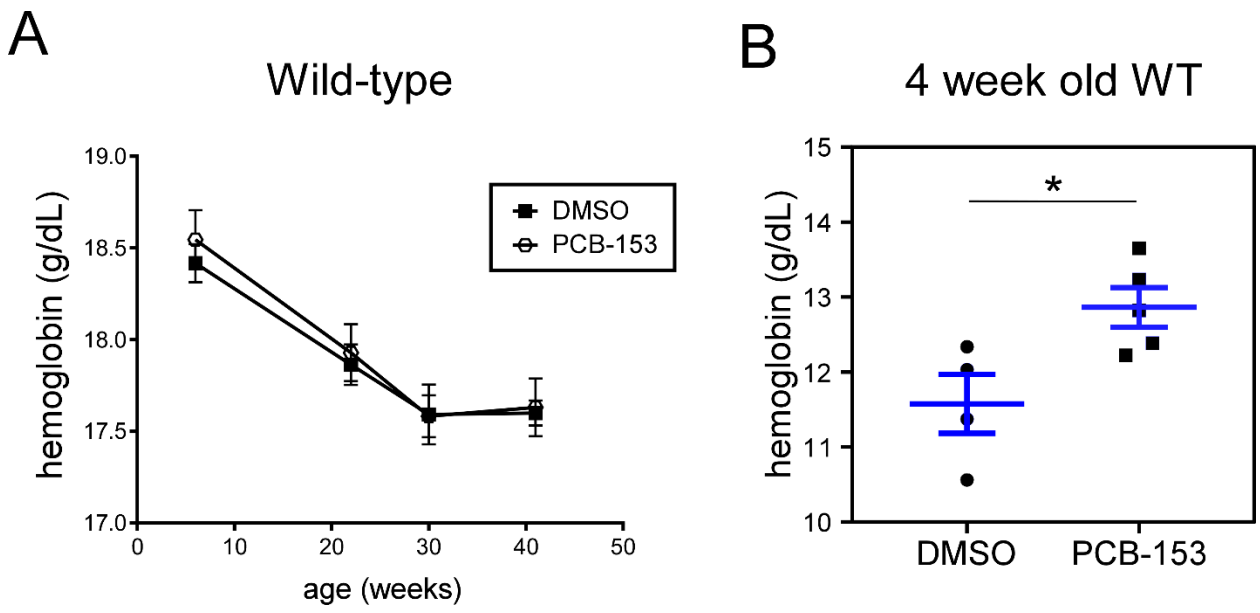

<u>Supplemental Figure 4.1</u>: Blood hemoglobin levels of wild-type mice throughout lifespan. Hemoglobin levels of wild-type (WT) mice exposed to either PCB-153 or vehicle (DMSO) at 6 to 40 weeks of age as measured by the blood analyzer (A). Blood hemoglobin values in WT mice at 4 weeks of age perinatally exposed to either PCB-153 or DMSO, as determined by hemoglobin assay kit (B)

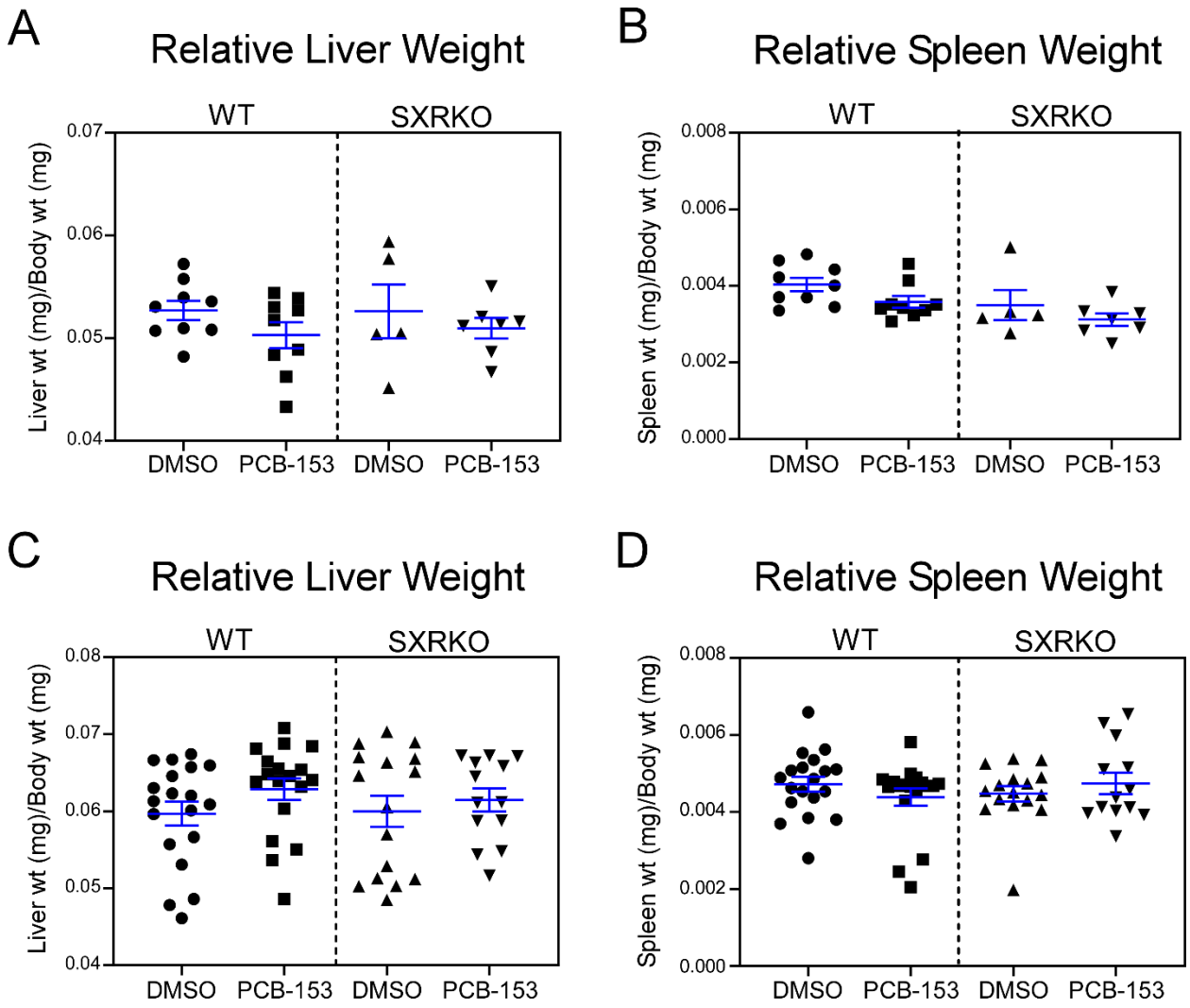

<u>Supplemental Figure 4.2</u>: Relative spleen weights of dams and pups from PCB-153 exposure study. Relative liver weights (A) and spleen weights (B) for DMSO and PCB-153 exposed WT and SXRKO dams. Relative liver weights (C) and spleen weights (D) for perinatally exposed WT and SXRKO mice at 4 weeks of age.

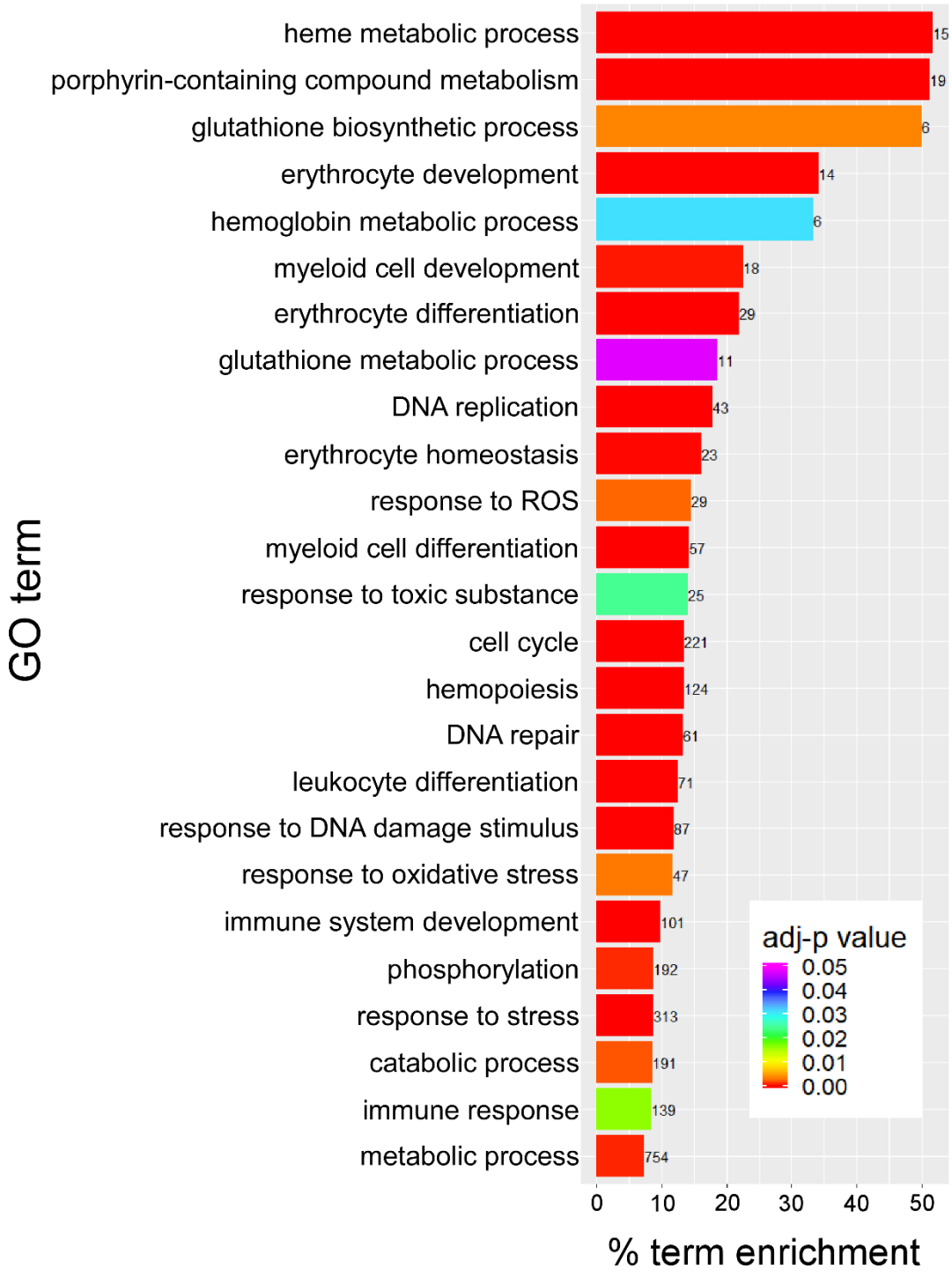

<u>Supplemental Figure 4.3</u>: Gene Ontology (GO) term enrichment of spleen RNA-seq data set comparing SXRKO mice exposed to PCB-153 vs SXRKO mice exposed to vehicle (DMSO). GO term enrichment of select biological processes (BP) of SXRKO PCB vs SXRKO DMSO in the spleen RNA-seq dataset. Number of significant genes within each term is to the right of the bar.

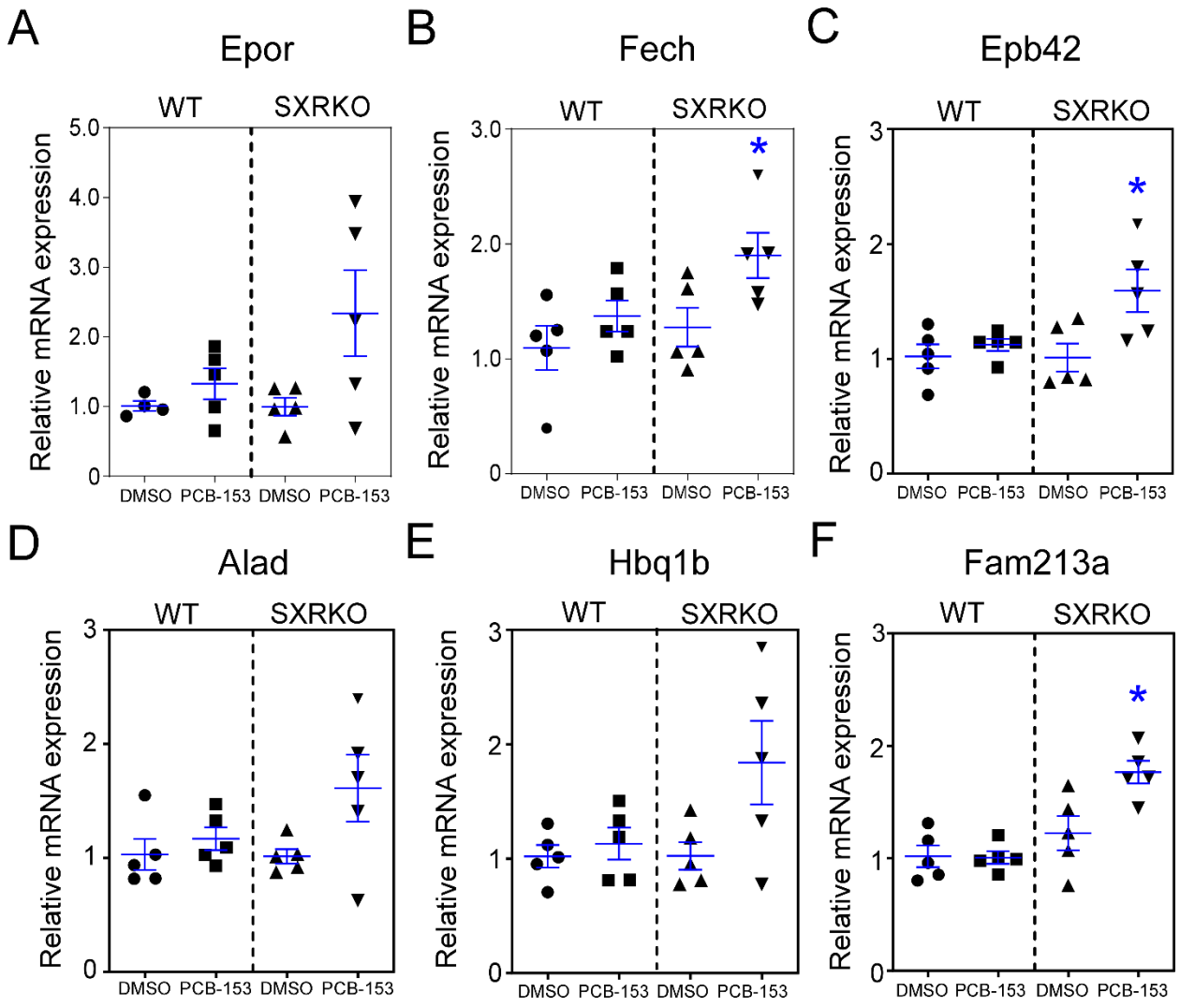

<u>Supplemental Figure 4.4</u>: qPCR validation of select differentially expressed genes (DEGs) related to erythrocyte development and heme metabolism in the spleen. Relative mRNA expression of Epor (A), Fech (B), Epb42 (C), Alad (D), Hbq1b (E), and Fam213a (F) determined by qPCR analysis compared to Actb housekeeping gene.

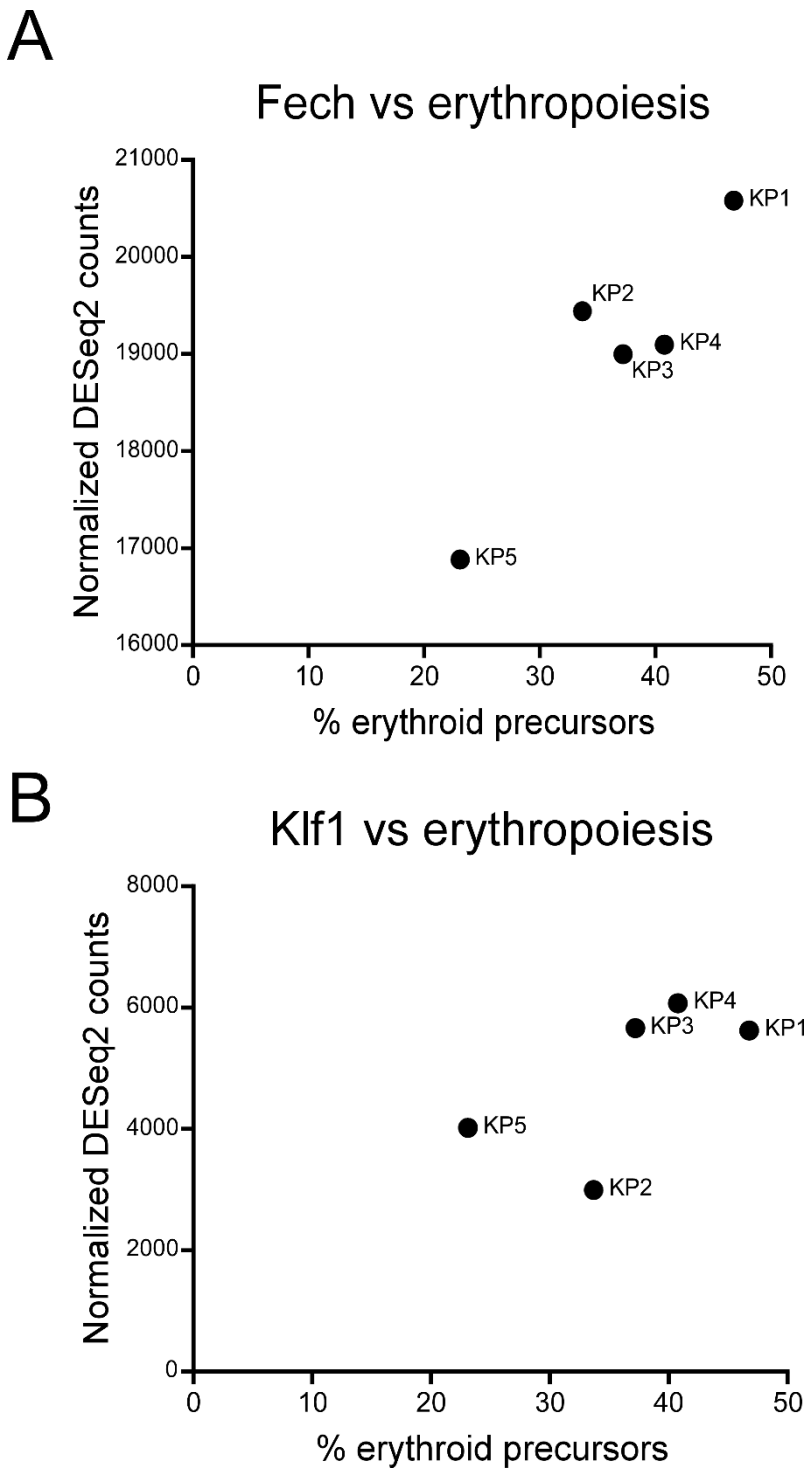

<u>Supplemental Figure 4.5</u>: mRNA expression of erythrocyte development and heme metabolism genes correlates with level of erythropoiesis in SXRKO mice exposed to PCB-153. Plots of percentage of splenic erythroid precursors vs normalized DESeq2 counts in the spleen dataset for A) Fech and B) Klf1. KP= SXRKO mice exposed to PCB-153.

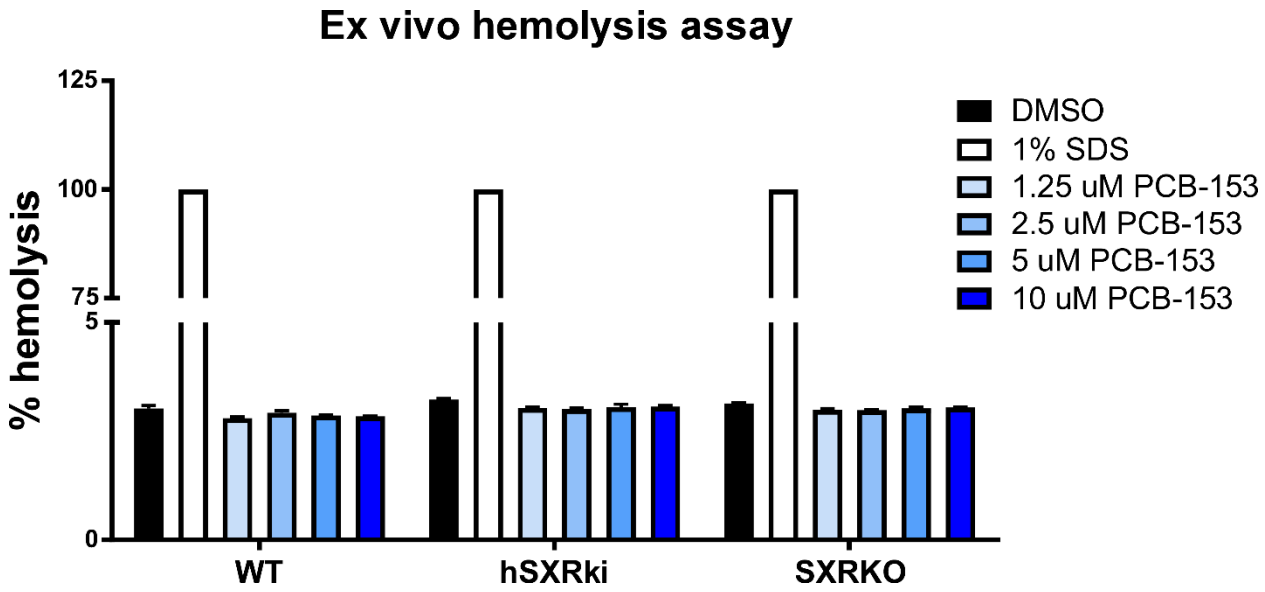

<u>Supplemental Figure 4.6</u>: PCB-153 does not induce hemolysis of red blood cells *ex vivo*. *Ex vivo* hemolysis assay of red blood cells (RBCs) from WT (n=3) and SXRKO mice (n=3) treated ex vivo to vehicle (DMSO), positive control (1% SDS), and four different concentrations of PCB-153.

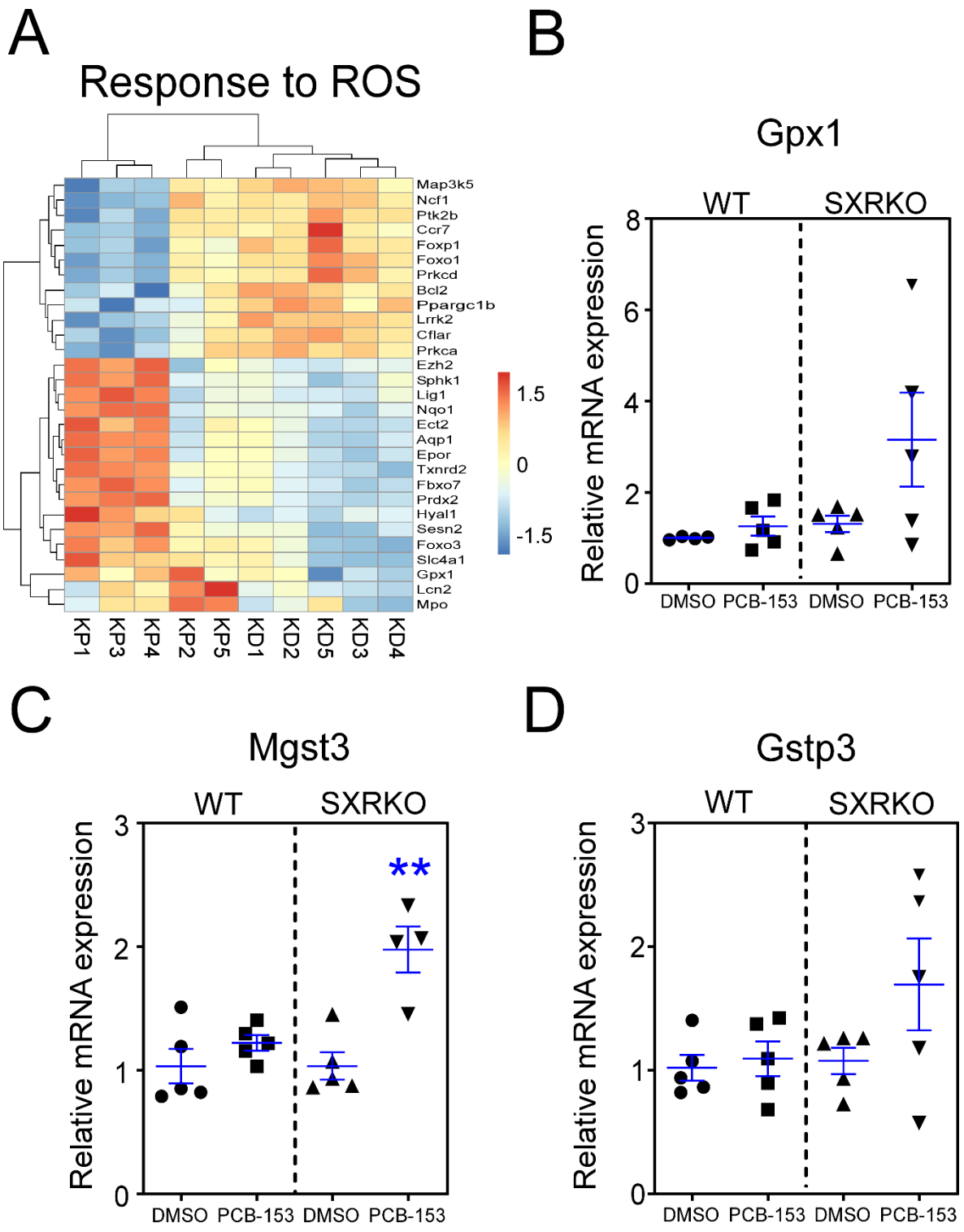

<u>Supplemental Figure 4.7</u>: Differentially expressed genes (DEGs) related to oxidative stress in the spleen of SXRKO mice exposed to PCB-153 vs vehicle (DMSO). Heatmap of DEGs in the GO term of Response to reactive oxygen species (ROS) (A). qPCR validation of the antioxidant gene Gpx1 (B) and glutathione S-transferase genes, Mgst3 (C) and Gstp3 in the spleen compared to Actb housekeeping gene

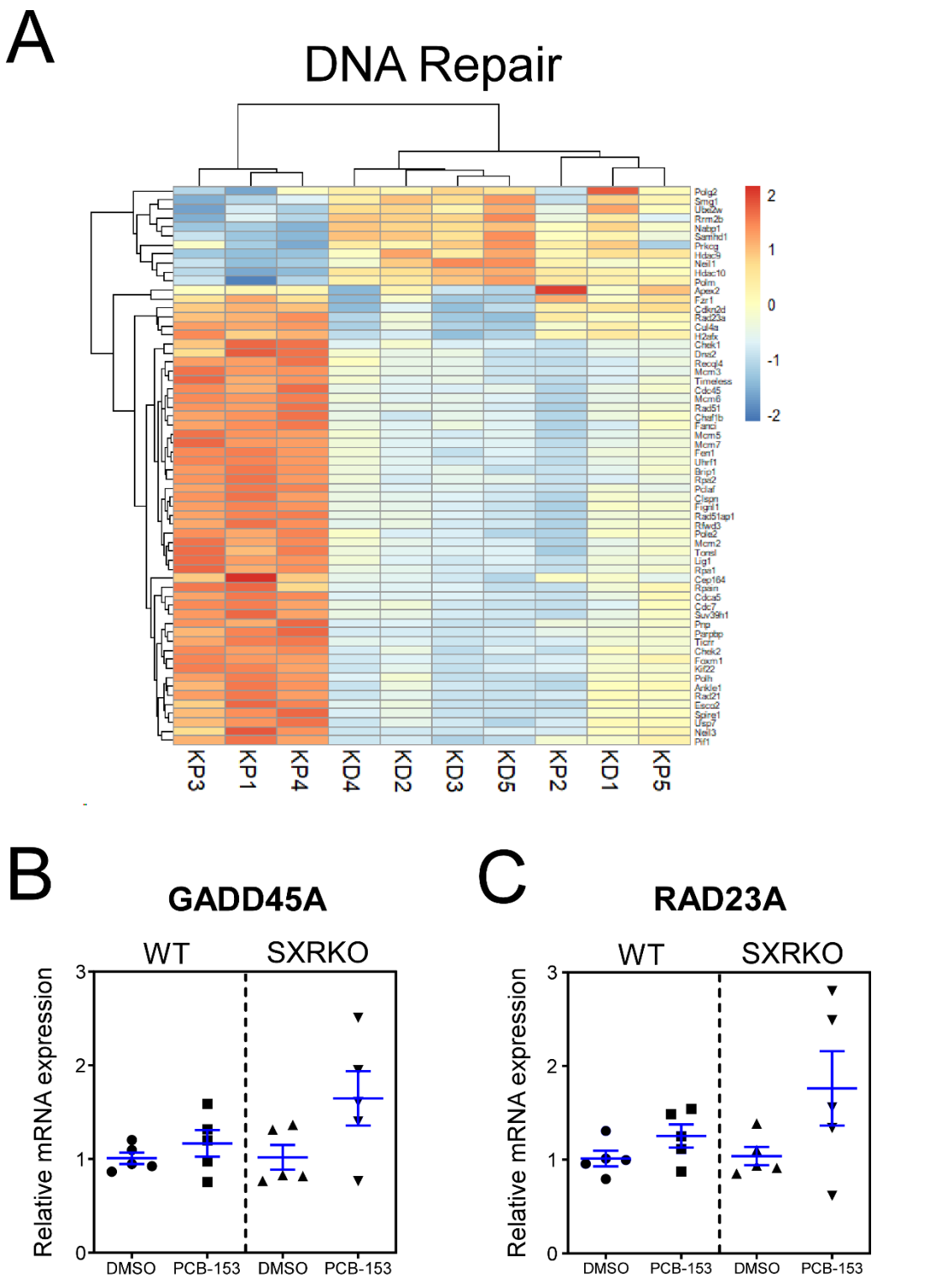

<u>Supplemental Figure 4.8</u>: Increased DNA repair genes in the spleen of SXRKO mice exposed to PCB-153. Heatmap of significant differentially expressed genes within the GO term of DNA repair between spleens of SXRKO mice exposed to PCB-153 vs DMSO (A). qPCR validation of Gadd45a (B) and Rad23a (C).

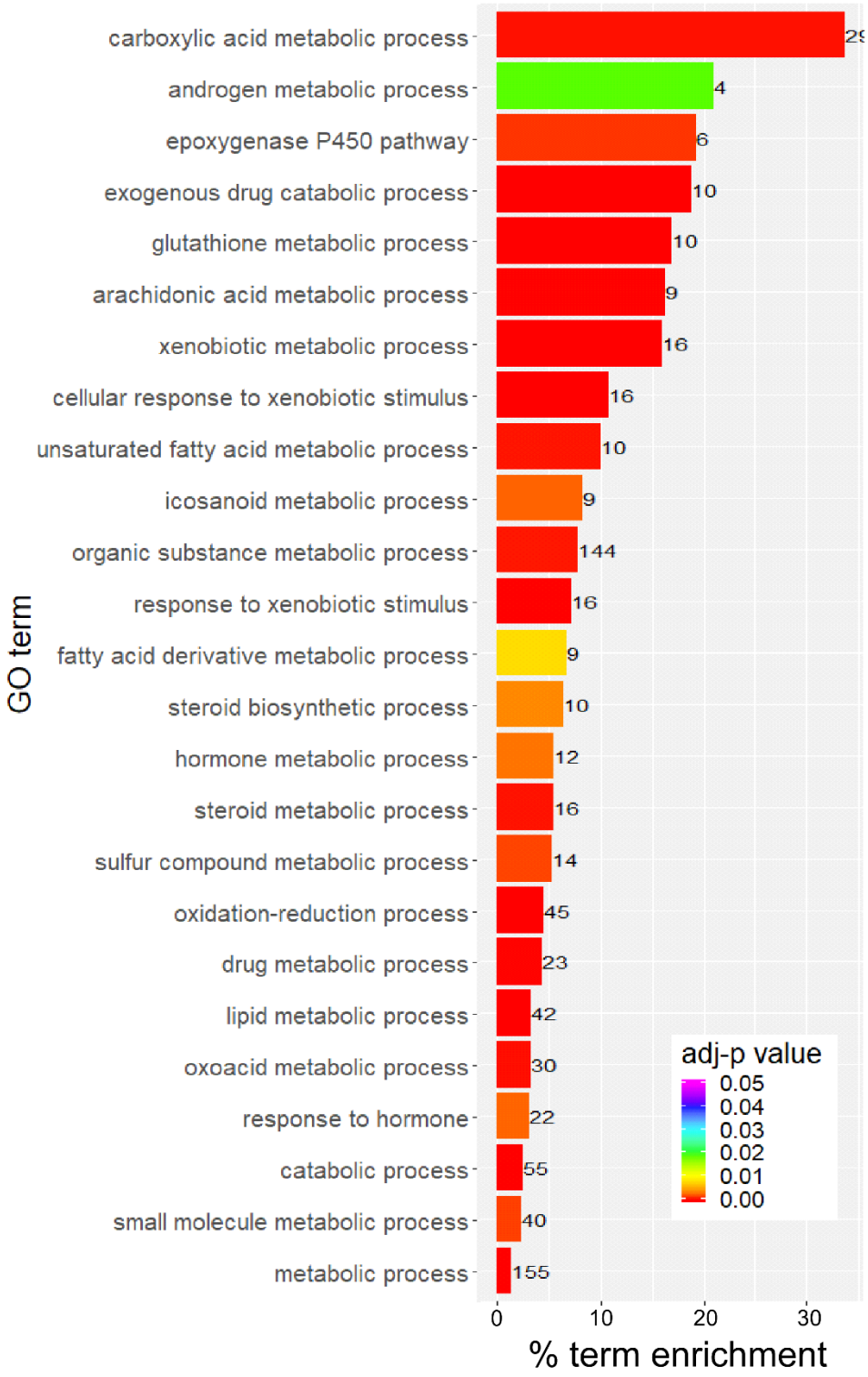

<u>Supplemental Figure 4.9</u>: Gene Ontology (GO) term enrichment of liver RNA-seq dataset comparing SXRKO vs wild-type mice exposed to vehicle (DMSO). GO term enrichment of select biological processes (BP) of SXRKO DMSO vs WT DMSO in the liver RNA-seq dataset. Number of significant genes within each term is to the right of the bar.

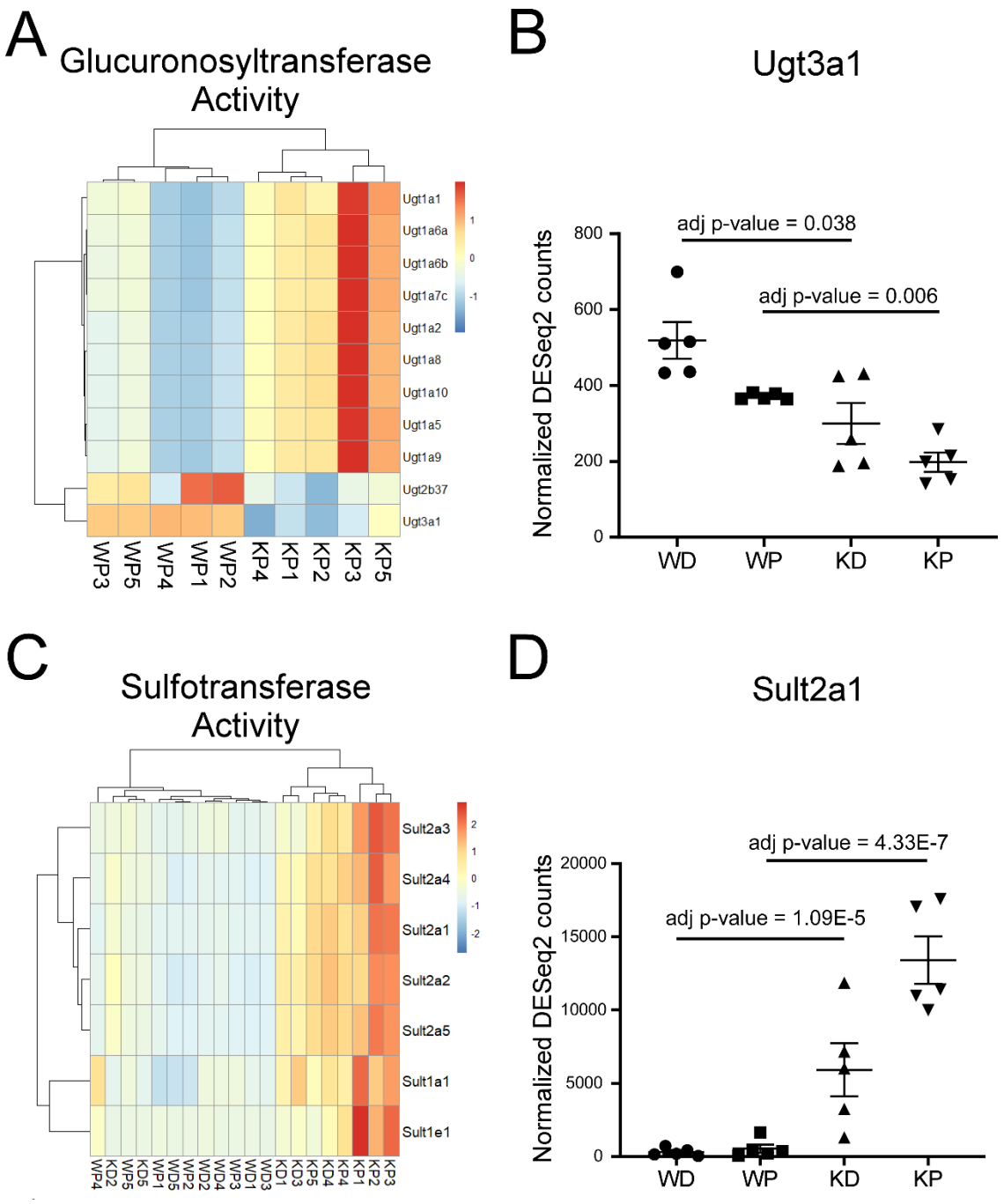

<u>Supplemental Figure 4.10</u>: Differential expression of various UGT and SULT genes between WT and SXRKO mice and with PCB-153 exposure. Heatmap of DEGs related to glucuronosyltransferase activity in the livers between SXRKO and WT mice exposed to PCB-153 (A). Normalized counts of Ugt3a1 obtained from DESeq2 (B). Heatmap of DEGs related to sulfotransferase activity, comparing all groups (C). Normalized counts of Sult2a1 obtained from DESeq2 analysis (D). Lines demonstrate the comparisons that were significant as determined by DESeq2 using the criteria listed in the materials and methods. Adjusted p-values determined by DESeq2 analysis are displayed above lines for corresponding comparisons.

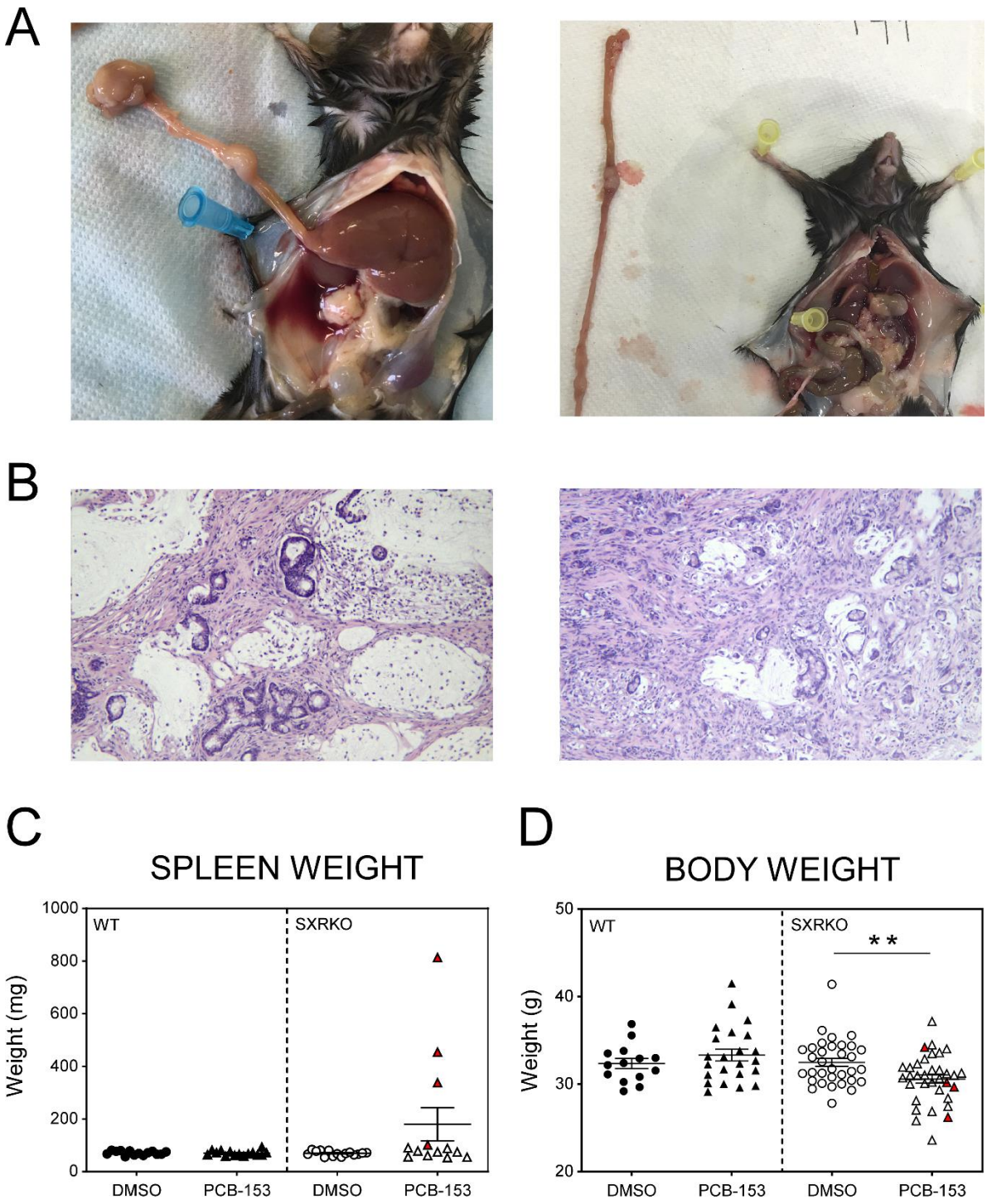

<u>Supplemental Figure 4.11</u>: Tumor location, body weights, and spleen weights of mice chronically exposed to PCB-153. Representative images of SXRKO mice chronically exposed to PCB-153 displaying tumors in the upper small intestine near the duodenum-jejunum junction (A). Representative histology images of the intestinal tumors at 40X total magnification (B). Spleen weights (C) and body weights (D) of chronically exposed mice. Tumor bearing mice are indicated with red symbols in panel C and D.

Supplemental Table 4.1: qPCR primer sequences

Gene (mouse)	Forward primer	Reverse primer
36B4/Rplp0	AAGCGCGTCCTGGCATTGTCT	CCGCAGGGGCAGCAGTGGT
Actb	GGCTGTATTCCCCTCCATCG	CCAGTTGGTAACAATGCCATGT
Fech	GACCGAGACCTCATGACACTTCC	ATAACTCATCCAGCAGCTTCACCA
Klf1	GAGCCCTCCAAGAAACTTTCCT	TCAGACCGCCACCACTTGAG
Epor	CGGGATGGACTTCAACTACAGC	AACACCAGAAACGCACGGAG
Prxd2	GGACTACAGAGGGAAGTACG	TGAACTGAGAGTCCACAGAC
Gpx1	CGTTTGAGTCCCAACATCTC	ATCGTTCATCTCGGTGTAGTC
Gstp1	TCCTTTGCCGATTACAACTTGC	AGTCCACTACTGTTTGCCATTGC
Gadd45a	GCTGCTACCTCTGCTTACCTCTG	CCTTCCATTGTGATGAATGTGGGT
Rad23a	AGATGTTGAATGAGCCTCCCG	TGCCTTCAGCCTTTCTATAGCC
Blvrb	CAGGTTATGAGGTGACGGTG	CCACAGTCTTGTCCACATCGG
Gstp3	GTGACCTTGGATGTTTGGGAGC	CTTTGCCATAGAGCCCGAAGGA
Mgst3	TACAGCACAGATCCTGAGAACG	TAAACACCTCCCACCGTTAGGA
Epb42	GACAGTCCTTCACTATCACCCTG	TGGCTTGGGTCTTATTGATCTTGG
Alad	CAGTGCCTCCAACCTCATCTATCC	GACGCCAAAGATCAGGACACAG
Hbq1b	AGACTTCAGCCCAGAGATGC	GAGACTATAGAACCCTGTATCCC
Fam213a	GCAGACCTGATGTCCTTGAAGC	ATGAACATCATCTTCCGCCTCTC
Cyp2b10	GTGCCCACAGACAAATCTCCA	GGACTTCTCCTTCTCCATGCG

Supplemental Table 4.2: Deaths at 5 weeks of age

		DMSO	PCB-153
COHORT 1	WT	0/6 (0%)	0/13 (0%)
	SXRKO	0/15 (0%)	**3/17 (17.6%)**
COHORT 2	WT	0/13 (0%)	0/10 (0%)
	SXRKO	0/3 (0%)	**2/10 (20%)**

Supplemental Table 4.3: WT blood parameters over time

	Week 6		Week 21-22		Week 30		Week 40	
	WT DMSO	**WT PCB**	**WT DMSO**	**WT PCB**	**WT DMSO**	**WT PCB**	**WT DMSO**	**WT PCB**
WBC(10^3/mm3)	14.8±2.8	14.8±3.7	22±10.4	24.1±6.1	23.5±5.5	26.7±5.5	26.5±6.2	26.3±3.6
RBC (10^6/mm3)	10.6±0.6	11.2±0.7	11.1±0.4	11.2±0.4	10.7±0.5	10.7±0.4	10.2±0.2	10.3±0.8
HGB (g/dL)	18.4±0.4	18.5±0.7	17.8±0.4	17.9±0.7	17.5±0.6	17.5±0.5	17.6±0.1	17.6±0.5
HCT (%)	58.6±2.5	61±2.6	55.8±3.4	55.8±1.9	52.8±2.8	52.7±2.1	51.4±1.4	51.1±3.5
MCV (fl)	55.1±1.9	54.4±2	49.1±0.7	49.7±0.8	48.9±0.9	49.2±0.7	50.1±1.1	49.1±1.1
MCH (pg)	17.3±1	16.5±1.3	15.9±0.4	15.9±0.5	16.3±0.6	16.3±0.5	17.1±0.4	17±0.8
MCHC (g/dL)	31.5±1.3	30.3±1.3	32.4±0.9	32.1±1.1	33.3±1.2	33.3±1	34.2±0.9	34.5±1.2
RDW (%)	15.7±1.7	14.5±1.4	13.8±0.5	13.9±0.5	13.8±0.4	13.9±0.3	14.1±0.3	14.3±0.2
PLT (10^3/mm3)	955.5±562	581.1±531.7	822±395.7	561.2±303.6	776.6±502.6	707.6±252.3	871.5±523.4	961.4±521.5
MPV (fl)	6.7±0.4	6.3±0.5	6±0.6	5.8±0.3	6.1±0.4	6.1±0.2	6.2±0.2	6.1±0.2
LYM (%)	82.2±4.3	82.9±5.1	74±3.7	74.1±6.9	71.8±6.9	71.6±6.1	72.5±5.6	71.3±4.3
MON (%)	2.9±0.4	2.9±0.4	4±0.3	3.9±0.4	3.9±0.5	4±0.3	4±0.5	4±0.3
GRA (%)	14.8±3.9	14.1±4.8	21.9±3.4	21.8±6.5	24.2±6.4	24.3±5.8	23.4±5.2	24.6±4.1

Values presented as mean±SD

asterisks indicate significance compared to vehicle treated group for same age. *p<0.05, **p<0.01, ***p<0.001 determined by t-test

Supplemental Table 4.4: SXRKO blood parameters over time

	Week 6		Week 22		Week 30		Week 40	
	SXRKO DMSO	**SXRKO PCB**	**SXRKO DMSO**	**SXRKO PCB**	**SXRKO DMSO**	**SXRKO PCB**	**SXRKO DMSO**	**SXRKO PCB**
WBC(10^3/mm3)	14.7±5	16.3±4	21.3±3.9	19.8±6.5	25.3±5.8	21.9±4.1	22±5.8	19.1±7.4
RBC (10^6/mm3)	11.8±1	11.1±0.8	11.2±0.4	11±0.4	11.1±0.5	10.9±0.5	10.5±0.5	10.6±0.8
HGB (g/dL)	18.7±1.1	****17.8±0.7**	18.3±0.5	*****17.7±1**	18.3±0.5	*****17.7±0.4**	18±0.3	*****17.6±0.7**
HCT (%)	63.2±4.6	***58.8±4.3**	56.4±1.9	55.1±2.6	55.3±2.8	54.1±2.6	53.2±2.6	53.3±4.8
MCV (fl)	53.7±1.9	53±3	50±0.6	49.8±0.7	49.7±0.7	49.5±0.9	50.3±0.8	49.6±0.7
MCH (pg)	15.9±1.1	16.1±1.1	16.3±0.4	16±0.8	16.5±0.7	16.2±0.5	17±0.6	16.5±0.8
MCHC (g/dL)	29.5±1.1	30.3±1.5	32.5±1	32.2±1.9	33.2±1.5	32.8±1.1	33.9±1.3	33.1±1.9
RDW (%)	13.9±0.8	***15.2±1.6**	14.2±0.5	14.4±0.5	13.9±0.4	13.1±3.3	14±0.5	14.1±0.5
PLT (10^3/mm3)	335.3±384.7	432±343.2	602.4±290.9	684.5±299	646.6±377.5	751.1±366.9	1051±581	980.6±531.7
MPV (fl)	6.4±0.3	6.7±0.6	5.6±0.1	5.6±0.2	6.1±0.2	6±0.2	5.9±0.3	5.8±0.2
LYM (%)	80.8±6.5	77.5±7.7	78.6±1.5	76.1±5.4	71.3±4.9	73.9±4.9	72.5±5.5	71.2±6
MON (%)	3.4±0.8	3.5±0.7	3.9±0.1	3.9±0.4	4.1±0.4	4.9±4	4±0.4	4.1±0.4
GRA (%)	15.6±6	18.9±7.1	17.4±1.5	19.9±5.1	24.5±4.6	22.1±4.6	23.3±5.2	24.6±5.7

Values presented as mean±SD

asterisks indicate significance compared to vehicle treated group for same age. *p<0.05, **p<0.01, ***p<0.001 determined by t-test

CHAPTER 5

Mice lacking the Steroid and Xenobiotic Receptor (SXR/PXR) are not more susceptible to the hemolytic and oxidative stress induced by phenylhydrazine

Summary:

In **Chapter 4**, we reported that mice lacking the Steroid and Xenobiotic Receptor (SXR/PXR) developed a phenotype of oxidative stress and hemolytic anemia following exposure to the environmental toxicant, PCB-153. We asked whether this phenotype in SXR knockout (SXRKO) mice was specific to PCB-153 exposure or if SXRKO mice had a general increased susceptibility to oxidative stress. To test this, we utilized the phenylhydrazine (PHZ) model of chemical-induced oxidative stress and hemolytic anemia. Wild-type (WT) and SXRKO mice were injected interperitoneally with PHZ at 4 weeks of age and the resulting anemia and oxidative stress monitored. We discovered that there was no differential effect of PHZ induced anemia or oxidative stress between WT and SXRKO mice, investigating ROS production in red blood cells (RBCs) and multiple blood parameters. The compensatory erythropoiesis was also unchanged between male WT and SXRKO mice at both 2 and 7 days post PHZ injection. Interestingly, female SXRKO mice showed elevated compensatory erythropoiesis 7 days after the initial injection, despite having no difference in hematocrit, RBC count, or hemoglobin. Overall, these results demonstrate that SXRKO mice do not have a general susceptibility to oxidative stress, thus supporting our previous findings that it is the altered metabolism profile of SXRKO mice and the resulting accumulation of toxic xenobiotic metabolites that induce oxidative stress and hemolytic anemia.

Introduction

Many xenobiotic chemicals lead to oxidative stress-induced hemolytic anemia[40, 161]. This can be because of direct action of the parent compound or as the result of a toxic metabolite(s) produced by the body. These compounds often deplete cellular glutathione levels, oxidize hemoglobin, or cause cell membrane damage in red blood cells (RBCs), leading to cell rupture or phagocytosis by macrophages[161, 190, 191]. There are several genetic mutations in both humans and rodent models that have demonstrated increased susceptibility to oxidative stress and chemical induced hemolytic anemia[163, 171, 192].

Polychlorinated biphenyls (PCBs) are persistent organic pollutants known to induce many adverse health effects in exposed individuals[110]. Both the parent compounds and their metabolites can induce oxidative stress[39, 174, 193, 194]. We previously reported that mice lacking the steroid and xenobiotic receptor SXR/PXR, SXRKO mice, developed oxidative stress-induced hemolytic anemia with exposure to PCB-153, and this phenotype was accompanied by an accumulation of hydroxylated metabolites of PCB-153 (**Chapter 4**).

Therefore, we asked if the observed phenotype of oxidative stress and hemolytic anemia in SXRKO mice exposed to PCB-153 was due to an increased susceptibility to oxidative stress and/or anemia due to the loss of SXR. To study this, we implemented the phenylhydrazine (PHZ) model of oxidative stress-induced anemia. PHZ rapidly and reproducibly induces oxidative stress that targets the red blood cells (RBCs) leading to hemolytic anemia[41]. This phenotype is easily observed in wild-type (WT) mice with no genetic mutations. If SXRKO mice had an inherent susceptibility to oxidative stress and/or anemia, independent of xenobiotic metabolites, we would expect to observe an elevated response to PHZ (e.g. elevated oxidative stress, more severe anemia) compared to WT controls. We administered PHZ to 4 week old WT

and SXRKO mice and monitored the content of reactive oxygen species (ROS) in the blood, spleen, and bone marrow, multiple blood parameters, and the compensatory erythropoiesis. We observed no difference in the ROS content or blood parameters between WT and SXRKO mice following PHZ injection, indicating that SXRKO mice are not susceptible to all inducers of oxidative stress. This is consistent with our findings from **Chapter 4** that the hemolytic anemia was the result of the accumulation of hydroxylated PCB-153 metabolites due to an altered metabolism profile of SXRKO mice.

Materials and methods

Mouse maintenance: WT and SXRKO (C57BL/6J) mice were equally maintained and housed by the Blumberg lab at the University of California, Irvine. SXRKO mice were descendants from a colony of 129SVEV mice from the Salk institute and were backcrossed onto C57BL/6J background strain for 6 generations to obtain an essentially pure C57BL/6J background. Mice were housed in micro-isolator cages in a temperature-controlled room (25–28°C) with a 12-h light/dark cycle. Water and food (5P14 ProLab RMH 2500, LabDiet) were provided ad libitum. Animals were treated humanely and all procedures were approved by the Institutional Animal Care and Use Committee of the University of California, Irvine.

Phenylhydrazine induced hemolytic anemia: Male and female WT and SXRKO mice (4 weeks of age) were injected with 40 µg/kg BW of phenylhydrazine hydrochloride (Sigma) intraperitoneally for two consecutive days. A control group of mice injected with vehicle (PBS) were also included. Extra nestlets and water-soaked food pellets were placed in the mouse cages following PHZ administration. Blood was monitored starting at Day 0 and every 2 days following. Mice were euthanized either 2 or 7 days after the first PHZ injection.

Complete blood count: Whole blood (20 µL) was collected every 2 days from the saphenous vein of the mice. Blood was collected using heparinized capillary tubes. Blood parameters were measured on a VetABC hematology analyzer (scil Animal Care Company) within 4 hours of blood collection. Blood parameters measured included: white blood cell count (WBC), red blood cell count (RBC), hematocrit (HCT), hemoglobin (HGB), mean corpuscular volume (MCV), mean cell hemoglobin (MCH), mean corpuscular hemoglobin concentration (MCHC), red blood cell distribution width (RDW), platelet count (PLT), lymphocyte count (LYM), monocyte count (MON), and granulocyte count (GRA).

Tissue and blood collection: Mice were euthanized by isoflurane overdose. Whole blood was collected by cardiac puncture. An aliquot of whole blood (20 µL) was set aside for blood analysis and CM-H_2DCFDA staining. Spleen tissue was dissected and placed on ice for splenocyte isolation. Legs were dissected and placed in ice-cold PBS for bone marrow isolation.

Spleen and bone marrow cell isolation: Spleen tissue was physically dissociated using a petri dish and syringe plunger in 1 mL of cold PBS containing 1% FBS. Bone marrow cells were extracted from the tibia and femur by flushing cold PBS + 1% FBS buffer into the marrow cavity using a 25 gauge needle. Erythrocytes were lysed by incubating cell suspensions in ACK lysis buffer (150 mM NH4Cl, 10 mM KHCO3, 0.1 mM Na2EDTA) for 5 min. Cells were washed and resuspended in FACS buffer (PBS, 1% FBS, 0.02% sodium azide) for antibody staining and flow cytometric analysis.

ROS detection: whole blood was diluted 1:500 in Hank's balanced salt solution (HBSS). Spleen and bone marrow cells were diluted to $4x10^6$ cells/mL in HBSS. Cell aliquots (50µL) were combined with an equal volume of 20µM CM-H_2DCFDA, (chloromethyl-2',7'-dichlorofluorescein diacetate--Ex/Em: 502/523 nm , Thermo Fisher Scientific) in HBSS+2% FBS and incubated for 15 minutes at 37˚C. Stained cells were washed twice with cold FACS buffer (PBS, 1% FBS, 0.02% sodium azide), then proceeded to antibody staining for flow cytometric analysis.

Flow cytometry: CM-H2DCFDA stained spleen and bone marrow cells were stained with an antibody cocktail of anti-mouse TER119-APC (TONBO biosciences) and CD71-PE (eBioscience), and for 15 min. Cells were washed with cold FACS buffer (PBS, 1% FBS, 0.02% sodium azide) and measured on a BD FortessaX20 cytometer within one hour. Data was analyzed using FlowJo software (Treestar).

Statistical analysis: Data visualization and statistical analyses were conducted in Prism 8 (GraphPad Software). Ten biological replicates per group were used for phenylhydrazine injections, half were euthanized 2 days after the first injection and the other half were euthanized 7 days after the first injection. Unpaired t-test was used to determine statistical significance: * = p-value <0.05, ** = p-value <0.01, ***= p-value <0.001, #= p-value <0.0001

Results

WT and SXRKO mice show equal responses to phenylhydrazine-induced ROS and hemolytic anemia 2 days after injection

Male and female WT and SXRKO mice at 4 weeks of age (n=10 per group) were injected with 40 µg/kg BW of phenylhydrazine (PHZ) on two consecutive days. Control mice were injected with PBS. We used mice at 4 weeks of age because this was the age we observed the hemolytic anemia in our previous study (**Chapter 4**). Half of the mice were dissected 2 days after the initial injection, which is when the anemia is the most robust[41]. At this timepoint, we observed a significant increase in reactive oxygen species (ROS) content in the RBCs of mice injected with PHZ compared to PBS injected mice (Figure 5.1A). We observed no difference in RBC ROS content between WT and SXRKO mice of either gender. Interestingly, female mice showed a higher percentage of CM-H2DCFDA+ cells compared to males. Complete blood counts of whole blood obtained via cardiac puncture revealed that PHZ injected mice were anemic, as measured by decreases in RBC count, hematocrit, and blood hemoglobin levels (Figure 5.1B-D). We observed no differences between WT and SXRKO mice or between genders for these three parameters.

Erythropoiesis is induced when animals are anemic to replenish lost RBCs[159, 160]. Bone marrow is the normal site of erythropoiesis, but it can also be observed in the spleen during times of RBC stress[160]. PHZ injected mice had increased erythropoiesis in both the bone marrow and spleen 2 days after the initial PHZ injection (Figure 5.2). Erythropoiesis was mostly evident in the bone marrow at this time point (Figure 5.2A). We observed no difference in the percentage of erythroid precursors between WT and SXRKO mice in either tissue. These results demonstrate

that WT and SXRKO mice do not have differential responses to PHZ in terms of oxidative stress, anemia, and compensatory erythropoiesis that occurs 2 days following the injection.

Comparable induction and recovery of anemia between WT and SXRKO mice up to 6 days after phenylhydrazine injection

The blood of the remaining mice that were not dissected on day 2 was continuously monitored every 2 days. We observed that RBC count dropped 2 days after the first injection and didn't show recovery until day 6; this trend was observed for both male (Figure 5.3A) and female (Figure 5.4A) mice. There were no differences between WT and SXRKO mice at any timepoint (Figure 5.3A, Figure 5.4A). Hematocrit dropped significantly at day 2, began recovering by day 4, and was completely recovered by day 6 (Figure 5.3B, 5.4B). This trend was observed for both males (Figure 5.3B) and females (Figure 5.4B). Male SXRKO mice showed a significant increase in hematocrit before PHZ injection and then a significant decrease at day 2 (Figure 5.3B). However, these findings were not consistent with day 2 measurements of the other half of the injected mice that were dissected on day 2 (Figure 5.1C). No differences in hematocrit between WT and SXRKO were observed in female mice at any time point (Figure 5.4B).

Elevated compensatory erythropoiesis in SXRKO mice

By day 6 we observed full recovery of RBC content and hematocrit, indicating that there was sufficient erythropoiesis occurring since the induction of the anemia by PHZ. We analyzed the residual amount of erythroid precursors at day 7 in the PHZ injected mice. We observed that PHZ injected male mice still contained an increased percentage of erythroid precursors in both the bone marrow and spleen compared to the PBS injected mice, although the increase was only statistically significant with the SXRKO males (Figure 5.5). There was no difference between WT and SXRKO males. Interestingly, we observed increased erythropoiesis in PHZ injected

female SXRKO mice compared to PHZ injected female WT mice in both the bone marrow and spleen (Figure 5.5). However, the percentages for either group were not different than the PBS injected controls. These results suggest that SXRKO mice may have a delayed inhibition of the compensatory erythropoiesis that becomes induced in response to anemia.

Discussion

Phenylhydrazine is a chemical known to induce both oxidative stress and hemolytic anemia and these effects have been demonstrated in several strains of mice[41, 195]. Elevated levels of ROS in the RBCs, and more severe changes to blood parameters following PHZ injection have been observed in mice with mutations or knockouts of several genes, demonstrating that loss of these genes leads to increased susceptibility to oxidative stress[192, 196]. We administered PHZ to WT and SXRKO mice to assess whether SXRKO mice were more susceptible to oxidative stress and/or anemia. We observed no differences between WT and SXRKO mice in RBC ROS content or in any blood parameter tested following injection of PHZ. These results demonstrated that SXRKO mice are not genetically more susceptible to PHZ induced oxidative stress or anemia. We infer that this may apply to other direct inducers of oxidative stress.

These results support our previous findings that it is the altered metabolism of SXRKO mice that leads to accumulation of toxic PCB-153 metabolites that induce oxidative stress and anemia. PHZ does not require the transformation into a metabolite to induce the toxic effects and we infer that this is why WT and SXRKO mice showed an equal response to PHZ exposure. Metabolites of other xenobiotics, such as those of primaquine, have demonstrated to induce oxidative stress and anemia[40]. I hypothesize that SXRKO mice would demonstrate stronger toxicity with primaquine exposure compared to WT mice, similar to what was observed with PCB-153 exposure in **Chapter 4**. It may be interesting to investigate the effects of primaquine exposure between WT and SXRKO mice in the future.

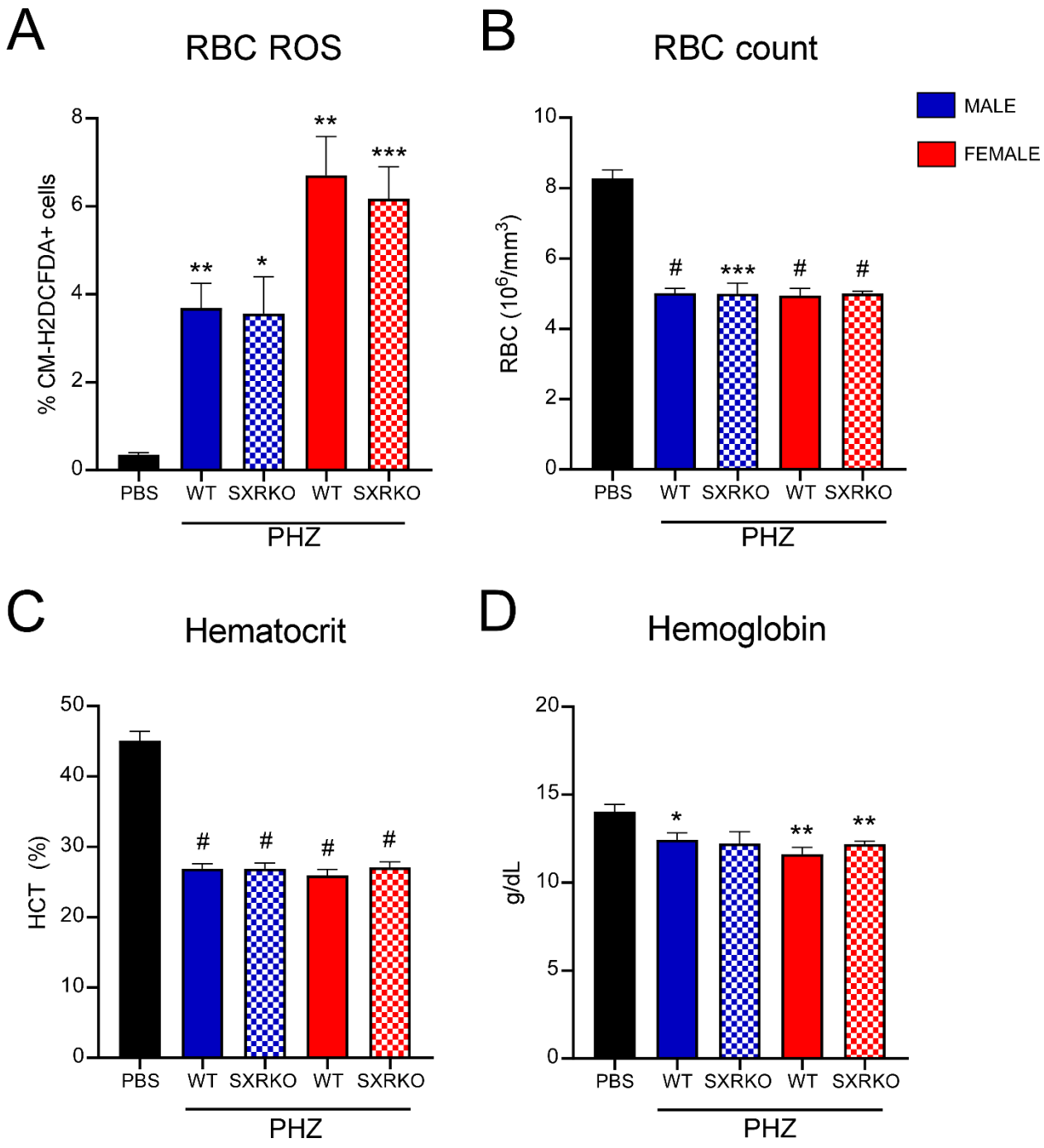

Figure 5.1 Oxidative stress and anemia in WT and SXRKO mice 2 days following PHZ injection. Red blood cell (RBC) ROS content determined by CM-H2DCFDA staining (A), RBC count (B), hematocrit (C) and hemoglobin level (D) in WT and SXRKO mice 2 days after initial PHZ injection. PHZ groups: n=5 per group, PBS group: n=3.

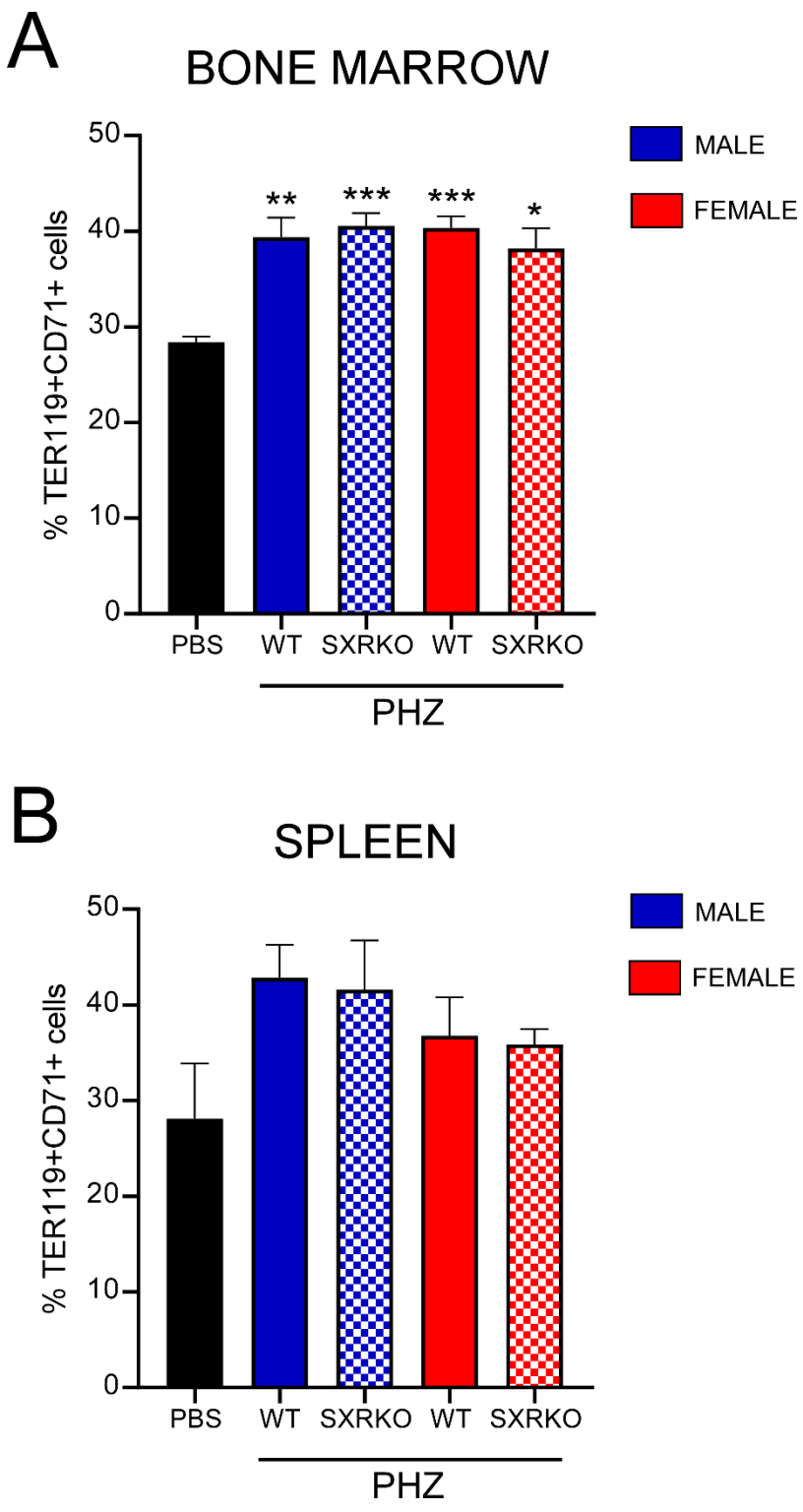

<u>Figure 5.2</u> Erythropoiesis in WT and SXRKO mice 2 days following PHZ injection. Percentage of erythroid precursors in the bone marrow (A) and spleen (B) determined by flow cytometry, gating on TER119+/CD71+ cells, in WT and SXRKO mice 2 days after initial PHZ injection. PHZ groups: n=5 per group, PBS group: n=3.

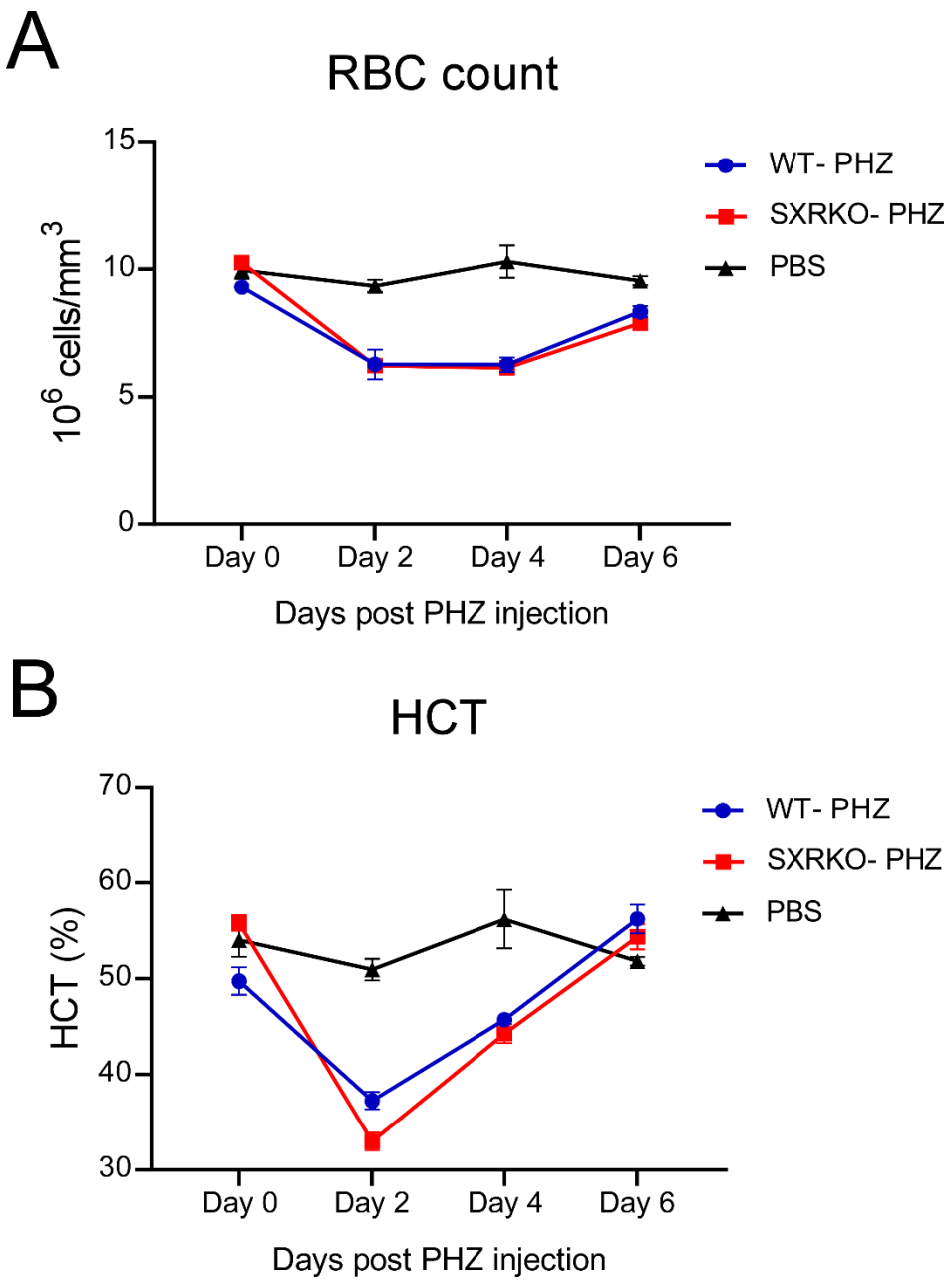

<u>Figure 5.3</u> Blood parameters of male WT and SXRKO mice over time. RBC count (A) and HCT (B) in WT and SXRKO male mice measured every 2 days starting at Day 0 before PHZ injection and ending 6 days later. PHZ groups: n=5 per group for each time point, PBS group: n=3 for each timepoint.

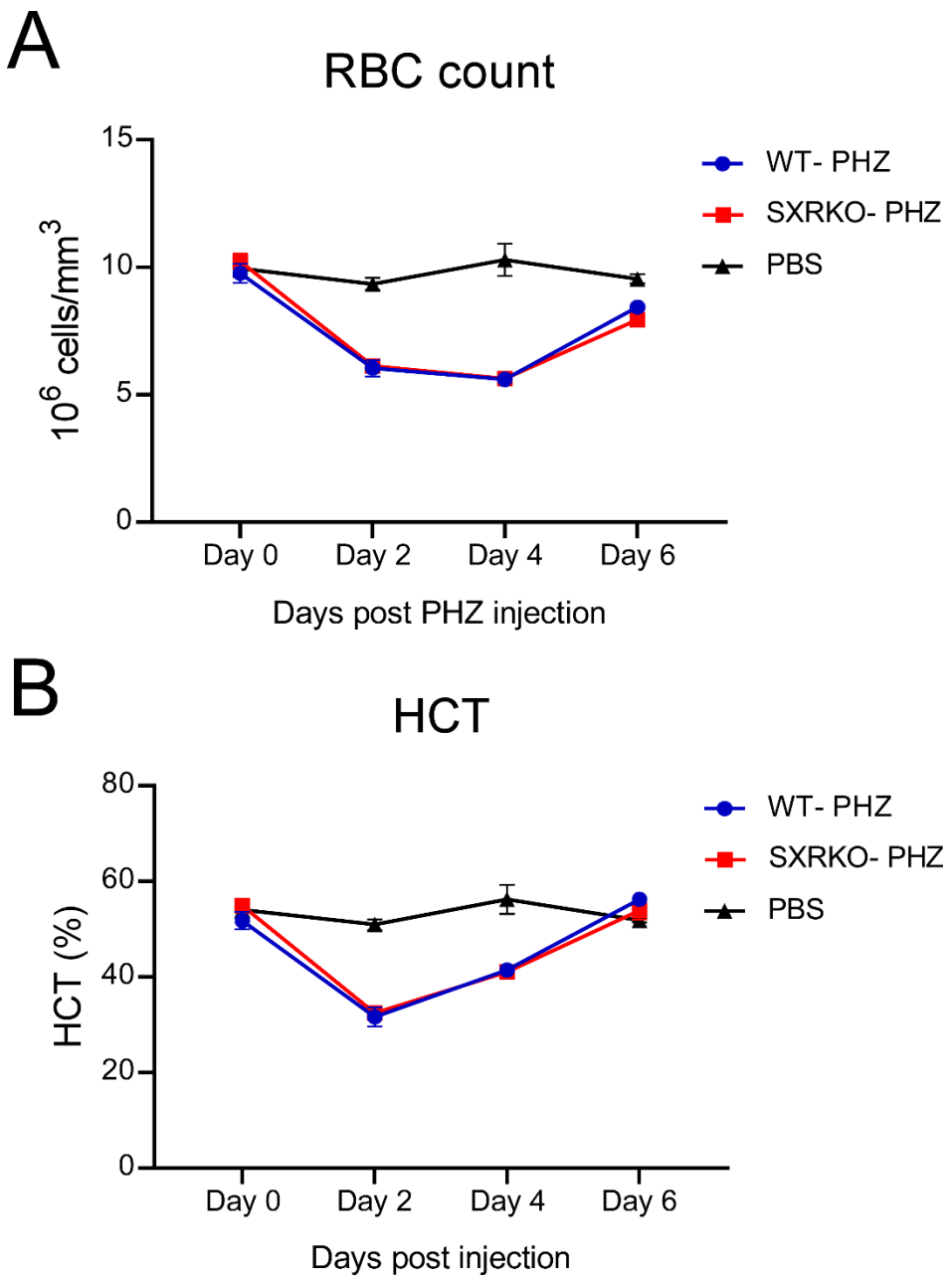

Figure 5.4 Blood parameters of female WT and SXRKO mice over time. RBC count (A) and HCT (B) in WT and SXRKO female mice measured every 2 days starting at Day 0 before PHZ injection and ending 6 days later. PHZ groups: n=5 per group for each time point, PBS group: n=3 for each timepoint.

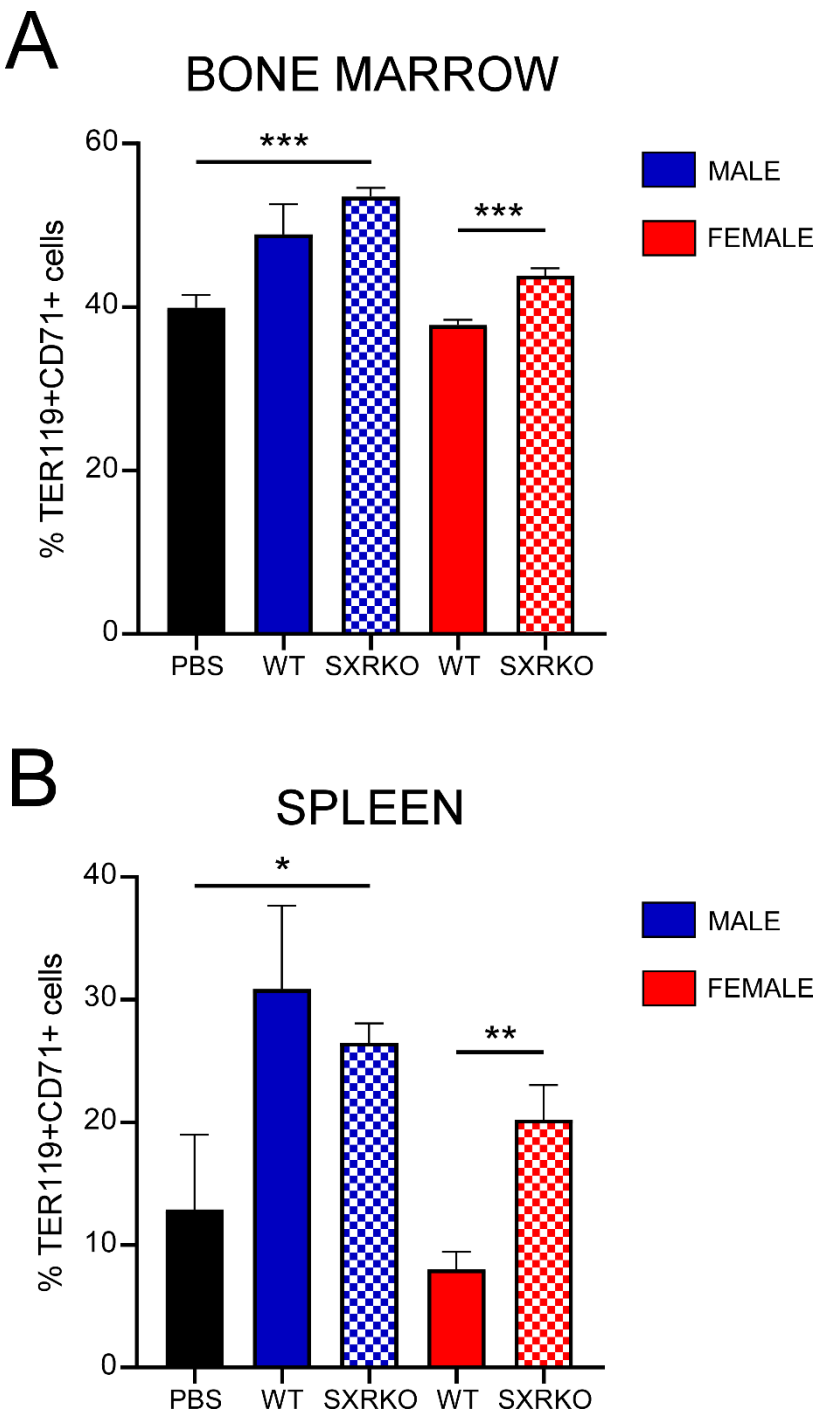

<u>Figure 5.5</u> Erythropoiesis in WT and SXRKO mice 7 days following PHZ injection. Percentage of erythroid precursors in the bone marrow (A) and spleen (B) determined by flow cytometry, gating on TER119+/CD71+ cells, in WT and SXRKO mice 7 days after initial PHZ injection. PHZ groups: n=5 per group, PBS group: n=3.

CONCLUDING REMARKS

The steroid and xenobiotic receptor, SXR/PXR, is a master regulator of xenobiotic metabolism. It has become increasingly apparent that SXR plays additional roles and that perturbing its function can lead to adverse health consequences. This dissertation investigated new roles for SXR in interactions with the diet and gut microbiome (Part I), and xenobiotic-induced oxidative stress (Part II). These studies established SXR as a candidate bridge between the gut microbiome and its impact on host health and provide further evidence of the important role of SXR in the protection against adverse effects induced by xenobiotics.

The studies in Part I demonstrated that the diet and gut microbiome do not impact the development of the B-1a B cell lymphoma phenotype in SXRKO mice. They did demonstrate that SXR can impact intestinal inflammation (**Chapter 2**) and gene expression of tight junction proteins (**Chapter 3**) in response to changes in the gut microbiome, which can lead to an increased innate immune response, observed as increased percentage of B-1a cells in the peritoneal cavity (**Chapter 3**). These results suggest that SXR and the gut microbiome interact and that this interaction impacts the host. These findings pave the way for more investigations into the impact of the gut microbiome on other phenotypes reported for SXRKO mice (e.g. intestinal permeability) or in combination with xenobiotic exposure in mice with a functional SXR, to better understand the role of SXR in microbiome-induced health effects.

Part II of this dissertation revealed that SXR is important for the proper metabolism and clearance of harmful xenobiotic metabolites, which otherwise can cause oxidative stress leading to adverse health consequences. Oxidative-stress induced hemolytic anemia was observed in SXRKO mice exposed to the environmental toxicant, PCB-153, and was accompanied by

increased accumulation of a hydroxylated PCB-153 metabolite (**Chapter 4**). No differences in oxidative stress or hemolytic anemia were observed between wild-type and SXRKO mice exposed to phenylhydrazine, an oxidative stress-inducing xenobiotic that does not require biological activation into a metabolite to induce its toxic effects (**Chapter 5**). These results demonstrated that the oxidative stress observed in SXRKO mice by exposure to some xenobiotics is due to the role of SXR in the proper metabolism and clearance of the harmful metabolites rather than SXR playing a direct function in the protection against general oxidative stress. It would be interesting to investigate whether SXR plays a similar role after exposure to other xenobiotic chemicals that have metabolites capable of inducing oxidative stress and anemia. These include pharmaceutical agents, such as primaquine, and other xenobiotic toxicants, such as polybrominated diphenylethers (PBDEs) and polybrominated biphenyls (PBBs).

Overall, the studies in this dissertation revealed new adverse health consequences related to SXR loss-of-function and set the stage for future investigations of these roles to provide more insight into human relevance. There are currently 9,451 reported single nucleotide polymorphisms (SNPs) of human SXR in the NCBI dbSNP, many of which can impact the expression of SXR itself and/or that of its target genes[42, 43]. In addition, human SXR polymorphisms have been linked to various functional consequences, including altered metabolism, increased inflammation, and susceptibility to disease[44-46]. Some xenobiotics and pharmaceutical drugs have shown to suppress SXR signaling[188, 189] and antagonists of SXR are actively being developed to be used as pharmaceutical drugs[48]. Our studies suggest that both genetic and chemical inhibition of SXR might predispose humans to altered responses to the gut microbiome and to increased oxidative stress due to altered metabolism of certain xenobiotics,

both of which are associated with negative adverse health consequences. Pharmaceutical research aims to inhibit SXR function and activity due to its role in drug-drug interactions, but our studies suggest that inhibiting SXR may have adverse physiological impacts. The health consequences of SXR inhibition should be investigated more carefully before use in humans. In addition, these studies suggest that targeting SXR activation could possibly be beneficial to humans exposed to various toxicants, such as PCBs, to reduce the accumulation of the toxic metabolites.

REFERENCES

1. Mangelsdorf, D. J.; Thummel, C.; Beato, M.; Herrlich, P.; Schütz, G.; Umesono, K.; Blumberg, B.; Kastner, P.; Mark, M.; Chambon, P.; Evans, R. M., The nuclear receptor superfamily: the second decade. *Cell* **1995,** *83* (6), 835-839.
2. Robinson-Rechavi, M.; Garcia, H. E.; Laudet, V., The nuclear receptor superfamily. *Journal of Cell Science* **2003,** *116* (4), 585.
3. Francis, G. A.; Fayard, E.; Picard, F.; Auwerx, J., Nuclear Receptors and the Control of Metabolism. *Annual Review of Physiology* **2003,** *65* (1), 261-311.
4. McKenna, N. J.; Lanz, R. B.; O'Malley, B. W., Nuclear Receptor Coregulators: Cellular and Molecular Biology*. *Endocrine Reviews* **1999,** *20* (3), 321-344.
5. Casey, S. C.; Nelson, E. L.; Turco, G. M.; Janes, M. R.; Fruman, D. A.; Blumberg, B., B-1 cell lymphoma in mice lacking the steroid and xenobiotic receptor, SXR. *Molecular Endocrinology* **2011,** *25* (6), 933-943.
6. Blumberg, B.; Sabbagh, W.; Juguilon, H.; Bolado, J.; van Meter, C. M.; Ong, E. S.; Evans, R. M., SXR, a novel steroid and xenobioticsensing nuclear receptor. *Genes Dev* **1998,** *12* (20), 3195-205.
7. Hurst, C. H.; Waxman, D. J., Interactions of Endocrine-active environmental chemicals with the nuclear receptor PXR. *Toxicological and Environmental Chemistry* **2005,** *87* (3), 299-311.
8. Staudinger, J. L.; Ding, X.; Lichti, K., Pregnane X receptor and natural products: beyond drug–drug interactions. *Expert Opinion on Drug Metabolism & Toxicology* **2006,** *2* (6), 847-857.
9. Xie, W.; Barwick, J. L.; Simon, C. M.; Pierce, A. M.; Safe, S.; Blumberg, B.; Guzelian, P. S.; Evans, R. M., Reciprocal activation of xenobiotic response genes by nuclear receptors SXR/PXR and CAR. *Genes and development* **2000,** *14* (23), 3014-3023.
10. Geick, A.; Eichelbaum, M.; Burk, O., Nuclear receptor response elements mediate induction of intestinal MDR1 by rifampin. *Journal of Biological Chemistry* **2001,** *276* (18), 14581-14587.
11. Staudinger, J.; Liu, Y.; Madan, A.; Habeebu, S.; Klaassen, C. D., Coordinate Regulation of Xenobiotic and Bile Acid Homeostasis by Pregnane X Receptor. *Drug Metabolism and Disposition* **2001,** *29* (11), 1467.
12. Xie, W.; Barwick, J. L.; Downes, M.; Blumberg, B.; Simon, C. M.; Nelson, M. C.; Neuschwander-Tetri, B. A.; Brunt, E. M.; Guzelian, P. S.; Evans, R. M., Humanized xenobiotic response in mice expressing nuclear receptor SXR. *Nature* **2000,** *406* (6794), 435.
13. Guengerich, F. P., CYTOCHROME P-450 3A4: Regulation and Role in Drug Metabolism. *Annual Review of Pharmacology and Toxicology* **1999,** *39* (1), 1-17.
14. Kotiya, D.; Jaiswal, B.; Ghose, S.; Kaul, R.; Datta, K.; Tyagi, R. K., Role of PXR in Hepatic Cancer: Its Influences on Liver Detoxification Capacity and Cancer Progression. *PLOS ONE* **2016,** *11* (10), e0164087.
15. Zhou, C.; Tabb, M. M.; Nelson, E. L.; Grün, F.; Verma, S.; Sadatrafiei, A.; Lin, M.; Mallick, S.; Forman, B. M.; Thummel, K. E.; Blumberg, B., Mutual repression between steroid and xenobiotic receptor and NF-κB signaling pathways links xenobiotic metabolism and inflammation. *The Journal of Clinical Investigation* **2006,** *116* (8), 2280-2289.
16. Sui, Y.; Xu, J.; Rios-Pilier, J.; Zhou, C., Deficiency of PXR decreases atherosclerosis in apoE-deficient mice. *Journal of Lipid Research* **2011,** *52* (9), 1652-1659.

17. Wada, T.; Gao, J.; Xie, W., PXR and CAR in energy metabolism. *Trends in Endocrinology & Metabolism* **2009,** *20* (6), 273-279.
18. Dubrac, S.; Elentner, A.; Ebner, S.; Horejs-Hoeck, J.; Schmuth, M., Modulation of T lymphocyte function by the pregnane X receptor. *The Journal of Immunology* **2010,** *184* (6), 2949-2957.
19. Teng, S.; Piquette-Miller, M., The involvement of the pregnane X receptor in hepatic gene regulation during inflammation in mice. *Journal of Pharmacology and Experimental Therapeutics* **2005,** *312* (2), 841-848.
20. Gu, X.; Ke, S.; Liu, D.; Sheng, T.; Thomas, P. E.; Rabson, A. B.; Gallo, M. A.; Xie, W.; Tian, Y., Role of NF-κB in Regulation of PXR-mediated Gene Expression: A MECHANISM FOR THE SUPPRESSION OF CYTOCHROME P-450 3A4 BY PROINFLAMMATORY AGENTS. *Journal of Biological Chemistry* **2006,** *281* (26), 17882-17889.
21. Venkatesh, M.; Mukherjee, S.; Wang, H.; Li, H.; Sun, K.; Benechet, Alexandre P.; Qiu, Z.; Maher, L.; Redinbo, Matthew R.; Phillips, Robert S.; Fleet, James C.; Kortagere, S.; Mukherjee, P.; Fasano, A.; Le Ven, J.; Nicholson, Jeremy K.; Dumas, Marc E.; Khanna, Kamal M.; Mani, S., Symbiotic Bacterial Metabolites Regulate Gastrointestinal Barrier Function via the Xenobiotic Sensor PXR and Toll-like Receptor 4. *Immunity* **2014,** *41* (2), 296-310.
22. Dring, M. M.; Goulding, C. A.; Trimble, V. I.; Keegan, D.; Ryan, A. W.; Brophy, K. M.; Smyth, C. M.; Keeling, P. W. N.; O'Donoghue, D.; O'Sullivan, M.; O'Morain, C.; Mahmud, N.; Wikström, A. C.; Kelleher, D.; McManus, R., The Pregnane X Receptor Locus Is Associated With Susceptibility to Inflammatory Bowel Disease. *Gastroenterology* **2006,** *130* (2), 341-348.
23. Sookoian, S.; Castaño, G. O.; Burgueño, A. L.; Gianotti, T. F.; Rosselli, M. S.; Pirola, C. J., The nuclear receptor PXR gene variants are associated with liver injury in nonalcoholic fatty liver disease. *Pharmacogenetics and Genomics* **2010,** *20* (1).
24. Ouyang, N.; Ke, S.; Eagleton, N.; Xie, Y.; Chen, G.; Laffins, B.; Yao, H.; Zhou, B.; Tian, Y., Pregnane X receptor suppresses proliferation and tumourigenicity of colon cancer cells. *British Journal Of Cancer* **2010,** *102*, 1753.
25. Shreiner, A. B.; Kao, J. Y.; Young, V. B., The gut microbiome in health and in disease. *Curr Opin Gastroenterol* **2015,** *31* (1), 69-75.
26. Borenstein, S. G.; Peter, J. T.; Elhanan, Metagenomic systems biology of the human gut microbiome reveals topological shifts associated with obesity and inflammatory bowel disease. **2012**.
27. Chassaing, B.; Darfeuille-Michaud, A., The commensal microbiota and enteropathogens in the pathogenesis of inflammatory bowel diseases. *Gastroenterology* **2011,** *140* (6), 1720-28.
28. Frank, D. N.; Robertson, C. E.; Hamm, C. M.; Kpadeh, Z.; Zhang, T.; Chen, H.; Zhu, W.; Sartor, R. B.; Boedeker, E. C.; Harpaz, N.; Pace, N. R.; Li, E., Disease phenotype and genotype are associated with shifts in intestinal-associated microbiota in inflammatory bowel diseases. *Inflamm Bowel Dis* **2011,** *17* (1).
29. Caparrós-Martín, J. A.; Lareu, R. R.; Ramsay, J. P.; Peplies, J.; Reen, F. J.; Headlam, H. A.; Ward, N. C.; Croft, K. D.; Newsholme, P.; Hughes, J. D.; O'Gara, F., Statin therapy causes gut dysbiosis in mice through a PXR-dependent mechanism. *Microbiome* **2017,** *5* (1), 95.
30. EPA, U. S. Learn about Polychlorinated Biphenyls (PCBs). https://www.epa.gov/pcbs/learn-about-polychlorinated-biphenyls-pcbs.
31. EPA, U. S., EPA Bans PCB Manufacture; Phases Out Uses. 1979.

32. Gährs, M.; Roos, R.; Andersson, P. L.; Schrenk, D., Role of the nuclear xenobiotic receptors CAR and PXR in induction of cytochromes P450 by non-dioxinlike polychlorinated biphenyls in cultured rat hepatocytes. *Toxicology and Applied Pharmacology* **2013,** *272* (1), 77-85.
33. Al-Salman, F.; Plant, N., Non-coplanar polychlorinated biphenyls (PCBs) are direct agonists for the human pregnane-X receptor and constitutive androstane receptor, and activate target gene expression in a tissue-specific manner. *Toxicology and Applied Pharmacology* **2012,** *263* (1), 7-13.
34. Tabb, M. M.; Kholodovych, V.; Grün, F.; Zhou, C.; Welsh, W. J.; Blumberg, B., Highly chlorinated PCBs inhibit the human xenobiotic response mediated by the steroid and xenobiotic receptor (SXR). *Environmental Health Perspectives* **2004,** *112* (2), 163-169.
35. Lille-Langøy, R.; Goldstone, J. V.; Rusten, M.; Milnes, M. R.; Male, R.; Stegeman, J. J.; Blumberg, B.; Goksøyr, A., Environmental contaminants activate human and polar bear (Ursus maritimus) pregnane X receptors (PXR, NR1I2) differently. *Toxicology and applied pharmacology* **2015,** *284* (1), 54-64.
36. Pacyniak, E. K.; Cheng, X.; Cunningham, M. L.; Crofton, K.; Klaassen, C. D.; Guo, G. L., The Flame Retardants, Polybrominated Diphenyl Ethers, Are Pregnane X Receptor Activators. *Toxicological Sciences* **2007,** *97* (1), 94-102.
37. An, J.; Li, S.; Zhong, Y.; Wang, Y.; Zhen, K.; Zhang, X.; Wang, Y.; Wu, M.; Yu, Z.; Sheng, G.; Fu, J.; Huang, Y., The cytotoxic effects of synthetic 6-hydroxylated and 6-methoxylated polybrominated diphenyl ether 47 (BDE47). *Environmental Toxicology* **2011,** *26* (6), 591-599.
38. Henkler, F.; Brinkmann, J.; Luch, A., The Role of Oxidative Stress in Carcinogenesis Induced by Metals and Xenobiotics. *Cancers* **2010,** *2* (2).
39. Oakley, G. G.; Devanaboyina, U.-s.; Robertson, L. W.; Gupta, R. C., Oxidative DNA damage induced by activation of polychlorinated biphenyls (PCBs): implications for PCB-induced oxidative stress in breast cancer. *Chemical research in toxicology* **1996,** *9* (8), 1285-1292.
40. Bowman, Z. S.; Oatis, J. E.; Whelan, J. L.; Jollow, D. J.; McMillan, D. C., Primaquine-induced hemolytic anemia: susceptibility of normal versus glutathione-depleted rat erythrocytes to 5-hydroxyprimaquine. *Journal of Pharmacology and Experimental Therapeutics* **2004,** *309* (1), 79-85.
41. Angulo, O.; Gandrillon, O.; Crauste, F., Investigating the role of the experimental protocol in phenylhydrazine-induced anemia on mice recovery. *J Theor Biol* **2018,** *437*, 286-298.
42. Zhang, B.; Xie, W.; Krasowski, M. D., PXR: a xenobiotic receptor of diverse function implicated in pharmacogenetics. *Future Medicine* **2008**.
43. NCBI Nr1i2[Gene Name] - SNP - NCBI. https://www.ncbi.nlm.nih.gov/pubmed/ (accessed May 31, 2019).
44. Lim, Y.-P.; Liu, C.-H.; Shyu, L.-J.; Huang, J.-d., Functional characterization of a novel polymorphism of pregnane X receptor, Q158K, in Chinese subjects. *Pharmacogenetics* **2005,** *15* (5), 337-341.
45. Dring, M. M.; Goulding, C. A.; Trimble, V. I.; Keegan, D.; Ryan, A. W.; Brophy, K. M.; Smyth, C. M.; Keeling, P. N.; O'Donoghue, D.; O'Sullivan, M., The pregnane X receptor locus is associated with susceptibility to inflammatory bowel disease. *Gastroenterology* **2006,** *130* (2), 341-348.

46. Karlsen, T. H.; Lie, B. A.; Frøslie, K. F.; Thorsby, E.; Broomé, U.; Schrumpf, E.; Boberg, K. M., Polymorphisms in the steroid and xenobiotic receptor gene influence survival in primary sclerosing cholangitis. *Gastroenterology* **2006,** *131* (3), 781-787.
47. Lin, W.; Wang, Y.-M.; Chai, S. C.; Lv, L.; Zheng, J.; Wu, J.; Zhang, Q.; Wang, Y.-D.; Griffin, P. R.; Chen, T., SPA70 is a potent antagonist of human pregnane X receptor. *Nature Communications* **2017,** *8* (1), 741.
48. Staudinger, J. L., Clinical applications of small molecule inhibitors of Pregnane X receptor. *Molecular and cellular endocrinology* **2019**.
49. Lim, Y.-P.; Cheng, C.-H.; Chen, W.-C.; Chang, S.-Y.; Hung, D.-Z.; Chen, J.-J.; Wan, L.; Ma, W.-C.; Lin, Y.-H.; Chen, C.-Y.; Yokoi, T.; Nakajima, M.; Chen, C.-J., Allyl isothiocyanate (AITC) inhibits pregnane X receptor (PXR) and constitutive androstane receptor (CAR) activation and protects against acetaminophen- and amiodarone-induced cytotoxicity. *Archives of Toxicology* **2015,** *89* (1), 57-72.
50. Kliewer, S. A.; Goodwin, B.; Willson, T. M., The Nuclear Pregnane X Receptor: A Key Regulator of Xenobiotic Metabolism. *Endocrine Reviews* **2002,** *23* (5), 687-702.
51. Kawana, K.; Ikuta, T.; Kobayashi, Y.; Gotoh, O.; Takeda, K.; Kawajiri, K., Molecular Mechanism of Nuclear Translocation of an Orphan Nuclear Receptor, SXR. *Molecular Pharmacology* **2003,** *63* (3), 524.
52. Wei, P.; Zhang, J.; Dowhan, D.; Han, Y.; Moore, D., Specific and overlapping functions of the nuclear hormone receptors CAR and PXR in xenobiotic response. *The pharmacogenomics journal* **2002,** *2* (2), 117.
53. Zhou, C.; Tabb, M. M.; Nelson, E. L.; Grün, F.; Verma, S.; Sadatrafiei, A.; Lin, M.; Mallick, S.; Forman, B. M.; Thummel, K. E., Mutual repression between steroid and xenobiotic receptor and NF-κB signaling pathways links xenobiotic metabolism and inflammation. *The Journal of clinical investigation* **2006,** *116* (8), 2280-2289.
54. Tilman, D.; Clark, M., Global diets link environmental sustainability and human health. *Nature* **2014,** *515*, 518.
55. Landes, N.; Birringer, M.; Brigelius-Flohé, R., Homologous metabolic and gene activating routes for vitamins E and K. *Molecular Aspects of Medicine* **2003,** *24* (6), 337-344.
56. Landes, N.; Pfluger, P.; Kluth, D.; Birringer, M.; Ruhl, R.; Bol, G. F.; Glatt, H.; Brigelius-Flohe, R., Vitamin E activates gene expression via the pregnane X receptor. *Biochem Pharmacol* **2003,** *65* (2), 269-73.
57. Satsu, H.; Hiura, Y.; Mochizuki, K.; Hamada, M.; Shimizu, M., Activation of Pregnane X Receptor and Induction of MDR1 by Dietary Phytochemicals. *Journal of Agricultural and Food Chemistry* **2008,** *56* (13), 5366-5373.
58. David, L. A.; Maurice, C. F.; Carmody, R. N.; Gootenberg, D. B.; Button, J. E.; Wolfe, B. E.; Ling, A. V.; Devlin, A. S.; Varma, Y.; Fischbach, M. A.; Biddinger, S. B.; Dutton, R. J.; Turnbaugh, P. J., Diet rapidly and reproducibly alters the human gut microbiome. *Nature* **2013,** *505*, 559.
59. Blaser, I. C.; Martin, J., The human microbiome: at the interface of health and disease. *Nature Reviews Genetics* **2012,** *13* (4), 260.
60. Greenblum, S.; Turnbaugh, P. J.; Borenstein, E., Metagenomic systems biology of the human gut microbiome reveals topological shifts associated with obesity and inflammatory bowel disease. *Proceedings of the National Academy of Sciences* **2012,** *109* (2), 594.
61. Kreznar, J. H.; Keller, M. P.; Traeger, L. L.; Rabaglia, M. E.; Schueler, K. L.; Stapleton, D. S.; Zhao, W.; Vivas, E. I.; Yandell, B. S.; Broman, A. T.; Hagenbuch, B.; Attie,

A. D.; Rey, F. E., Host genotype and gut microbiome modulate insulin secretion and diet-induced metabolic phenotypes. *Cell Rep* **2017,** *18* (7), 1739-50.
62. Turnbaugh, P. J.; Backhed, F.; Fulton, L.; Gordon, J. I., Diet-induced obesity is linked to marked but reversible alterations in the mouse distal gut microbiome. *Cell Host Microbe* **2008,** *3* (4), 213-23.
63. Yang, I.; Eibach, D.; Kops, F.; Brenneke, B.; Woltemate, S.; Schulze, J.; Bleich, A.; Gruber, A. D.; Muthupalani, S.; Fox, J. G.; Josenhans, C.; Suerbaum, S., Intestinal microbiota composition of interleukin-10 deficient C57BL/6J mice and susceptibility to Helicobacter hepaticus-induced colitis. *PLoS One* **2013,** *8* (8), e70783.
64. Zhou, C.; Verma, S.; Blumberg, B., The steroid and xenobiotic receptor (SXR), beyond xenobiotic metabolism. *Nuclear receptor signaling* **2009,** *7* (1), nrs. 07001.
65. Caporaso, J. G.; Kuczynski, J.; Stombaugh, J.; Bittinger, K.; Bushman, F. D.; Costello, E. K.; Fierer, N.; Peña, A. G.; Goodrich, J. K.; Gordon, J. I.; Huttley, G. A.; Kelley, S. T.; Knights, D.; Koenig, J. E.; Ley, R. E.; Lozupone, C. A.; McDonald, D.; Muegge, B. D.; Pirrung, M.; Reeder, J.; Sevinsky, J. R.; Turnbaugh, P. J.; Walters, W. A.; Widmann, J.; Yatsunenko, T.; Zaneveld, J.; Knight, R., QIIME allows analysis of high-throughput community sequencing data. *Nature Methods* **2010,** *7*, 335.
66. Edgar, R. C.; Haas, B. J.; Clemente, J. C.; Quince, C.; Knight, R., UCHIME improves sensitivity and speed of chimera detection. *Bioinformatics* **2011,** *27* (16), 2194-2200.
67. DeSantis, T. Z.; Hugenholtz, P.; Larsen, N.; Rojas, M.; Brodie, E. L.; Keller, K.; Huber, T.; Dalevi, D.; Hu, P.; Andersen, G. L., Greengenes, a Chimera-Checked 16S rRNA Gene Database and Workbench Compatible with ARB. *Applied and Environmental Microbiology* **2006,** *72* (7), 5069.
68. Edgar, R. C., Search and clustering orders of magnitude faster than BLAST. *Bioinformatics* **2010,** *26* (19), 2460-2461.
69. Zakrzewski, M.; Proietti, C.; Ellis, J. J.; Hasan, S.; Brion, M.-J.; Berger, B.; Krause, L., Calypso: a user-friendly web-server for mining and visualizing microbiome–environment interactions. *Bioinformatics* **2016,** *33* (5), 782-783.
70. Livak, K. J.; Schmittgen, T. D., Analysis of Relative Gene Expression Data Using Real-Time Quantitative PCR and the 2−ΔΔCT Method. *Methods* **2001,** *25* (4), 402-408.
71. Jin, C.; Lagoudas, G. K.; Zhao, C.; Bullman, S.; Bhutkar, A.; Hu, B.; Ameh, S.; Sandel, D.; Liang, X. S.; Mazzilli, S.; Whary, M. T.; Meyerson, M.; Germain, R.; Blainey, P. C.; Fox, J. G.; Jacks, T., Commensal Microbiota Promote Lung Cancer Development via gammadelta T Cells. *Cell* **2019,** *176* (5), 998-1013.e16.
72. McCarthy, I.; James, S.; Dominique, G.; Jeremy K. Nicholson, M.-E. D.; Richard, H. B.; Ayo, T.; Olivier, C.; Christine, B.; Alice, R.; Jane, F.; Roger, T.; Véronique, B.; John, C. L.; Steve, C. M.; Elaine, H.; Mark, Metabolic profiling reveals a contribution of gut microbiota to fatty liver phenotype in insulin-resistant mice. **2006**.
73. Michan, S.; Sinclair, D., Sirtuins in mammals: insights into their biological function. *Biochemical Journal* **2007,** *404* (1), 1.
74. Yeung, F.; Hoberg, J. E.; Ramsey, C. S.; Keller, M. D.; Jones, D. R.; Frye, R. A.; Mayo, M. W., Modulation of NF-κB-dependent transcription and cell survival by the SIRT1 deacetylase. *The EMBO journal* **2004,** *23* (12), 2369-2380.
75. Wellman, A. S.; Metukuri, M. R.; Kazgan, N.; Xu, X.; Xu, Q.; Ren, N. S. X.; Czopik, A.; Shanahan, M. T.; Kang, A.; Chen, W.; Azcarate-Peril, M. A.; Gulati, A. S.; Fargo, D. C.;

Guarente, L.; Li, X., Intestinal Epithelial Sirtuin 1 Regulates Intestinal Inflammation During Aging in Mice by Altering the Intestinal Microbiota. *Gastroenterology* **2017,** *153* (3), 772-786.
76. Zhang, Y.; Wang, X.-l.; Zhou, M.; Kang, C.; Lang, H.-d.; Chen, M.-t.; Hui, S.-c.; Wang, B.; Mi, M.-t., Crosstalk between gut microbiota and Sirtuin-3 in colonic inflammation and tumorigenesis. *Experimental & Molecular Medicine* **2018,** *50* (4), 21.
77. Li, W.; Khor, T. O.; Xu, C.; Shen, G.; Jeong, W.-S.; Yu, S.; Kong, A.-N., Activation of Nrf2-antioxidant signaling attenuates NFκB-inflammatory response and elicits apoptosis. *Biochemical Pharmacology* **2008,** *76* (11), 1485-1489.
78. Kulkarni, S. R.; Donepudi, A. C.; Xu, J.; Wei, W.; Cheng, Q. C.; Driscoll, M. V.; Johnson, D. A.; Johnson, J. A.; Li, X.; Slitt, A. L., Fasting Induces Nuclear Factor E2-Related Factor 2 and ATP-Binding Cassette Transporters via Protein Kinase A and Sirtuin-1 in Mouse and Human. *Antioxidants & Redox Signaling* **2013,** *20* (1), 15-30.
79. Aleksunes, L. M.; Klaassen, C. D., Coordinated regulation of hepatic phase I and II drug-metabolizing genes and transporters using AhR-, CAR-, PXR-, PPARα-, and Nrf2-null mice. *Drug Metabolism and Disposition* **2012,** *40* (7), 1366-1379.
80. Venugopal, R.; Jaiswal, A. K., Nrf2 and Nrf1 in association with Jun proteins regulate antioxidant response element-mediated expression and coordinated induction of genes encoding detoxifying enzymes. *Oncogene* **1998,** *17* (24), 3145-3156.
81. Franklin, C. L.; Ericsson, A. C., Microbiota and reproducibility of rodent models. *Lab animal* **2017,** *46* (4), 114-122.
82. Markle, J. G. M.; Frank, D. N.; Mortin-Toth, S.; Robertson, C. E.; Feazel, L. M.; Rolle-Kampczyk, U.; von Bergen, M.; McCoy, K. D.; Macpherson, A. J.; Danska, J. S., Sex Differences in the Gut Microbiome Drive Hormone-Dependent Regulation of Autoimmunity. *Science* **2013,** *339* (6123), 1084.
83. Org, E.; Mehrabian, M.; Parks, B. W.; Shipkova, P.; Liu, X.; Drake, T. A.; Lusis, A. J., Sex differences and hormonal effects on gut microbiota composition in mice. *Gut Microbes* **2016,** *7* (4), 313-322.
84. Clemente, Jose C.; Ursell, Luke K.; Parfrey, Laura W.; Knight, R., The Impact of the Gut Microbiota on Human Health: An Integrative View. *Cell* **2012,** *148* (6), 1258-1270.
85. Dumas, M.-E.; Barton, R. H.; Toye, A.; Cloarec, O.; Blancher, C.; Rothwell, A.; Fearnside, J.; Tatoud, R.; Blanc, V.; Lindon, J. C.; Mitchell, S. C.; Holmes, E.; McCarthy, M. I.; Scott, J.; Gauguier, D.; Nicholson, J. K., Metabolic profiling reveals a contribution of gut microbiota to fatty liver phenotype in insulin-resistant mice. *Proceedings of the National Academy of Sciences* **2006,** *103* (33), 12511.
86. Jin, C.; Lagoudas, G. K.; Zhao, C.; Bullman, S.; Bhutkar, A.; Hu, B.; Ameh, S.; Sandel, D.; Liang, X. S.; Mazzilli, S.; Whary, M. T.; Meyerson, M.; Germain, R.; Blainey, P. C.; Fox, J. G.; Jacks, T., Commensal Microbiota Promote Lung Cancer Development via γδ T Cells. *Cell* **2019,** *176* (5), 998-1013.e16.
87. Li, Y.; Kundu, P.; Seow, S. W.; de Matos, C. T.; Aronsson, L.; Chin, K. C.; Karre, K.; Pettersson, S.; Greicius, G., Gut microbiota accelerate tumor growth via c-jun and STAT3 phosphorylation in APCMin/+ mice. *Carcinogenesis* **2012,** *33* (6), 1231-8.
88. Scher, J. U.; Sczesnak, A.; Longman, R. S.; Segata, N.; Ubeda, C.; Bielski, C.; Rostron, T.; Cerundolo, V.; Pamer, E. G.; Abramson, S. B.; Huttenhower, C.; Littman, D. R., Expansion of intestinal Prevotella copri correlates with enhanced susceptibility to arthritis. In *eLife*, 2013; Vol. 2.

89. Denning, T. L.; Norris, B. A.; Medina-Contreras, O.; Manicassamy, S.; Geem, D.; Madan, R.; Karp, C. L.; Pulendran, B., Functional specializations of intestinal dendritic cell and macrophage subsets that control Th17 and regulatory T cell responses are dependent on the T cell/APC ratio, source of mouse strain, and regional localization. *J Immunol* **2011,** *187* (2), 733-47.
90. Ericsson, A. C.; Hagan, C. E.; Davis, D. J.; Franklin, C. L., Segmented Filamentous Bacteria: Commensal Microbes with Potential Effects on Research. In *Comp Med*, 2014; Vol. 64, pp 90-8.
91. Ericsson, A. C.; Davis, J. W.; Spollen, W.; Bivens, N.; Givan, S.; Hagan, C. E.; McIntosh, M.; Franklin, C. L., Effects of Vendor and Genetic Background on the Composition of the Fecal Microbiota of Inbred Mice. *PLOS ONE* **2015,** *10* (2), e0116704.
92. Ivanov, II; Atarashi, K.; Manel, N.; Brodie, E. L.; Shima, T.; Karaoz, U.; Wei, D.; Goldfarb, K. C.; Santee, C. A.; Lynch, S. V.; Tanoue, T.; Imaoka, A.; Itoh, K.; Takeda, K.; Umesaki, Y.; Honda, K.; Littman, D. R., Induction of intestinal Th17 cells by segmented filamentous bacteria. *Cell* **2009,** *139* (3), 485-98.
93. Wu, H. J.; Ivanov, II; Darce, J.; Hattori, K.; Shima, T.; Umesaki, Y.; Littman, D. R.; Benoist, C.; Mathis, D., Gut-residing segmented filamentous bacteria drive autoimmune arthritis via T helper 17 cells. *Immunity* **2010,** *32* (6), 815-27.
94. Cai, X.; Carlson, J.; Stoicov, C.; Li, H.; Wang, T. C.; Houghton, J., Helicobacter felis Eradication Restores Normal Architecture and Inhibits Gastric Cancer Progression in C57BL/6 Mice. *Gastroenterology* **2005,** *128* (7), 1937-1952.
95. Maggio-Price, L.; Treuting, P.; Zeng, W.; Tsang, M.; Bielefeldt-Ohmann, H.; Iritani, B. M., Helicobacter Infection Is Required for Inflammation and Colon Cancer in Smad3-Deficient Mice. *Cancer Research* **2006,** *66* (2), 828.
96. Berg, R. D.; Garlington, A. W., Translocation of certain indigenous bacteria from the gastrointestinal tract to the mesenteric lymph nodes and other organs in a gnotobiotic mouse model. *Infect Immun* **1979,** *23* (2), 403-411.
97. Fouts, D. E.; Torralba, M.; Nelson, K. E.; Brenner, D. A.; Schnabl, B., Bacterial translocation and changes in the intestinal microbiome in mouse models of liver disease. *Journal of Hepatology* **2012,** *56* (6), 1283-1292.
98. Emani, R.; Alam, C.; Pekkala, S.; Zafar, S.; Emani, M. R.; Hänninen, A., Peritoneal Cavity is a Route for Gut-Derived Microbial Signals to Promote Autoimmunity in Non-Obese Diabetic Mice. *Scandinavian Journal of Immunology* **2015,** *81* (2), 102-109.
99. Sun, Z.; Wang, X.; Andersson, R., Role of Intestinal Permeability in Monitoring Mucosal Barrier Function. *Digestive Surgery* **1998,** *15* (5), 386-397.
100. Llewellyn, S. R.; Britton, G. J.; Contijoch, E. J.; Vennaro, O. H.; Mortha, A.; Colombel, J.-F.; Grinspan, A.; Clemente, J. C.; Merad, M.; Faith, J. J., Interactions Between Diet and the Intestinal Microbiota Alter Intestinal Permeability and Colitis Severity in Mice. *Gastroenterology* **2018,** *154* (4), 1037-1046.e2.
101. Donaldson, G. P.; Lee, S. M.; Mazmanian, S. K., Gut biogeography of the bacterial microbiota. *Nat Rev Microbiol* **2016,** *14* (1), 20-32.
102. Flemer, B.; Lynch, D. B.; Brown, J. M. R.; Jeffery, I. B.; Ryan, F. J.; Claesson, M. J.; Riordain, M.; Shanahan, F.; Toole, P. W., Tumour-associated and non-tumour-associated microbiota in colorectal cancer. *Gut* **2017,** *66* (4), 633.

103. Jahani-Sherafat, S.; Alebouyeh, M.; Moghim, S.; Ahmadi Amoli, H.; Ghasemian-Safaei, H., Role of gut microbiota in the pathogenesis of colorectal cancer; a review article. *Gastroenterol Hepatol Bed Bench* **2018,** *11* (2), 101-109.
104. Bekele, A. Z.; Koike, S.; Kobayashi, Y., Genetic diversity and diet specificity of ruminal Prevotella revealed by 16S rRNA gene-based analysis. *FEMS Microbiology Letters* **2010,** *305* (1), 49-57.
105. Baxter, N. T.; Zackular, J. P.; Chen, G. Y.; Schloss, P. D., Structure of the gut microbiome following colonization with human feces determines colonic tumor burden. *Microbiome* **2014,** *2* (1), 20.
106. Zackular, J. P.; Baxter, N. T.; Iverson, K. D.; Sadler, W. D.; Petrosino, J. F.; Chen, G. Y.; Schloss, P. D., The Gut Microbiome Modulates Colon Tumorigenesis. *mBio* **2013,** *4* (6), e00692-13.
107. Kleinstern, G.; Maurer, M. J.; Liebow, M.; Habermann, T. M.; Koff, J. L.; Allmer, C.; Witzig, T. E.; Nowakowski, G. S.; Micallef, I. N.; Johnston, P. B.; Inwards, D. J.; Thompson, C. A.; Feldman, A. L.; Link, B. K.; Flowers, C.; Slager, S. L.; Cerhan, J. R., History of autoimmune conditions and lymphoma prognosis. *Blood Cancer J* **2018,** *8* (8), 73-73.
108. Viau, M.; Zouali, M., B-lymphocytes, innate immunity, and autoimmunity. *Clinical Immunology* **2005,** *114* (1), 17-26.
109. Duan, B.; Morel, L., Role of B-1a cells in autoimmunity. *Autoimmunity Reviews* **2006,** *5* (6), 403-408.
110. Safe, S. H., Polychlorinated biphenyls (PCBs): environmental impact, biochemical and toxic responses, and implications for risk assessment. *Critical reviews in toxicology* **1994,** *24* (2), 87-149.
111. Weisglas-Kuperus, N.; Vreugdenhil, H. J.; Mulder, P. G., Immunological effects of environmental exposure to polychlorinated biphenyls and dioxins in Dutch school children. *Toxicology letters* **2004,** *149* (1-3), 281-285.
112. Rasmussen, J.; Rowan, D.; Lean, D.; Carey, J., Food chain structure in Ontario lakes determines PCB levels in lake trout (Salvelinus namaycush) and other pelagic fish. *Canadian Journal of Fisheries and Aquatic Sciences* **1990,** *47* (10), 2030-2038.
113. Muir, D. C.; Norstrom, R. J.; Simon, M., Organochlorine contaminants in Arctic marine food chains: accumulation of specific polychlorinated biphenyls and chlordane-related compounds. *Environmental Science and Technology* **1988,** *22* (9), 1071-1079.
114. Ampleman, M. D.; Martinez, A.; DeWall, J.; Rawn, D. F. K.; Hornbuckle, K. C.; Thorne, P. S., Inhalation and Dietary Exposure to PCBs in Urban and Rural Cohorts via Congener-Specific Measurements. *Environmental Science & Technology* **2015,** *49* (2), 1156-1164.
115. Norström, K.; Czub, G.; McLachlan, M. S.; Hu, D.; Thorne, P. S.; Hornbuckle, K. C., External exposure and bioaccumulation of PCBs in humans living in a contaminated urban environment. *Environment International* **2010,** *36* (8), 855-861.
116. Faroon, O. M.; Samuel Keith, L.; Smith-Simon, C.; De Rosa, C. T.; Organization, W. H., Polychlorinated biphenyls: human health aspects. 2003.
117. Dekoning, E. P.; Karmaus, W., PCB exposure in utero and via breast milk. A review. *Journal of Exposure Science and Environmental Epidemiology* **2000,** *10* (3), 285.
118. Fein, G. G.; Jacobson, J. L.; Jacobson, S. W.; Schwartz, P. M.; Dowler, J. K., Prenatal exposure to polychlorinated biphenyls: effects on birth size and gestational age. *The Journal of pediatrics* **1984,** *105* (2), 315-320.

119. Jacobson, J. L.; Jacobson, S. W.; Humphrey, H. E., Effects of exposure to PCBs and related compounds on growth and activity in children. *Neurotoxicology and Teratology* **1990,** *12* (4), 319-326.
120. Curran, C. P.; Nebert, D. W.; Genter, M. B.; Patel, K. V.; Schaefer, T. L.; Skelton, M. R.; Williams, M. T.; Vorhees, C. V., In utero and lactational exposure to PCBs in mice: adult offspring show altered learning and memory depending on Cyp1a2 and Ahr genotypes. *Environmental Health Perspectives* **2011,** *119* (9), 1286-1293.
121. Čechová, E.; Scheringer, M.; Seifertová, M.; Mikeš, O.; Kroupová, K.; Kuta, J.; Forns, J.; Eggesbø, M.; Quaak, I.; de Cock, M., Developmental neurotoxicants in human milk: Comparison of levels and intakes in three European countries. *Science of the Total Environment* **2017,** *579*, 637-645.
122. van den Berg, M.; Kypke, K.; Kotz, A.; Tritscher, A.; Lee, S. Y.; Magulova, K.; Fiedler, H.; Malisch, R., WHO/UNEP global surveys of PCDDs, PCDFs, PCBs and DDTs in human milk and benefit–risk evaluation of breastfeeding. *Archives of toxicology* **2017,** *91* (1), 83-96.
123. Pirard, C.; Compere, S.; Firquet, K.; Charlier, C., The current environmental levels of endocrine disruptors (mercury, cadmium, organochlorine pesticides and PCBs) in a Belgian adult population and their predictors of exposure. *International journal of hygiene and environmental health* **2018,** *221* (2), 211-222.
124. Safe, S.; Bandiera, S.; Sawyer, T.; Robertson, L.; Safe, L.; Parkinson, A.; Thomas, P. E.; Ryan, D. E.; Reik, L. M.; Levin, W., PCBs: structure–function relationships and mechanism of action. *Environmental Health Perspectives* **1985,** *60*, 47-56.
125. Kafafi, S. A.; Afeefy, H. Y.; Ali, A. H.; Said, H. K.; Kafafi, A. G., Binding of polychlorinated biphenyls to the aryl hydrocarbon receptor. *Environmental Health Perspectives* **1993,** *101* (5), 422-428.
126. Okey, A. B.; Riddick, D. S.; Harper, P. A., The Ah receptor: mediator of the toxicity of 2, 3, 7, 8-tetrachlorodibenzo-p-dioxin (TCDD) and related compounds. *Toxicology letters* **1994,** *70* (1), 1-22.
127. Gaspar-Ramírez, O.; Pérez-Vázquez, F. J.; Salgado-Bustamante, M.; González-Amaro, R.; Hernandez-Castro, B.; Pérez-Maldonado, I. N., DDE and PCB 153 independently induce aryl hydrocarbon receptor (AhR) expression in peripheral blood mononuclear cells. *Journal of Immunotoxicology* **2015,** *12* (3), 266-272.
128. Strathmann, J.; Schwarz, M.; Tharappel, J. C.; Glauert, H. P.; Spear, B. T.; Robertson, L. W.; Appel, K. E.; Buchmann, A., Pcb 153, a Non-dioxin–like Tumor Promoter, Selects for β-catenin (catnb)–mutated Mouse Liver Tumors. *Toxicological Sciences* **2006,** *93* (1), 34-40.
129. Haave, M.; Bernhard, A.; Jellestad, F. K.; Heegaard, E.; Brattelid, T.; Lundebye, A.-K., Long-term effects of environmentally relevant doses of 2, 2', 4, 4', 5, 5'hexachlorobiphenyl (PCB153) on neurobehavioural development, health and spontaneous behaviour in maternally exposed mice. *Behavioral Brain Functions* **2011,** *7* (1), 3.
130. Lu, Z.; Lee, E. Y.; Robertson, L. W.; Glauert, H. P.; Spear, B. T., Effect of 2, 2′, 4, 4′, 5, 5′-hexachlorobiphenyl (PCB-153) on hepatocyte proliferation and apoptosis in mice deficient in the p50 subunit of the transcription factor NF-κB. *Toxicological Sciences* **2004,** *81* (1), 35-42.
131. Hamers, T.; Kamstra, J. H.; Cenijn, P. H.; Pencikova, K.; Palkova, L.; Simeckova, P.; Vondracek, J.; Andersson, P. L.; Stenberg, M.; Machala, M., In vitro toxicity profiling of ultrapure non–dioxin-like polychlorinated biphenyl congeners and their relative toxic contribution to PCB mixtures in humans. *Toxicological Sciences* **2011,** *121* (1), 88-100.

132. Spinelli, J. J.; Ng, C. H.; Weber, J. P.; Connors, J. M.; Gascoyne, R. D.; Lai, A. S.; Brooks-Wilson, A. R.; Le, N. D.; Berry, B. R.; Gallagher, R. P., Organochlorines and risk of non-Hodgkin lymphoma. *International journal of cancer* **2007,** *121* (12), 2767-2775.
133. Bonefeld-Jørgensen, E. C.; Andersen, H. R.; Rasmussen, T. H.; Vinggaard, A. M., Effect of highly bioaccumulated polychlorinated biphenyl congeners on estrogen and androgen receptor activity. *Toxicology* **2001,** *158* (3), 141-153.
134. Giera, S.; Bansal, R.; Ortiz-Toro, T. M.; Taub, D. G.; Zoeller, R. T., Individual polychlorinated biphenyl (PCB) congeners produce tissue-and gene-specific effects on thyroid hormone signaling during development. *Endocrinology* **2011,** *152* (7), 2909-2919.
135. Brody, J. G.; Moysich, K. B.; Humblet, O.; Attfield, K. R.; Beehler, G. P.; Rudel, R. A., Environmental pollutants and breast cancer: epidemiologic studies. *Cancer* **2007,** *109*, 2667-2711.
136. Hardell, L.; Andersson, S.-O.; Carlberg, M.; Bohr, L.; van Bavel, B.; Lindström, G.; Björnfoth, H.; Ginman, C., Adipose tissue concentrations of persistent organic pollutants and the risk of prostate cancer. *Journal of Occupational Environmental Medicine* **2006,** *48* (7), 700-707.
137. Miki, Y.; Suzuki, T.; Tazawa, C.; Blumberg, B.; Sasano, H., Steroid and xenobiotic receptor (SXR), cytochrome P450 3A4 and multidrug resistance gene 1 in human adult and fetal tissues. *Molecular and Cellular Endocrinology* **2005,** *231* (1), 75-85.
138. European Food Safety, A., Opinion of the Scientific Panel on contaminants in the food chain [CONTAM] related to the presence of non dioxin-like polychlorinated biphenyls (PCB) in feed and food. *EFSA Journal* **2005,** *3* (11), 284.
139. Evans, B. C.; Nelson, C. E.; Shann, S. Y.; Beavers, K. R.; Kim, A. J.; Li, H.; Nelson, H. M.; Giorgio, T. D.; Duvall, C. L., Ex vivo red blood cell hemolysis assay for the evaluation of pH-responsive endosomolytic agents for cytosolic delivery of biomacromolecular drugs. *JoVe* **2013,** (73), e50166.
140. Andrews, S., FastQC: a quality control tool for high throughput sequence data. 2010.
141. Dobin, A.; Davis, C. A.; Schlesinger, F.; Drenkow, J.; Zaleski, C.; Jha, S.; Batut, P.; Chaisson, M.; Gingeras, T. R., STAR: ultrafast universal RNA-seq aligner. *Bioinformatics* **2013,** *29* (1), 15-21.
142. Liao, Y.; Smyth, G. K.; Shi, W., featureCounts: an efficient general purpose program for assigning sequence reads to genomic features. *Bioinformatics* **2013,** *30* (7), 923-930.
143. Love, M. I.; Huber, W.; Anders, S., Moderated estimation of fold change and dispersion for RNA-seq data with DESeq2. *Genome biology* **2014,** *15* (12), 550.
144. Supek, F.; Bošnjak, M.; Škunca, N.; Šmuc, T., REVIGO Summarizes and Visualizes Long Lists of Gene Ontology Terms. *PLOS ONE* **2011,** *6* (7), e21800.
145. Milanowski, B.; Lulek, J.; Lehmler, H. J.; Kania-Korwel, I., Assessment of the disposition of chiral polychlorinated biphenyls in female mdr 1a/b knockout versus wild-type mice using multivariate analyses. *Environment International* **2010,** *36* (8), 884-892.
146. Kania-Korwel, I.; Shaikh, N. S.; Hornbuckle, K. C.; Robertson, L. W.; Lehmler, H. J., Enantioselective disposition of PCB 136 (2,2 ',3,3 ',6,6 '-hexachlorobiphenyl) in C57BL/6 mice after oral and intraperitoneal administration. *Chirality* **2007,** *19* (1), 56-66.
147. Kania-Korwel, I.; Hornbuckle, K. C.; Peck, A.; Ludewig, G.; Robertson, L. W.; Sulkowski, W. W.; Espandiari, P.; Gairola, C. G.; Lehmler, H. J., Congener-specific tissue distribution of aroclor 1254 and a highly chlorinated environmental PCB mixture in rats. *Environmental Science & Technology* **2005,** *39* (10), 3513-3520.

148. Wu, X. A.; Pramanik, A.; Duffel, M. W.; Hrycay, E. G.; Bandiera, S. M.; Lehmler, H. J.; Kania-Korwel, I., 2,2 ',3,3 ',6,6 '-Hexachlorobiphenyl (PCB 136) Is Enantioselectively Oxidized to Hydroxylated Metabolites by Rat Liver Microsomes. *Chemical Research in Toxicology* **2011,** *24* (12), 2249-2257.
149. Kania-Korwel, I.; Duffel, M. W.; Lehmler, H. J., Gas Chromatographic Analysis with Chiral Cyclodextrin Phases Reveals the Enantioselective Formation of Hydroxylated Polychlorinated Biphenyls by Rat Liver Microsomes. *Environmental Science & Technology* **2011,** *45* (22), 9590-9596.
150. Uwimana, E.; Li, X. S.; Lehmler, H. J., 2,2 ',3,5 ',6-Pentachlorobiphenyl (PCB 95) Is Atropselectively Metabolized to para-Hydroxylated Metabolites by Human Liver Microsomes. *Chemical Research in Toxicology* **2016,** *29* (12), 2108-2110.
151. Siatecka, M.; Bieker, J. J., The multifunctional role of EKLF/KLF1 during erythropoiesis. *Blood* **2011,** *118* (8), 2044-2054.
152. Kops, G. J. P. L.; Dansen, T. B.; Polderman, P. E.; Saarloos, I.; Wirtz, K. W. A.; Coffer, P. J.; Huang, T.-T.; Bos, J. L.; Medema, R. H.; Burgering, B. M. T., Forkhead transcription factor FOXO3a protects quiescent cells from oxidative stress. *Nature* **2002,** *419* (6904), 316-321.
153. Marinkovic, D.; Zhang, X.; Yalcin, S.; Luciano, J. P.; Brugnara, C.; Huber, T.; Ghaffari, S., Foxo3 is required for the regulation of oxidative stress in erythropoiesis. *The Journal of clinical investigation* **2007,** *117* (8), 2133-2144.
154. Grimm, F. A.; Hu, D.; Kania-Korwel, I.; Lehmler, H.-J.; Ludewig, G.; Hornbuckle, K. C.; Duffel, M. W.; Bergman, Å.; Robertson, L. W., Metabolism and metabolites of polychlorinated biphenyls. *Critical reviews in toxicology* **2015,** *45* (3), 245-272.
155. Daidoji, T.; Gozu, K.; Iwano, H.; Inoue, H.; Yokota, H., UDP-glucuronosyltransferase isoforms catalyzing glucuronidation of hydroxy-polychlorinated biphenyls in rat. *Drug Metabolism and Disposition* **2005,** *33* (10), 1466-1476.
156. Igarashi, K.; Kitajima, S.; Aisaki, K.-i.; Tanemura, K.; Taquahashi, Y.; Moriyama, N.; Ikeno, E.; Matsuda, N.; Saga, Y.; Blumberg, B.; Kanno, J., Development of humanized steroid and xenobiotic receptor mouse by homologous knock-in of the human steroid and xenobiotic receptor ligand binding domain sequence. *The Journal of Toxicological Sciences* **2012,** *37* (2), 373-380.
157. Guo, Y. L.; Lambert, G. H.; Hsu, C.-C., Growth abnormalities in the population exposed in utero and early postnatally to polychlorinated biphenyls and dibenzofurans. *Environmental Health Perspectives* **1995,** *103* (suppl 6), 117-122.
158. Jacobson, J. L.; Jacobson, S. W.; Humphrey, H. E., Effects of in utero exposure to polychlorinated biphenyls and related contaminants on cognitive functioning in young children. *The Journal of pediatrics* **1990,** *116* (1), 38-45.
159. Paulson, R. F.; Shi, L.; Wu, D.-C., Stress erythropoiesis: new signals and new stress progenitor cells. *Current opinion in hematology* **2011,** *18* (3), 139.
160. Bozzini, C.; Barrio Rendo, M.; Devoto, F.; Epper, C., Studies on medullary and extramedullary erythropoiesis in the adult mouse. *American Journal of Physiology* **1970,** *219* (3), 724-728.
161. Beutler, E., Drug-induced hemolytic anemia. *Pharmacological Reviews* **1969,** *21* (1), 73-103.
162. Fibach, E.; Rachmilewitz, E., The role of oxidative stress in hemolytic anemia. *Current molecular medicine* **2008,** *8* (7), 609-619.

163. Han, Y.-H.; Kim, S.-U.; Kwon, T.-H.; Lee, D.-S.; Ha, H.-L.; Park, D.-S.; Woo, E.-J.; Lee, S.-H.; Kim, J.-M.; Chae, H.-B., Peroxiredoxin II is essential for preventing hemolytic anemia from oxidative stress through maintaining hemoglobin stability. *Biochem Biophys Res Commun* **2012,** *426* (3), 427-432.
164. Iuchi, Y.; Kibe, N.; Tsunoda, S.; Suzuki, S.; Mikami, T.; Okada, F.; Uchida, K.; Fujii, J., Implication of oxidative stress as a cause of autoimmune hemolytic anemia in NZB mice. *Free Radic Biol Med* **2010,** *48* (7), 935-944.
165. Meister, A.; Anderson, M. E., Glutathione. *Annual review of biochemistry* **1983,** *52* (1), 711-760.
166. Townsend, D.; Tew, K.; Tapiero, H., The importance of glutathione in human disease. *Biomedicine pharmacotherapy* **2003,** *57* (3-4), 145.
167. Al-Anati, L.; Viluksela, M.; Strid, A.; Bergman, Å.; Andersson, P. L.; Stenius, U.; Högberg, J., Hydroxyl metabolite of PCB 180 induces DNA damage signaling and enhances the DNA damaging effect of benzo [a] pyrene. *Chemico-biological interactions* **2015,** *239*, 164-173.
168. Sandal, S.; Yilmaz, B.; Carpenter, D. O., Genotoxic effects of PCB 52 and PCB 77 on cultured human peripheral lymphocytes. *Mutation Research/Genetic Toxicology and Environmental Mutagenesis* **2008,** *654* (1), 88-92.
169. Han, Y.; Liu, Q.; Hou, J.; Gu, Y.; Zhang, Y.; Chen, Z.; Fan, J.; Zhou, W.; Qiu, S.; Zhang, Y., Tumor-induced generation of splenic erythroblast-like Ter-cells promotes tumor progression. *Cell* **2018,** *173* (3), 634-648. e12.
170. Hayes, J. D.; Flanagan, J. U.; Jowsey, I. R., Glutathione transferases. *Annu. Rev. Pharmacol. Toxicol.* **2005,** *45*, 51-88.
171. Beutler, E.; Dunning, D.; Dabe, I.; Forman, L., Erythrocyte glutathione S-transferase deficiency and hemolytic anemia. *Blood* **1988,** *72* (1), 73-77.
172. Lee, K. A.; Kim, S. H.; Woo, H. Y.; Hong, Y. J.; Cho, H. C., Increased frequencies of glutathione S-transferase (GSTM1 and GSTT1) gene deletions in Korean patients with acquired aplastic anemia. *Blood* **2001,** *98* (12), 3483-3485.
173. Silva, D. G. H.; Junior, E. B.; de Souza Torres, L.; Júnior, O. R.; de Castro Lobo, C.; Bonini-Domingos, C. R.; de Almeida, E. A. J. B. C., Molecules,; Diseases, Relationship between oxidative stress, glutathione S-transferase polymorphisms and hydroxyurea treatment in sickle cell anemia. **2011,** *47* (1), 23-28.
174. Dreiem, A.; Rykken, S.; Lehmler, H.-J.; Robertson, L. W.; Fonnum, F. J. T.; pharmacology, a., Hydroxylated polychlorinated biphenyls increase reactive oxygen species formation and induce cell death in cultured cerebellar granule cells. **2009,** *240* (2), 306-313.
175. Burchell, B.; Coughtrie, M. W.; therapeutics, UDP-glucuronosyltransferases. *Pharmacology* **1989,** *43* (2), 261-289.
176. Gamage, N.; Barnett, A.; Hempel, N.; Duggleby, R. G.; Windmill, K. F.; Martin, J. L.; McManus, M. E., Human Sulfotransferases and Their Role in Chemical Metabolism. *Toxicological Sciences* **2005,** *90* (1), 5-22.
177. Liu, Y.; Smart, J. T.; Song, Y.; Lehmler, H.-J.; Robertson, L. W.; Duffel, M. W., Structure-Activity Relationships for Hydroxylated Polychlorinated Biphenyls as Substrates and Inhibitors of Rat Sulfotransferases and Modification of These Relationships by Changes in Thiol Status. *Drug Metabolism and Disposition* **2009,** *37* (5), 1065.
178. Liu, Y.; Apak, T. I.; Lehmler, H.-J.; Robertson, L. W.; Duffel, M. W., Hydroxylated polychlorinated biphenyls are substrates and inhibitors of human hydroxysteroid sulfotransferase SULT2A1. *Chemical research in toxicology* **2006,** *19* (11), 1420-1425.

179. Shevtsov, S.; Petrotchenko Evgeniy, V.; Pedersen Lars, C.; Negishi, M., Crystallographic analysis of a hydroxylated polychlorinated biphenyl (OH-PCB) bound to the catalytic estrogen binding site of human estrogen sulfotransferase. *Environmental Health Perspectives* **2003,** *111* (7), 884-888.
180. Mesnier, A.; Champion, S.; Louis, L.; Sauzet, C.; May, P.; Portugal, H.; Benbrahim, K.; Abraldes, J.; Alessi, M.-C.; Amiot-Carlin, M.-J., The transcriptional effects of PCB118 and PCB153 on the liver, adipose tissue, muscle and colon of mice: highlighting of Glut4 and Lipin1 as main target genes for PCB induced metabolic disorders. *PLoS One* **2015,** *10* (6), e0128847.
181. Birnbaum, L. S., Distribution and excretion of 2,3,6,2′,3′,6′- and 2,4,5,2′,4′,5′-hexachlorobiphenyl in senescent rats. *Toxicology and Applied Pharmacology* **1983,** *70* (2), 262-272.
182. Peters, A.; Festing, M., Population density and growth rate in laboratory mice. *Laboratory Animals* **1990,** *24* (3), 273-279.
183. Garcia, J. F., Changes in blood, plasma and red cell volume in the male rat, as a function of age. *American Journal of Physiology* **1957,** *190* (1), 19-24.
184. Patandin, S.; Koopman-Esseboom, C.; De Ridder, M. A.; Weisglas-Kuperus, N.; Sauer, P. J., Effects of environmental exposure to polychlorinated biphenyls and dioxins on birth size and growth in Dutch children. *Pediatric research* **1998,** *44* (4), 538.
185. Chu, I.; Poon, R.; Yagminas, A.; Lecavalier, P.; Håkansson, H.; Valli, V.; Kennedy, S.; Bergman, Å.; Seegal, R.; Feeley, M., Subchronic toxicity of PCB 105 (2, 3, 3′, 4, 4′-pentachlorobiphenyl) in rats. *Journal of Applied Toxicology* **1998,** *18* (4), 285-292.
186. Tryphonas, L.; Arnold, D. L.; Zawidzka, Z.; Mes, J.; Charbonneau, S.; Wong, J., A Pilot Study in Adult Rhesus Monkeys (M. mulatta) Treated with Aroclor 1254 for Two Years. *Toxicologic Pathology* **1986,** *14* (1), 1-10.
187. Ji, K.; Choi, K.; Giesy, J. P.; Musarrat, J.; Takeda, S., Genotoxicity of Several Polybrominated Diphenyl Ethers (PBDEs) and Hydroxylated PBDEs, and Their Mechanisms of Toxicity. *Environmental Science & Technology* **2011,** *45* (11), 5003-5008.
188. Krausova, L.; Stejskalova, L.; Wang, H.; Vrzal, R.; Dvorak, Z.; Mani, S.; Pavek, P., Metformin suppresses pregnane X receptor (PXR)-regulated transactivation of CYP3A4 gene. *Biochemical pharmacology* **2011,** *82* (11), 1771-1780.
189. Smutny, T.; Pavek, P., Resveratrol as an inhibitor of pregnane X receptor (PXR): another lesson in PXR antagonism. *Journal of pharmacological sciences* **2014,** *126* (2), 177-178.
190. De Franceschi, L.; Fattovich, G.; Turrini, F.; Ayi, K.; Brugnara, C.; Manzato, F.; Noventa, F.; Stanzial, A. M.; Solero, P.; Corrocher, R., Hemolytic anemia induced by ribavirin therapy in patients with chronic hepatitis C virus infection: role of membrane oxidative damage. *Hepatology* **2000,** *31* (4), 997-1004.
191. Johnson, R. M.; Ravindranath, Y.; el-Alfy, M.; Goyette, G., Jr., Oxidant damage to erythrocyte membrane in glucose-6-phosphate dehydrogenase deficiency: correlation with in vivo reduced glutathione concentration and membrane protein oxidation. *Blood* **1994,** *83* (4), 1117.
192. Angelillo-Scherrer, A.; Burnier, L.; Lambrechts, D.; Fish, R. J.; Tjwa, M.; Plaisance, S.; Sugamele, R.; DeMol, M.; Martinez-Soria, E.; Maxwell, P. H.; Lemke, G.; Goff, S. P.; Matsushima, G. K.; Earp, H. S.; Chanson, M.; Collen, D.; Izui, S.; Schapira, M.; Conway, E. M.; Carmeliet, P., Role of Gas6 in erythropoiesis and anemia in mice. *The Journal of clinical investigation* **2008,** *118* (2), 583-596.

193. Song, Y.; Wagner, B. A.; Witmer, J. R.; Lehmler, H.-J.; Buettner, G. R., Nonenzymatic displacement of chlorine and formation of free radicals upon the reaction of glutathione with PCB quinones. *Proc Natl Acad Sci U S A* **2009,** *106* (24), 9725-9730.
194. Zhu, Y.; Kalen, A. L.; Li, L.; Lehmler, H.-J.; Robertson, L. W.; Goswami, P. C.; Spitz, D. R.; Aykin-Burns, N., Polychlorinated-biphenyl-induced oxidative stress and cytotoxicity can be mitigated by antioxidants after exposure. *Free Radical Biology and Medicine* **2009,** *47* (12), 1762-1771.
195. Moreau, R.; Tshikudi Malu, D.; Dumais, M.; Dalko, E.; Gaudreault, V.; Romero, H.; Martineau, C.; Kevorkova, O.; Dardon, J. S.; Dodd, E. L.; Bohle, D. S.; Scorza, T., Alterations in bone and erythropoiesis in hemolytic anemia: comparative study in bled, phenylhydrazine-treated and Plasmodium-infected mice. *PLoS One* **2012,** *7* (9), e46101.
196. Wang, S.; Dale, G. L.; Song, P.; Viollet, B.; Zou, M. H., AMPKalpha1 deletion shortens erythrocyte life span in mice: role of oxidative stress. *J Biol Chem* **2010,** *285* (26), 19976-85.

APPENDIX

```
########################
#STAR HPC Cluster Script#
########################

#generate genome index on HPC cluster
module purge
module load gcc/6.4.0 STAR/2.6.0c
STAR --runThreadN 12 \
--runMode genomeGenerate \
--genomeDir
/bio/regusqui/PCB_RNAseq/mm10/STARindexENSEMBLandEncode \
--genomeFastaFiles
/bio/regusqui/PCB_RNAseq/mm10/ENSEMBLfasta/Mus_musculus.GRCm38.d
na.primary_assembly.fa \
--sjdbGTFfile
/bio/regusqui/PCB_RNAseq/mm10/ENCODEmouseAnnotation/gencode.vM20
.annotation.gtf \
--sjdbOverhang 99

#Align fastq files to mouse genome (repeated for each file)
STAR --runThreadN 16 \
--genomeDir /dfs3/bio/regusqui/PCB_RNAseq/mm10/STARindexENSEMBL
\
--readFilesIn
/dfs3/bio/regusqui/PCB_RNAseq/liver/fastq_files/reSequencedFiles
/KP2-GCCAAT-Sequences.txt.gz \
--readFilesCommand zcat \
--outFileNamePrefix
/dfs3/bio/regusqui/PCB_RNAseq/liver/newBAMfiles/WD1_ \
--outSAMtype BAM Unsorted SortedByCoordinate

####################
# Rsubread R Script #
####################

#install Rsubread
if (!requireNamespace("BiocManager", quietly = TRUE))
+ install.packages(BiocManager)
BiocManager::install("Rsubread", version = "3.8")
library("Rsubread")

#set input and output directories
dir_input <- "/dfs3/bio/regusqui/PCB_RNAseq/liver/newBAMfiles/"
dir_output <- "/dfs3/bio/regusqui/PCB_RNAseq/liver/Rsubread/"
setwd(dir_output)

#specify GTF file
```

```
gtf.file <-
"/dfs3/bio/regusqui/PCB_RNAseq/mm10/ENSEMBLannotation/Mus_muscul
us.GRCm38.95.gtf"

#load STAR BAM files
WD1 <- paste0(dir_input, "WD1_Aligned.out.bam")
WD2 <- paste0(dir_input, "WD2_Aligned.out.bam")
WD3 <- paste0(dir_input, "WD3_Aligned.out.bam")
WD4 <- paste0(dir_input, "WD4_Aligned.out.bam")
WD5 <- paste0(dir_input, "WD5_Aligned.out.bam")
WP1 <- paste0(dir_input, "WP1_Aligned.out.bam")
WP2 <- paste0(dir_input, "WP2_Aligned.out.bam")
WP3 <- paste0(dir_input, "WP3_Aligned.out.bam")
WP4 <- paste0(dir_input, "WP4_Aligned.out.bam")
WP5 <- paste0(dir_input, "WP5_Aligned.out.bam")
KD1 <- paste0(dir_input, "KD1_Aligned.out.bam")
KD2 <- paste0(dir_input, "KD2_Aligned.out.bam")
KD3 <- paste0(dir_input, "KD3_Aligned.out.bam")
KD4 <- paste0(dir_input, "KD4_Aligned.out.bam")
KD5 <- paste0(dir_input, "KD5_Aligned.out.bam")
KP1 <- paste0(dir_input, "KP1_Aligned.out.bam")
KP2 <- paste0(dir_input, "KP2_Aligned.out.bam")
KP3 <- paste0(dir_input, "KP3_Aligned.out.bam")
KP4 <- paste0(dir_input, "KP4_Aligned.out.bam")
KP5 <- paste0(dir_input, "KP5_Aligned.out.bam")
bam.files <-
c(WD1,WD2,WD3,WD4,WD5,WP1,WP2,WP3,WP4,WP5,KD1,KD2,KD3,KD4,KD5,KP
1,KP2,KP3,KP4,KP5)

#Run Rsubread to obtain exon counts
counts <- featureCounts(files = bam.files,
                        annot.ext = gtf.file,
                        isGTFAnnotationFile = TRUE,
                        GTF.featureType = "exon",
                        GTF.attrType = "gene_name",
                        allowMultiOverlap = TRUE,
                        isPairedEnd = FALSE,
                        nthreads = 24,
                        countMultiMappingReads = TRUE,
                        strandSpecific = 0)

# Get counts in data frame
liver_unsorted_counts.df <- as.data.frame(counts$counts)

# Simplify column names
```

```
colnames(liver_unsorted_counts.df) <-
sub("X.dfs3.bio.regusqui.PCB_RNAseq.liver.newBAMfiles.", "",
colnames(liver_unsorted_counts.df))
colnames(liver_unsorted_counts.df) <- sub("_Aligned.out.bam",
"", colnames(liver_unsorted_counts.df))

# Save data frame file
write.table(liver_unsorted_counts.df,
file=paste0(dir_output,"liver_unsorted_counts.txt"),quote=F,col.
names=T,row.names=T,sep="\t")

###################
# DESeq2 R Script #
###################

# Load DESeq2
BiocManager::install("DESeq2", version = "3.8")
library("DESeq2")

# Set new input output and working directory
dir_input <- "/dfs3/bio/regusqui/PCB_RNAseq/liver/Rsubread/"
dir_output <- "/dfs3/bio/regusqui/PCB_RNAseq/liver/DESeq2/"
setwd(dir_output)

# Load Rsubread count file
counts <- paste0(dir_input, "liver_unsorted_counts.txt"
countData <- read.table(counts, as.is=T, header=T, row.names=1)


# Define experimental design
samples <- c("WD1", "WD2", "WD3", "WD4", "WD5", "WP1", "WP2",
"WP3", "WP4", "WP5", "KD1", "KD2", "KD3", "KD4", "KD5", "KP1",
"KP2", "KP3", "KP4", "KP5")
condition <- c("WD", "WD", "WD", "WD", "WD", "WP", "WP", "WP",
"WP", "WP", "KD", "KD", "KD", "KD", "KD", "KP", "KP", "KP",
"KP", "KP")
type <- "single-read"
liver_colData <- data.frame(condition=condition, type=type,
row.names=samples)

#DEG analysis
liver_dds_unsorted <- DESeqDataSetFromMatrix(countData =
countData, colData = liver_colData, design = ~ condition)
liver_dds_unsorted <- DESeq(liver_dds_unsorted)
liver_DESeq2results_KDvsWD_alpha0.05 <-
results(liver_dds_unsorted, alpha=0.05, contrast =
c("condition", "KD", "WD"))
```

```
liver_DESeq2results_KPvsKD_alpha0.05 <-
results(liver_dds_unsorted, alpha = 0.05, contrast =
c("condition", "KP", "KD"))
liver_DESeq2results_KPvsWP_alpha0.05 <-
results(liver_dds_unsorted, alpha = 0.05, contrast =
c("condition", "KP", "WP"))
liver_DESeq2results_WPvsWD_alpha0.05 <-
results(liver_dds_unsorted, alpha = 0.05, contrast =
c("condition", "WP", "WD"))
write.table(liver_DESeq2results_KDvsWD_alpha0.05, file =
paste0(dir_output, "liver_KDvsWD_alpha0.05.txt"), quote = F,
col.names = T, sep = "\t")
write.table(liver_DESeq2results_KPvsKD_alpha0.05, file =
paste0(dir_output, "liver_KPvsKD_alpha0.05.txt"), quote = F,
col.names = T, sep = "\t")
write.table(liver_DESeq2results_KPvsWP_alpha0.05, file =
paste0(dir_output, "liver_KPvsWP_alpha0.05.txt"), quote = F,
col.names = T, sep = "\t")
write.table(liver_DESeq2results_WPvsWD_alpha0.05, file =
paste0(dir_output, "liver_WPvsWD_alpha0.05.txt"), quote = F,
col.names = T, sep = "\t")

#obtain normalized counts
liver_dds_unsorted <- estimateSizeFactors(liver_dds_unsorted)
norm_liver_counts <- counts(liver_dds_unsorted, normalized=TRUE)
write.csv(norm_liver_counts, file="norm_liver_counts.csv")
```